Dissertation
submitted to the Combined Faculties for Natural Sciences and for Mathematics
of the Ruperto-Carola University of Heidelberg, Germany
for the degree of

Doctor of Natural Sciences

presented by:
Diplom Meteorologin Linda Smoydzin
born in: Krumbach

Oral examination: 04.06.2008

Modelling Gas Phase and Aerosol Phase Chemistry in the Atmospheric Boundary Layer

Zusammenfassung

Organische Substanzen, welche sich an der Ozeanoberfläche ansammeln, können häufig im Laufe des Bildungsprozesses von Seesalzaerosolen in diese eingeschlossen werden und Oberflächenfilme auf den Partikeln bilden. Solch ein organischer Film kann den beidseitigen Austausch von Gasphasen Substanzen mit Aerosolpartikeln herabsetzen und damit chemische Zyklen in der maritimen Grenzschicht beeinflussen. Dieser Aspekt der Atmosphärenchemie wird mit Hilfe eines eindimensionalen numerischen Modells im ersten Teil dieser Arbeit untersucht, in dem unter anderem Abschätzungen zur Lebenszeit eines organischen Oberflächenfilms gegeben werden. Desweiteren wird gezeigt, in wie weit die Intensität des Effektes der organischen Filme von den Konzentrationen der organischen Substanzen sowie der Größenordnung der Phasentransferlimitierung abhängt.

Im zweiten Teil der Arbeit werden Ozon - Zerstörungsprozesse und die Bildung aussergewöhnlich hoher Brom Konzentrationen über dem Toten Meer untersucht. Es wird analysiert, wie groß der Beitrag von bromhaltigen Substanzen, welche direkt aus dem Wasser des Toten Meeres ausgasen, an der Gesamtbrombilanz ist, indem der Gasaustausch dieser Spezies explizit im Modell betrachtet wird. Es wird gezeigt, das nur unter Berücksichtigung dieses Prozesses hohe BrO und korrespondierend niedrige Ozon Werte in der Größenordnung, wie sie am Toten Meer gemessen wurden, in den Modellstudien simuliert werden können.

Abstract

Organic material from the ocean's surface microlayer can be incorporated into sea salt aerosol particles often producing a surface film on the aerosol. Such an organic coating can reduce the mass transfer between the gas phase and the aerosol phase influencing sea salt chemistry in the marine boundary layer. This aspect of atmospheric chemistry is investigated using a numerical one-dimensional model in the first part of this thesis. Estimates for the lifetime of the surface coating are given. Furthermore, it is showed in which way the intensity of the effect of an organic film depends on the concentrations of the organic species as well as the order of magnitude of the the mass transfer reduction.

The second part of the thesis deals with the investigation of O_3 depletion events and extraordinary high bromine levels along the Dead Sea. The contribution of degassing bromine species out of the Dead Sea water to the total bromine budget is investigated by including this process explicitly in a numerical model. It is showed that only when considering this process it is possible to simulate high mixing ratios for BrO and low mixing ratios for O_3 in agreement to field measurements.

Contents

Chapter 1

Introduction

1.1 Foreword and outline of this thesis

Part I

Based on an increasing number of field measurements as well as laboratory studies, the objective of part I of this thesis is to investigate the potential impact of film forming organic compounds on atmospheric chemistry as well as their effect on diffusional growth of aerosol particles. It is assumed that organic surface films decrease the mass transfer between the aerosol phase and the gas phase. A one-dimensional numerical model is used and by considering uncertainties regarding the magnitude of uptake reduction, the concentrations of organic compounds in sea salt aerosol particles and the oxidation rate of the organics, the possible influence of organic surfactants on gas and liquid phase chemistry with a special focus on halogen chemistry is analysed.

The introduction of part I of this thesis gives an overview of recent field measurements (Chapter 3) and laboratory measurements dealing with the occurrence and relevance of organic compounds in the atmosphere. Afterwards it is explained in which way heterogeneous surface reactions are treated in the model (Section 4.1) and thus how the atmospheric processing of the organic surface films is calculated. An important aspect is the lifetime of an organic surface film which is investigated (Section 4.3.1). Furthermore, the actual effect on gas phase as well as aerosol phase chemistry is addressed (Section 4.3.2) as well as the effect on diffusional growth of aerosol particles under cloud free as well as cloudy conditions (Chapter 5).

Part II

Measurements of O_3 and BrO concentrations over the Dead Sea indicate that Ozone Depletion Events (ODE) widely known to happen in polar regions are also likely to occur over the Dead Sea due to the very high bromine content of the Dead Sea water. However, BrO and O_3 levels as they are detected cannot solely be explained by high Br^- levels in the Dead Sea water and the release of gas phase halogen species out of sea borne aerosol particles and their conversion to reactive halogen species. It is likely that other sources for reactive halogen compounds are required to explain the observed concentrations for BrO and O_3. To include an additional source for gas phase halogen compounds, air-sea exchange between the Dead Sea water and the atmosphere is calculated explicitly for bromine, chlorine and iodine species. The effect of different meteorological background conditions and potential uncertainties regarding the source strength by direct degassing of halogen species or regarding the concentrations of halogens in the Dead Sea water itself is investigated in part II of this thesis.

After giving an introduction (Chapter 8) several model scenarios are presented, both excluding (Section 9.1) and including iodine chemistry (Section 9.3).

1.2   Halogen Chemistry

Halogen compounds are naturally released into the atmosphere over large parts of the globe, especially in polar and coastal regions as well as over the ocean. However, anthropogenically emitted chlorofluorocarbons (CFC's) finally directed scientific interest to halogens. Molina and Rowland (1974) were the first to point out the impact of CFC's within the process of stratospheric ozone destruction. A decade later, Farman et al. (1985) discovered the springtime Antarctic ozone hole that builds up annually in the stratosphere with varying extend. It is formed when the first sunlight of the year initialises photochemistry which is necessary to activate halogen chemistry.
CFC's are relatively unreactive under tropospheric conditions but get photolytically destroyed in the stratosphere leading to the formation of the radical Cl reacting with ozone and thus leading to its destruction:

$$
\begin{aligned}
CFC + h\nu & \longrightarrow Cl + CFC \\
2(Cl + O_3) & \longrightarrow 2(ClO + O_2) \\
ClO + ClO + M & \longrightarrow Cl_2O_2 + M \\
Cl_2O_2 + h\nu & \longrightarrow Cl + ClO_2 \\
ClO_2 + M & \longrightarrow Cl + O_2 \\
\hline
net : 2O_3 + h\nu & \longrightarrow 3O_2
\end{aligned}
\tag{1.1}
$$
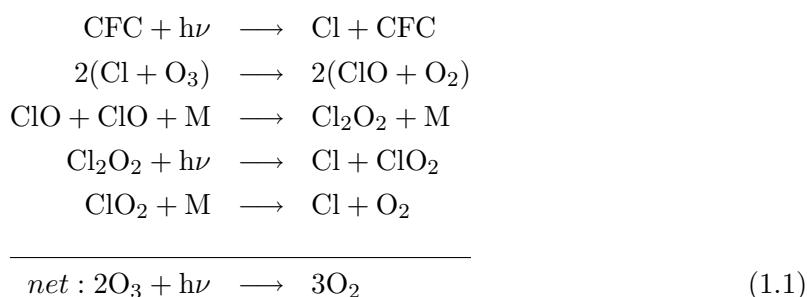
Within one catalytic cycle, two molecules of ozone are destroyed (Solomon, 1990). The formation of the dimer Cl_2O_2 by ClO self-reaction and its subsequent photolysis is a key step in the catalytic cycle. Even though this process was meant to be understood, recently published absorption cross sections of Cl_2O_2 by Pope et al. (2007) that would lead to a lower yield of ClO and lower O_3 loss rates than using values as in past years took this topic back into a scientific focus. However, those new measurements were doubted quickly by von Hobe et al. (2007).
Even though man made CFCs are by far the largest source for stratospheric chlorine, naturally or anthropogenically produced methyl chloride (CH_3Cl) also contributes to the chlorine budget. CH_3Cl can be broken up by reaction with OH (leading to the formation of reactive chlorine compounds) in the troposphere. However, as it has continuous sources, significant fractions can still reach the stratosphere. Methyl bromide (CH_3Br, naturally or anthropogenically emitted) is the major stratospheric bromine source. Bromine atoms have the potential to destroy ozone much more efficiently on equivalent reaction pathways like chlorine however, chlorine is much more abundant in the stratosphere.

Even more importance was assigned to halogen chemistry as scientists became aware that not only the stratosphere but also the troposphere can be affected by halogen - ozone interactions. Oltmans and Komhyr (1986) and Bottenheim et al. (1986) were the first who detected an almost complete destruction of ozone in the Arctic boundary layer. Tropospheric ozone depletion events (ODE's) affecting the whole boundary layer can last for several days and can affect thousands of square kilometres. During extreme events ozone

is even destroyed almost completely (Murayama et al., 1992; Solberg et al., 1996; Wessel et al., 1998; Jones et al., 2006). Barrie et al. (1988) and Barrie et al. (1989) were the first who suggested those ozone depletion events to be initiated by Br atom chain reaction. In the following years indications for a correlation between tropospheric ozone depletion events and bromine chemistry were found by several groups (Bottenheim et al., 1990; McConnell et al., 1992; Foster et al., 2001; Spicer et al., 2002). During periods of low O_3 mixing ratios, extraordinary large amounts of BrO (≈ 30 pmol/mol) were detected. Hausmann and Platt (1994) could measure BrO for the first time in the polar boundary layer using Differential Optical Absorption Spectroscopy (DOAS). These first measurements were confirmed by numerous field campaigns in the Arctic (Tuckermann et al., 1997; Martinez et al., 1999; Avallone et al., 2003; Hönninger et al., 2004b) as well as the Antarctic (Kreher et al., 1997; Frieß et al., 2004). Lehrer et al. (1997) also found a correlation between ozone depletion events and high concentrations of filterable bromine in aerosols collected at Spitsbergen. The large spacial extend of ODE's can be seen very well from satellite (Wagner and Platt, 1998; Richter et al., 1998; Wagner et al., 2001; Richter et al., 2002; Hollwedel et al., 2004). Even though ODE's are in general restricted to the boundary layer it might be possible that under certain meteorological conditions transport of significant amounts of BrO into the free troposphere might be possible (McElroy et al., 1999; Frieß et al., 2004).

Several years after the first observations of ozone depletion events in polar regions, Nagao et al. (1999) detected a decrease in O_3 mixing ratios at sunrise in the marine boundary layer (MBL). They suggest that this depletion event is also triggered by reactions of bromine with O_3.

The most important source for gas phase chlorine and bromine species in the marine troposphere are sea salt aerosols. When air bubbles burst at the ocean surface, formed for example by wave breaking, small as well as larger jet droplets - sea salt aerosols - are formed from the thin water film building the barrier between the air bubble and the atmosphere. If strong winds are blowing over the water surface even larger spray droplets can be formed. A detailed description of this process can be found in Pruppacher and Klett (1997). The chemical release mechanism of halogen species out of aerosol particles will be described in detail below (see Section 1.3).

Apart from degassing out of sea salt aerosols, halogens can be emitted directly from the ocean in the form of halocarbons formed by phytoplankton and algae. Bromocarbons were detected at several places and might be an important bromine source especially in coastal regions (Carpenter et al., 1999; Quack and Wallace, 2003). A model study done by Warwick et al. (2006) indicates that halocarbon emissions from tropical forests contribute much more to the global bromocarbon budget than emissions from the ocean. The contribution of bromocarbons, with methyl bromide being the most abundant bromocarbon, to total tropospheric bromine is not negligible and might be of importance especially for the upper part of the troposphere (Yang et al., 2005).

Even though more than 70% of the earth's surface is covered by saline waters from which sea salt aerosols are generated which are the most important bromine sources (together with the snowpack in polar regions and organo-halogens in coastal regions), only little is known about the global distribution of halogen compounds in general.

With regard to bromine and chlorine species, only very few data sets for the open ocean are available. Leser et al. (2003) report mean boundary layer BrO mixing ratios in the range of 1 - 3.6 pmol/mol based on their data collected on a ship cruise in the Atlantic off

West-Africa. Unexpectedly high nighttime Cl_2 mixing ratios were found at the coast of Long Island, New York with maximum values of up to 150 pmol/mol (Spicer et al., 1998). At the same site also Br_2 was detected (Foster et al., 2001; Spicer et al., 1998).
Mixing ratios of 38-268 pmol/mol of $HCl^\star$ ($HCl^\star = HCl$, $HOCl$, $ClNO_2$, $ClONO_2$) and $Cl^\star$ ($Cl^\star = Cl_2$, $HOCl$) mixing ratios of 26-245 pmol/mol were detected near Miami by Keene et al. (1993) and Pszenny et al. (1993) using a tandem mist chamber to sample chlorine gases. Using the same technique, $HCl^\star$ was detected in the range of 39-263 pmol/mol in Hawaii an $Cl^\star$ was in the range of 26-48 pmol/mol at the same site (Pszenny et al., 2004). On a ship cruise in the Atlantic, Keene et al. (2005) detected maximum $Cl^\star$ mixing ratios of up to 200 pmol/mol.
Indirect estimates for chlorine concentrations in the troposphere can be given as certain hydrocarbons are removed from the atmosphere via reactions with radicals like OH or Cl. The rates of these reactions differ by several orders of magnitude. Wingenter et al. (1996) give estimates for Cl concentrations in the North Atlantic of $3.3 \cdot 10^4$ - $6.5 \cdot 10^4$ atoms/cm^3. Cl concentrations in the same order of magnitude were estimated at the Christmas Islands (Wingenter et al., 2005, $8.4 \cdot 10^4$ - $5.7 \cdot 10^4$ atoms/cm^3). Furthermore, indirect estimates of summer and annual mean Cl concentrations ($6.5 \cdot 10^3$ atoms/cm^3 and $3.6 \cdot 10^3$ atoms/cm^3 respectively) are given by Allan et al. (2001b)
Even though organic precursor compounds are a minor source for gas phase chlorine and bromine in the marine boundary layer, they turned out to be one of the most important sources for gas phase iodine species. Several algae species emit iodocarbons like CH_3I, CH_2I_2, CH_2IBr or CH_2ICl. This process seems to be significant in coastal areas with strong tides (Carpenter et al., 1999, 2000; Peters et al., 2005). Certain types of algae, if present in coastal regions are apparently also able to directly inject molecular iodine into the atmosphere when exposed to air during low tide (Saiz-Lopez and Plane, 2004; Mc Figgans et al., 2004; Peters et al., 2005; Saiz-Lopez et al., 2006b). Indications also exist, that I_2 is emitted directly from open ocean waters as originally proposed by Garland and Curtis (1981). Iodine chemistry gained increasing attention within the last decade as I atoms can react with ozone in the same way as chlorine and bromine atoms do. Therefore iodine compounds take part in the halogen related ozone destruction process (Vogt et al., 1999a; Saiz-Lopez and Plane, 2004; McFiggans et al., 2000). The contribution of iodine chemistry to ozone depletion events was found to be of potential significance especially in Antarctica (Saiz-Lopez et al., 2007b,c). Furthermore, it was shown by several laboratory studies that iodine compounds are able to form new particles (Hoffmann et al., 2001; Jimenez et al., 2003; Burkholder et al., 2004) which can act as reaction surfaces especially in the coastal marine boundary layer and might potentially grow to become cloud condensation nuclei. Several measurements and model studies deal with the question how efficient this process is, how often it occurs and whether it is more a local phenomenon or whether it is of global importance.
O'Dowd et al. (2002) could show in a smog-chamber experiment that new particles can be formed from condensable iodine vapours that are formed by photolysis of iodocarbons. O'Dowd et al. (2002) suggest that concentrations of condensable iodine vapours in the marine boundary layer are sufficient to influence marine particle formation. However, Mc Figgans et al. (2004) found that molecular iodine which is released directly from algae is most likely the dominant precursor species for new particle formation. They further state out, that more research is needed to understand under which conditions iodine vapours form new particles in competition with condensational growth of iodine compounds on already existing particles. The importance of the role of I_2 in the process of new parti-

cle formation, at least in coastal regions, was confirmed by Saiz-Lopez et al. (2006b) who present in-situ measurements of I_2 and ultra-fine aerosol. Saiz-Lopez et al. (2006b) further investigated the particle formation process via iodine vapours in a numerical model. They came to the conclusion that particles formed by this process can grow to a significant size and make an important contribution to the total number of condensation nuclei at least on a regional scale. Pechtl et al. (2006) performed model studies with focus on the role of homomolecular homogeneous OIO nucleation. They found that in general OIO is more important for the growth of newly formed particles than for the formation of new nuclei.

The majority of halogen measurements refer to halogen oxides detected in coastal regions. One site, that has probably the highest data coverage is Mace Head, at the Irish west coast. Apart from gaining information about bromine oxide concentrations which reach maximum values of 6 pmol/mol at Mace Head (Saiz-Lopez et al., 2004), numerous measurements concentrate on the detection of iodine species. Iodine oxide (IO) was detected in Mace Head by several groups, with maximum mixing ratios of 7 pmol/mol (Alicke et al., 1999; Saiz-Lopez et al., 2004; Peters et al., 2005; Allan et al., 2001a). Furthermore the oxygenated iodine compound OIO could be detected (Saiz-Lopez et al., 2004; Allan et al., 2001a) during night time with mixing ratios of up to 10 pmol/mol (Saiz-Lopez et al., 2006a). In contrast to the measurements at Mace Head where OIO was only detected during night time, Stutz et al. (2007) detected OIO also at daytime in the Gulf of Maine. At the same site IO was detected during day time with mixing ratios of 4 pmol/mol. The measurements taken at the Gulf of Maine reveal the question how complete our present understanding of iodine reaction pathways really is.
Iodine Oxide was detected at several other coastal sites like Tasmania (Allan et al., 2000, IO_{max}: 2.2 pmol/mol), Tenerife (Allan et al., 2000, IO_{max}: 3.5 pmol/mol), Kerguelen, an island in the Indian Ocean (Hönninger and Platt, 2002, IO_{max}: 9.8 pmol/mol) as well as at the North Sea coast in Germany (Peters et al., 2005, IO_{max}: 2.1 pmol/mol) and at the French Atlantic coast (Peters et al., 2005, IO_{max}: 7.7 pmol/mol).
Iodine Oxide mixing ratios in the Antarctic even exceed those detected in coastal regions (Frieß et al., 2001; Saiz-Lopez et al., 2007c). Saiz-Lopez et al. (2007c) report maximum IO mixing ratios in polar spring of up to 20 pmol/mol. Apparently, IO is distributed homogeneously within the polar boundary layer as can be concluded from satellite data recently presented by two groups (Saiz-Lopez et al., 2007a; Schönhardt et al., 2008) whereas a numerical model shows a strong vertical gradient in IO mixing ratios. Saiz-Lopez et al. (2007c) suggest that potentially the photolysis of higher iodine oxides provide a missing IO source. If Saiz-Lopez et al. (2007c) include this process in their model, IO is distributed more homogeneously in the boundary layer. However, photolysis rates of higher iodine oxides are unknown.
In contrast to mid-latitudinal coastal regions where air-exposed algae is assumed to be the strongest source for gas-phase iodine compounds, phytoplankton which colonises the underside of sea ice produces iodocarbons such as CH_2I_2, CH_2IBr in polar regions. Those species then provide a source of inorganic iodine in the boundary layer (Saiz-Lopez et al., 2007b). Furthermore, Saiz-Lopez and Boxe (2008) propose a new release mechanism for iodine from the sea-ice surface via the biological production of iodide and hypoiodous acid from marine algae.
Regarding iodine chemistry, a lot of open questions remain. Apart from the uncertainties regarding new particle formation and reactions involving (higher) iodine oxides, one uncertainty is related to aqueous phase iodine chemistry. Numerical models predict an

accumulation of iodate within aerosol particle (Pechtl et al. (2007) and references therein) whereas measurements do not show this phenomenon (Baker, 2004, 2005; Gilfedder et al., 2007). However, Pechtl et al. (2007) could reduce the accumulation of IO_3^- in their model by using a new aqueous phase iodine mechanism.

Apart from providing a potentially very efficient ozone sink, halogens can influence the oxidation capacity of the atmosphere via several additional reaction pathways.
Halogen Oxides can react with HO_2 ($BrO + HO_2 \longrightarrow HOBr + O_2$) to form hypohalous acids which can either get photolysed ($HOX + h\nu \longrightarrow X + OH$) or which are taken up by aerosol particles. This reaction pathway can lead to a shift of the $[HO_2]/[OH]$ ratio if the loss of HO_2 via halogen oxide reaction is large compared to other loss processes. If the uptake of HOX is more efficient than photolysis, gas phase HO_2 is lost increasing the shift in $[HO_2]/[OH]$. It is most likely that such a shift mainly occurs only in clean air masses (Bloss et al., 2005).
In the presence of high NO_x ($NO + NO_2$) concentrations, halogen oxides can further react with NO

$$XO + NO \longrightarrow X + NO_2. \tag{1.2}$$

As this reaction converts NO into NO_2, reactions between halogen oxides and NO can lead to a shift in the $[NO]/[NO_2]$ ratio. Halogen oxides can further react with NO_2 which leads to the formation of halogen nitrates

$$XO + NO_2 \overset{M}{\rightleftharpoons} XONO_2. \tag{1.3}$$

Halogen Nitrates can photolyse, decompose thermally or react with water on particle surfaces.
Furthermore, halogen compounds can influence the tropospheric sulfur cycle. DMS (dimethyl sulphate) that gets emitted out of the ocean is the most important sulphate source in the marine boundary layer. DMS gets mainly oxidised to SO_2 which is the most important precursor species for sulphate aerosols in the MBL. In the presence of halogens, DMS can react efficiently with BrO which leads to a decreased SO_2 formation (von Glasow and Crutzen, 2004).
Apart from oceanic sources, halogens can be also produced by other natural as well as anthropogenic pathways. Bobrowski et al. (2003) were the first to detected BrO in plumes of passively degassing volcanos. Other measurements followed to confirm that discovery (Lee et al., 2005; Oppenheimer et al., 2006; Bobrowski et al., 2007). Bromine oxide, chlorine oxide as well as iodine oxide were also measured over Salt Lakes, however this aspect of halogen chemistry will be discussed in great detail in Part II of this thesis. Bromocarbons are further emitted from salt marshes as reported by Bill et al. (2002) and Rhew et al. (2002).
A recent review by von Glasow and Crutzen (2007) gives a detailed overview of tropospheric halogen chemistry based on our current understanding.

1.3 Halogen Reaction Mechanism

As was mentioned above, the most important source for gas phase chlorine and bromine compounds in the troposphere are sea salt aerosols. In this section a short description of the most important reactions being responsible for the cycling of bromine and chlorine
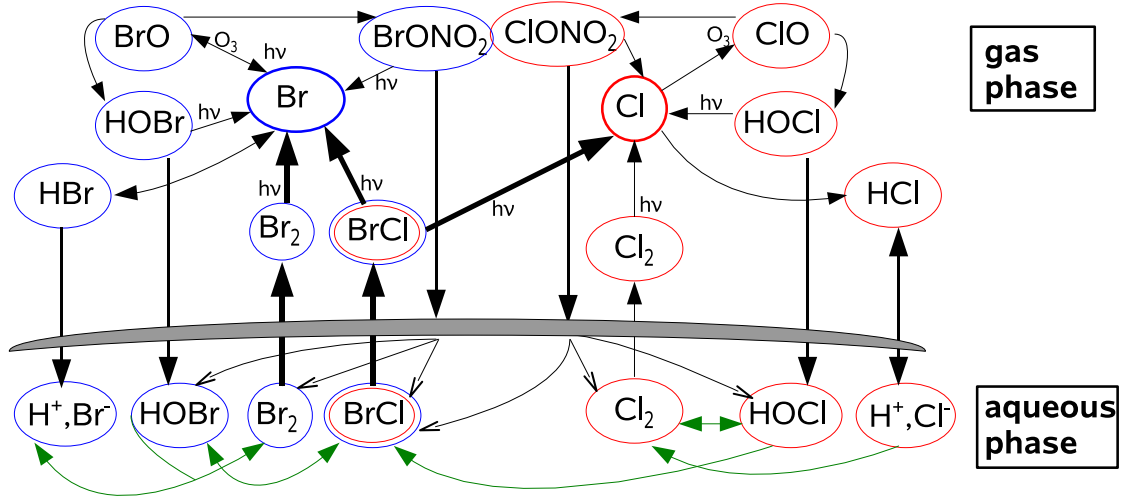
Figure 1.1: Bromine and chlorine cycling between aerosol phase and gas phase.

species between the gas phase and the aerosol phase is given. Several pathways for the release of halogens from salt particles and the recycling on particles are known and are described in the following.

Fan and Jacob (1992) suggested an autocatalytic conversion of Br^- into Br_2:

$$
\begin{align}
HOBr_{(g)} &\longrightarrow HOBr_{(aq)} \tag{1.4} \\
HOBr_{(aq)} + Br^- + H^+ &\longleftrightarrow H_2O + Br_{2(aq)} \tag{1.5} \\
Br_{2(aq)} &\longrightarrow Br_{2(g)} \tag{1.6} \\
Br_{2(g)} + h\nu &\longrightarrow 2Br \tag{1.7} \\
2(Br + O_3 &\longrightarrow BrO + O_3) \tag{1.8} \\
2(BrO + HO_2 &\longrightarrow HOBr_{(g)} + O_2) \tag{1.9} \\
2\,HOBr_{(g)} &\longrightarrow 2HOBr_{(aq)} \tag{1.10}
\end{align}
$$

$$\textbf{Cycle I } net : 2\,O_3 + 2\,HO_2 + 2\,Br^- + 2\,H^+ \longrightarrow Br_2 + 4\,O_2 + 2\,H_2O \tag{1.11}$$
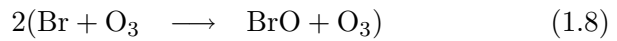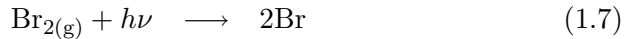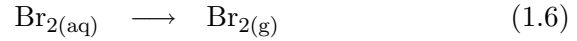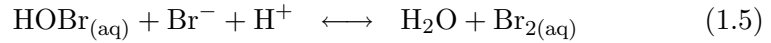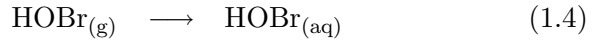
Hypobromous acid (HOBr) which is highly soluble, is taken up into sea salt particles from the gas phase. It undergoes reaction with bromide and H^+ producing water and $Br_{2(aq)}$ (Reaction 1.5). Br_2 is only slightly soluble and degasses quickly out of the aerosol (Reaction 1.6). During day time, gas phase Br_2 gets rapidly photolysed to form bromine atoms (Reaction 1.7) which then can react with O_3 leading to the formation of bromine oxide (Reaction 1.8). If sufficient bromine is available in the atmosphere this reaction can efficiently destroy O_3. BrO can react with HO_2 which leads to the production of $HOBr_{(g)}$ (Reaction 1.9) that is mainly taken up into sea salt particles due to its high solubility (Reaction 1.10) and can again take part in aqueous phase reactions. If bromide concentrations within the aqueous phase are large enough and the bromine loss process in the gas phase is not too large, cycle I (see Reaction 1.11 and Fig. 1.1) leads to an exponential release of bromine. As this process intensifies itself, it was given the name *bromine explosion* (Platt and Janssen, 1995).

Vogt et al. (1996a) introduced a similar reaction pathway via the conversion of Br^- into

$BrCl_{(aq)}$.

$$
\begin{array}{rcll}
HOBr_{(g)} & \longrightarrow & HOBr_{(aq)} & (1.12) \\
HOBr_{(aq)} + Cl^- + H^+ & \longleftrightarrow & H_2O + BrCl_{(aq)} & (1.13) \\
BrCl_{(aq)} & \longrightarrow & BrCl_{(g)} & (1.14) \\
BrCl_{(g)} + h\nu & \longrightarrow & Br + Cl & (1.15) \\
Br + O_3 & \longrightarrow & BrO + O_3 & (1.16) \\
BrO + HO_2 & \longrightarrow & HOBr_{(g)} + O_2 & (1.17) \\
HOBr_{(g)} & \longrightarrow & HOBr_{(aq)} & (1.18)
\end{array}
$$

$$
\textbf{Cycle II } net : O_3 + HO_2 + Br^- + H^+ \longrightarrow Cl + 2O_2 + H_2O \quad (1.19)
$$
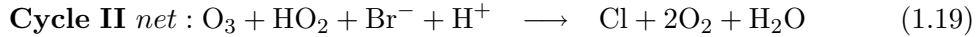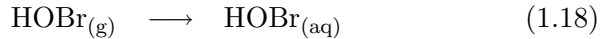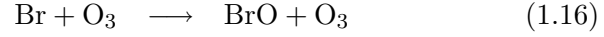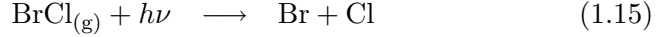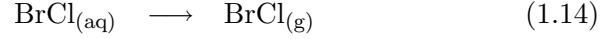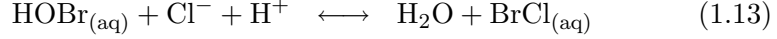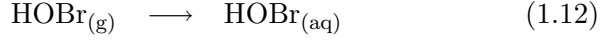
Instead of reaction with H^+ and Br^-, $HOBr_{(aq)}$ can further undergo reaction with H^+ and Cl^- (Reaction 1.13) leading to the formation of $BrCl_{(aq)}$ which is also released into the gas phase (Reaction 1.14). Upon photolysis $BrCl_{(g)}$ gets decomposed into one bromine and one chlorine atom (Reaction 1.15). The bromine atom follows mainly the same reaction pathway as in cycle I as described above, i.e. reaction with O_3 and formation of BrO which can further react to form $HOBr_{(g)}$ (Reactions 1.16 - 1.18 are equivalent to Reactions 1.8 - 1.10).

The chlorine atom can undergo an equivalent reaction path as the bromine atom (see Figure 1.1). However, those reactions are much slower and less effective for chlorine compounds. Even though aqueous phase Cl_2 is formed by a similar reaction as $Br_{2(aq)}$ and gets photolysed in the gas phase to form 2 Cl atoms, this reaction is only a minor contribution to total gas phase chlorine. The most important source for gas phase chlorine is the release of hydrochloric acid (HCl) out of aerosol particles due to acid displacement. When very strong and highly soluble acids (like H_2SO_4 or HNO_3) are taken up into particles and Cl^- concentrations are sufficiently large ($HCl \rightleftharpoons Cl^- + H^+$), HCl degasses out of aerosol particles. As HBr has a much higher effective solubility compared to HCl it is not affected by acid displacement.

In contrast to gas phase bromine chemistry, where mainly reactive species are formed (Br_2, BrO), the dominantly produced gas phase chlorine species are unreactive (like HCl). The main sink reaction for (reactive) chlorine is reaction with hydrocarbons (mainly $Cl+RH\longrightarrow HCl+R$) leading also to the formation of the hardly reactive hydrochloric acid. Furthermore, it has to be mentioned that aqueous phase chlorine and bromine chemistry are strongly linked via interhalogen equilibria. Reaction cycles I (see Reaction 1.11) and II (see Reaction 1.19) lead to the formation of $Br_{2(aq)}$ and $BrCl_{(aq)}$ respectively. However, the formation of $Br_{2(aq)}$ might proceed via an intermediate step (Vogt et al., 1996a):

$$
\begin{array}{rcll}
HOBr + Cl^- + H^+ & \longleftrightarrow & H_2O + BrCl_{(aq)} & (1.20) \\
BrCl_{(aq)} + Br^- & \longleftrightarrow & Br_2Cl^- & (1.21) \\
Br_2Cl^- & \longrightarrow & Br_{2(aq)} + Cl^- & (1.22) \\
Br_{2(aq)} & \longrightarrow & Br_{2(g)} & (1.23)
\end{array}
$$
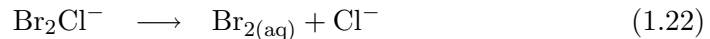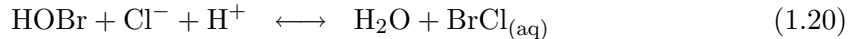
The above explained cycles I and II lead to a quick destruction of gas phase O_3. The aqueous phase BrCl to Br_2 yield, i.e. whether reaction cycle I or II is more efficient depends on the Cl^- to Br^- ratio within the particle (Fickert et al., 1999). Further the amount of outgassing BrCl and Br_2 is strongly pH dependant (Keene et al., 1998). Both reaction

cycles - I and II - only play a role in aerosols that are at least slightly acidified (pH < 6.5) and become more important with decreasing pH values. However, the acid displacement process (release of HCl out of aerosols) requires stronger acidified aerosols to be highly effective thus reactive bromine species are in general released more easily into the gas phase than reactive chlorine species in the MBL.

In Section 1.2 it was mentioned that in areas where sufficient NO_x concentrations are available, BrO (and ClO) can react with NO as well as with NO_2. The product $BrONO_2$ is either decomposed photolytically (to Br and NO_3) or can react heterogeneously on aerosol surfaces. A product of this heterogeneous reaction is aqueous phase HOBr, the important precursor of reactive bromine compounds. Again, the same reaction mechanism takes also place for chlorine compounds but less effective. As the small sulphate particles (in terms of the model terminology particles with a dry radius smaller than $0.5\,\mu$m, see Section 2.4.2) account for the largest fraction of total particles, their total surface area is large compared to the total surface area of the bigger but fewer sea salt particles (in terms of the model terminology particles with a dry radius larger than $0.5\,\mu$m). Thus the heterogeneous decomposition of $BrONO_2$ is especially efficient on the small (mainly) sulphate particles as the overall uptake is much faster than on larger particles (mainly sea salt) (Sander et al., 1999; von Glasow et al., 2002a, the differing uptake properties will be discussed later in more detail). Even though sea salt (large) aerosols are the most important primary sources for halogens in the MBL, sulphate (small) aerosols provide a surface for uptake and aqueous phase recycling of halogen species.

Under atmospheric conditions yielding to very high bromine oxide mixing ratios, the self reaction of BrO ($BrO+BrO\longrightarrow 2Br+O_2$) which increases the ozone destruction rate by bromine chemistry gains in importance. If both halogen compounds (bromine and chlorine) are abundant, the reaction between BrO and ClO, which is much faster than the BrO self reaction might play a role in the halogen gas phase cycling as the reaction leads to the reactive species BrCl.

In general, nearly all of the above described reaction mechanisms (as shown in Figure 1.1) for chlorine and bromine are also valid for iodine compounds (see Fig.1.2). However, some important differences in the iodine release and recycling require an additional explanation as well as uncertainties in the iodine reaction mechanism:

Measurements indicate, that aerosol particles are rather a sink for iodine species than a source (like for bromine and chlorine). As was already mentioned above in Section 1.2, a discrepancy exists between model simulations which predict an accumulation of IO_3^- in the aerosol phase (Pechtl et al., 2007, and references therein). Such a trend cannot be observed this clearly in field measurements which sometimes show non-negligible I^- concentrations in aerosol particles and not such a strong accumulation of iodate like predicted in numerical models (Baker, 2004, 2005; Gilfedder et al., 2007). The lack of knowledge of aqueous phase iodine reaction pathways and accurate reaction rate coefficients leads to an uncertainty in the calculation of the recycling potential of aerosol particles with regard to iodine compounds.

As was mentioned above, the most important iodine sources are biogenic alkyl iodides as well as the direct release of molecular iodine I_2 by various phytoplankton species and algae. Gas phase iodocarbons are photolysed to from I atoms which can react with O_3 on equivalent reaction paths like bromine atoms ($I+O_3\longrightarrow IO+O_2$). However, in contrast to tropospheric bromine and chlorine chemistry, the self reaction of IO leading to the formation of OIO is supposed to be of major importance for the formation of new particles from iodine vapours. OIO can act either as a precursor species for higher iodine oxides (e.g.
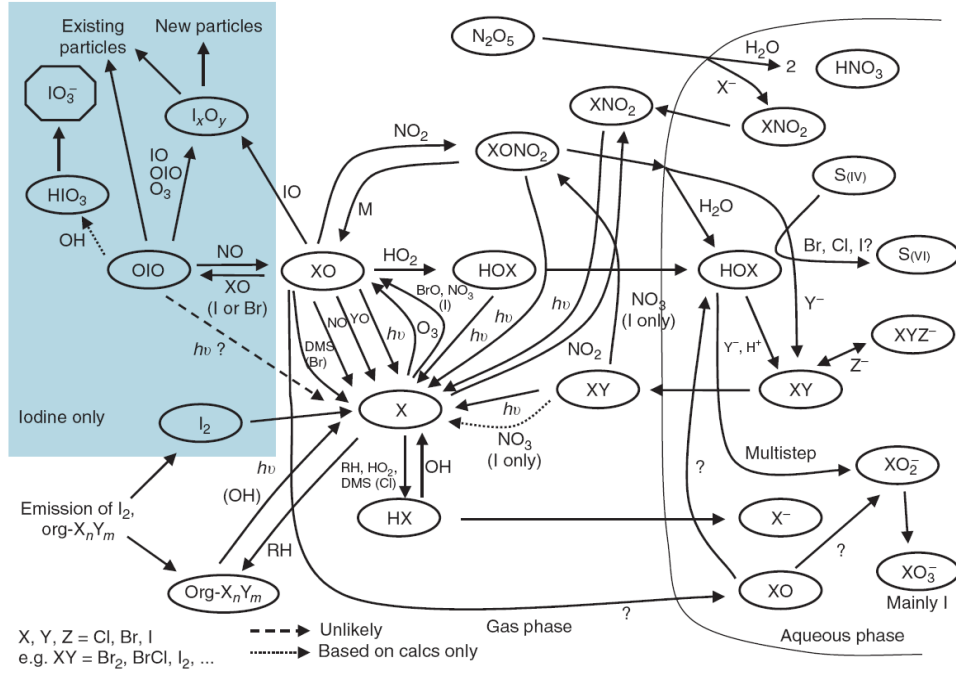
Figure 1.2: Schematic overview of the major halogen-related reactions in the gas and aqueous phase. The shaded area indicates reactions that are of importance only for iodine. This plot is taken from von Glasow and Crutzen (2007)

I_2O_5) which are assumed to take part in cluster formation leading to the formation of new particles. Or OIO can condense on existing particles enhancing their growth potential. Furthermore, it is still not ruled out that OIO photolyses and forms potentially I and O_2 (Ashworth et al., 2002). However, the exact mechanism and the role of iodine in particle formation still remains unclear with a lot of question marks related to I_xO_y reactions and under which ambient conditions particle formation via iodine vapours is facilitated. An overview of the most important iodine reactions as included in the model MISTRA is given in Figure 1.2.

Chapter 2

Model description

The one dimensional numerical model MISTRA was once designed to study microphysical processes in marine stratus clouds in the cloud topped planetary boundary layer. The original model version developed by Bott et al. (1996) calculated atmospheric radiation with a δ-two-stream approximation and turbulence is parameterised by means of a 1.5-order, turbulent kinetic energy (TKE) closure based on the level 2.5 model of Mellor and Yamada (1982). In recent years the model was extended by a chemistry scheme describing reactions in the gas phase, the aerosol phase and cloud droplets (von Glasow et al., 2002a,b). Latest model developments focused on iodine chemistry in the gas phase as well as in aerosol particles (Pechtl et al., 2007). Pechtl et al. (2006) implemented a two-step nucleation parameterisation into the model to study the role of iodine in the formation of new particles. To study chemical processes in polar regions, Piot and von Glasow (2007) developed a polar version of MISTRA.

2.1 Numerical Setup

Within the standard model version as it is used in part I of this thesis, the atmosphere is divided into 100 equidistant layers reaching an altitude of 1000 m. Each layer has a height of 10 meters except for the lowest model level which is infinitesimally thin and which is only used to calculate exchanges between the surface and the overlaying atmosphere. Above an altitude of 1000 m the model grid is spaced logarithmically up to an altitude of 2000 m.
The model timestep for updating meteorological parameters such as temperature, humidity and the particle size distribution is 10 s and for updating photolysis rates it is 2 min.
For calculating atmospheric chemistry, all chemical reactions in the gas phase, in the aerosol phase as well as aqueous phase equilibria and phase transfer reactions are treated as a set of coupled differential equations. The kinetic preprocessor (KPP) is a software tool used for simulating the chemical system in a computational efficient and user-friendly way as it allows rapid changes in the chemistry scheme (Damian et al., 2002). For integrating the stiff system of ordinary differential equations describing the set of chemical reactions, a Rosenbrock third-order-solver (ROS3) using adjusted timesteps is used (Sandu et al., 1997). The timestep for this procedure is chosen automatically and can vary between 10^{-10} s for conditions of low liquid water content in aerosol particles or cloud drops and 10 s if only gas phase reactions are calculated.

2.2   Meteorology

The set of prognostic equations for the horizontal components of the wind speed (u,v), the specific humidity (q) and the potential temperature (θ) is given by:

$$\frac{\partial u}{\partial t} = -w\frac{\partial u}{\partial z} - \frac{\partial}{\partial z}K_m\frac{\partial u}{\partial z} + f(v - v_g) \tag{2.1}$$

$$\frac{\partial v}{\partial t} = -w\frac{\partial v}{\partial z} - \frac{\partial}{\partial z}K_m\frac{\partial v}{\partial z} + f(u - u_g) \tag{2.2}$$

$$\frac{\partial q}{\partial t} = -w\frac{\partial q}{\partial z} - \frac{\partial}{\partial z}K_h\frac{\partial q}{\partial z} + \frac{C}{\rho} \tag{2.3}$$

$$\frac{\partial \theta}{\partial t} = -w\frac{\partial \theta}{\partial z} - \frac{\partial}{\partial z}K_h\frac{\partial \theta}{\partial z} - \left(\frac{p_0}{p}\right)^{R/c_p}\frac{1}{c_p\rho}\left(\frac{\partial E_r}{\partial z} + l_{12}C\right) \tag{2.4}$$

where f is the Coriolis parameter, u_g and v_g are the geostrophic wind components, K_m and K_h are the turbulent exchange coefficients for momentum and heat, l_{12} is the latent heat of condensation, C is the condensation rate which is determined diagnostically from the below explained particle growth equation, E_r is the net radiative flux density, ρ the density of the air, p the air pressure, p_0 the air pressure at the surface, R the gas constant for dry air, c_p the specific heat of dry air at constant pressure.

The first term on the right hand side in Equations 2.1 - 2.4 describes large scale subsidence. Regarding the general assumptions for the model setup, the vertical component of the wind speed (w) should vanish everywhere in order to conserve the total mass of the system. However, large scale subsidence is essential to control the observed quasi-steady structure of a marine stratiform cloud (Bott et al. (1996) and references therein). The second term on the right hand side in Equations 2.1 - 2.4 describes the turbulent vertical transport of the quantities u, v, q, θ. The last term on the right side in Equations 2.1 - 2.2 describes the coriolis force whereas the last term on the right side in Equation 2.4 stands for changed in the temperature (θ) due to radiation as well as condensation. As already stated out above, turbulence is treated with the 2.5 Mellor and Yamada (1982) model with modifications e.g. for the mixing length (l) as described in Bott et al. (1996). The following prognostic equation for the TKE $e = (\overline{u'u'} + \overline{v'v'} + \overline{w'w'})/2$ is solved:

$$\frac{\partial e}{\partial t} = -w\frac{\partial e}{\partial z} - \frac{\partial}{\partial z}\left(\overline{e'w'}\right) + \frac{(2e)^{3/2}}{l}(S_mG_m + S_hG_h - \epsilon) \tag{2.5}$$

with ϵ=1/16.1 describing the dissipation of TKE. The first term on the right hand side of the equation describes again subsidence, the second term vertical mixing, S_mG_m and S_hG_h are dimensionless shear and buoyancy production terms. The turbulent exchange coefficients K_h and K_m are determined in dependency on S_hG_h and S_mG_m as explained in detail in Bott et al. (1996).

2.3   Microphysics

Microphysics is treated using a two-dimensional particle size distribution $f(a,r)$ depending on the dry radius (a) and the total radius (r) of the aerosol. The dry radius a is the radius of a particle it had without any water being present. The total radius r of a particle is the radius a particle has that has a dry radius a and contains a certain amount of water contributing to the total size of a particle. The two-dimensional particle grid as shown

schematically in Figure 2.1 is divided into 70 by 70 logarithmically equidistant spaced size classes. Under cloud free conditions, the minimum dry radius is chosen to be 0.01 μm and the maximum dry radius is 15 μm. The associated total radii range from 0.01 μm to 60 μm.

Upon model initialisation particles contain a water coating according to the equilibrium radius of the dry nucleus at the ambient relative humidity. Particle growth due to diffusion including radiation effects is calculated following the approach by Davies (1985) and Pruppacher and Klett (1997):

$$r\frac{dr}{dt} = \frac{1}{C_1}\left(C_2\left(\frac{S_a}{S_r} - 1\right) - \frac{F_r(a,r) - m_w(a,r)c_w\frac{dT}{dt}}{4\pi r}\right) \tag{2.6}$$

The coefficients C_1 and C_2 are defined as follows:

$$C_1 = \rho_w l_{21} + \frac{\rho_w C_2}{D_v^\star S_r \rho_s} \qquad C_2 = kT\left(\frac{l_{21}}{R_v T} - 1\right)^{-1} \tag{2.7}$$

The parameter $m_w(a,r)$ stands for the liquid water mass of a particle, c_w is the specific heat of water and ρ_w the density of water, ρ_s the saturation vapour density, R_v the gas constant for water vapour, k is the thermal conductivity, l_{21} is the latent heat of evaporation, $F_r(a,r)$ is the net flux of radiation absorbed by an individual droplet with dry radius a and wet radius r. This flux is explicitly calculated with the δ-two-stream approximation and thus the feedbacks between radiation and particle growth can be considered. $D_v^\star$ is the diffusivity of air corrected for gas kinetic effects and calculated after Pruppacher and Klett (1997):

$$D_v^\star = \frac{D_v}{\zeta} \tag{2.8}$$

$$D_v = 0.211\left(\frac{T}{T_0}\right)^{0.194}\left(\frac{p}{p_0}\right) \tag{2.9}$$

$$\zeta = \frac{a}{a+\Delta} + \frac{D_v}{a\alpha_c}\left(\frac{2\pi M_w}{RT}\right)^{1/2} \tag{2.10}$$

M_w is the molecular weight of water, T and p the atmospheric temperature and pressure, T_0= 273.15 K, p_0=1013.25 hpa, a is the dry radius of a particle. The equation calculating diffusional growth was derived under the assumption that the water vapour pressure is homogeneously distributed around a particle. However, this assumption is not valid anymore directly at the particle surface where the water vapour pressure is much larger than in the ambient air. The simple assumption of homogenous water vapour pressure around a particle is roughly valid up to a distance from the droplet called the vapour jump length Δ. Thus the corrections for gas kinetic effects are included in the above written equation. The mass accommodation coefficient for water vapour α_c=0.036 describes the probability that a gas after diffusing to the particle surface really sticks to the surface. The parameters S_a and S_r stand for the ambient saturation ratio and the saturation ratio required for equilibrium at the particle's surface respectively. The latter one is calculated via the Köhler equation:

$$S_r = exp\left(\frac{A}{r} - \frac{B}{r^3}\right) \tag{2.11}$$

with the parameters A (Kelvin/Curvature term) and B (Raoult/Solution term) given by:

$$A = \frac{2M_w\sigma_w}{RT\rho_w} \qquad B = \frac{3\nu m_s M_w}{4\pi M_s \rho_w} \qquad (2.12)$$

and the parameters stand for: M_w is the molecular weight of water, M_s is the molecular weight of the solute, m_w is the mass of water and m_s the mass of the solute, ν is the number of ions that one salt molecule dissociates into, σ is the surface tension and r the total particle radius.

The equilibrium saturation ratio (S_r) over a particle varies with the radius of the particle. The radius at which the equilibrium saturation ratio is maximum (= critical saturation ratio, S_c) is called the critical radius (r_c). If particles have a radius exceeding their critical radius, these particles are called 'activated'.

2.4   Chemistry

2.4.1   Gas phase chemistry

Chemical reactions in the current version of MISTRA can be explicitly treated in the gas phase as well as within aerosol particles. Heterogeneous reactions as well as phase transfer reactions are also calculated explicitly. The prognostic equation for the concentration of a gas phase chemical species c_g (in mol/m$^3_{air}$) as implemented in the model includes turbulent exchange, deposition on the ocean surface (D_{dep}), chemical production (P) and
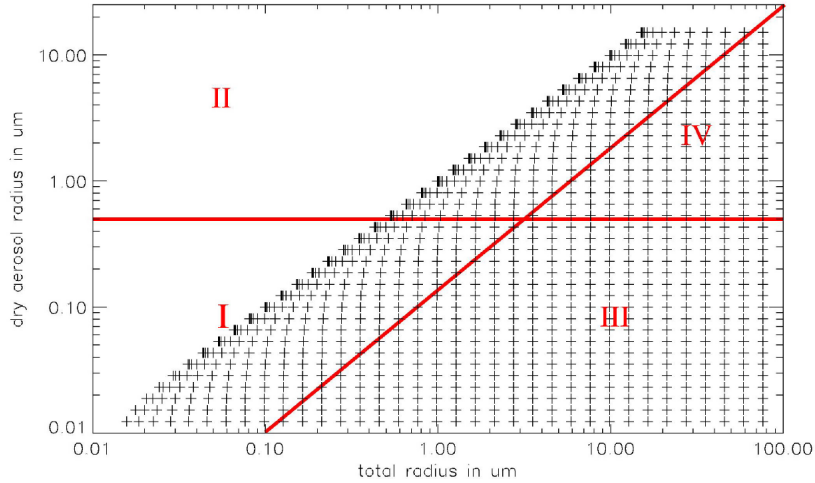
Figure 2.1: Two-dimensional particle spectrum as a function of the dry aerosol radius (a) and the total (=wet) particle radius (r). Added are the chemical bins. I: Sulphate aerosol bin, II: Sea salt aerosol bin, III: Sulphate cloud droplet bin, IV: Sea salt cloud droplet bin. For simplicity a 35x35 grid is plotted whereas in the model 70x70 bins are used.

destruction (L), emission (E) and exchange with the aqueous phase:

$$\frac{\partial c_g}{\partial t} = \frac{\partial}{\partial z}\left(K_h\rho\frac{\partial c_g/\rho}{\partial z}\right) - D_{dep} + P - Lc_g$$

$$+E - \sum_{i=1}^{n_{kc}} \overline{k_{t,i}}\left(LWC_i c_g - \frac{c_{a,i}}{k_H^{cc}}\right) \tag{2.13}$$

where k_H^{cc} is the dimensionless Henry constant obtained by $k_H^{cc} = k_H RT$ (k_H is in mol/ (m^{3}Pa)), LWC_i and $c_{a,i}$ are the dimensionless liquid water content (in m$^3_{aq}$/m$^3_{air}$) and aqueous phase concentration of the aerosol size class i (in mol/m$^3_{air}$), n_{kc} is the number of aqueous classes and $k_{t,i}$ is the mass transfer coefficient. The treatment of heterogeneous reactions in the model and the meaning of the mass transfer coefficient is explained in detail below in Section 4.1.

2.4.2   Aqueous phase chemistry

Aqueous phase chemistry is treated in only four different size classes in the model as it would be very time consuming to calculate aerosol/droplet phase chemistry in each of the 70 x 70 microphysical bins. Thus the grid is subdivided into four size classes as it is shown in Figure 2.1. The size of particles in bin I ranges from 0.01 - 0.5 μm (with respect to the dry radius) and the size of those particles being present in bin II ranges from 0.5 - 15 μm (again with respect to the dry radius). Particles in bin I are referred to as sulphate aerosols and particles in bin II as sea salt aerosols indicating also the different initial chemical composition of the particles in those two size classes. However, during model integration several processes alter the chemical composition and size of the aerosol particles so that they can grow into the size range of bin II from bin I (or shrink from bin II into the size range of bin I).
When water uptake onto the aerosol let the total radius increase strong enough that it exceeds the dry radius by a factor of ten, roughly corresponding to the equilibrium radius of the aerosol as calculated by the Köhler equation, particles are treated as cloud droplets and are moved into the size classes III (referred to as sulphate droplets) and IV (referred to as sea salt droplets). Again particles can be shifted between the different bins due to growth/shrinking processes. For calculating chemistry in the aqueous phase a mean radius for each of the four bins is calculated every timestep. Thus chemistry is calculated in aerosol particles/droplets with mean properties calculated from all particles being present in the corresponding bin. In each of the four size classes the following prognostic equation for the concentration $c_{a,i}$ (in mol/m$^3_{air}$) of each chemical species is solved:

$$\frac{\partial c_{a,i}}{\partial t} = -w\frac{\partial c_{a,i}}{\partial z} + \frac{\partial}{\partial z}\left(K_h\rho\frac{\partial c_{a,i}/\rho}{\partial z}\right) - D_{dep} + P - Lc_{a,i}$$

$$+E + P_{pc} + \overline{k_{t,i}}\left(LWC_{l,i} c_{a,i} - \frac{c_{a,i}}{k_H^{cc}}\right) \tag{2.14}$$

The term P_{pc} accounts for the transport of chemical species from the aerosol to the cloud droplet regime and vice versa. All other variables have equivalent meanings as given above for the prognostic equation for gas phase concentrations.

2.4.3 Photolysis

Photolysis frequencies are calculated online using the method of Landgraf and Crutzen (1998). The following integral

$$J_x = \int_I \sigma_x(\lambda_w)\Phi_x(\lambda_w)F_{act}(\lambda_w)d\lambda_w \tag{2.15}$$

calculates the photolysis frequency J_x for a species x from the spectral actinic flux $F_{act}(\lambda_w)$ (λ_w is the wavelength, σ_x the absorption cross section, Φ_x the quantum yield, I is the photochemically active spectral interval). For computational efficiency reasons Landgraf and Crutzen (1998) suggest a method using only 8 spectral bins:

$$J_x = \sum_{i=1}^{8} J_{i,x}^a \cdot \delta_i \tag{2.16}$$

where $J_{i,x}^a$ is the photolysis rate for a purely absorbing atmosphere. The factor δ_i

$$\delta_i = \frac{F_{act}(\lambda_{w,i})}{F^a(\lambda_{w,i})} \tag{2.17}$$

describes the effect of scattering by air molecules, aerosol and cloud particles, which is significant in the spectral range $202.0\,\text{nm} < \lambda_w < 752.5\,\text{nm}$. $F^a(\lambda_{w,i})$ is the actinic flux of a purely absorbing atmosphere. The rates $J_{i,x}^i$ are precalculated with a fine spectral resolution and are approximated during runtime from lookup tables or by using polynomials. For a more detailed description of the calculation of photolysis rates see Landgraf and Crutzen (1998) or von Glasow et al. (2002a).

2.4.4 Deposition and Emission

The emission of sea salt particles from the ocean by bubble bursting at low wind speeds is calculated using the parameterisation by Monahan et al. (1986). The following equation describes the flux F (in particles/(m^2 s μm)) of particles with a radius r at a relative humidity of $80\,\%$ per unit area of sea surface and per increment of particle radius and time:

$$\frac{dF}{dr} = 1.373\,u_{10}^{3.41}r^{-3}(1 + 0.057 \cdot r^{1.05}) \times 10^{1.19exp(-B^2)} \tag{2.18}$$

with B=(0.208-$\log r$)/0.65, u_{10} is the wind speed at $10\,\text{m}$ altitude. An additional parameterisation which is used for higher wind speeds is also implemented in the model (Smith et al., 1993).
The emission of gas phase species from the surface are prescribed in the model.

The removal of gases out of the atmosphere through deposition is calculated with a resistance model after Wesely (1989a). The dry deposition velocity (v_g^{dry}) of gases at the surface can be viewed as the sum of a series of resistances

$$v_g^{dry} = \frac{1}{R_a + R_m + R_c} \tag{2.19}$$

where R_a is the aerodynamic resistance between a reference height z and the surface (z_0):

$$R_a = \frac{1}{\kappa u_\star}\left(ln\frac{z}{z_0} + \Phi_s(z, L)\right) \tag{2.20}$$

with the friction velocity $u_\star$ and the von Karman constant κ=0.4. The stability function Φ_s included in the equation above is calculated from Monin-Obukhov similarity theory and depends on the reference height z and the Monin-Obukhov length L. The dry deposition velocity further depends on the resistance to molecular diffusion through the surface layer:

$$R_m = \frac{1}{u_\star(Sc^{-2/3} + 10^{-3/St})} \tag{2.21}$$

The Schmidt number can be written as $Sc = \nu/D$ and the Stokes number as $St = w_t u_\star^2/(g\nu)$ with ν being the dynamic viscosity of air and D the diffusion coefficient. The surface resistance due to physical, chemical or biological interactions is calculated as follows:

$$R_c = \frac{2.54 \cdot 10^4}{H^\star T u_\star} \tag{2.22}$$

with the effective Henry's law coefficient $H^\star$ and the temperature T.

Part I

Organic Surface Films on Sea Salt Aerosols

Chapter 3

Introduction - Organic Aerosols

Aerosol particles are important constituents of the global climate system. With their ability to scatter solar radiation aerosols influence the global energy budget and affect climate directly. Furthermore, they serve as cloud condensation nuclei (CCN) and influence cloud properties like the number distributions and size of droplets. As the scattering of solar radiation depends on these quantities, aerosols also have an indirect effect on the global energy budget.

In the marine boundary layer sulphate and sea salt aerosols which originate from bubble bursting at the ocean surface are the most important particles which can act as CCN.

Apart from their role in cloud processes, aerosol particles are important for atmospheric chemistry as they can take up gas phase species, recycle them and release them back into the gas phase. Furthermore sea salt aerosol particles can be the source for gas phase constituents like halogen species.

3.1 Field Measurements

In recent years scientist became more and more interested in organic compounds being present in the atmosphere as gas phase species as well as dissolved in aerosol particles (Novakov and Penner, 1993; Jacobson et al., 2000). A steadily increasing number of measurements indicate that organic aerosols are very common over large parts of the globe. Organic compounds have various sources - natural ones as well as anthropogenic ones. Over the continents the most important natural sources are emissions from plants. Some organic compounds that are emitted as gas phase species can rapidly condense on existing particles or can form new particles, so-called secondary organic aerosols (SOA). SOA-aerosols gained a lot of attention in recent years as they are supposed to be important to consider for calculations of the first and second indirect aerosol effect. It is assumed that their ability to act as a CCN differs significantly from that of other types of aerosols. Recent reviews about the sources and possible role of volatile organic compounds (VOC's, such compounds that remain in the gas phase) and the formation of secondary organic aerosols are given by Fuzzi et al. (2006) and Kanakidou et al. (2005).

Apart from the above mentioned VOC's and SOA's, one other group of organic compounds has gained increasing attention in recent years: long chain organic compounds, mainly fatty acids that are able to form surface films on aerosol particles. An overview of several fatty acids and dicarboxylic acids is given in Tables 10.9 and 10.10 in the Appendix. For nearly one century it has been known that some organic molecules are able to form

surface films on particles and that those can have an effect on phase interactions between the gas and the liquid phase. The first laboratory experiments where performed focusing on the evaporation efficiency of water vapour in presence of an organic coating (Rideal, 1924). As it became more and more possible to determine the chemical composition or at least to determine the inorganic and organic mass fraction of aerosol particles, scientists became aware that large numbers of organic compounds are emitted naturally including fatty acids. Over the continents, fatty acids are mainly derived from anthropogenic emissions (e.g. diesel fuel, coal burning or meat cooking, Rogge et al., 1991, 1993; Schauer et al., 1999a; Oros and Simoneit, 2000) but possibly also from natural sources (Simoneit and Mazurek, 1982; BinAbas et al., 1995; Schauer et al., 1999b; Pio et al., 2001; Oros and Simoneit, 2001; Cheng et al., 2004).

Organic compounds have also natural sources in the marine boundary layer. Both dissolved organic matter and decomposition products from algae accumulate in the surface microlayer. The thickness of this layer depends on the biological activity. Organic matter can be directly incorporated in marine particles when gas bubbles burst at the surface. Furthermore, rising gas bubbles scavenge organic material in the water column when they rise towards the surface. A third way for inclusion of organic matter into sea salt aerosol particles is uptake from the gas phase into airborne particles.

Most of the measurements that are discussed below distinguish either between water soluble organic compounds (WSOC) and water insoluble organic compounds (WIOC). WSOC are organic compounds that get dissolved into aerosols but mostly have a lower solubility than inorganic salts. Fatty acids e.g. belong to the WIOC as they do not get totally dissolved in the aerosol but stay at its surface and form a coating. That however, does not necessarily mean that all WIOC are able to form a surface film.

One of the first field measurements of fatty acid concentrations in the marine boundary layer was done by Marty et al. (1979). They found total fatty acid concentrations in seawater of $3 \text{-} 200\,\mu\text{g/l}$ and assumed that concentrations are enriched in the oceanic microlayer by a factor of $2 \text{-} 5$ and in aerosols even by a factor of $50 \text{-} 90$, based on measurements in the North-Eastern Atlantic. Inspired by such kinds of measurements, Gill et al. (1983) brought up the idea that organic surfactants (e.g. fatty acids) which can be present on sea salt aerosols might be of potential importance for the atmosphere as they might affect processes like droplet activation and droplet growth by decreasing the mass transfer between the gas phase and the aerosol phase. This suggestion further motivated people to find out whether organic compounds are present over large parts of the ocean or if their inclusion in aerosol particles is only a very local phenomenon. Recent measurements have shown that the organic mass fraction in marine particles can be up to 60% especially in regions with high biological activity (O'Dowd et al., 2004). Even in areas where only small amounts of microorganisms are present in sea water like the Carribean (Novakov et al., 1997; Russell et al., 2002) and Cape Grim (Middlebrook et al., 1998) non-negligible organic mass fractions were detected. Organic concentrations in marine particle samples vary up to a few orders of magnitude since the biological activity varies and since the organic mass fraction is much larger in the smaller particle modes than in larger modes (O'Dowd et al., 2004). Cavalli et al. (2004) collected aerosol samples at Mace Head and report concentrations of water insoluble organic compounds of $0.66\,\mu\text{g/m}^3$ in the submicron and $0.26\,\mu\text{g/m}^3$ in the supermicron mode whereas Sempere and Kawamura (2003) report dicarboxylic acid concentrations of only a few ng/m^3 in the western Pacific.

As organic compounds are large in number and complexity most chemical analyses of sea salt aerosols can only give information about functional groups being present in the

samples. The measurements from Mace Head have further shown that about 60% of the total organic mass fraction is water insoluble. The functional groups detected are mainly carbonyl compounds and carboxylic acids (Russell et al., 2002; Mochida et al., 2002; Sempere and Kawamura, 2003; Cavalli et al., 2004) which might be decomposition products of longer chain fatty acids. Fatty acids are compounds that are known to be surface active meaning that they are able to form a film on the aerosol which can decrease the mass transfer between the gas phase and the liquid phase as discussed by Gill et al. (1983). Furthermore, Kawamura and Gagosian (1987) detect ω-oxocarboxylic acids in marine aerosols that were sampled in areas with clean air masses (Marshall Islands and North Pacific). Compounds containing nine carbon atoms (C_9) were most abundant in the samples. This finding is supposed to be related to the structure of longer chain organic molecules as numerous of those have a double bond at the C_9 position (e.g. oleic acid, linoleic acid) which is quickly broken up by chemical reactions. It might further explain why unsaturated long chain organic compounds are either not detected very frequently or only in very small concentrations. Data from two field campaigns presented by Kawamura and Gagosian (1987) support this conclusion: Steric acid (a very long chain saturated fatty acid, C_{18}, see Table 10.10) was found in low concentrations ranging from 0.083 to $0.2\,\mathrm{ng/m^3}$. Oleic acid (a very long chain unsaturated fatty acid, C_{18}, see Table 10.10) was detected only once during the campaigns with concentrations of about $0.043\,\mathrm{ng/m^3}$. Kawamura and Gagosian (1987) assume phytoplankton to be the main source for the ω-oxocarboxylic acids detected in marine aerosol samples but they also consider bacteria as another potential source.

Fatty acids were further identified in marine aerosol samples collected in the Western Pacific with total concentrations of $7.6\text{-}20.7\,\mathrm{ng/m^3}$. Apparently the concentrations of low molecular weight fatty acids (LFAs, $C_{12}\text{-}C_{19}$) decreased in winter and increased in summer. A reverse behaviour was observed for high molecular weight fatty acids ($C_{20}\text{-}C_{35}$) (Fang et al., 2002). Mochida et al. (2002) collected aerosols in the North Pacific and found concentrations of low molecular weight fatty acids of $0.8\text{-}24\,\mathrm{ng/m^3}$. In agreement with Fang et al. (2002), they detected maximum concentrations in spring correlated with higher biological activity (based on chlorophyll-α data). Mochida et al. (2002) estimate the average coverage of LFAs on sea salt aerosols to be only 0.3-14% with strong seasonal variablity. Based on work done by Barger and Garrett (1976) who suggest, referring to their measurements that 5-15% of sea salt mass are fatty acids, Mochida et al. (2002) assume that long chain fatty acids comprise only 4% of all film forming compounds (FFCs) that might be incorporated in sea salt particles. If it was possible to detect more abundant FFCs in the marine atmosphere, the process of organic film formation might be of importance as stated out by Mochida et al. (2002).

Masslinger et al. (2003) confirm the presence of large organic mass fractions in marine aerosols samples. However, the analysis technique this group used, was not appropriate to give more detailed information regarding which organic compounds are present in the samples and in which concentrations. Putaud et al. (2000) determined the mass composition of MBL aerosols and found mean values of 37% non-sea-salt sulphate, 21% sea salt and 20% organic compounds. Similar results are reported from Kaku et al. (2006). Aerosol particles collected from an airplane over the North-East Pacific contained an organic mass fraction of 8% of the total aerosol mass. However, it is questionable whether this mass fraction has to be considered as significant or not.

During the ACE-Asia campaign aerosol particles were collected on an island at the Korean coast (Yang et al., 2004). In those samples, WSOC mass is about half the mass of sulphate and accounts for two-third of the total organic carbon mass. Roughly 14% of the WSOC

mass was assigned to mono- and dicarboxylic acids, aliphatic amines and amino acids. Oxalic acid was the most abundant single species that could have been detected. It was not possible to determine more precisely the organic constituents accounting for the rest of the WSOC mass. However, it was assumed that a large mass fraction are polymeric materials.

Yoon et al. (2007) investigated the physicochemical properties of aerosols in the North Atlantic. In summer when biological activity is high they found WSOC concentrations of $0.2 \, \mu\text{gC/m}^3$ and in winter when biological activity is lower WSOC concentration were lower than $0.05 \, \mu\text{gC/m}^3$. The organic mass fraction therefore seems to be strongly correlated with phytoplankton production. Furthermore, the authors report, that the WSOC accounts for 10-50% of the total organic compounds (TCs) with highest percentage in spring.

Apart from those field measurements which can give concentrations of organic compounds or at least can detect several functional groups being present in aerosol samples and their concentrations, those measurements do not give any information of the distribution of the organics within the aerosol particles. Such information is necessary to be able to quantify the theory that some of the organic species - presumably long chain fatty acids in the range C_{12} - C_{18} - are forming surface films on real atmospheric aerosol particles.

Only two publications exist that get close to proof this theory. Russell et al. (2002) could detect functional groups being present in aerosol particles, mainly aromatic, alkyl, ketonic carbonyl and carboxylic carbonyl groups like already mentioned above. They can further see that the organic composition on the surface of the particle is enhanced in shorter chain and more oxygenated groups and suggest surface active carboxylic acids forming organic coatings. However, the detection of shorter chain and more oxygenated groups indicates that these compounds have already undergone atmospheric processing and are potentially follow-up products of longer chain organic compounds. Even though those organic groups were detected at the surface of a particle it does not automatically indicate that they still influence mass transfer between the phases.

Tervahattu et al. (2002a) could give more striking evidence of a surface film on their aerosol samples. However, Tervahattu et al. (2002a) sampled particles at the south coast of Finland and although the air masses on the sampling day came from the North Atlantic, aerosols have undergone atmospheric processing over the European continent. Tervahattu et al. (2002a) found a morphological proof of the existence of an organic surface coating on aerosols as they found that the particles do not have a solid shape but are pulsating. On a follow up paper Tervahattu et al. (2002b) present the chemical analysis of the same samples they used for the investigations of the shape of the particles and detected biogenic fatty acids, mainly palmitic acid. Tervahattu et al. (2005) could also detect fatty acids in continental sulphate aerosols.

As the variety of organic compounds is large and as different organic compounds can have significantly differing effects on aerosol properties the most discussed ones are introduced now.

3.2   Which organic compounds are able to form surface films?

Based on the definition of Seidl (2000) and Gill et al. (1983) all organic compounds that contain less than 12 carbon atoms are too volatile to form a surface film and those containing more than 18 carbon atoms are not thermodynamically stable anymore to form a film.

This leads to the definition that those organics can form surface films that contain about 12 to 18 carbon atoms and have a straight carbon chain. Further Seidl (2000) and Gill et al. (1983) build up the conception that the hydrophilic group of the organic molecule is attracted by the water within a particle and the hydrophobic group is facing the air (see Figure 3.1 b and c). The carbon chain length determines the water solubility of the organic compound, its gas-particle portioning and the state of the film. Figure 3.1 gives a schematically overview of different types of surface films. Figure 3.1 a shows a 'liquid condensed' surface film where the organic molecules stick to the particle with one end but their tails can still move freely around the particle. It is supposed that shorter chain organic molecules form such kinds of films. Both other schematic plots show 'solid condensed' films where molecules are well ordered around the particle. It has to be pointed out that the above described idea of an organic surface film is a theoretical model. It is highly idealised especially regarding the amount of different chemical compounds that are in reality present at the same time on one particle and that form all together one surface film. It is unlikely that such a well organised film as shown in 3.1 would build up in reality due to the complexity of organic compounds.

3.3 Which aerosol properties are affected by a surface film?

Surface coatings can reduce the phase transfer between the gas and the aerosol phase as they are literally an additional barrier for gas phase molecules that condense onto particles or liquid molecules that evaporate from a droplet.

Since the first publication by Rideal (1924) who found a reduction of the evaporation efficiency of water vapour out of a droplet in presences of an organic surface film, a series of similar results were published (Snead and Zung, 1968; Garrett, 1971; Kocmond et al., 1972; Rubel and Gentry, 1984; Otani and Wang, 1984; Seaver et al., 1992). Most of those articles deal with effects on evaporation of water out of a droplet but Rubel and Gentry (1984) could show that the effect on condensation is on the same order of magnitude as that on evaporation. Even in the 1960's scientists were aware that a reduced evaporation/condensation efficiency might have a significant influence on the diffusional growth process of cloud droplets, cloud number distribution as well as the development of precipitation and the evolution of fog. Bigg et al. (1969) performed an experiment where they released a 200 g mixture of hexadecanol and octadecanol as finely divided smoke into a valley where fog development is very likely and was expected on the experiment days. In

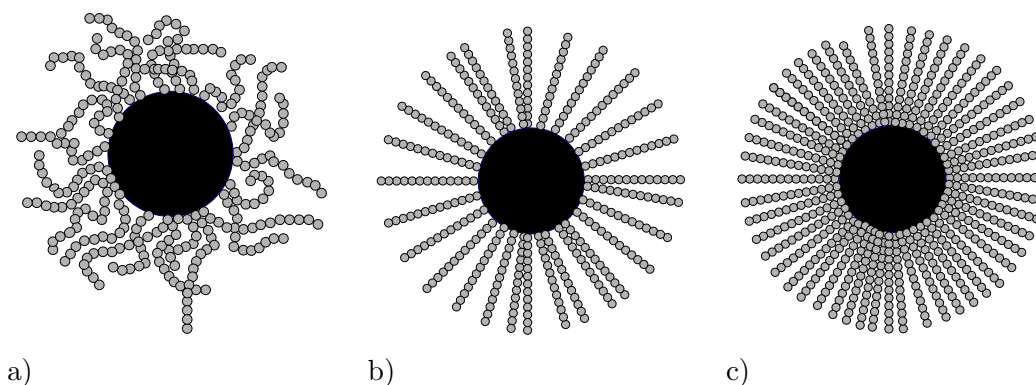a)   b)   c)

Figure 3.1: Model conception of an organic surface film on a sea salt particle.

all cases a deviation from the expected fog evolution process was observed. However, it is not possible to exclude that this was a natural process and fog would not have developed either with or without the release of the surface active organic compounds.

Apart from water vapour, the phase transfer of all kinds of gases that undergo uptake on aerosol particles (or such species that degas out of particles) can theoretically be influenced by a surface film. However, the latest laboratory measurements show different results regarding the degree of uptake reduction. While N_2O_5 uptake on sea salt aerosols covered by an organic coating seems to be decreased by a factor of 3-4 up to a factor of 42 (Thornton and Abbatt, 2005; Badger et al., 2006; Neill et al., 2006) there are measurements which show that uptake of water vapour on particles with a palmitic acid coating is not affected significantly (Garland et al., 2005). Brown et al. (2006) have collected aerosol particles over the American continent and could show that the uptake coefficient for N_2O_5 on these particles varies with ambient conditions including the organic mass fraction in the aerosol. As nearly all laboratory studies deal with the uptake of water vapour or N_2O_5 and as even those measurements give differing results it is still an open question if the uptake of all kinds of gases is affected in the same way. Further it is not well known how large the effect of an uptake reduction really is and if all kinds of film forming compounds affect mass transfer in the same way especially in consideration of the large number of different organic compounds. Nothing is known about the structure of an organic surface film on real atmospheric particles. It is not known if the organic coating has to be as tightly packed as suggested in Figure 3.1 c where nearly two monolayers exist and one organic molecule is directly positioned adjacent to the neighbouring one to inhibit phase transfer. Or is a coating as indicated in Figure 3.1 b sufficient to reduce mass transfer between the phases where not even one complete monolayer is present? Again it is reminded that this point of view of an organic coating is rather a conceptual model.

A few model calculations exist, dealing with the potential effect of a reduced uptake of water vapour on the activation potential of aerosol particles. Chuang (2006) performed sensitivity studies with a parcel model regarding the sensitivity of droplet growth with respect to a reduced thermal and condensational accommodation coefficient as well as dissolution behaviour of organics. They concluded that activation only was sensitive to changes if the mass accommodation coefficient was decreased below some critical value of 0.1 - 0.001 depending on the droplet size. Classical Köhler theory which is based on an equilibrium assumption between the particle and its environment sometimes overpredicts the number of droplets that are activated compared to measurements. Nenes et al. (2001) suggest that this equilibrium assumption might not be correct for certain aerosol populations. However, they find that a reduced mass transfer only slightly decreases the number of activated particles and the authors suggest that this phenomenon might be regionally important, either in areas with large anthropogenic organic emissions or in marine areas with highly active phytoplankton production, but most likely not globally. Feingold and Chuang (2002) also performed parcel-model studies and assumed film forming compounds being present on some of the aerosol particles (mainly ammonium sulphate). Their finding is that the growth of those particles that are at the beginning of the simulation coated by organics (they assume that the surface coating breaks up with time) is delayed due to the delayed water vapour uptake. Those particles that are not coated can grow much faster as more water vapour is available for them. This leads to larger but fewer cloud droplets. In a field measurement the timescale of condensational growth of aerosol particles was investigated (Chuang, 2003). Only 0 - 2 % of all particles show a delayed growth depending on their size and the season. The delay is assumed to be associated with an organic sur-

face film inhibiting water vapour uptake on particle. The percentage of those potentially coated particles is extremely low and only if much more of those particles existed they would be important to consider for e.g. indirect aerosol effects. However, the delayed droplet growth might be important regionally for the CCN activation as lifted particles only have a certain time to collect water vapour to get activated as Chuang (2003) conclude. In a more recent field campaign at several sites in the United States with the same focus, the fraction of aerosols showing a delayed growth behaviour was at some days up to 60% (Ruehl et al., 2008).

Summarising, the above discussed work indicates that the effect of a delayed droplet growth due to a limited water vapour uptake due to an organic coating - if it is important at all - it might be rather regionally important but not globally. It has also to be mentioned again that the global coverage of aerosol characterisation experiments is poor. The measurements mentioned above only cover very small parts of the ocean and it is impossible to know if there are regions where regularly a significant fraction of particles might be affected by a surface coating or not.

3.4 Atmospheric processing of surface films

Although an increasing number of measurements give indications of the presence and potential effects of organic surface films, it is still a challenge to determine the contribution from the oceanic surface microlayer to the initial chemical composition of sea salt particles which is important for understanding the complete reaction cycles taking place in the atmosphere. Ellison et al. (1999) have developed an inverted micelle model (i.e. long chain organic molecules that are attached to an aerosol with their hydrophilic end and the hydrophobic end is facing the air) to describe atmospheric processing of organic surface films of biological origin on sea borne aerosol particles.

As mentioned above little is known about the detailed chemical composition of the organic mass fraction so that it is very difficult to assess the chemical reactions that take place on the organic aerosol surface and within the aerosol. What has been shown in many studies, however, is that the surfactant coating undergoes chemical reaction with atmospheric oxidants like O_3 or OH which leads to the destruction of the organic coating on the aerosol. Most of the published laboratory studies dealing with the reactive uptake of O_3 on coated particles use oleic acid as a proxy for surface active compounds like fatty acids (de Gouw and Lovejoy, 1998; Moise and Rudich, 2002; Smith et al., 2002; Morris et al., 2002; Thornberry and Abbatt, 2004; Hearn and Smith, 2004; Katrib et al., 2005a; Hearn et al., 2005; Knopf et al., 2005) Although the measurements agree quite well in the value for the reactive uptake coefficient it is questionable and has been pointed out in several of these studies (Smith et al., 2002; Knopf et al., 2005) if these numbers can be applied under atmospheric conditions where an organic film would consist of a large number of different surfactants. One reason why we maybe should handle these data with care are the large discrepancies in oleic acid lifetimes in the laboratory where the molecules only survive a few seconds to minutes opposed to the lifetimes in the atmosphere which seem to be a few days (Rogge et al., 1991). Robinson et al. (2006) calculated the oxidation lifetime of condensed phase organic aerosol constituents as a function of particle size and compared the results to the age of an aerosol particle in air masses which are affected by regional transport. They suggest that a reactive uptake coefficient for O_3 on organic aerosols nearly two orders of magnitude lower than reported from laboratory measurements would be more realistic.

Furthermore, measurements deal with the oxidation of organic monolayers by NO_3 and OH. Both oxidation processes seem to happen on similar time scales (Bertram et al., 2001; Knopf et al., 2006). The uptake of Cl and Br by organic surfaces was also investigated (Moise and Rudich, 2001). Additionally to the investigation of the ozonolysis of oleic acid, reactive uptake coefficients of O_3 on linoleic acid (Moise and Rudich, 2002; Hearn and Smith, 2004; Thornberry and Abbatt, 2004), linolenic acid (Thornberry and Abbatt, 2004), oleyl alcohol (Hearn and Smith, 2004), peroxides (Thomas et al., 2001), lauric acid/oleic acid mixtures, myristic acid/oleic acid mixtures (Knopf et al., 2005) or stearic acid/oleic acid mixtures (Katrib et al., 2005a) were determined. However, values are all on the same order of magnitude as for the O_3 - oleic acid system ($\gamma \approx 10^{-4}$ - 10^{-3}). In addition to the already mentioned processes at the gas phase - surfactant interface the surfactants might also be attacked at the surfactant-aqueous phase interface. However, it was not possible to find any information about this process in the literature. Apart from the uncertainties regarding the destruction rate of the film even less is known about reaction products that are formed by the reaction between the organic film with gas phase oxidants and further reactions that take place after the primary oxidation of the surface film. Several laboratory studies also deal with the detection of reaction products from the heterogeneous reaction between O_3 and oleic acid (Katrib et al., 2004; Asad et al., 2004; Hung et al., 2005; Ziemann, 2005; Zahardis et al., 2005; Katrib et al., 2005b; Zahardis et al., 2006; Mochida et al., 2006; Vesna et al., 2007; Hung and Ariya, 2007). However, regarding the uncertainties with respect to the reactive uptake coefficient, the yield of certain products is subject to uncertainties. A large fraction of reaction products staying in the aerosol phase are suggested to be dicarboxylic acids or at least are supposed to be compounds that further react to form dicarboxylic acids. Furthermore, a certain fraction of organics is also observed to degas out of the aerosol immediately after primary ozonolysis reactions take place (e.g. Moise and Rudich, 2002; Hearn and Smith, 2004). A recent review about the ozone - oleic acid system was published by Zahardis and Petrucci (2007).

3.5 Effect of WSOC on microphysical aerosol properties

Water soluble organic compounds can influence microphysical aerosol properties in various ways. The best known and most often investigated effect is the reduction of the surface tension of droplets. Molecules in the droplets interior are within a symmetrical attractive force field (Pruppacher and Klett, 1997). Molecules on the surface of a droplet experience a net force towards the interior of the droplet as intermolecular attractive forces tend to minimise the surface area of the drop. Pure water droplets have a very high surface tension due to the water's strong hydrogen bonds. This effect is diminished in the presence of dissolved organic compounds having a polar group (Facchini et al., 1999). Thus WSOC decrease the surface tension of a droplet. Further WSOC modify the droplets solubility as the solubility of the dissolved organic compounds is in general lower than that of inorganic salts (as was already mentioned above). Most of the existing studies deal with the influence of those two effects on the activation behaviour of aerosol particles.

In general droplet activation is described by Köhler theory (see Equation 2.12). Shulman et al. (1996) present a parcel model study based on laboratory data regarding the gradual dissolution behaviour of only slightly soluble organic compounds which they found alters the shape of the classical Köhler curve. The effect of a reduced surface tension considered by itself leads to a reduction of the critical supersaturation of the particles and at the same time to an increase in the critical radius. This effect might increase droplet activation

leading to a greater number of CCN. The authors assume that the overall effect of a stepwise dissolution of the organics and the reduction of the surface tension is however, a delay in droplet activation. The authors point out that this effect would not only be valid for organics but for all kinds of only slightly soluble molecules incorporated into aerosol particles. Li et al. (1998) come to the same conclusion based on a model study and point out that such an effect, if globally relevant has to be taken into account when discussing the indirect aerosol effects. Facchini et al. (1999) only consider the effect of a reduced surface tension on the Köhler curve (based on field data) and find that a decrease of the surface tension by 30% leads to an increase of droplet numbers by 20% but at the same time the mean droplet radius is decreased by about 6%. Shantz et al. (2003) and Lohmann et al. (2004) compare the activation behaviour of particles containing slightly soluble organics to that of pure ammonium sulphate and find in both cases a delayed particle growth in presence of the organics and a smaller activated aerosol fraction. Ervens et al. (2005) presented a model study where they could show that the impact of organic aerosol constituents on the microphysical properties of the aerosol might have been overestimated by others as the effects caused by an alteration of the aerosol's solubility, molecular weight and surface tension counteract one another and lead to only small changes compared with cases where these effects are ignored. The study presented by Ervens et al. (2005) is the only one that does not only take into account the modification of the surface tension and solubility by organic aerosol constituents but also the influence on molecular weight and the potential changes from ideal dissolution behaviour.

Several other researchers investigated the effect of dissolved organic compounds on the activation behaviour of aerosol particles - model studies as well as laboratory studies. As they all consider different regimes and different aspects of how organics might influence droplet activation, the results differ significantly and the assumed effect on the number of activated particles (N) varies from -86 % ΔN (Shantz et al., 2003) to +110 % ΔN (Mircea et al., 2002).

A *decrease* in the number of activated particles was estimated by: Shantz et al. (2003) (ΔN_{max}= -86 %), Lohmann et al. (2004) (ΔN_{max}= -76 to -35 %), Ervens et al. (2004) (ΔN_{max}= -50 to 0 %, either decrease or effect negligible), Hegg et al. (2001) (ΔN_{max}= -40 %), Shulman et al. (1996) (ΔN_{max}= < 0 %), Nenes et al. (2002) (ΔN_{max}= -5 to +25 %, either increase or decrease in dependance of the organic mass fraction), Rissman et al. (2004) (ΔN= 0 %), Giebl et al. (2002) (ΔN_{max}= -25 to 0 %, decrease or effect negligible in dependence of the organic mass fraction and choice of organic species), Ming and Russell (2004) (ΔN_{max}= -57 to +6 %, small increase for some tested organics).

An *increase* in the number of activated particles was estimated by: Mircea et al. (2002) (ΔN_{max}= +110 %), Alfonso and Raga (2004) (ΔN_{max}= +35 %), Anttila and Kerminen (2002) (ΔN_{max}= -8 to +4 %), Bilde and Svenningsson (2004) (ΔN_{max}= -30 to +30 %, increase or decrease to the same extend), Facchini et al. (1999) (ΔN_{max}= +20 %).

3.6   Motivation

Recent laboratory experiments, field campaigns and model studies give more and more indications about the specification and concentration of organic compounds and their role in the atmosphere. However, all existing model studies only deal with the question in which way either a reduced water vapour uptake due to an organic surface film might affect droplet growth or in which way dissolved organic compounds can have an impact on aerosol growth and activation. As pointed out in the introduction above, especially the latter point is difficult to assess and different model approaches give significantly differing results. However, in all those model studies mentioned, organic concentrations are prescribed and set to constant values or only their effects are parameterised. Thus the model simulations presented in this thesis focus on the effect of a reduced mass transfer between the aerosol and the gas phase due to an organic surface film. Oxidation of the film with gas phase species like O_3 or OH is treated explicitly in the model as well as gas phase and aerosol phase chemistry, like explained in Section 2.4 (Model description).

The first question that is addressed is the lifetime of a surface coating. Measurements show that especially in regions of the oceans that have a high biological activity the fraction of organic compounds being incorporated into aerosol particles is a common phenomenon as measurements show. We know further that surfactants are among those organics. However, no measurements can give information whether surfactants are also present in aged marine particles or only in freshly emitted sea salt aerosols. Thus reactive uptake coefficients derived from laboratory experiments for O_3 and OH on surfactants are applied in the model to study the timescale of atmospheric processing of an organic surface film. In general, organic surface films could to be able to influence atmospheric chemistry on two ways: (i) Atmospheric processing of the surface film and its follow up products might have an impact on the atmospheric oxidation capacity and on atmospheric reaction cycles. (ii) A reduced mass transfer due to the surface coating might influence gas- and aqueous phase chemistry.

Those potential effects of an organic surface film on chemistry in the marine boundary layer are discussed in the following.

Chapter 4

Influence of Organic Surface Films on Atmospheric Chemistry

4.1 Treatment of surface reactions in the model

[1] The prognostic equation for gas phase concentrations as calculated in the model was explained in Section 2.4.1. As mentioned above, a focus should be put on limitations of mass transfer from gas to liquid and liquid to gas phase which is described by the sum term of Equation 2.13. The rate coefficients for heterogeneous reactions and phase transfer reactions depend on the mass transfer coefficient k_t for non-reactive uptake of gas molecules to the surface of particles (Schwartz, 1986) which is given by:

$$k_t = \left(\frac{r^2}{3D_g} + \frac{4r}{3\bar{v}\alpha} \right)^{-1} \tag{4.1}$$

with the particle radius r, the mean molecular speed $\bar{v} = \sqrt{8RT/(M\pi)}$ (M is the molar mass), the accommodation coefficient α and the gas phase diffusion coefficient D_g which can be approximated by $D_g = \lambda\bar{v}/3$ using the mean free path λ.

In this setup the parameter influenced by the organic coating is the accommodation coefficient which describes the probability that a gas phase molecule impinging on the particle is taken up.

To determine the rate coefficients for the transfer reactions k_t has to be multiplied with the LWC for the forward reaction (k_f) describing uptake of gaseous species and with the dimensionless Henry coefficient k_H^{cc} for the backward reaction (k_b) describing release of liquid phase species (Sander, 1999).

$$k_f = k_t \cdot LWC \cdot c_g \tag{4.2}$$
$$k_b = k_t \cdot \frac{c_a}{k_H^{cc}} \tag{4.3}$$

To simulate organic surface films every sea salt particle which is emitted from the ocean is assumed to contain organic compounds. Based on the cross section area of one molecule of oleic acid, it was assumed that one molecule of an organic compound covers $20 \cdot 10^{-20}\,\mathrm{m}^2$ of the sea salt aerosol surface. For a particle radius of $3\,\mu$m an organic concentration of

---

[1]Parts of this Chapter have been published by: L. Smoydzin and R. von Glasow, 'Do organic surface films on sea salt aerosols influence atmospheric chemistry? - a model study', ACP,7,5555-5567,2007

about 0.5 nmol/l is needed to form a complete monolayer on one particle. In the following, surfactant concentrations refer to the total sea salt particle spectrum so that the required oleic acid concentration to cover all sea salt particles would be about 70 mmol/l for a typical particle spectrum with an average radius of $3\,\mu$m.

As soon as the organic concentration is large enough to form a monolayer on the aerosol, the accommodation coefficients (α) for gas phase species are decreased in the model. According to Equation 4.1, a reduction of α by one order of magnitude would lead to a decrease in the transfer coefficient (k_t) of about 50% for a particle with a radius of $0.8\,\mu$m. Figure 4.1 shows the effect for various reduction factors as a function of particle radius. For the uptake of gaseous species with large transfer coefficients close to the diffusion limit for large particles (as sea salt particles) a reduction of the accommodation coefficient leads to nearly no differences in the transfer coefficient (Figure (4.1), r=10^{-5} m).

To describe the heterogeneous reaction between gas phase oxidants and the organic surfactants a reactive uptake rate is calculated with Equation 4.1 by replacing the accommodation coefficient α with the reactive uptake coefficient γ. That means that a reactive uptake coefficient is used instead of an unreactive uptake coefficient. Replacing α by γ is strictly only valid if the diffusion corrections for the measured reactive uptake coefficients were low. However, regarding the range of reported reactive uptake coefficients and regarding the uncertainties related to these values one can replace α by γ without causing a large error. By using this approach to calculate a first order reaction rate of the gas phase oxidants with the surfactant, both the loss of the oxidant and the chemical destruction of the surfactant is calculated. Therefore the chemical lifetime of the surfactant is calculated explicitly. In contrast to an approach following the Langmuir-Hinshelwood mechanism (for example Pöschl et al., 2001, 2005) no time-dependant reactive uptake coefficients are used as the surface film in the model gets completely destroyed by reaction and so the factors that lead to the determination of time-dependant uptake/reaction rates in a laboratory experiment do not account for the model approach.

4.2 Setup of model runs

All model runs were performed for summer time (solar declination 20°) under clean marine conditions characterised by relatively low NO_x and O_3 mixing ratios (initial mixing ratios are: 20 nmol/mol O_3, 9 pmol/mol NO_2, 1.6 pmol/mol NO). A typical marine background aerosol size distribution (Hoppel and Frick, 1990) with an initial surface area of $70\,\mu$m^2/cm^3 is used. The initial and boundary conditions were chosen such that no clouds form during the simulation time and the boundary layer height is kept constant at about 700 m. The temperature in the lowest model levels is about 15°C and relative humidity increases from 65% near the ocean surface to 85% at the top of the boundary layer.

All model runs are initialised with the same fields for chemistry and meteorology which are taken from a two day model run without organic emissions in order to have a spin up for the model. The simulation time for all runs is three days and each run starts at midnight. For all cases except the base case sea salt particles contain organic compounds when they are emitted from the ocean. This setup can be understood as follows: The model column moves over the clean ocean and after two days it crosses for three days an area with high biological activity where organic material gets incorporated into sea salt aerosols.

To quantify the uncertainties regarding the concentrations of organic compounds being present in sea salt aerosols, the magnitude of uptake reduction, the oxidation rate of the
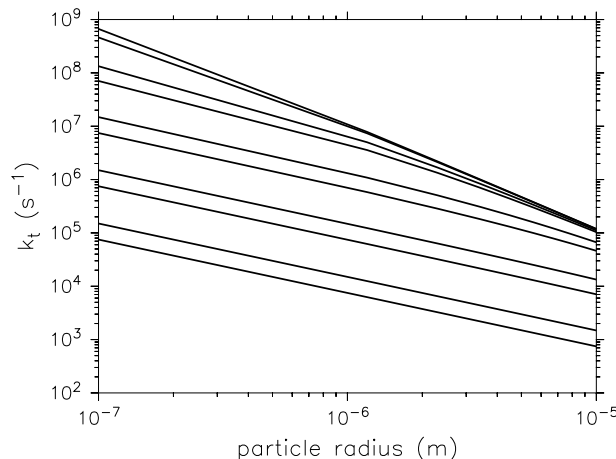
Figure 4.1: Transfer coefficient k_t as a function of particle radius and accommodation coefficient α calculated after Equation 4.1. The largest value chosen for α was 1 (resulting in the largest values for k_t; $k_t = 7 \cdot 10^8$ for $r = 10^{-7}$) and the lowest value was $\alpha = 5 \cdot 10^{-5}$ (resulting in the lowest value for k_t; $k_t = 7 \cdot 10^4$ for $r = 10^{-7}$). α was decreased stepwise by a factor of 0.5 from 1 to $5 \cdot 10^{-5}$. The different lines refer to the transfer coefficient calculated with different accommodation coefficients. Note the logarithmic scaling of the axes.

organics and the organic fractions being oxidised by reaction with ozone or OH four different scenarios were considered. In the following it is referred to the different scenarios with Roman numbers I-IV and to the different cases with Arabic numbers 1-6.

Scenario I:
The model runs for scenario I were performed to investigate the potential influence of different organic concentrations in sea salt aerosols. As mentioned above organic concentrations might vary by more than three orders of magnitude as they are strongly depending on ambient conditions.
For all cases of this scenario it is assumed that the surface film only comprises of oleic acid, which is used as a proxy for long chain organic surfactants and that the film is destroyed by reaction between oleic acid and O_3 using literature values for the reactive uptake coefficient (Knopf et al., 2005). The accommodation coefficients of all species are decreased by a factor of 10 if an organic coating is present. The initial oleic acid concentrations are varied (case 1-3).

Scenario II:
The reactive uptake coefficients which is used for the heterogeneous reactions between the organic film compounds and gas phase radicals were all determined under laboratory conditions using single compound organic particles or particles covered by a single-compound-film. However, even a surface film consisting of only two different compounds changes the reactivity of the film (Katrib et al., 2005a). In reality a surface film consists of a large number of different organic compounds. A mixed film might alter the chemical properties of a coated aerosol significantly in contrast to the laboratory studies. Therefore model runs were performed with different reactive uptake coefficients for O_3 on oleic acid. For this scenario the initial organic concentration was kept constant for all cases and all ac-

Scenario I			Scenario II		
$\alpha = 0.1 \cdot \alpha_\circ$	case 1:	OA=80 mmol/l	OA=80 mmol/l	case 1:	$\gamma_{(OA)}$=7.9·10^{-4}
$\gamma_{(OA)}$=7.9·10^{-4}	case 2:	OA=400 mmol/l	$\alpha = 0.1 \cdot \alpha_\circ$	case 2:	$\gamma_{(OA)}$=1·10^{-5}
	case 3:	OA=800 mmol/l		case 3:	$\gamma_{(OA)}$=1·10^{-6}

Scenario III			Scenario IV		
$\alpha = 0.1 \cdot \alpha_\circ$	case 1:	OA =390 mmol/l	OA=400 mmol/l	case 1:	$\alpha = 0.25 \cdot \alpha_\circ$
$\gamma_{(OA)}$=7.9·10^{-4}		Org=390 mmol/l	$\gamma_{(OA)}$=7.9·10^{-4}	case 2:	$\alpha = 0.1 \cdot \alpha_\circ$
$\gamma_{(Org)}$=0.1	case 2:	OA =70 mmol/l		case 3:	$\alpha = 0.025 \cdot \alpha_\circ$
		Org=78 mmol/l			
	case 3:	OA =47 mmol/l			
		Org=62 mmol/l			
$\gamma_{(OA)}$=1·10^{-5}	case 4:	OA =39 mmol/l	OA=70 mmol/l	case 4:	$\alpha = 0.25 \cdot \alpha_\circ$
		Org=55 mmol/l	Org=78 mmol/l	case 5:	$\alpha = 0.1 \cdot \alpha_\circ$
	case 5:	OA =39 mmol/l	$\gamma_{(Org)}$=0.1	case 6:	$\alpha = 0.025 \cdot \alpha_\circ$
		Org=47 mmol/l			
	case 6:	OA =39 mmol/l			
		Org=39 mmol/l			

Table 4.1: $\alpha_\circ$: accommodation coefficient, α: decreased accommodation coefficient, **OA**: initial concentration of oleic acid (respectively **ORG**) which sea salt particles contain when they are emitted from the ocean, $\gamma_{(OA)}$: reactive uptake coefficient for O_3 on oleic acid, $\gamma_{(Org)}$: reactive uptake coefficient for OH on 'ORG'.

commodation coefficients were reduced in the same way as in scenario I.

Scenario III:
The uncertainty regarding the real composition of an organic film leads to the question how many surface molecules are really oxidised by reaction with O_3 and how many molecules react with other oxidants like OH. In scenario III the film consists of different mass fractions of oleic acid (which reacts with O_3) and 'ORG' which is an unspecified organic compound which we assume to react with OH. The reactive uptake coefficient for this reaction is taken from Bertram et al. (2001). Again the accommodation coefficients are reduced by one order of magnitude if an organic film is present. Initial concentrations of both of the organic species were varied indicating that a film has different [ORG]/[oleic acid] ratios.

Scenario IV:
Finally the sensitivity of atmospheric gas and aerosol phase chemistry to different magnitudes of uptake reduction is studied. In cases 1-3 of scenario IV the organic surface film consists again only of oleic acid which reacts with O_3. The initial oleic acid concentration was the same for all three cases (same setup as case I.2). In cases 4-6 the film consists of oleic acid and ORG (same setup as case III.2). The magnitude of the decrease of the accommodation coefficients was varied.

4.3 Results

4.3.1 Lifetime of the organic film

Organic surface films on sea salt particles can only have an effect on atmospheric chemistry if they have a lifetime long enough so that they can be transported to higher levels of the MBL.

4.3.1.1 Scenario I

For case 1 of scenario I (blue dash-dotted line, Figure 4.2 I a,b,c) it was assumed that the initial oleic acid concentration for freshly emitted sea salt aerosols is large enough to form exactly one monolayer on the aerosol. The plots Ia, IIa and IIIa of Figure 4.2 show the maximum altitude where particles with a complete monolayer can be found. As can be seen in Figure 4.2 (Ia), for case I.1 (blue dash-dotted line) the organic coating is already destroyed within the lowest 30 meters of the boundary layer because the reaction of oleic acid with O_3 is very fast. For case I.2 (green dotted line, Figure 4.2 I a,b,c) and case I.3 (red dashed line, Figure 4.2 I a,b,c) higher initial organic concentrations were assumed. As a consequence, coated particles can be found at higher atmospheric levels during the whole simulation time (90 m for case I.2, 140 m (day)-200 m (night) for case I.3). The differences for case I.3 (red dashed line) between day and night can be explained with the diurnal variation of the turbulence structure in the MBL. Turbulent transport over the ocean is stronger during night than during day as the air cools down stronger at night than the ocean surface thus inducing thermal turbulence. That explains why coated particles can reach higher levels during night than during day when the sea salt source and the only sink reaction for organic surfactants stay unchanged.

However, the assumptions which were made in scenario I are considered as unrealistic and are not used for further investigations. After three days of model run time a dramatic decrease in O_3 concentrations by 30% for case I.3 can be seen compared to the base run without an organic coating (black line, Figure 4.2, Ic). For case I.1 and case I.2 where oleic acid concentrations are lower the differences are smaller (ΔO_3: 20% for case I.2, ΔO_3: 8% for case I.1). This effect is caused by the new sink reaction for O_3 with oleic acid. With a reactive uptake coefficient of $\gamma = 7.9 \cdot 10^{-4}$, the O_3 destruction rate by the heterogeneous reaction with oleic acid is 0.008 pmol/mol·s which results in the difference of 3.75 nmol/mol (for case I.3) after three days simulation time. Such a strong O_3 loss is rather unrealistic.

4.3.1.2 Scenario II

Therefore, in scenario II the reactive uptake coefficients for O_3 on oleic acid are decreased. Initial oleic acid concentrations in freshly emitted sea salt particles are 80 mmol/l for all three cases of scenario II. This is the concentration required to form exactly one monolayer on all sea salt particles. To be able to compare the effects of varying uptake coefficients, scenario II.1 equals scenario I.1 (blue dash-dotted line in Figure 4.2 I, II).

For case II.3 (red dashed line Figure 4.2 II a,b) the reactive uptake coefficient for O_3 on oleic acid was decreased by two orders of magnitude compared to laboratory data. The initial oleic acid concentration of 80 mmol/l is now sufficiently large for the presence of coated particles at 500 m altitude during the whole simulation time of three days, without an unrealistically strong O_3 destruction (Fig. 4.2 II c). By changing the reactivity of the film by one order of magnitude (case II.2, green dotted line, Figure 4.2, IIa,b) coated particles
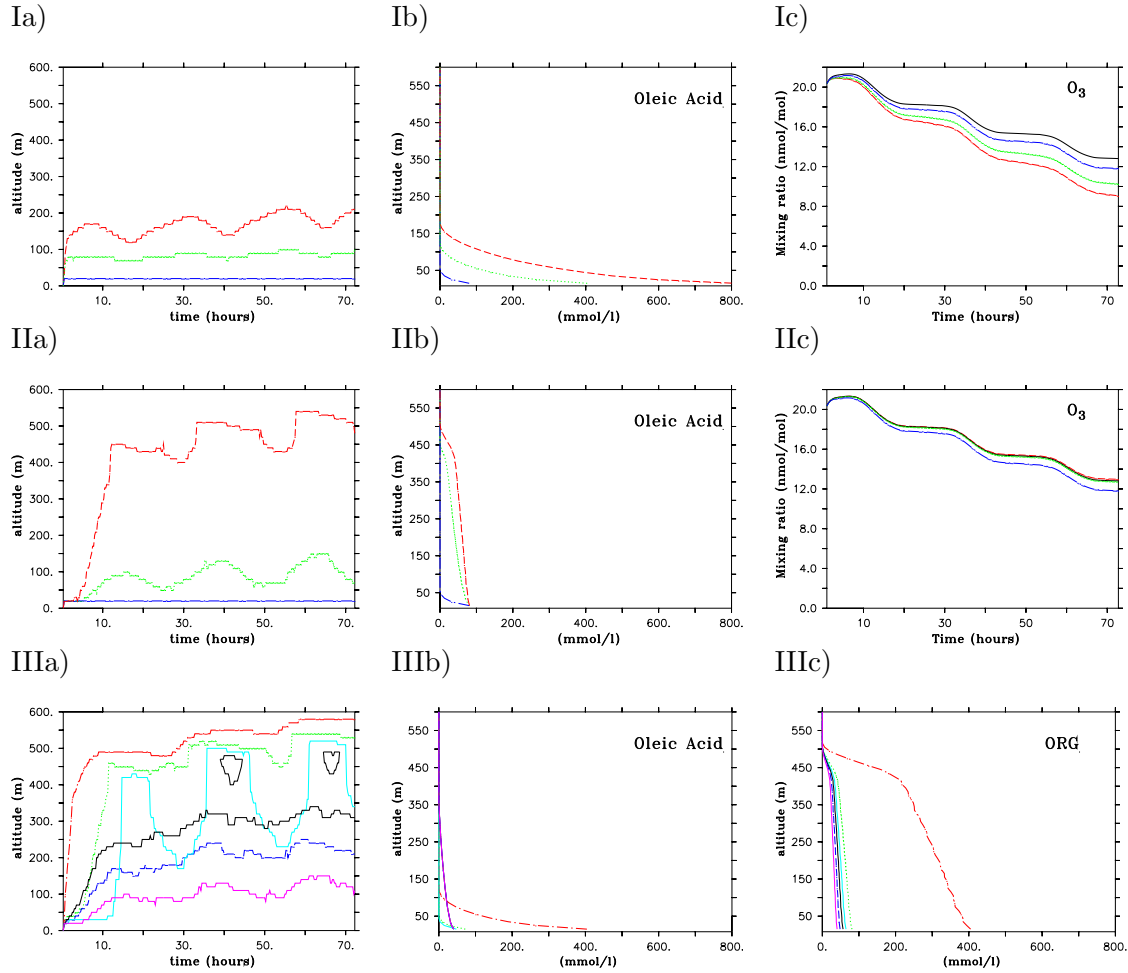
Figure 4.2: The colour code for the plots is as follows:
Plots for cases of **Scenario I (I a, b, c):** base case (black solid line), I.1 (blue dash-dotted line), I.2 (green dotted line), I.3 (red dashed line). Plots for cases of **Scenario II (II a, b, c):** II.1 (blue dash-dotted line), II.2 (green dotted line), II.3 (red dashed line). Plots for cases of **Scenario III (III a, b, c):** III.1 (red dash-dotted line), III.2 (green dotted line), III.3 (light blue solid line), III.4 (black solid line), III.5 (blue solid line), III.6 (purple solid line).
Figures I **a**, II **a**, III **a**: Levels below which sea salt aerosols are coated with an organic film. Figures I **b**, II **b**, III **b**: Vertical profile of oleic acid concentrations at noon, third day of simulation. As for scenario III, case III.4, III.5 and III.6 initial oleic acid concentrations were the same, the lines for these cases are on top of each other (III b).
Figure **I c, II c**: 3-day time series of gas phase O_3 mixing ratios at 50 m altitude. The time is given in hours since model start. Figure III **c**: Vertical profile of 'ORG' concentrations at noon, third day of simulation.

a)   b)   c)

Scenario III.1   Scenario III.2   Scenario III.5

d)

Sea Salt aerosol radius
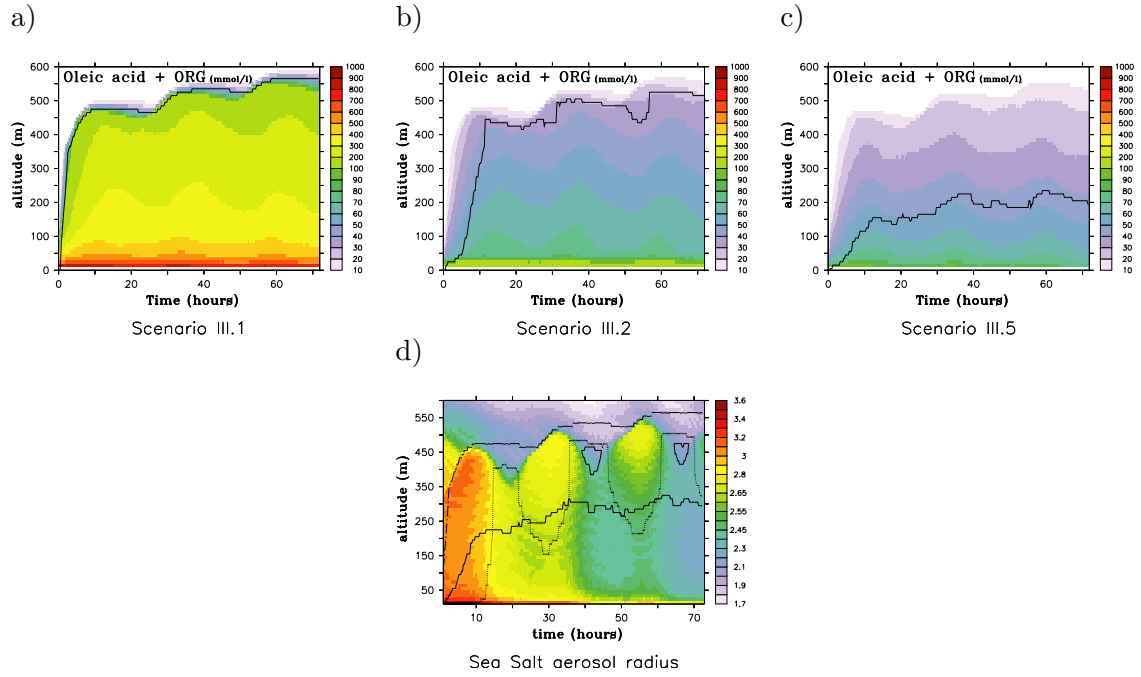
Figure 4.3: Plots in the top row show oleic acid + ORG concentrations (shaded, in mmol/l) for case III.1 (a), case III.2 (b) and case III.5 (c). The black lines show the maximum altitude, where totally coated particles can still be found for the corresponding scenarios. Figure d) shows the vertical distribution of the sea salt aerosol radius for case III.1 (in μm, shaded). The black lines show the maximum altitude, where coated particles can still be found for case III.3 (black dotted line), case III.1 (black dash-dotted line) and case III.4 (black line).

can be found up to about 100 m. However, in this case coated particles reach higher altitudes during day than during night, which is the reverse of what was seen in case I.3 (red dashed-line, Fig. 4.2, Ia). O_3 mixing ratios decrease during day time as the assumed NO_x concentrations for very clean marine conditions are too low to reproduce the amount of O_3 that is photochemically destroyed. During night time O_3 mixing ratios stay constant (Fig. 4.2, IIc). As the heterogeneous reaction between O_3 and oleic acid is one order of magnitude slower in case II.2 and II.3 than in case I.3 and as O_3 mixing ratios decrease permanently during day time as mentioned above, the reaction with oleic acid gets slower leading to a less efficient destruction of the surface film. Whereas, during night time O_3 mixing ratios stay constant leading to a constant destruction of the film and thus totally coated particles are transported to lower maximum altitudes than during day.

In case I.1 the reaction rate between O_3 and oleic acid is fast enough so that the decrease in O_3 mixing ratios does not limit the destruction of the film and thus vertical transport controls the maximum altitude at which coated sea salt aerosols can be found.

4.3.1.3   Scenario III

The lifetime of the organic surface film can also be increased when it is assumed that only a small fraction of the organic constituents react with O_3 using the laboratory-derived reactive uptake coefficient and that the largest fraction of the surfactants reacts with OH. For such a scenario an initial concentration of 62 mmol/l for 'ORG' and an oleic acid con-

centration of about $47\,$mmol/l is sufficient to transport coated particles into upper levels of the boundary layer (case III.3, light blue line, Figure 4.2 ,III a). However, in case III.3 coated particles reach altitudes greater than $200\,$m only during day and the first hours of the nights. As explained above, turbulent transport in the MBL is stronger during night than during day. For case I.3 this lead to a larger maximum altitude where coated particles can be found during night ($200\,$m, see Figure 4.2, I a). For all cases of scenario III (and also cases II.2, II.3) it leads to the opposite effect because stronger turbulent transport also leads to a higher relative humidity during night in the upper levels of the MBL so that aerosol growth is facilitated leading to larger aerosol particles. That means that at altitudes of $200\,$m to $700\,$m the organic concentration which is needed to form a complete monolayer is slightly larger during night than during day. To visualise this effect, Figure 4.3 d shows the vertical distribution of the sea salt aerosol radius. The black lines show again the maximum altitude, where coated particles can still be found for case III.3 (black dotted line), case III.1 (black dash-dotted line) and case III.4 (black line). As background conditions do not vary between the different cases, the vertical distribution of the radii is almost the same for all cases and thus the sea salt radius is only plotted for case III.1.

The concentration differences between cases III.1 (red dash-dotted line, Figure 4.2 III a,b,c), III.2 (green dotted line, Figure 4.2 III a,b,c), III.3 (light blue line, Figure 4.2 III a,b,c) and III.4 (black line, Figure 4.2 III a,b,c) at these altitudes are very small but sufficiently large to find coated particles at $500\,$m altitude also during night in case III.1 and III.2 but not in case III.3. and III.4. This can best be seen in Figure 4.3 a -c which show the vertical distribution of the sum of oleic acid and ORG concentrations for cases III.1 (a), III.2 (b) and III.5 (c). In case III.5 (blue dashed line, Figure 4.2 III a,b,c) and case III.6 (purple line, Figure 4.2 III a,b,c) where oleic acid and 'ORG' concentrations were low ($39 \text{-} 55\,$mmo/l) but the reactivity of the film was decreased ($\gamma_{OA}=10^{-5}$), coated particles can reach at least an altitude of about $100\,$m to $300\,$m.

As all model runs are initialised with the same fields for meteorology and chemistry, the boundary layer height and its structure is the same for all cases. Therefore, in none of the presented cases particles with a complete monolayer can be found in altitudes exceeding $500\,$m independently of the initial oleic acid and ORG concentrations.

Even though the reactive uptake coefficient for OH on organic aerosols is much larger than for O_3 on oleic acid the reaction rate for the reaction $OH + ORG$ is not as fast as for $O_3 +$ oleic acid. OH is a very short lived radical with concentrations that are several orders of magnitude lower than for O_3 and with gas phase sink reactions up to three orders of magnitude faster than the heterogeneous reaction with the organic film. In contrast to this the reaction with the surfactants becomes one of the fastest O_3 sink reactions leading to its strong destruction as discussed above. This explains the slow destruction of the organic film if it predominantly reacts with OH. For scenario III the lifetime of the film is further increased because OH is not present during night and no other sink reaction for the organic surfactants ('ORG') are taken into account.

4.3.1.4   Summary

To summarise the results from Section 4.3.1 one can say:

- If 50% of the organics were to react with OH and 50% with O_3 and reactive uptake coefficients determined in the laboratory are valid under atmospheric conditions, then the initial concentration of both species have to be larger than $40\,$mmol/l so

Figure 4.4: **Scenario III:** Time evolution of gas phase mixing rations at $50\,\mathrm{m}$ altitude for three days (midnight day 1 - midnight day 3). The time is given in hours since model start. Case III.1 (red, dash-dotted), case III.2 (green, dotted), case III.5 (blue, dashed), base case (black, solid line). $Br_{tot}=HBr+HOBr+BrNO_2+BrNO_3+2\cdot Br_2+BrCl+Br+BrO$ $Cl_{tot}=HCl+HOCl+ClNO_2+ClNO_3+2\cdot Cl_2+Cl+ClO+OClO+\ 2\cdot Cl_2O_2+BrCl$

that coated particles are present at least in the lowest 50 meters of the MBL or above.

- If more than 50% of the organics react with OH, an initial ORG concentration of $70\,\mathrm{mmol/l}$ and an initial oleic acid concentration of 78 mmol/l is enough to find covered particles even at 400-500 meters altitude (case III.2).

- To survive long enough in the atmosphere to be important, either i) the largest fractions of the organic film have to be compounds that react with OH (or at least that do not react with O_3) when assuming that measured reactive uptake coefficients are correct (cases III.2, III.3), or ii) if about 50% of the organics should react with O_3 (cases II.2, III.6) the reaction rates have to be at least a factor of five smaller than those derived in the laboratory.

4.3.2   Effects of reduced mass transfer on chemistry

The net effect of the decreased mass transfer due to an organic coating on atmospheric chemistry mainly depends on the lifetime of the film. Therefore results from scenario II and III are very similar and only scenario III is discussed in more detail in this section. It can be expected that especially those species are influenced by the decreased mass transfer
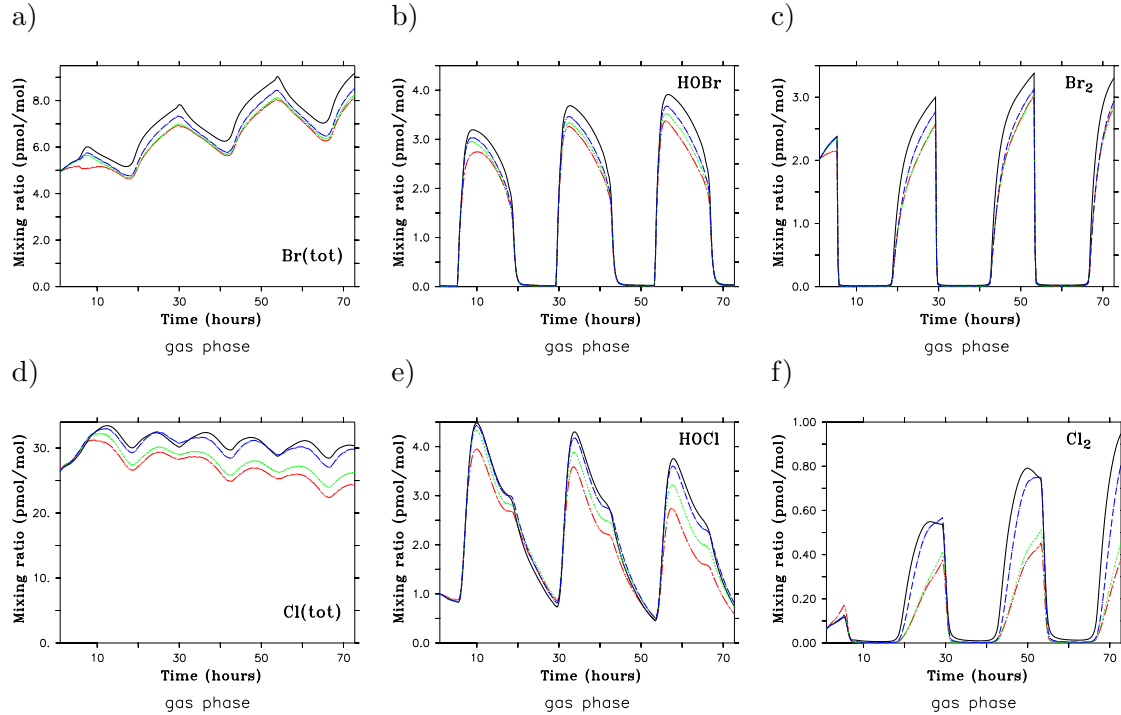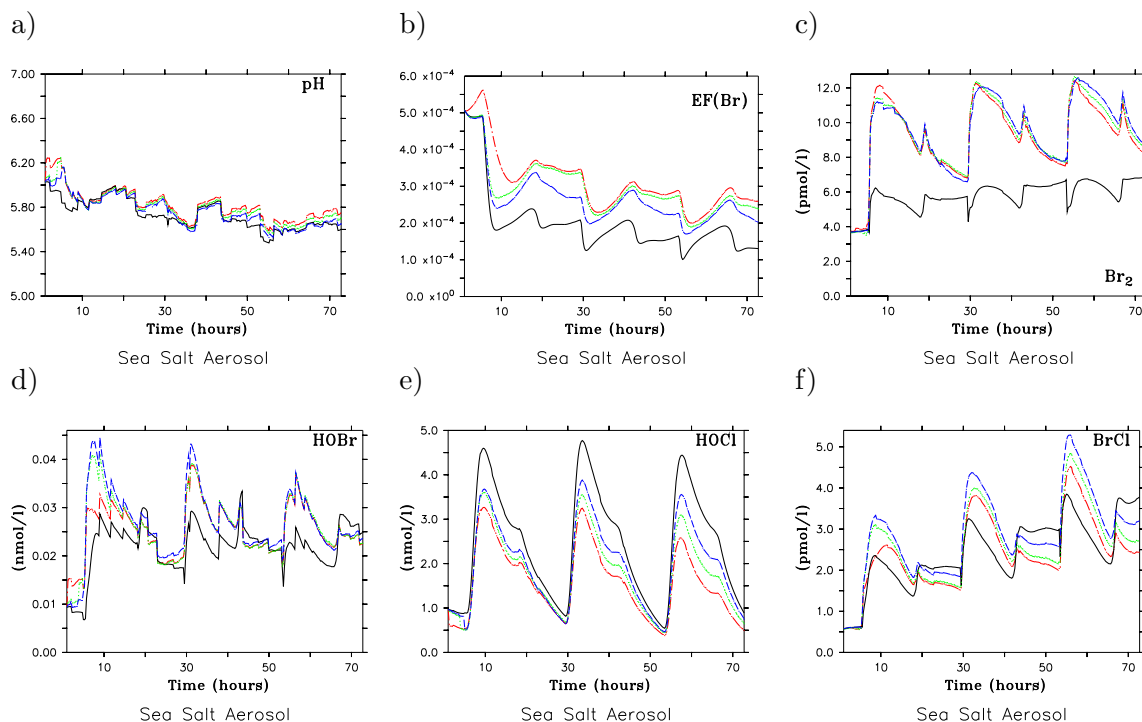
Figure 4.5: **Scenario III:** Time evolution of aqueous phase concentrations at $50\,m$ altitude for three days (midnight day 1 - midnight day 3). The time is given in hours since model start. Case III.1 (red, dash-dotted), case III.2 (green, dotted), case III.5 (blue, dashed), base case (black, solid line).

due to an organic coating that i) directly take part in heterogeneous reactions or uptake processes; or ii) species that take part in acid catalysed reactions.

Sea salt aerosols get rapidly acidified in the atmosphere by uptake of acids like HNO_3 or H_2SO_4. These processes are slowed down by the organic surface film leading to slightly higher gas phase concentrations and lower aqueous phase concentrations of HNO_3 ($\Delta HNO_{3(aq)}$: 1 - $3\,nmol/l = 10\text{-}40\%$ for case III.1) in contrast to the base case whereas differences in H_2SO_4 concentrations in the gas phase as well as in the aqueous phase are negligibly small. Although the uptake of acids is decreased by one order of magnitude for all cases of scenario III, the decrease of H^+ concentrations in sea salt particles is relatively small and the aerosol pH is hardly changed when it is compared with the base case (Figure 4.5). Only in the case with highest rates for the surface reaction (case III.1, red dashed line) the pH increases from 5.60 to 5.65 at day three of the simulation. These differences are too small to significantly influence aqueous phase chemistry and acid catalysed aqueous phase reactions.

The following discussion is mainly focused on tropospheric halogen chemistry because concentrations of halogen species are strongly controlled by exchange processes between the gas and the aqueous phase as well as by the acidity of the aerosol.

4.3.2.1 Effect on halogen chemistry

In Figure 4.4 the mixing ratios of total gas phase bromine (Fig. 4.4 a) and chlorine (Fig. 4.4 d) species are plotted. For all cases the mixing ratios are lower than without an organic

coating (black line) which has to be attributed to the decreased mass transfer out of the liquid phase. However, the difference after three days of simulation time for case III.1 is only 9% for total bromine. For gas phase chlorine mixing ratios the same effect can be observed but the differences are larger (10% - 20% for case III.1). This trend can be observed for nearly all species, i.e. ΔCl: 20 - 30%, ΔClO: 20 - 40%, ΔCl$_2$: 50 - 80%, ΔHOCl: 10 - 30% versus ΔBr: 5 - 15%, ΔBrO: 15 - 25%, ΔBr$_2$: 20 - 30% or ΔHOBr: 15 - 20% (numbers refer to case III.1, see Fig. 4.4 b, c, e, f). For both other cases of scenario III the differences are even smaller. Hardly any difference in total chlorine mixing ratios can be seen for case III.5 (blue dash-dotted line).

During day, one of the main sources for gas phase Cl and Br is the photolysis of BrCl which degasses out of the aerosol. Due to the organic coating less BrCl gets into the gas phase leading to a reduced Cl and Br production by this reaction pathway (Figure 1.1). A second important source for Br is the photolysis of Br$_2$ which also degasses more slowly out of the aerosol when an organic coating is present. A corresponding source for Cl is photolysis of Cl$_2$. However, this reaction is about 80% slower than photolysis of Br$_2$. Thus night time Br$_2$ mixing ratios are in all cases about a factor of three larger than night time Cl$_2$ mixing ratios (Fig. 4.4 c, f). The lower Br and Cl gas phase concentrations in the presence of an organic surface coating lead to lower concentrations of their reaction products like HOBr, BrONO$_2$ and, respectively, HOCl, and ClONO$_2$ which are taken up by the aerosol or take part in heterogeneous surface reactions (ClONO$_2$, BrONO$_2$). Uptake and surface reactions are also slowed down so that less bromine and chlorine are transported from the gas phase into the aerosol phase compared to the base case.

In Figure 4.5 concentrations of HOBr (Fig. 4.5 d) and HOCl (Fig. 4.5 e) in the aqueous phase (= sea salt aerosol phase) are plotted. It can be seen that at day time HOCl concentrations decreased and HOBr concentrations increased when an organic coating was present on sea salt aerosols compared to the base case (ΔHOCl $\approx$ +(30 - 50%), ΔHOBr $\approx$ -(20%), again numbers refer to case III.1, red dash-dotted line in Fig. 4.5). A very important reaction for starting bromine chemistry in the aqueous phase is the conversion of Br$^-$ into Br$_2$ or BrCl by the following reactions:

$$HOBr + Br^- + H^+ \quad \longleftrightarrow \quad Br_2 \qquad (4.4)$$
$$HOBr + Cl^- + H^+ \quad \longleftrightarrow \quad BrCl \qquad (4.5)$$
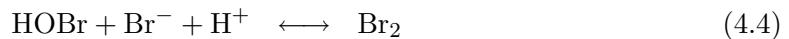
Both reactions are equilibrium reactions which usually produce Br$_2$ and BrCl in the forward reactions. If the organic film is present, Br$_2$ and BrCl accumulate in the aqueous phase because the transfer into the gas phase is decreased (Fig. 4.5 c, f). As a consequence the reverse reactions gain in importance and produce HOBr and Br$^-$ leading to larger HOBr aqueous phase concentrations compared to the base case. Equivalent reactions take place including HOCl instead of HOBr leading in general to the production of Cl$_2$ and BrCl.

$$HOCl + Cl^- + H^+ \quad \longleftrightarrow \quad Cl_2 \qquad (4.6)$$
$$HOCl + Br^- + H^+ \quad \longrightarrow \quad BrCl \qquad (4.7)$$
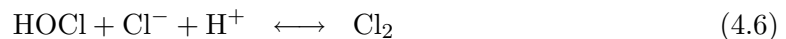
However, these reactions are slower and the backward reaction of Reaction 4.7 is negligible. As a result, with an organic coating even more HOCl is consumed and converted into BrCl (via Reaction 4.7) because of larger Br$^-$ concentrations. Br$^-$ concentrations are slightly larger if particles contain a surfactant monolayer as the equilibrium of Reaction 4.4 is shifted more towards the backward reaction, i.e. the production of HOBr and Br$^-$.

The shifting of the equilibria due to the decreased mass transfer between gas phase and liquid phase explains the *increase* in concentrations of aqueous phase bromine species. For aqueous phase chlorine this shift does not take place which explains the *decrease* in concentrations in comparison with the base case.

During night time, differences in HOCl and HOBr concentrations between the base case and the cases assuming an organic coating on the aerosol particles are smaller. As sunlight is required to activate the cycling of halogen species between the gas phase and the aerosol phase, uptake processes are in general of lower importance during night time which explains why ΔHOBr and ΔHOCl is smaller at darkness. It was pointed out above, that BrCl accumulates in the aerosol during day time (Fig. 4.5 f). However, BrCl concentrations in cases III.1, III.2, III.5 are lower than in the base case during night. During daytime the net flux of BrCl is directed out of the aerosol into the gas phase where BrCl gets quickly photolysed. During night time, when the main BrCl sink reaction (i.e. photolysis) does not take place the net flux of BrCl is directed from the gas phase into the aerosol. As the uptake of BrCl is decreased in case of an organic surface film, aqueous phase concentrations are lower than in the base case during night. At the same time, gas phase BrCl mixing ratios are slightly larger during night time if aerosols are coated by surfactants compared to the base case.

Figure 4.5 also shows the bromine enrichment factor which is defined as follows:

$$EF(Br) = \frac{\left(\frac{[Br^-]}{[Na^+]}\right)_{particle}}{\left(\frac{[Br^-]}{[Na^+]}\right)_{seawater}} \tag{4.8}$$

The Br enrichment factor is about 30 - 40% higher for case III.1 (red dashed line) compared to the base run. Case III.1 shows the largest differences because the lifetime of the organic coating is longer than in other cases and sea salt aerosols which contain a surfactant monolayer reach larger altitudes than in the other simulated cases. Aqueous phase bromine species like HOBr, BrCl, HBr show differences in the range of 30% compared to the base case (in contrast to about 20% in the gas phase). HOCl aqueous phase concentrations decrease by about 40-50%. Aqueous phase chemistry seems to be affected more by organic coatings than gas phase chemistry.

As less aqueous phase chlorine is present in model runs with a surfactant coating even less chlorine can degas in comparison to bromine and in comparison with the base case. This explains why gas phase chlorine concentrations decrease much stronger than bromine concentrations. When less gas phase chlorine is produced, smaller amounts can also be taken up by the aerosol so that the effect intensifies itself.

Comparing the different cases assuming an organic coating on sea salt aerosols, not all species are affected to the same extent by the different model setups. Hardly any difference can be seen between case III.1, III.2 and III.3 for $Br_{2(aq)}$, $HOBr_{(aq)}$ or $Br_{2(g)}$ concentrations whereas the decrease in $Cl_{2(g)}$, $HOBr_{(g)}$, $HOCl_{(g)}$ or $HOCl_{(aq)}$ concentrations is much larger in case III.1 (red dash-dotted line in Fig. 4.4, 4.5) than in case III.5 (blue dashed line in Fig. 4.4, 4.5).

4.3.2.2 Effect on non-halogen chemistry

Apart from halogen chemistry other species are also affected by the decreased mass transfer due to the organic film. Plots in the bottom row of Figure 4.6 show aqueous phase concentrations of NO_3^- (d), SO_2^{4-} (e) and HO_2 (f). Higher aqueous phase concentrations for
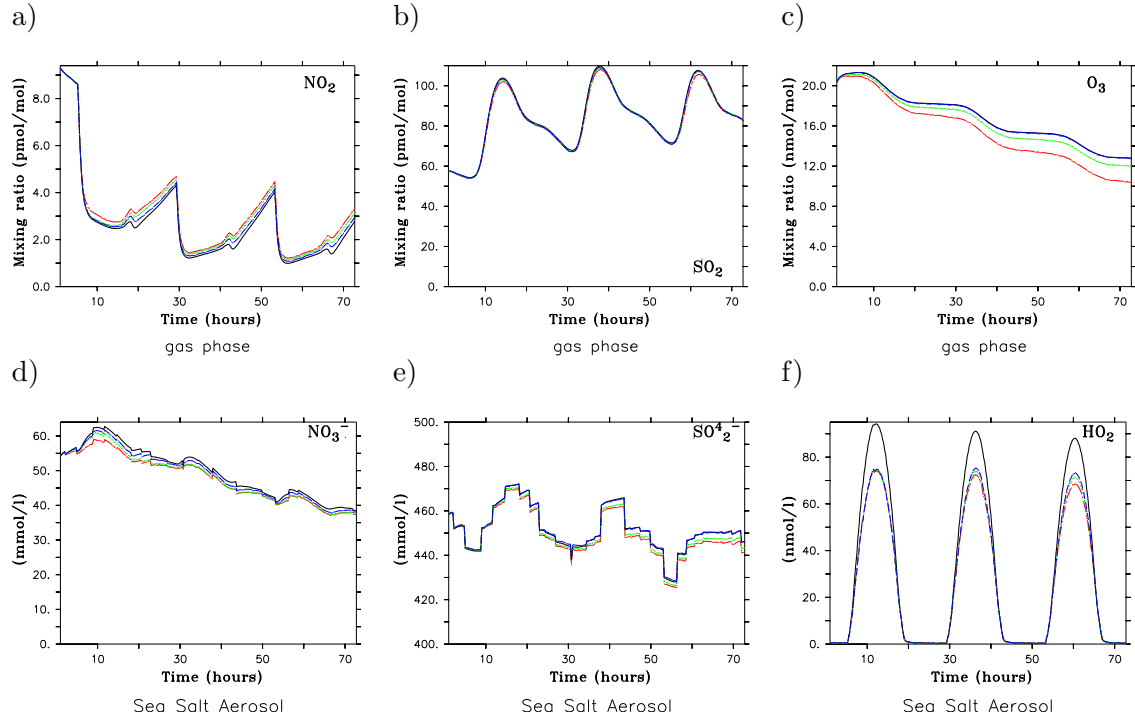
Figure 4.6: **Scenario III:** Time evolution of gas phase mixing ratios (top row) and aqueous phase concentrations in sea salt aerosols (bottom row) at 50 m altitude for three days (midnight day 1 - midnight day 3). The time is given in hours since model start. Case III.1 (red, dash-dotted), case III.2 (green, dotted), case III.5 (blue, dashed), base case (black, solid line).

NO_2 (ΔNO_2: -100%, not plotted), NO_2^- (ΔNO_2^-: -100%, not plotted), HONO (ΔHONO: (-20)-(-100)%, not plotted) and lower aqueous phase concentrations for HO_2 (ΔHO_2: 20%) or HNO_3 (ΔHNO_3: 10-40%, not plotted) can be observed as the concentrations of theses species directly depend on exchange processes between the aerosol and the gas phase. However, the absolute concentrations of all those species are very low so that the relatively small deviation from the base case does not influence any other processes. HNO_3 quickly dissociates in the aerosol phase into H^+ and NO_3^-. Even though the uptake of HNO_3 is decreased, almost no difference can be seen in aqueous phase concentrations of NO_3^- between e.g. case III.1 and the base case (ΔNO_3^-: 3%). The influence of the decreased uptake coefficients on the sulfur cycle is also negligible. The difference between aqueous phase sulphate concentrations in case III.1 and the base case is less than 1% (Fig. 4.6 e).

Plots in the top row of Figure 4.6 show gas phase mixing ratios of NO_2 (a), SO_2 (b) and O_3 (c). For the gas phase nearly no difference in NO, NO_2 or N_2O_5 concentrations are found. However, all model runs were performed under clean marine conditions with very low NO_x mixing ratios. No differences between cases III.1, III.2 or III.5 and the base case can be seen in SO_2 mixing ratios or any sulfur containing species.

In Section 4.3.1 the loss of O_3 due to the heterogeneous reaction with the organic surfactants was discussed in detail. For case III.1 where oleic acid concentrations are highest for all cases of scenario III, the decrease in O_3 mixing ratios within three days is still significant (Fig. 4.6 c).
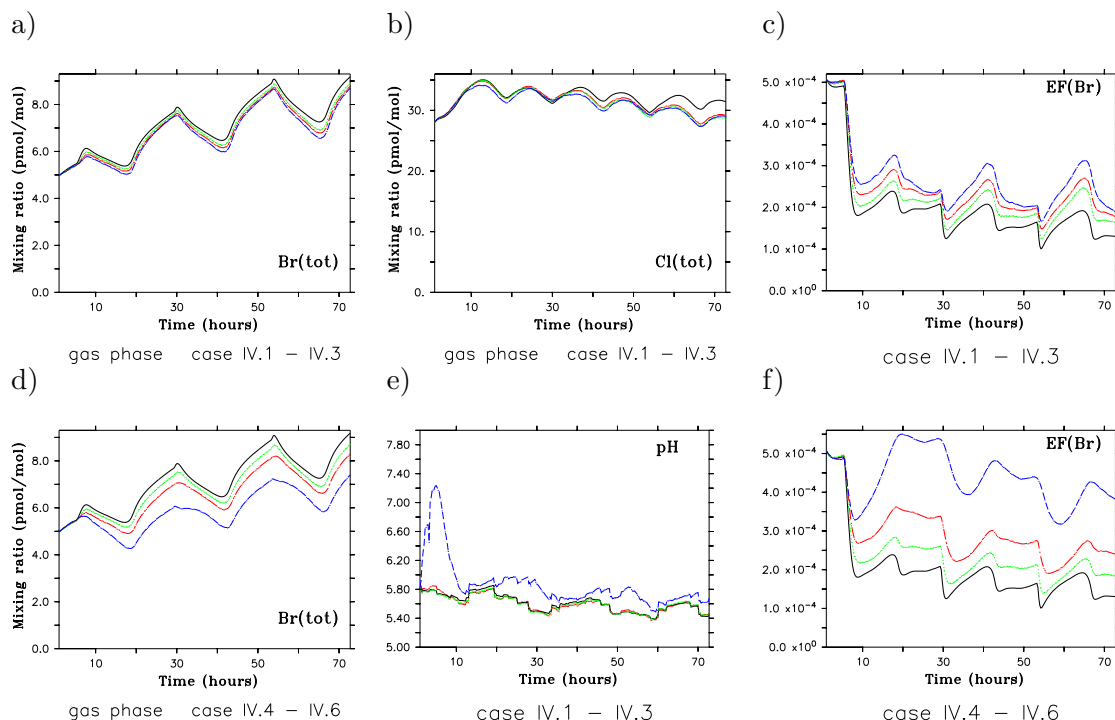
Figure 4.7: **Scenario IV:** All plots show time series at 70 m altitude for three days (midnight day 1 - midnight day 3). Plots (a, b, c, e) refer to cases IV.1 - IV.3. The colour code is as follows: case IV.1 (green, dotted), case IV.2 (red, dash-dotted), case IV.3 (blue, dashed), base case (black, solid line). Plots d), f) refer to cases IV.4 - IV.6. The colour code is as follows: case IV.4 (green, dotted), case IV.5 (red, dash-dotted), case IV.6 (blue, dashed), base case (black, solid line).

4.3.2.3   Impact of magnitude of uptake decrease

In all scenarios discussed above it was assumed that if sea salt aerosols are completely covered with an organic monolayer the accommodation coefficient is reduced by one order of magnitude. Literature values for the strength of uptake reduction vary from a factor of 3-4 (Thornton and Abbatt, 2005) to a factor of 42 (Badger et al., 2006). To quantify how chemistry responds to different uptake behaviour onto sea salt aerosols sensitivity studies were performed where the accommodation coefficients for gas phase species were reduced by various orders of magnitude (Table 4.1, scenario IV). For cases IV.1 - IV.3 the initial organic concentrations were relatively small so that the maximum altitude where particles with a complete monolayer can be found is 90 m (similar setup than for case I.2, Figure 4.2, Ia, green line). For cases IV.4 - IV.6 the same initial conditions were chosen as for case III.2 so that coated particles can be found at 400 m altitude during the whole simulation time (Figure 4.2, IIIa, green dotted).

In Figure 4.7 time series of total gas phase chlorine and total gas phase bromine concentrations at 50 m altitude are plotted for scenario IV. Apparently gas phase chemistry is not very sensitive to the magnitude of uptake reduction for cases IV.1 - IV.3 (Figure 4.7 a-d). A decrease of the accommodation coefficient by a factor of 4 (case IV.1) leads to 4% smaller concentrations for total Br and about 6% smaller concentrations for total Cl compared to the base case. The concentrations hardly decrease any further (6% for Br and Cl) in

case IV.3 where uptake was decreased by about two orders of magnitude. Similar effects can be observed for nearly all gas phase species. As a decrease of the accommodation coefficient by two orders of magnitude leads to a decrease of the mass transfer coefficient by about one order of magnitude only (Figure 4.1) the differences in reaction rates for the cases of scenario IV are less than one order of magnitude.

Larger differences between the three cases can be observed for the liquid phase like it can be expected from the results from scenario III. The Br enrichment factor is increased by 10-30% for case IV.1, 20-40% for case IV.2 and 40-90% for case IV.3 compared to the base case. The differences increase with simulation time indicating that the enrichment of Br in the aerosol due to the organic coating gets stronger the longer the monolayer is present. Sea salt pH does not increase significantly for cases IV.1 and IV.2 but it increases from about 5.6 (base case, day 3) to about 6.4 for case IV.3. In comparison with the results from scenario III a long-lived organic coating with a relatively low uptake reduction (scenario III) has more influence on atmospheric chemistry than a short-lived organic monolayer with a relatively large uptake reduction (scenario IV, case 1-3).

For cases IV.4 - IV.6 where the lifetime of the organic coating is long, chemistry is much more sensitive to the magnitude of uptake reduction as can be seen in Figure 4.7 (e) and (f). When the destruction of the organic coating is slow and the accommodation coefficient is reduced by about two orders of magnitude total bromine concentrations decrease by about 20 % and the enrichment factor increases even by about 100 %.

While discussing the effect of the magnitude of uptake reduction in this section it was said that the effect of a reduced mass transfer starts to get significant when the accommodation coefficient is reduced by a factor of at least 0.1 and more. However, these sensitivity studies are rather conceptual investigations that can point out potential effects, but measurements have still to confirm that a reduction of the accommodation coefficient by a factor of 0.1 might happen in the real atmosphere.

Chapter 5

Influence of organic surface films on diffusional growth of aerosols

For all of the above discussed cases of scenarios I-IV, it was assumed, that the mass accommodation coefficient for water vapour (α_c) and thus diffusional growth of aerosol particles is not affected by the organic surface film. In general the uptake of all gases should be affected by the surfactants in a similar way. However, under cloud free conditions the diffusion of water vapour onto sea salt particles is low anyway. No difference in the size of the particles or their mean radius, i.e. the sea salt radius that is used for calculating chemistry can be seen whether reducing the accommodation coefficient for water vapour or not reducing it. Thus the additional decrease of the accommodation coefficient for water vapour can be neglected under cloud free conditions.

Under cloudy conditions, diffusional growth of aerosol particles is of more significance such that decreasing the uptake of water vapour onto particles containing an organic surface film might alter the aerosol size distribution and potentially the mean radius of the particle spectrum, i.e. the sea salt/sulphate aerosol radius (see Section 2.4.2). Therefore, a set of model runs was additionally performed under cloudy conditions which are discussed in the following.

5.1 Setup of model runs

To study the sensitivity of the model to changes in the water vapour diffusion rate, at first six model runs were performed letting the model run without calculating chemistry. The meteorological conditions and the initial setup are the same for all of the six simulations. Again, the model is run for three days to have a spin up and the following three days are discussed in this section. Start of the simulation is at midnight (day 1) and the end is again at midnight (day 3). Meteorological conditions are such that a cloud develops immediately between 300 and 800 m altitude. Temperature decreases from 15°C in the lowest model levels to 8°C in the upper parts of the boundary layer and relative humidity increases respectively from 80% directly above the ocean surface to 100% in the cloud layer at the top of the boundary layer. Diffusional growth in the model is calculated following the approach of Pruppacher and Klett (1997) as described in detail in Section 2.3.

For scenario DEF the accommodation coefficient for water vapour (α_c) is left on its default value of $3.6 \cdot 10^{-2}$. For scenario ALL$_1$ α_c is reduced for all particles by a factor of 0.5, for scenario ALL$_2$ by a factor of 0.1 and for scenario ALL by a factor of 0.05. For scenario

SEA only particles in the sea salt size range, i.e. particles with a dry radius larger than $0.5\,\mu$m are assumed to be affected by a reduction of α_c by a factor of 0.05 and in scenario SUL only particles in the sulphate size range respectively. Thus it is assumed that in scenario ALL, all particles are coated completely with an organic surface film for the whole simulation time, for scenario SUL only the sulphate aerosols and for scenario SEA only sea salt particles.

An overview of the different model runs is given in Table 5.1.

DEF	$\alpha_c = \alpha_c$	for all particles
ALL$_1$	$\alpha_c = \alpha_c \cdot 0.5$	for all particles
ALL$_2$	$\alpha_c = \alpha_c \cdot 0.1$	for all particles
ALL	$\alpha_c = \alpha_c \cdot 0.05$	for all particles
SUL	$\alpha_c = \alpha_c \cdot 0.05$	only for particles in sulphate size range
SEA	$\alpha_c = \alpha_c \cdot 0.05$	only for particles in sea salt size range

Table 5.1: Overview of model runs under cloudy conditions without calculating chemistry.

5.2   Results

5.2.1   Cloudy conditions without chemistry

In all model runs discussed in Chapter 4 it was assumed, that only sea salt particles are affected by an organic coating mainly because of the lack of knowledge how long chain, marine derived organic compounds could be incorporated into sulphate aerosol particles. In this section the effect of a reduced water vapour uptake on either all particles (ALL), or only sulphate particles (SUL) or only sea salt particles (SEA) is investigated. In all cases the accommodation coefficient is decreased by a factor of 0.05. Results for those three cases are discussed in the following.

Figure 5.1 a shows the aerosol number distribution, integrated over all dry radii (with respect to Figure 2.1, integrated over the y-axis), in a cloud layer at 700 m altitude at noon (12:00) of the third day of simulation time for cases DEF (black line), SEA (green dotted line), SUL (blue line) and ALL (red dash-dotted line). Figure 5.1 b shows the number of activated particles (again integrated over all dry radii) at 700 m altitude at 12:00 day 3 and Figure 5.1 c shows the liquid water content of the cloud at day 3 of simulation time at 700 m altitude. Obviously hardly any difference can be seen between cases DEF and SEA as well as ALL and SUL, i.e. the green dotted line almost covers the black line and the red dash-dotted line covers almost the blue line in all plots in Figure 5.1. As the total number of sea salt aerosols is very low, modifying only the water vapour uptake onto these particles has not influence on the total aerosol particle number distribution. Furthermore, with respect to absolute numbers, sulphate aerosol particles are the most prevalent ones. Thus changing the water vapour uptake onto these particles leads to almost the same effect as reducing the accommodation coefficient for all particles.

  Due to the similarities of the cases DEF and SEA as well as SUL and ALL, in the following it is only referred to cases DEF and ALL and these two cases are compared. The character of the three-modal aerosol distribution can very well be seen in the three maxima for all cases. Comparing scenarios DEF and ALL, two general differences can be seen: (i) The spectrum is shifted to smaller radii for case ALL compared to case DEF. (ii) Maxima (minima) in the number distribution are more pronounced in case ALL than in

a)   b)   c)

Particle number distribution   Particle Nb of activ. particles at 700m   Liquid water content at 700m

Figure 5.1: Plots show the particle number distribution (integrated over all dry radii, a) and the number of activated particles (integrated over all dry radii, b) at noon of the third day of simulation time at 700 m altitude. The liquid water content at 700 m altitude for the third day of simulation time (6:00 day 3 - 18:00 day 3) is shown in Figure (c). The colour code for the plots is as follow: black solid line (DEF), green dotted line (SEA), blue solid line (SUL), red dash-dotted line (ALL).

case DEF.
Due to the limited water vapour diffusion, growth of particles in case ALL is slowed down compared to case DEF. As a consequence, much more particles can be found in the 'small size range' between 0.1 and 1 μm in case ALL, compared to case DEF. At the same time much less particles can be found in the larger particle mode (1 - 10 μm) in case ALL compared to case DEF. Furthermore, the absolute minimum size of particles has shifted to a smaller value in case ALL (0.08 μm in DEF, 0.06 μm in ALL). Additionally the maximum of the largest mode has shifted to smaller radii in case ALL (7.5 μm in DEF, 5.1 μm in ALL). As a further consequence of the inhibited growth process in case ALL, less particles get activated as can be seen in Figure 5.1 b. Particles are regarded as 'activated' if their (wet) radius is larger than their critical radius (see Section 2.3). As more particles

a)   b)   c)

Δ N$_{act}$ (%), DEF $-$ ALL   Particle number distribution   Nb of activ. particles at 700m
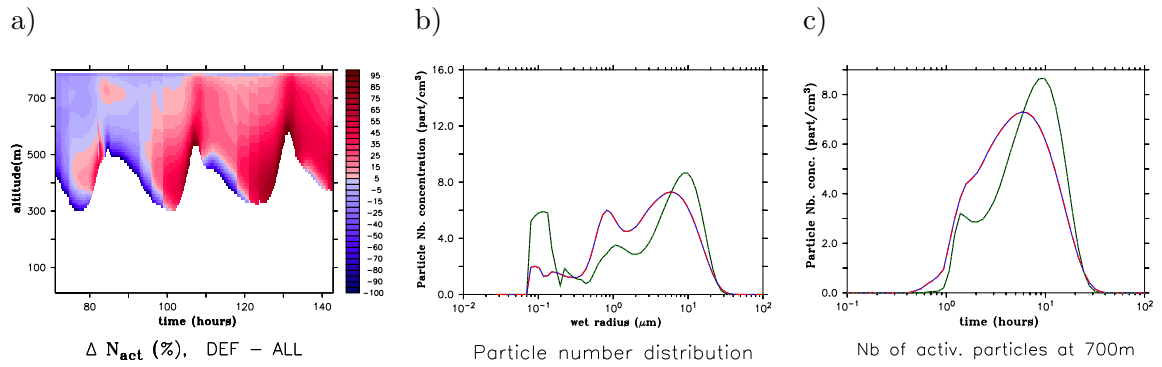
Figure 5.2: Plot (a) shows the relative difference in the number of activated particles in the cloud layers between cases DEF and ALL for the three days of simulation time (midnight day 1 - midnight day 3). Plots (b) and (c) show the particle number distribution (integrated over all dry radii) and the number of activated particles (integrated over all dry radii) at noon at day 1 of the simulation time at 700 m altitude. The colour code for the plots is as follow: black solid line (DEF), green dotted line (SEA), blue solid line (SUL), red dash-dotted line (ALL).

a)   b)   c)

Particle number distribution   Number of activated particles   Liquid water content at 700m
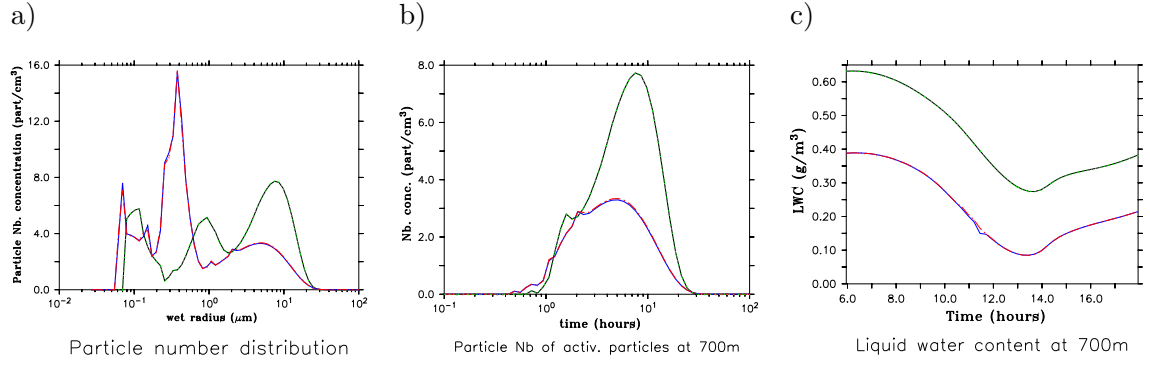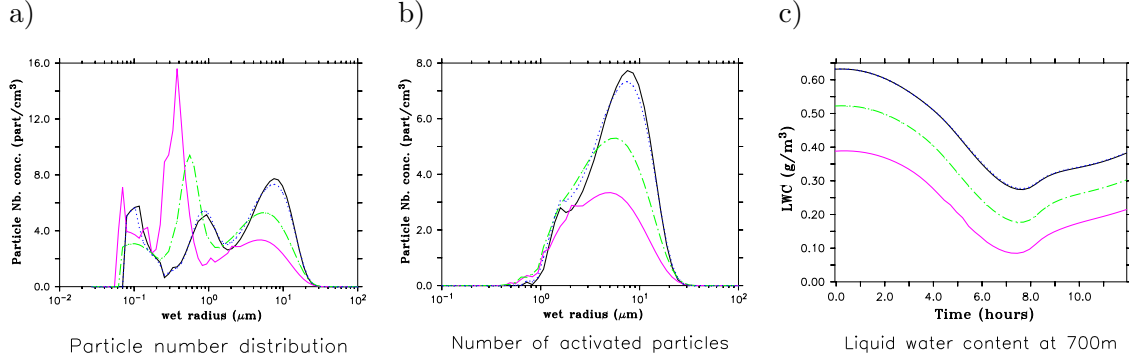
Figure 5.3: Plots show the particle number distribution (integrated over all dry radii, a) and the number of activated particles (integrated over all dry radii, b) at noon of the third day of simulation time at 700 m altitude. The liquid water content at 700 m altitude for the third day of simulation time (6:00 day 3 - 18:00 day 3) is shown in Figure (c). The colour code for the plots is as follow: black solid line: DEF, blue-dotted line: ALL_1, green dash-dotted line: ALL_2, purple solid line: ALL

exceeding their critical radius and thus having a comparatively higher water content in case DEF, the cloud liquid water content in this case is also higher than in case ALL (see Fig. 5.1 c).

Thus in general, the potential of the cloud in case ALL to form rain droplets is lower than in case DEF. Furthermore, as more smaller particles are present in case ALL, the properties of the cloud with respect to light scattering differs from that of the cloud in case DEF.

However, looking at the aerosol number distribution and the number of activated particles in cases DEF and ALL at day 1, exactly the opposite effect as discussed above can be observed, i.e. more activated particles can be found in a cloud layer in the case where the accommodation coefficient for water vapour was reduced by a factor of 0.05. Figure 5.2 a shows the relative difference in the number of activated particles between case DEF and case ALL all over the cloud for the three days of simulation time. If the difference has a positive sign this corresponds to more activated particles in case DEF and a negative sign means more activated particles in case ALL. The thickness of the cloud increases during day and decreases during night time.

Even though the accommodation coefficient of water vapour is decreased in case ALL, particles can still take up water and grow. However, they grow to less larger sizes than in case DEF. Even though at day 1 more particles get activated in case ALL, these particles are only slightly larger than their critical radius, whereas in case DEF particles grow further and reach sizes that are significantly larger than their critical radius, i.e. in the size range 0.5 - 6 μm more activated particles can be found in case ALL than in case DEF whereas in the size range $> 6\,\mu$m more activated particles can be found in case DEF (see Fig. 5.2 b, c). The maximum in the curve describing the number of activated particles is at $\approx 10\mu$m for case DEF, whereas it is at $\approx 4\mu$m in case ALL (Fig. 5.2 b, c). When the vertical extent of the cloud starts to decrease during day time, i.e. when the ambient saturation ratio decreases, water evaporates from the particles and they shrink. In case ALL, the majority of those particles that are activated have a size only exceeding their critical radius slightly. When water vapour evaporates from these particles, they shrink quickly to a size such that their radius is below the critical radius. Thus these particles

are not activated anymore.

In case DEF those particles that have grown into the activated size range could take up comparatively more water than particles in case ALL. Even though these particles become smaller as soon as water vapour evaporates from them, they still have radii exceeding the critical radii. Thus more particles stay activated during day (see Fig. 5.2 a at time = 80 h, 100 h = morning day 1 and day 2).

This 'turnover' affects the whole cloud from day 2 onward as the ambient relative humidity as well as the liquid water content of the cloud decrease with time in case ALL compared to case DEF. This is an indirect feedback of the different cloud properties due to the limited water vapour uptake in case ALL compared to case DEF. As the relative humidity decreases with time in case ALL, the saturation ratio in the cloud is lower and particle growth is less facilitated than in case DEF.

In general the relative difference in the number of activated particles is largest in the lowest cloud levels. However, the absolute number of activated particles in this region of the cloud is negligibly small.

Feingold and Chuang (2002) performed similar sensitivity studies with a parcel model, assuming that only a certain fraction of aerosol particles is affected by an organic coating and experience a reduction of the water vapour diffusion. Feingold and Chuang (2002) observe a spectral broadening in both directions, towards the larger and the smaller particles whereas in case ALL (as well as case SUL) only a broadening of the spectrum towards smaller radii can be observed. Feingold and Chuang (2002) use slightly differing parameters determining their initial aerosol number distribution and they assume that the organic surfactants are equally distributed on particles of all size ranges. Feingold and Chuang (2002) conclude, that those particles not being coated by surfactants can grow more rapidly as they do have to compete with fewer particles for the available amount of water vapour. Thus for those particles growth is more facilitated and the spectrum also broadens towards the larger particles. This process is intensified by coagulation, a process that is not included in the standard version of MISTRA. Thus the second phenomenon cannot be observed in the model studies done in this thesis. Even though the accommodation coefficient was only reduced for small particles in case SUL, the additional available amount of water is not sufficient to let larger particles grow to even larger sizes in case SUL than in case DEF.

Due to the uncertainties about the magnitude of uptake reduction, again several sensitivity model runs were performed to test various reduction factors of the accommodation coefficient and their influence on diffusional growth. For case ALL_1 α_c is reduced by a factor of 0.5, for case ALL_2 by a factor of 0.1 for case ALL by a factor of 0.05, which is the case already discussed above. For an overview of the model runs, see Table 5.1

Figure 5.3 a) shows again the particle number distribution with respect to the wet radius and integrated over all dry radii, the number of activated particles is shown in Figure 5.3 b and the cloud liquid water content in Figure 5.3 c for cases DEF (black line) ALL_1 (blue dotted line), ALL_2 (green dash-dotted line) and ALL (purple line). All three plots are again drawn in a cloud layer at 700 m altitude at noon of the third day of simulation time. As can be seen in Figure 5.3 a, reducing the accommodation coefficient by only a factor of 0.5 (ALL_1, blue dotted line), has hardly any effect on the aerosol size distribution. In case ALL_2 however, the spectrum shows already the same shift to smaller particles as discussed above. The number of activated particles is also significantly lower in case ALL_2

compared to DEF. Reducing the accommodation coefficient further by a factor of 0.05 (ALL), the spectrum shifts further to smaller particles, the number of activated particles further decrease as well as the liquid water content as discussed above.

5.2.2 Cloudy conditions with Chemistry

A set of model runs was also performed under cloudy conditions including the explicit treatment of chemistry in the model. However, regarding the above discussed results regarding the lifetime of the organic surface coating and regarding the effect of a reduced accommodation coefficient of water vapour only affecting diffusional growth of sea salt particles, it is not necessary to discuss those model simulations in detail as no other effect on chemistry as showed in Chapter 4 can be seen and as the aerosol size distribution is not affected, not even the sea salt radius is affected.

Initial ORG concentrations of 720 mmol/l and oleic acid concentrations of 320 mmol/l have to be assumed to find coated particles in at least the lowest 100 m of the cloud, i.e. the total load of organics is about a factor of 1.3 higher than the total organic concentration that were assumed for scenario III.1. However, those concentrations are still too low to get significant concentrations of organic surfactants on sea salt *droplets* such that they could also form a complete coating on those large particles. Furthermore, the absolute number of sea salt *aerosols* within the cloud is negligibly small.

Chapter 6

Summary of results

The influence of a reduced mass transfer between the gas phase and the aerosol phase caused by an organic surfactant coating on tropospheric chemistry with a special focus on halogen species was investigated. In general the simulations show, that gas phase bromine and chlorine concentrations decrease in the presence of an organic monolayer on sea salt aerosols. Chlorine gas phase chemistry is affected stronger than bromine chemistry. The effect of a reduced mass transfer on aqueous phase chemistry is stronger than on gas phase chemistry leading to an increase in bromine concentrations and a decrease in chlorine concentrations.

Even though the presence of a coating reduces the uptake of acids, the pH of the sea salt aerosol is not influenced until uptake was decreased by nearly two orders of magnitude.

The impact of the lifetime of the organic surface film and therefore the height at which coated particles can still be found within the MBL, is larger than the variation of the order of magnitude of the uptake reduction. I.e. reducing the accommodation coefficient by more than one order of magnitude but having coated particles only in the lowest $100\,\mathrm{m}$ of the boundary layer has a negligible effect on gas as well as aerosol phase chemistry whereas an uptake reduction on the same order of magnitude leads to a much larger, non-negligible effect if coated sea salt particles can be found all over the boundary layer.

In order to study the effects of a reduced mass transfer due to an organic surface film being present on sea salt aerosols, assumptions had to be made regarding:

(i) The density of organic molecules on the aerosol surface. The assumption was made that one molecule of oleic acid is located directly next to the adjacent molecule but as stated out already in the introduction in Section 3.3 it might be possible that organics do not have to be packed this tightly on the aerosol surface to influence mass exchange between gas and liquid phase. (ii) The reactive uptake coefficients for gas phase oxidants on organic surfactants. Even though numerous measurements for uptake coefficients exist the published values are not applicable under atmospheric conditions as the large loss in O_3 due to the heterogeneous reaction with surfactants is not considered as realistic and as the field data indicate that the lifetime of e.g. oleic acid is larger than in laboratory experiments. Therefore sensitivity studies were necessary to show the range of resulting different lifetimes dependant on the reactive uptake coefficients and to show the effect of different lifetimes of a surface coating on atmospheric chemistry. (iii) The composition of the film and decomposition products. As a realistic composition of the film is unknown the surface activity of decomposition products is not known. Every assumption about the reactivity of decomposition products and their ability to be surface active would be speculative so that no further reactions of the initial components of the monolayer were

taken into account in the model simulations. It should be kept in mind that in reality a lot more reactions on the aerosol surface take place that might increase or further decrease the lifetime of the organic coating and that might increase or decrease the reactivity of the film compared to the laboratory measurements. Thus, overall it is very difficult to assess this aspect properly.

The model simulations have shown that assuming that the majority of organic surfactants react with ozone and using the reactive uptake coefficient reported from laboratory studies O_3 concentrations decrease dramatically after three days of simulation time. This effect let the assumption arise that either a multicomponent coating alters uptake behaviour in such a way that reactive uptake coefficients from laboratory studies cannot be applied under atmospheric conditions as discussed above or that only a very small fraction of the organic surfactants react with O_3 and the largest fraction reacts with OH or NO_3. It is likely that a combination of both effects accounts for organic particles in reality.

Regarding the effect of a reduced accommodation coefficient for water vapour (α_c) on microphysical aerosol properties, only reducing α_c for sea salt particles has no effect on the aerosol number distribution whereas the net effect of reducing α_c for only sulphate particles or all particles is a shift of the aerosol number distribution to smaller particles and a smaller number of activated particles.
Decreasing the uptake of water vapour onto sea salt particles under cloudy conditions does not alter the ('mean') sea salt radius and thus has not effect on chemistry in the model.

Chapter 7

Discussion and Conclusions

Motivated by the increasing number of field campaigns identifying a significant organic mass fraction in marine particles as well as laboratory studies dealing with the investigation of the oxidation process of long chain organic surface active compounds, this model study was performed to study the potential impact of organic surface films on atmospheric chemistry.

In general, organic surface films are assumed to be able to influence atmospheric chemistry on two ways, like stated out in Section 3.6 ('Motivation'): (i) Atmospheric processing of the surface film and its follow up products might have an impact on the atmospheric oxidation capacity and on atmospheric reaction cycles. (ii) A reduced mass transfer due to the surface coating might influence gas- and aqueous phase chemistry.

The first aspect is more difficult to assess because of our limited understanding of the structure and the chemical processing of the organic surface coating.

7.1 Atmospheric Processing

With respect to the literature dealing with the ozonolysis of potential surfactants, the atmospheric processing of organic surface films itself has been suggested to have a large impact on atmospheric chemistry (e.g. Bertram et al., 2001; Moise and Rudich, 2002). However, due to all the well known uncertainties and unknown components of the surfactant chemistry it is not possible to quantify this suggestion.

Regarding the influence of the additional heterogeneous reaction between a gas phase species and the organic surfactant on the primary gas phase oxidants itself, it can be seen in the results from this model study, that gas phase OH mixing ratios are hardly affected due to the additional heterogeneous reactions with the surfactants. This is mainly because of the very short lifetime of OH as discussed in Section 4.3.1.

For O_3 no such clear conclusion can be drawn. Reactive uptake coefficients as reported from laboratory experiments are in the range of $7 \cdot 10^{-4}$ - $7 \cdot 10^{-3}$ (Smith et al., 2002; Hearn and Smith, 2004). These large uptake coefficients lead to an approximate lifetime of oleic acid in the laboratory in the range of minutes to hours assuming O_3 mixing ratios of about 100 nmol/mol (Knopf et al., 2005). This result is in strong contrast to field measurements estimating a lifetime of oleic acid that is present in particles of days (Robinson et al., 2006; Rogge et al., 1991). However, Robinson et al. (2006) only analysed organic aerosol particles in areas with strong and continuous anthropogenic emissions. As was said in the introduction in Section 3.1, the strongest known sources for oleic acid are cooking as well

as traffic emissions. As the oleic acid concentrations in aerosol samples show a seasonal cycle, Robinson et al. (2006) further suggest that atmospheric processing of organic surfactants like fatty acids is more efficient in summer than in winter.

Using the reactive uptake coefficients in the model under clean marine conditions ($O_3 \approx$ 20 nmol/mol, mean $NO_2 \approx$ 3 pmol/mol), leads to a significant loss in O_3 mixing ratios compared to the case where no surface film effects were considered (Section 4.3.1.1). It was discussed in Section 4.3.1.1 that it can be assumed that a comparative O_3 loss of up to 30% (Scenario I.3) within three days due to the additional heterogeneous reaction between O_3 and oleic acid is rather unrealistic. Even though, the initial organic load on sea salt particles might even be overestimated - an aspect that will be discussed in more detail below - the organic surface film only comprising of oleic acid is destroyed rapidly within the first 200 m of the boundary layer. Thus with respect to field measurements and with respect to the initial oleic acid concentrations on sea salt aerosols needed for the presence of coated particles also in the upper part of the boundary layer, it can be assumed that scenario II using reduced reactive uptake coefficients of O_3 on oleic acid is the more realistic approach to include this process in a numerical model. Otherwise the concentrations of the surface active species reacting with O_3 have to be very low. However, as the reaction between O_3 and oleic acid - and most likely also with other long chain fatty acids having a double bond - is very fast, the surface film is broken up readily as the model simulations could show and thus at least the effect of the organic film on the mass transfer is negligibly small.

7.2   Decomposition products of the primary oxidation

The question, if and in which ways organic compounds that are decomposition products of an organic surface film can influence and interfere with known chemical cycles in the gas phase as well as in the liquid phase is not possible to answer based on the current state of knowledge. Two of the key questions that need to be answered by laboratory studies are: Are secondary reaction products still surface active? And what is their lifetime?

Almost all laboratory studies dealing with the detection of secondary reaction products from the oxidation of an organic surface film mostly use the oleic acid - ozone system or a similar two - component system. However, even for the well studied oleic acid - ozone - system it is apparently a challenge to determine reaction products.

Asad et al. (2004), Hearn et al. (2005) and Zahardis et al. (2005) suggest that among the reaction products from the ozonolysis of oleic acid that remain in the liquid phase, a large amount of water soluble organic compounds (= WSOC, e.g. dicarboxylic acids) can be found. Dicarboxylic acids are known to be able to decrease the surface tension of an atmospheric particle what potentially might enhance its capability to act as a CCN. However, the influence of WSOC on droplet growth and activation as well as their modification of the Köhler curve is also unclear under the current state of knowledge as was already discussed in the Introduction in Section 3.5.

Apparently a larger fraction of reaction products of the ozonolysis of oleic acid is immediately released into the gas phase in the form of nonanal (Moise and Rudich, 2002; Katrib et al., 2004). However, only one study exists dealing with the further processing of nonanal (Bowman et al., 2003) and its potential atmospheric relevance. Therefore, the uncertainty regarding the yields of products formed by reaction of nonanal and the reaction rates are very large.

It is almost impossible to determine reaction products in a laboratory experiment using a

more realistic multi-component surface film reacting with various gas phase oxidants. As the majority of laboratory studies deal with the detection of secondary products of the ozonolysis of oleic acid, it would maybe improve our understanding of the processing of organic surface films if numerous surfactant/gas phase oxidant systems would be investigated and we would at least get a better idea about the fraction of secondary products staying in the aqueous phase and the volatile fraction degassing rapidly. In order to be able to include follow up reactions of the primary oxidation of the surface film into a numerical model, reaction rates are needed that are based on more than just the ozonolysis of oleic acid.

It was mentioned several times above that the main reason for using oleic acid as a proxy for long-chain organic compounds in this model study is the lack of data regarding any other species. It is very obvious that considering only a two-component system as has been done in nearly all laboratory studies simplifies real atmospheric conditions. In case of oleic acid this leads to two very general problems: (i) Oleic acid has only very rare or only regionally limited sources mainly related to anthropogenic emissions. Thus oleic acid is of minor importance for studying atmospheric chemistry in rural areas or in the marine boundary layer. (ii) Reactive uptake coefficients of O_3 on oleic acid derived from laboratory studies are either not applicable under atmospheric conditions or the fraction of organic species containing a double bond and reacting with O_3 with those rates has to be very small such that O_3 mixing ratios are not affected by this heterogeneous reaction. However, several authors presenting laboratory measurements for the reactive uptake coefficients of O_3 on oleic acid are even aware of this discrepancy between laboratory results and field measurements (Smith et al., 2002; Zahardis et al., 2005).

Thus the work presented in this thesis should be a motivation to leave the oleic acid - ozone system and start studying organic systems and their processing that are of more relevance for the atmosphere. At least, a stronger focus should be put on reactions following the primary ozonolysis and their relevance under atmospheric conditions. Studying the oleic-acid ozone system is rather of interest from the point of view of a physical chemist but rather not from that of an atmospheric scientist studying chemistry in the marine boundary layer.

7.3   Lifetime and structure of the film

For accurately modelling the effect of a reduced mass transfer due to organic surfactants on sea salt aerosols it is very important to know how long the organic coating is complete and how far coated particles can be transported upward within the boundary layer because the longer the lifetime of the film the larger is its possible influence.

However, it could be shown in Section 4.3.1 that a lot of uncertainties exist so that small changes in the initial organic concentrations or the reactive uptake coefficients lead to large differences in the lifetime of the film.

It was pointed out in the introduction, that our current understanding of organic surface films is rather based on a model consumption than on real observations. It is still an open question how an organic coating is structured from the molecular point of view. With respect to the work done by Tervahattu et al. (2002a) who found particles that don't have a solid but a pulsating shape, it appears to be more likely that a film looks more like in Figure 3.1 a than in Figure 3.1 c, i.e. one end of the organic molecule sticks to the aerosol whereas its tail can move freely around the particle. Thus the molecules are not well ordered and do not have to be very densely packed on the aerosol surface to influence

mass transfer. However, still the question cannot be answered, how much the structure of the film depends on its chemical composition. Furthermore, it would be crucial to know how dense the surface film is. How tightly are the organic molecules packed on the aerosol surface? How strongly does this vary with chemical composition? This information is important to know to be able to give an estimate of organic concentrations that are needed to form an 'effective' surface coating, i.e. a surface coating that decreases mass transfer between the gas phase and the aerosol phase. In the model studies presented herein, the assumption was made that one molecule of oleic acid (or ORG) is located directly next to the adjacent molecule. However, as pointed out above, it might be possible that organics do not have to be packed this tightly on the aerosol surface to influence mass exchange between gas and liquid phase. Laboratory measurements show that a monolayer of loosely packed organic compounds can still have an influence on the uptake behaviour (Neill et al., 2006) so that initial surfactant concentrations and the related ozone loss might be overestimated in the model. A further question is: How strong does the uptake reduction depend on the chemical composition of the film? Are all surface active organic compounds able to reduce mass transfer of all uptaken/degassing species in the same way? Are we able to assess a realistic value for at least a mean mass transfer reduction due to an organic surface coating in the near future?

Regarding the number and complexity of organic compounds it is a challenge for the next decade to assess which of those long chain organic compounds and their reactions are of real importance for the atmosphere and should be treated in a numerical model explicitly.

7.4   Organic emission strength

Even though our understanding of the nature and processing of organic surface film might be improved with the help of laboratory studies, our knowledge about the spacial and temporal distribution of surfactants in the marine as well as continental boundary layer is still poor. Is it a common phenomenon that surfactants are incorporated into sea salt particles in the MBL or is it only a regional phenomenon depending strongly on the biological activity in the water? Apparently the seasonal cycle of organic concentrations in marine aerosol particles is strong. Is the incorporation of organic surfactants into sea salt aerosols and the related decrease in mass transfer only of importance in the marine boundary layer in spring when biological activity is largest? Are there hot spot regions where surfactants are continously emitted? Is the fraction of organic material accumulating in the oceanic surface microlayer large enough throughout the year such that the organic mass fraction within aerosols is still large enough to form surface coatings?

As mentioned in the Introduction in Section 3.1, concentrations of organic species or even the water soluble/water insoluble organic mass fraction as measured in aerosol samples vary by several orders of magnitude. Thus it is very difficult to implement the emission of surfactants into a numerical model. For all the model studies presented in this chapter it was assumed that initial organic concentrations are at least large enough to form one monolayer on sea salt aerosols. As it was explained in Section 4.1, it has to be assumed in this model, that either all or no sea salt particles are coated with surfactants as it is not possible to treat single particles in the model. Furthermore it has to be assumed that all sea salt particles have the same radius. This leads to the very large concentration of organic surfactants of up to $\approx 500\,\mathrm{mmol/l}$ ($\approx 3.5\,\mu\mathrm{g/m}^3_{air}$) that is roughly needed to form one monolayer on an aerosol population having a size of $2.6\,\mu\mathrm{m}$. Recently reported analysis of aerosol samples show organic mass fractions in the range of ng/m^3 (Sempere and Kawa-

mura, 2003) to $\mu g/m^3$ (Cavalli et al., 2004) whereas older measurements report values of $200\,\mu g/l$. The organic concentration that is needed to form one surfactant monolayer on one sea salt particle with a radius of $2.6\,\mu m$ in the model is $\approx 700\,\text{nmol/l}$ ($\approx 5\,\text{pg/m}^3_{air}$). Assuming an aerosol radius of only $0.1\,\mu m$ the sufficient organic concentration to form one surfactant monolayer would be $\approx 1\,\text{nmol/l}$ ($\approx 10^{-15}\,\text{g/m}^3_{air}$). Regarding the value of $200\,\mu g/l$ as reported by Marty et al. (1979), that refers to sea water concentrations, is even three orders of magnitudes larger than concentrations needed in the model to form a monolayer on the whole spectrum of particles. Marty et al. (1979) suggest that fatty acid concentrations are even enriched in aerosol particles. However as values from these old measurements differ significantly from more recent measurements the question arises whether the data presented by Marty et al. (1979) are artifacts of the sampling technique or whether they maybe collected samples in a 'hot spot' region?

Comparing organic initial concentrations as used in the model with data from Sempere and Kawamura (2003) (reporting concentrations on the order of ng/m^3) or Cavalli et al. (2004) (reporting concentrations on the order of $\mu g/m^3$), they had to be in upper limit range of reported concentrations to have a lifetime long enough to have at least a small effect on atmospheric chemistry.

Based on those measurements and the knowledge of the average cross section of a long chain organic molecule that is used to calculated the sufficient surfactant concentration to form one monolayer, the load of film-forming compounds in sea salt particles is more likely to lead to a formation of a surface film only on the smallest sea salt particles. Is this the case in reality? If only the smallest sea salt particles contain a complete surfactant coating, is the fraction of those particles large enough to have an impact on atmospheric chemical or microphysical processes?

If the organic surface film does not have to be as dense as assumed in this model study, and only half the surface of the aerosol particle has to be directly covered with surfactants, organic concentrations in the model are still very large compared to latest measurements.

Additionally to the above mentioned uncertainties regarding organic emissions, atmospheric processing of the surface film or the order of magnitude of uptake reduction due to an organic surface film, we have only very few indications of the occurrence of surface films on atmosphere particles and we practically have no knowledge about their lifetime in the atmosphere.

Within the Introduction in Section 3.1 the field experiments done by Chuang (2003) and Ruehl et al. (2008) were mentioned who investigated the timescale of droplet growth. As said already above, they found that on numerous days the percentage of particles showing a delayed growth was very small whereas there were several days and locations where a large fraction of particles showed a delayed growth behaviour compared to the expected growth based on equilibrium (Köhler) theory. The authors suggest droplet growth is delayed because particles contain an organic surface film decreasing the water vapour diffusion to the droplet. They further find, that on those days, on that they detected a particularly large amount of particles that showed a delayed growth, air masses at the measurement site descended from aloft and had most likely undergone more than one cloud cycle. Several other studies give further indications that organic aerosols are present in the free troposphere (Murphy et al., 1998; Heald et al., 2005). This suggests that the lifetime of an organic film decreasing mass transfer is significantly longer than calculated in the above presented model studies. Ruehl et al. (2008) bring up the idea that those film forming organic compounds are less efficiently removed by wet deposition than more soluble com-

pounds and thus have a longer lifetime. However, this aspect is in contradiction to the very fast oxidation reactions of long chain surfactants. Even though surfactants were less efficiently removed by wet deposition, they should be destroyed rapidly by reaction. Is it possible that after the primary oxidation of the surface film hardly reactive surfactants are formed that have a very long lifetime? All laboratory and field measurements indicate that this is rather not the case. Even though organic aerosols are found in the free troposphere and even though organic compounds can be taken up into aerosols, those compounds are in general water soluble and not surface active. If the delayed droplet growth observed by Ruehl et al. (2008) is really related to an organic surface film, surface active compounds have to exist that hardly react with atmospheric oxidants like O_3, OH or NO_3. It should be clearly pointed out that Ruehl et al. (2008) only *suggest* that their observations can be explained with an organic surface film being present on the particles. However, it is not unlikely that their observations are not related at all to organic surface films.

Regarding the results from the model simulations presented in this thesis and regarding the information about organic surface films we can get from laboratory and field measurements, the effect of such organic surface films on atmospheric chemistry as well as microphysical aerosol properties in the marine boundary layer are negligibly small if the inclusion of surfactants into freshly emitted sea salt aerosols is considered to be the only source of surfactants. As fatty acids were also detected in continental sulphate aerosols, there might be regions on the globe where film-forming compounds might however, be of importance.
The overall question that has to be answered in the future is: Will it be possible to assess whether organic surface films really form naturally on atmospheric particles? And if they form on atmospheric particles; how long is their lifetime?

7.5 Requirements for future model studies

It is very difficult to draw a clear conclusion from the above presented model runs regarding the effect of an organic surface film on atmospheric chemistry due to the large range of uncertainties concerning the data from laboratory and due to the numerous assumptions that had to made in the model setup. However, this model study contributes to the understanding of the atmospheric processing of organic aerosols as well as the effect of the reduced mass transfer between the gas phase and the aerosol phase.

For future model studies more and detailed information regarding the following points is required:

- More detailed data from laboratory measurements are needed that give information how strongly the exchange between gas phase and aerosol phase is really affected by an organic coating. We need to know the magnitude of uptake reduction for various chemical species. It can be supposed that the influence of the organic coating varies depending on each species which is taken up by the aerosol.

- Can we assume that the release of aqueous phase species out of the aerosol is affected in the same way as the uptake of gas phase species into the aerosol?

- How tightly has the organic coating to be packed to influence mass exchange? Again, we need this information related to the uptake behaviour of various chemical species. The density of the organic coating determines the organic concentrations required to influence mass transfer and it determines indirectly the loss rate for gas phase oxidants which react with the surfactants.

- We need more measurements giving us data about organic surfactants which are found in the marine boundary layer and their concentrations.

- It is important to understand the process of surfactants forming films on aerosol particles and the process of destruction of this film by using oleic acid as a proxy for surfactants. However, in order to assess the importance for tropospheric chemistry we need a more realistic description of the composition of an organic surface film and its destruction rate.

- It could be showed that the effect of a reduced mass transfer strongly depends on the lifetime of a surface film in the atmosphere and the lifetime mainly depends on its chemical destruction. Reactive uptake coefficients for a variety of species are required as well as information in which way a mixed surface film alters its properties.

- Knowledge about the breakdown products of surfactants and their properties is required for a more in depth assessment of the problem. Current laboratory studies give information about secondary chemistry of the oleic acid-ozone system only. Even for this system the available information is not detailed enough. That makes the inclusion of these processes in atmospheric chemistry models difficult.

- How common are particles that are naturally coated by an organic surface film in the atmosphere?

Part II

Halogen and Ozone chemistry over the Dead Sea

Chapter 8

Introduction

8.1   Measurements and Motivation

Tropospheric ozone depletion events related to highly active bromine chemistry are widely known to take place in polar regions and were first observed by Barrie et al. (1988). Several years ago Hebestreit et al. (1999) detected a similar occurrence at the Dead Sea, Israel. On the first glance it is difficult to imagine that the same processes can lead to O_3 destruction in two regions of opposing environmental conditions such as the Arctic/Antarctic and the desert in Israel. Hebestreit et al. (1999) report maximum BrO mixing ratios of 86 pmol/mol, exceeding even mixing ratios in the arctic regions. O_3 levels dropped simultaneously below the detection limit of 2 nmol/mol. Those first measurements were taken on a peninsula separating the northern and southern part of the Dead Sea. On all measurement days with southerly winds Hebestreit et al. (1999) could observe a strong increase in BrO mixing ratios until noon. However, no BrO was found when the wind direction was northerly. Because of the correlation between the wind direction and the BrO concentrations, the authors assumed that the most important source for the very high gas phase bromine concentrations are the salt pans around the southern part of the Dead Sea as they are higher enriched with bromide than the northern part of the lake. Matveev et al. (2001) did BrO and O_3 measurements at the same site as Hebestreit et al. (1999) and obtained similar results regarding the high BrO mixing ratios (maximum BrO = 176 pmol/mol) and correlated O_3 depletion events when surface winds were southerly. However, in contrast to the first mentioned measurement campaign they could also detect large BrO levels when the wind direction was from North to South, even though under those conditions no O_3 depletion could be observed. An autocatalytic cycle - meaning the activation of bromine chemistry by the bromine explosion mechanism (Platt and Janssen, 1995) leading to the formation of reactive halogen species like BrO, followed by the recycling of bromine species through uptake and reactions in aerosol particles - was suggested to be responsible for the high BrO concentrations.

  Two long term measurement campaigns took place in 2001 (July to August) and 2002 (January, June to September) to get a deeper understanding of the chemical processes taking place at the Dead Sea. Ozone was even monitored continously for a 14-month period starting February 2001. This time data were collected at a site in the South, in the mid (West shore) and in the North of the Dead Sea as well as at an elevated site about 400 m above sea level about 20 km South of the northern end of the lake. Tas et al. (2003) and Tas et al. (2005) report high levels of BrO and low levels of O_3 on numerous days at all measurement sites, in summer time as well as in winter time, even though then less often
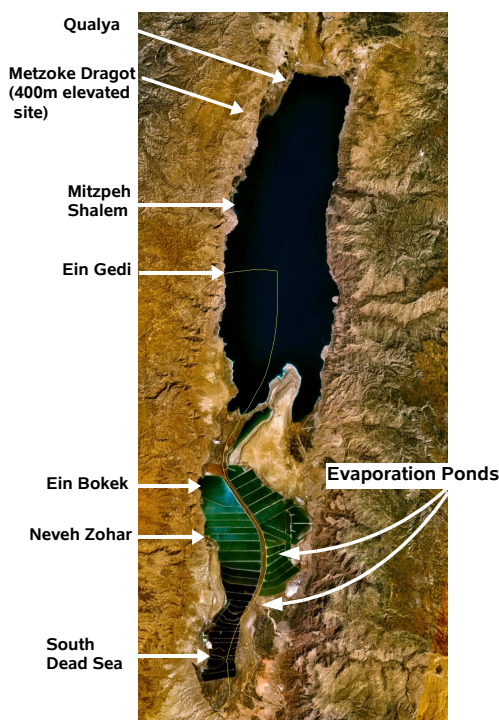
Figure 8.1: The Dead Sea from a satellite. Marked are the measurement sites.

and less intense. As on some days O_3 mixing ratios start to decrease nearly simultaneously at all measurement sites and no strong correlation between ozone depletion events and the wind direction could be found, the authors conclude that not only the salt pans in the South can be the source for gas phase bromine but that also the sea water in the northern part of the lake must be a strong bromine source. Matveev et al. (2001) present O_3 flight measurements taken at approximately 300 m altitude for four days. On one day O_3 levels are below 20 nmol/mol all over the Dead Sea, on one day only over the southern part, on one day only over the northern part and on one day no ozone depletion was observed anywhere.

A first very simple model study by Stutz et al. (1999) accompanying the measurements from Hebestreit et al. (1999) indicates that the formation of 0.5 nmol/mol BrO, which is about 5 times the absolute maximum measured BrO mixing ratio, would be required to destroy an average background level of about 60 nmol/mol O_3 within 2 - 3 hours. The latest model study by Tas et al. (2006) claims that the only source for the high bromine levels is the bromine explosion reaction taking place within sea salt aerosols released from the Dead Sea. The authors assume that the high bromide concentrations in the Dead Sea water and thus in sea salt aerosols are sufficient to produce those large BrO concentrations in the gas phase solely by the release of bromine species from sea salt particles. Furthermore, the authors assume that the most important recycling reaction is the heterogeneous decomposition of $BrONO_2$ on sulphate aerosols followed by the release of HOBr out of the particles into the gas phase. However, as Tas et al. (2006) do not calculate aqueous phase chemistry explicitly, use very simple parameterisations for the mentioned heterogeneous/aqueous phase reactions, choose a reaction rate for the bromine explosion reaction so that the model results agree best with the measurements and assume relatively arbi-

trary appearing O_3 fluxes into the domain of their one-dimensional model, the conclusions which are drawn from this study have to be thoroughly reconsidered.

Maybe the most astonishing measurements from the Dead Sea are presented by Zingler and Platt (2005) who detected up to 10 pmol/mol IO. Such levels of iodine oxide were observed before only in coastal regions where it is assumed that I_2 and organic iodine precursors related to large amounts of algae being exposed to the air during low tide are the most important precursor species for IO. As the Dead Sea is one of the most saline lakes in the world and as it is surrounded by a desert with hardly any vegetation it is very unlikely that organic iodine compounds can be produced in high concentrations. Thus it might be an even larger challenge to explain those high iodine oxide levels compared to the detected bromine oxide levels.

In the introduction in Section 1.2 it was mentioned that hardly any data is available with respect to gas phase bromine or chlorine mixing ratios from the midlatitude troposphere. Besides the Dead Sea two other salt lakes have turned out to be regions of highly active halogen chemistry within the midlatitudes. Stutz et al. (2002) could detect BrO mixing ratios of up to 6 pmol/mol at the Great Salt Lake, Utah, USA and at the same time they detected for the first time at all ClO with maximum mixing ratios of 15 pmol/mol. The authors assume that heterogeneous reactions on crystallised surface salt deposits on the shores of the lake release halogens by similar processes as the halogen release from the snowpack in the Arctic. They further assume that salt crystals might be lifted into the atmosphere and provide a reaction surface. The authors find a decrease in O_3 mixing ratios simultaneously to the daily BrO peak period, however, the decrease is far lower than for the Dead Sea region and cannot be considered as a depletion event. The Salar de Uyuni in Bolivia is the largest saltpan in the world. Hönninger et al. (2004a) found up to 20 pmol/mol BrO correlated with O_3 depletion events which were however still weaker than over the Dead Sea mainly because of the comparatively lower Br production. The authors suppose that concentrated acidic brines being present in huge amounts at the Salar support the activation of bromine chemistry by the bromine explosion mechanism.

The main question which is addressed in this work is to find an explanation for the measurements taken along the Dead Sea based on a reasonable chemistry mechanism. Two, very general points speak against the hypothesis brought up several times, that the standard bromine aerosol and gas phase chemistry also accounts for the very high BrO mixing ratios at the Dead Sea, only because the very high bromide content of the Dead Sea water and of sea salt aerosols. The wind speed over the Dead Sea is very low. Consequently the number of sea salt aerosol particles that are produced is low. As the relative humidity along the Dead Sea valley is very low, aerosol phase chemistry is likely to be of minor importance. A low aerosol liquid water content which consequently has to be the case if ambient relative humidity is extremely low, leads to a slow mass transfer between the aerosol and the gas phase. Thus, only a very limited amount of BrCl or Br_2 can be released out of particles as the total halogen cycling should be weak. Due to the dry conditions it has further to be taken into account that sea salt aerosol particles dry out quickly when they are transported vertically as the ambient relative humidity can be as low as 40% at an altitude of only 10 m above the water surface (Tas, personal communication). If such conditions are common along the Dead Sea, sea salt aerosols can be considered as sources for gas phase bromine species only in the lowest meters above the water. Regarding the meteorological background conditions such as low wind speed, very low ambient relative humidity and high temperature, the source for gas phase bromine species over the Dead

Sea due to degassing out of sea salt particles might even be weaker than over large parts of the open ocean so that an additional strong bromine source is required.

As the production of BrCl and Br_2 in the aerosol is pH dependant and the exchange process between the aerosol and the gas phase depends on the solubility of the species as well as their gas phase and aqueous phase concentrations, BrCl can only degas directly out of aerosols but not out of open ocean water with an average pH of about 8. The pH of Dead Sea water is much lower, leading to larger BrCl and Br_2 production rates in the water. This indicates that beside sea salt aerosols the Dead Sea water itself can be a direct source for gas phase bromine species as also suggested by Tas et al. (2006).

Figure 1.2 gives an overview of the potentially most important reactions leading to the formation of high BrO levels. The cycling of halogen species between aerosol particles and the gas phase was discussed in detail in Section 1.3. The only difference to the standard mechanism is the additional bromine source by degassing of bromine species like BrCl and Br_2 out of the Dead Sea water. A description of the treatment of the Dead Sea in the model MISTRA is given in the Section 8.3.3.

8.2   Background information about the Dead Sea

The Dead Sea is the lowest place on earth laying 415 m below sea level. It is located between the geographical coordinates 31°00'N, 31°50'N and 35°30'E. Being part of the Syrian-East African Rift Valley which reaches from the Taurus mountains in Turkey to East Africa, it expanses 75 km from North to South and 15 km from East to West where it is flanked by the Judean Mountains which exceed an altitude of 1000 m. Especially at the middle part of the lake the mountains arise steeply from the shores of the lake. On the East coast the Jordanian Moab Mountains stretch alongside the Dead Sea also reaching a height of about 1000 m. To the North and the South end of the lake the valley broadens and beyond the shores desert starts.

The Dead Sea is mainly fed by the river Jordan from the North and by perennial springs and streams in the East and West. As the Dead Sea has no outflow to the South it is a so-called terminal lake. As the air laying above the water is very hot and dry, the lake looses huge amounts of water by evaporation (400 cm/yr, Alpert et al., 1997). The average decrease of the sea level within one decade was estimated to be 0.8 m/yr (Anati and Shasha, 1989). The southern part of the Dead Sea, the so-called evaporation ponds, are separated from the northern part by a peninsula. This was however, not always the case. In the past the Dead Sea had a closed water surface but as the water level dropped more and more due to increased evaporation the Dead Sea was separated into two parts. The southern, very shallow basins - some of them have depth of only 1 - 2 m (see Fig. 8.1) - are fed with water from the the northern part by a channel. The evaporation ponds are used for industrial bromine production by the 'Dead Sea Works'.

In general the water of the Dead Sea has a very high acidity with pH values in the order of 5 (southern part) to 6 (northern part). Furthermore, the salinity of the water is very high. Bromide as well as chloride concentrations increase significantly from the northern part of the lake to the highly saline and acidic southern end. Cl^- and Br^- concentrations vary from 225 g/l and 6.1 g/l respectively in the North to about 405 g/l and 11 g/l in the South (Niemi et al., 1997). Thus the salinity of the water is about 12 times larger than for ocean water (Sverdrup et al., 1942) which has an average chloride content of about 19 g/l and a bromide content of 0.065 g/l. Therefore absolute bromide concentrations in the Dead Sea water are about a factor of 93 larger than in sea water.

As trace gas concentrations are always influenced by meteorological background conditions, local wind systems have to be analysed closer. Bitan (1977) collected a large surface wind data set at three sites (South, mid-North, North) along the Dead Sea. His finding was, that in the northern part of the lake the main wind direction was South to North and the opposite direction in the South. This wind system is driven by a lake breeze which develops due to thermal heating during the day and is in general related to winds blowing from the centre of a lake to the shore. The lake breeze is developed strongest in the late morning and afternoon hours. In the afternoon the local wind pattern is overlayed by strong downdrafts from the mountains in the west originating from the Mediterranean land-sea-circulation (Clarke, 1970; de Ridder and Gallee, 1998). Based on measurements and two-dimensional model calculations Alpert et al. (1997) report westerly and North westerly winds during the evening hours for the northern parts of the lake. However, Matveev et al. (2001) and Hebestreit et al. (1999) did BrO and O_3 measurements at the southern part of the Dead Sea as mentioned above, when southerly winds were dominant. Tas et al. (2003) also collected wind data together with their measurements of trace gas concentrations in the South, the mid and the North of the lake. Regarding their data the North shore is mainly influenced by southerly winds in agreement with Bitan (1977). The mid side is affected by northerly winds in summer and southerly winds in winter. At the southern measurement site it is more difficult to detect a main wind direction as according to Tas et al. (2003) on 65% of the measurement days the wind direction was between North and East-South-East and on the other days it was mainly South. Comparing all available wind data it can be said that the main wind direction is roughly either North to South or South to North. Even at noon and the early afternoon hours, when the lake breeze should be strongest, surface winds nearly never blow directly from the centre of the lake to the West (or East) shore as air masses are quickly canalised due to the topography.

No vertical wind profiles from the valley are available which would be helpful to understand the local flow pattern. Apart from the lake breeze and the regular downdrafts related with larger scale circulations, it has also to be influenced by the mountain breeze. In accordance to all reports the wind speed during day time is very low and lays in the range of 2-4 m/s.

As the Dead Sea is surrounded by a desert the temperature is very high with mean values of about 35 °C in summer. In the evening hours, when Mediterranean air masses reach the Dead Sea they are adiabatically warmed while descending. This process might slow down the cooling of surface air masses during the evening hours and the night (Bitan, 1977). Related to the hot air, relative humidity is very low with about 40 - 50 % only a few meters above the sea surface.

8.3   Model Description

For all presented model studies the one dimensional numerical model MISTRA is used which has been explained in detail in the introduction in Chapter 2. Changes have been made to the standard setup regarding the bin structure, the vertical grid and the lower boundary conditions as will be explained in the following sections. Furthermore, an aerosol size distribution for rural areas instead for clean marine conditions is used (Jaenicke, 1988). For all presented model runs for the Dead Sea, cloud free situations are assumed. Such a scenario is not unrealistic as the development of clouds over of the Dead Sea is limited mainly because of the low amount of available water.

8.3.1   The Boundary Layer Height in 'MISTRA'

The boundary layer height in the model is defined as the level where the buoyancy of an air parcel exceeds a threshold value of 10^{-5} K·m/s. Buoyancy (B_{uoy}) is defined as the vertical gradient of the virtual potential temperature ($\theta_v = (1+0.61q)\theta$). The vertical turbulent flux of momentum in the boundary layer is calculated using averaging methods:

$$
\begin{aligned}
B_{uoy} = \frac{\partial \theta_v}{\partial z} &= \overline{w'\theta_v'} \\
&= 0.61\,\theta\frac{\partial q}{\partial z} + (1+0.61q)\frac{\partial \theta}{\partial z} = 0.61\,\theta\,\overline{q'w'} + (1+0.61q)\,\overline{\theta'w'} \quad (8.1)
\end{aligned}
$$

Thus hot (T $\approx$ 35°C) and dry conditions (RH $\approx$ 45 %) as prevailing along the Dead Sea valley lead to a very high boundary layer in the model. Decreasing the temperature from such high values is followed by an increase in the relative humidity in the model and a comparatively lower boundary layer hight.

8.3.2   Activation of Aerosol-Chemistry

Due to the extremely dry conditions along the Dead Sea it is crucial to discuss shortly the way aerosol chemistry is triggered in MISTRA. In general, aerosol phase chemistry is always calculated in the corresponding bins if the ambient relative humidity is above the deliquescence humidity of sea salt (75%) or sulphate (70%) aerosols. It is known that soluble aerosol particles remain in a highly concentrated metastable aqueous state if they get dried out below their deliquescence humidity. Only when they reach the crystallisation humidity (40% for sulphate, 42% for sea salt) they can be considered as dry particles. As it can be assumed that freshly emitted sea salt particles are always present as an aqueous solution, sea salt chemistry is always calculated in the lowest model level (for model runs over a water surface). Aerosol phase chemistry is further calculated in the model on particles which once had exceeded the deliquescence point but afterwards had dried below it. Calculation of aqueous phase chemistry is however, terminated if the total water mass in one bin drops below a threshold value of 10^{-13} m$^3_{(aq)}$/m$^3_{(air)}$ or below the crystallisation humidity of the aerosol type. To re-activate aerosol phase chemistry again in such a layer, the ambient relative humidity has to exceed the deliquescence humidity of the particles. All model runs presented in this chapter are initialised with model runs that were ran over the desert for two days (this will be discussed in more detail in the model setup description in Section 8.4 below). Thus the relative humidity even in the lowest parts of the boundary layer is extremely low at least during day. As air masses near ground level cool down during the nights the related increase in relative humidity is strong enough to activate aerosol phase chemistry in at least the lowest 10 meters above ground. Thus aerosol phase chemistry is still active in a few of the lowest model layers when the model column is approaching the Dead Sea in the later morning hours.

8.3.3   The Dead Sea in MISTRA

As was explained in Section 2.4.2, the standard model setup allows the calculation of aerosol chemistry in four different size classes. The standard model setup uses two size

classes for the calculation of chemistry within aerosol particles (small particles are assumed to have an initial composition typical of sulphate aerosols and larger particles are initialised as purely sea salt particles) and two bins for chemistry on cloud droplets if the meteorological conditions are such that clouds are formed.

To be able to calculate air-sea exchange between the Dead Sea and the overlaying atmosphere, chemistry within the water of the lake is calculated explicitly. For all presented model runs, aerosol chemistry is treated in two size classes as explained in Section 2.4.2. A third bin is used to calculate aqueous phase bulk chemistry in the Dead Sea water. Figure 8.2 gives a simplified view of the possible interactions between gas phase, aerosol phase and water chemistry using the example of bromine chemistry. The assumption is made that the same reaction set which is used for aerosol phase chemistry is assumed to be also valid for chemistry in the water of the Dead Sea. As no heterogeneous reactions or phase transfer reactions are allowed, chemistry can be calculated independently of any radius. The only difference between calculation of chemistry in the water and the aerosol is the liquid water content which is set to one for calculations of chemistry within the Dead Sea water. The only possible interactions that are allowed between the Dead Sea water and the atmosphere is via air-sea exchange of trace gases as explained below and as is shown in Figure 8.2 using bromine chemistry as an example.

8.3.4 Air-Sea exchange

To describe the fluxes of gases across the air-sea interface a two-layer model as first presented by Liss and Slater (1974) is used. Assuming that the atmosphere and the water close to the interface are well mixed and that transport within the interface is only driven by molecular diffusion, the flux F (in mol/(m^{2}s)) across the interface reads

$$F = K_{tot}(c_w - Hp_g) \tag{8.2}$$

with K_{tot} being the transfer (or piston) velocity (in m/s), c_w is the aqueous phase concentration of a chemical tracer (in mol/m^3), H the henry constant (in mol/(m^{3}Pa)) and p_g
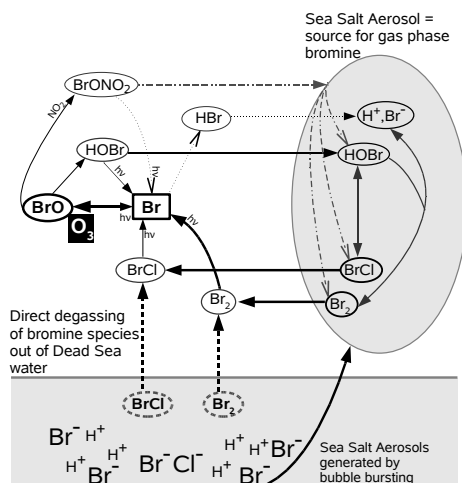

Figure 8.2: Simplified overview of the interacting chemistry in the water, the gas phase and aerosol particles.

(in Pa) the partial pressure of a gas phase species directly above the water surface. The piston velocity which is needed to calculate directly the changes in a concentration of a chemical species due to air-sea exchange is determined using a resistance model as follows:

$$K_{tot} \ = \ (R_g + R_w)^{-1} = \left(\frac{1}{K_w} + \frac{HRT}{K_g} \right)^{-1} \tag{8.3}$$

with the gas phase resistance R_g and the aqueous phase resistance R_w The variables used in that equation are the gas constant (R, in J/(molK)), the Temperature (T, in K), Henry's law coefficient (H, in mol/(m^{3}Pa)) and the exchange constants for the gas (K_g, in m/s) and the liquid phase (K_w, in m/s). Several slightly differing parameterisations exist to determine the liquid phase transfer constant from which the semi-empirical equation following Wanninkhof (1992) was chosen in this model setup:

$$K_w = \beta \cdot (u_{10})^2 \cdot \left(\frac{S_{liq}}{660} \right)^{-2/3} \tag{8.4}$$

β is an empirical constant ($2.8 \cdot 10^{-6} \cdot 0.31$ s/m), S_{liq} is the dimensionless Schmidt number for the liquid phase and u_{10} is the 10 meter wind speed. The gas phase exchange constant depends on the aerodynamic resistance (R_a, with z the height above the surface, z_0 the surface roughness length, $u\star$ the friction velocity and ϕ the potential temperature gradient calculated from similarity theory) and the molecular diffusion resistance (R_m, with Sc being the Schmidt number) and is calculated following Wesely (1989a).

$$
\begin{aligned}
K_g \ &= \ \frac{1}{R_a + R_m} \\
R_a \ &= \ \frac{1}{\kappa u_\star} \left(ln \left(\frac{z}{z_0} \right) + \phi \right) \\
R_m \ &= \ \frac{5}{u\star} Sc^{2/3}
\end{aligned}
\tag{8.5}
$$

Finally, the change of concentrations of gas phase species i by air-sea exchange can be described by

$$\frac{dc_i}{dt} = \frac{K_{tot}}{z} (c_w - c_i) \tag{8.6}$$

where c_i and c_w are gas and liquid phase concentrations of a tracer. This equation can be solved analytically, yielding

$$c_i(t) = c_{0_i} \cdot exp \left(-\frac{K_{tot}}{z} t \right) + (1 - exp \left(-\frac{K_{tot}}{z} t \right)) c_w. \tag{8.7}$$

The implementation of the air-sea exchange mechanism into the model MISTRA follows the work done by Pozzer et al. (2006) (and references therein) who explain in great detail the used parameterisations and their treatment in a numerical model.

It has further to be mentioned that dry deposition is not calculated for those species that undergo air-sea exchange as it is implicitly included in the approach explained above (Equation 8.6).

8.3.5 Vertical Model Grid

For studying the different formation mechanisms of BrO in detail it is crucial to be able to resolve chemical as well as meteorological process on a very fine model grid in the lowest 10 m in the atmosphere. A logarithmic grid for the vertical has been chosen with a grid spacing of 0.5 m for the lowest grid box above the water surface. Such a very high vertical resolution leads to difficulties regarding the calculation of turbulent exchange coefficients. All currently used parameterisations to calculate turbulent exchange coefficients are numerous years old and were developed for numerical models with a vertical grid spacing of at least 10 m or more. Thus the formulation of stability conditions used to parameterise (turbulent) surface fluxes (of heat and moisture) does not hold anymore for scales of less than a meter. As the computing capacity gets better and better, the question of new formulations of surface flux parameterisations will rise further.

Using the 'standard' formulation of surface fluxes with a grid spacing of 0.5 m in the lowest level in MISTRA would lead to random oscillations in all parameters either describing turbulent transport itself (turbulent exchange coefficients) or parameters that are dependant on turbulent exchange coefficients (temperature, humidity). To avoid this problem, two vertical grids are used in parallel. Meteorology is calculated on the standard 10 m equidistant grid which is necessary to determine turbulent exchange coefficients correctly. Turbulent exchange coefficients needed to calculate vertical transport of e.g. chemical tracers are interpolated on the small logarithmic grid with a grid spacing of 0.5 m in the lowest level. Regarding uncertainties e.g. with respect to the air-sea exchange or initial concentrations of tracers in the Dead Sea water, the error caused by using this method is small.

8.4 Model Setup
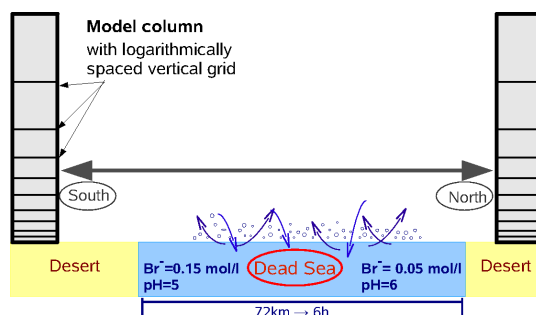
Figure 8.3: Schematically overview of pseudo-Lagrangian model setup.

8.4.1 Lagrangian - excluding iodine chemistry

To investigate bromine chemistry over the Dead Sea and related Ozone Depletion Events (ODE) at first a Lagrangian-kind model setup was chosen which is schematically shown in Figure 8.3. The model is first run over a land surface for two days in order to have a spin up. The temperature ranges from about 42°C directly above the ground to about 22°C at the top of the boundary layer during day. During the nights temperature decreases below 20°C close to the surface. Relative humidity increases from 40% in the lowest meters above the ground to a value of about 80% at the top of the boundary layer at about
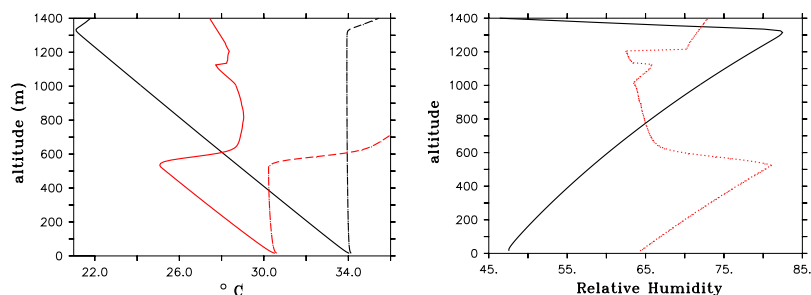
Figure 8.4: The plot on the left shows the vertical gradient of the temperature (°C, solid lines) and the potential temperature (°C, dashed lines) at 11:30 for scenarios **EXALL** (black) and **LOWBL** (red). The plot on the right shows the vertical gradient of the relative humidity (in %) at 11:30 for scenarios EXALL (black solid line) as well as scenario LOWBL (red dashed line).

1500 m altitude during day. During the night surface air masses cool down related with an increase of relative humidity up to 70%. This setup represents the environment of the Dead Sea as a desert. Figure 8.4 shows exemplarily vertical profiles of temperature, potential temperature and relative humidity for scenarios EXALL (black) and LOWBL (red, details of the scenarios will be given below). The temperature inversion indicates the boundary layer height.

Chemistry is initialised such that average background mixing ratios for O_3 are about 70 nmol/mol, 1 nmol/mol for NO_2 and approximately 0.3 nmol/mol for NO at the morning of day two in the initialisation model run. It is assumed that the moving model column reaches the Dead Sea at 10:00 on day two.

To initialise chemistry in the Dead Sea water, a separate model run was calculated, again for two days. No exchange with either the gas phase nor aerosol phase was allowed to take place for all chemical species in the water in order to have a spin up for the model.

As discussed above, the main surface wind direction over the Dead Sea is either North to South or South to North. Measurements indicate that on several days the wind direction in the North is southerly whereas it is simultaneously northerly in the South (initialised by the lake breeze). Even though an air parcel would be transported roughly above half the lake (southerly or northerly), before it could reach one of the measurement points in the North or respectively the South, it is assumed that the model column crosses the lake either from South to North or North to South. Obviously this model setup would only be completely valid for those days, when the wind direction all over the Dead Sea is the same. However, with this setup the influence of the gradient in chemical composition of the lake's water on gas phase concentrations can be taken into account as well as the influence of air masses originating in the desert North or South of the lake and their interactions with halogen containing air masses originating over the Dead Sea itself. By using this pseudo-Lagrangian approach no unrealistic or speculative assumptions about advection into the model domain have to be made.

With an average wind speed of 3 m/s it would take approximately six hours to transport an air parcel 72 km from the South end to the North end of the Dead Sea. During those six hours when the model is run over the water surface, the lower boundary conditions are changed representing the gradient in the acidity and salinity of the lake water as well as the slightly changing Br^-/Cl^- ratio which are factors that are assumed to be responsible

for the stronger and more often occurring O_3 depletion events over the southern part of the Dead Sea compared to the northern part. Br^- mixing ratios in the Dead Sea water are decreased from 0.15 mol/l (South) to 0.05 mol/l (North) and the pH of the lake is increased from 4.9 (South) to 6 (North). Obviously, this setup only changes the bromide content of the water and not the total salt content. One reason for this simplification is, that even the lowest named Cl^- concentrations for the Dead Sea water are very large compared to ocean water and should be no limitation to any kind of halogen chemistry. The second reason is that it should be the aim to constrain the model as little as possible. Thus only the effect of decreased Br^- and H^+ concentrations are to consider.

However, two model runs were performed using the very high Cl^- concentrations as measured in the evaporation ponds to initialise water chemistry in the South. In scenario CL_{HIGH} those high Cl^- concentrations stay constant (only Br^- and H^+ are forced to decrease) and in scenario CL_{DECR} also Cl^- concentrations are decreased with time to the minimum value measured in the North of the lake, which is the value that was used for calculating chemistry in all other model runs.

An overview of the different scenarios and the abbreviations of each calculated model run is given in Table 8.4. In all scenarios the model column moves over the Dead Sea from 10:00 until 16:00. Apart from scenarios NOSO it is assumed that the model crosses the lake from South to North. Furthermore, the dry and hot meteorological conditions lead to a boundary layer height that is constantly at 1300 m apart from scenarios SUB, EXLIM and LOWBL.

Overall, 13 different Lagrangian model scenarios were set up to simulate the effect of differing ambient conditions on the trace gas concentrations over the Dead Sea. One model run (NOEX) is calculated without including air-sea exchange only taking into account the 'standard' gas phase and aerosol phase chemistry of the model MISTRA. This setup is used as a kind of control run.

Direct degassing of the halogen species BrCl, Br_2 and Cl_2 out of the Dead Sea water into the atmosphere is calculated in scenario EX whereas in scenario EXALL additionally the air-sea exchange of HOBr, HOCl, HCl and HBr is considered. Eleven modifications of this scenario were set up: (1) For scenario SUB it is assumed that subsidence decreases the boundary layer height from about 1300 m to 700 m within the six hours of model run time. Such a scenario represents a day where the wind pattern over the Dead Sea is not affected by any large scale circulations in the morning hours but in the afternoon it is influenced by downdrafts originated by the land sea breeze as explained in the introduction. (2) For scenario EXLIM it is assumed that for the first two hours of simulation time vertical

Site	pH	Cl^- (g/l)	Cl^- (mol/l)	Br^- (g/l)	Br^- (mol/l)
North (Qalya)	5.9	225	6.34	6.1	0.08
Mid North (Mitzpeh Shalem)	5.7	225	6.34	6.9	0.09
Mid (Ein Gedi)	5.8	236	6.65	6.4	0.08
Evap. ponds (Ein Bokek)	5.5	306	8.62	8.3	0.10
South (Neveh Zohar)	5.0	345	9.72	9.6	0.12
South end	4.9	405	11.41	11	0.14

Table 8.1: The pH as well as Chloride and Bromide levels in the Dead Sea water. This table is composed on data given in Tas et al. (2005). These measurement sites can also be seen in Fig. 8.1.

transport is strongly limited. Such a situation might arise when hot and dry air masses that had been transported over the desert start to cross the water surface which is slightly cooler than the land surface. An inversion which is not very intense but strong enough to limit vertical transport builds up in the lowermost boundary layer. After a short time period it is compensated due to mixing of air masses. (3) It is assumed that in scenario NOSO the Dead Sea is crossed from North to South by the model column. Concentrations of Br^- and H^+ concentrations are increased with time opposite to as it was done in scenario EXALL. (4) Regarding the meteorological background conditions aerosol phase chemistry should only be important in the lower most part of the boundary layer as the relative humidity is extremely low. As mentioned above, the model is initialised such that relative humidity is about 47% in the lower most boundary layer (see Fig. 8.4). As those humidity conditions might not lead to an activation of aerosol phase chemistry in the model (mainly because the total water mass in aerosol particles might become too low, see Section 8.3.2), one model run (DRY) was calculated including heterogeneous reactions on 'dry' aerosol particles to enhance the potential of halogen recycling in the boundary layer. (5) To exclude uncertainties in the air-sea exchange process and to be able to exclude a potential effect of unrealistic feedbacks between the water chemistry and the gas phase chemistry, the fluxes of trace species from the water into the atmosphere (or vice versa) in scenario CONST are prescribed and stay constant with time (see table 8.3 for flux strength of tracers). (6, 7) From the measurements taken along the Dead Sea, it appears as if O_3 depletion events are more pronounced in the South. Salt pans which are mainly present in the southern part of the Dead Sea might be a strong bromine source in addition to the water and sea salt aerosols. Furthermore, it is possible that the air-sea parameterisation underestimates the flux of bromine species out of the very shallow and highly concentrated evaporation ponds in the South. Therefore in scenario ENH_1 and ENH_2 the fluxes of bromine species out of the Dead Sea water are increased in the first two hours of simulation time to simulate the potential additional bromine source. (8) To be able to evaluate the effect of a constantly lower boundary layer compared to scenario EXALL, scenario LOWBL was calculated where the initial meteorological conditions were chosen such, that the boundary layer hight is constantly at about 500 m. Therefore the temperature had to be decreased compared to scenario EXALL as can be seen in Fig. 8.4. (9) One Lagrangian scenario (HIGHRH) was calculated using different initial profiles for meteorology such that the relative humidity especially in the upper part of the boundary layer is higher than in the other Lagrangian scenarios. The further variations of scenario EXALL are the scenarios CL_{HIGH} and CL_{DECR} already mentioned above.

	Flux [pmol/(mol·s)] 10:00 (day 1) - 15:00 (day 2)	Flux [pmol/(mol·s)] 15:00 (day 2) - 24:00 (day 2)
O_3	0.078	6.829
NO_2	0.463	0.347

Table 8.2: Flux of O_3 and NO_2 into the model domain for the stationary model run (STAT).

8.4.2 Stationary runs - excluding iodine chemistry

To investigate the daily variation of trace gas concentrations at one single point above the Dead Sea (corresponding to a measurement site), in addition to the Lagrangian studies, a stationary model run over the South end of the Dead Sea (Dead Sea water with a pH of 4.9 and Br^- mixing ratios of 0.15 mol/l) was performed. The model run was initialised with the same fields for meteorology and chemistry as the Lagrangian studies, but the composition of the water as well as the composition of freshly emitted sea salt particles is not changed during the 38 hours of simulation time. The model runs start at the same time as the Lagrangian runs (10:00) and all presented plots show mixing ratios between 10:00 day 1 and 20:00 day 2. The boundary layer height, which is crucial for the magnitude of mixing ratios of tracers in the lower troposphere is constantly at about 1300 m altitude like e.g. in scenario EXALL indicating a well mixed boundary layer.

It is rather unrealistic, that the air at one particular site at the Dead Sea stays uninfluenced by the environment and thus advective fluxes of O_3 and NO_2 are assumed. As it is not possible to calculate advection into the model domain explicitly with a one-dimensional model, the strength of the fluxes is chosen somewhat arbitrarily such that in the evening of the second day of simulation time O_3 and NO_2 mixing ratios are in the same order of magnitude as at the beginning of the simulation. Therefore the advection of O_3 into the model domain was enhanced in the afternoon hours of day 2 of the simulation time. The strength of the advective fluxes of O_3 and NO_2 is given in Table 8.2. The inflow of both species into the model domain is assumed to be the same in all model levels.

Furthermore, it is idealised to assume that the measurement site was only affected by air masses originating over the desert and being totally uninfluenced by halogen chemistry as measurements also show at several days significant BrO mixing ratios at a site south of the Dead Sea even under southerly wind conditions (Tas et al., 2005). It is not realistic that one site is only slightly effected by its environment during the 2 days of simulation time which is assumed by admitting only an inflow of O_3 and NO_2. However, the setup was chosen like this to be better able to compare the Lagrangian and the stationary setup. The assumption of an inflow as well as the idealised initialisation is a strong constraint to the model. This scenario is not valid for representing accurately the conditions and daily variations at one site at the Dead Sea, but it should help to understand the general chemical mechanism and its sensitivity to changing background conditions.

Species	molec/(cm^{2}s)
HOCl	$7.5275 \cdot 10^3$
HOBr	$1.2044 \cdot 10^{10}$
HOI	$1.2044 \cdot 10^{10}$
Br$_2$	$1.1054 \cdot 10^{10}$
Cl$_2$	$4.5165 \cdot 10^2$
I$_2$	$1.2044 \cdot 10^{10}$
IBr	$2.7099 \cdot 10^9$
ICl	$9.0330 \cdot 10^8$
BrCl	$3.3121 \cdot 10^7$

Table 8.3: Fluxes of halogen species out of the Dead Sea water for scenario CONST and ICON.

8.4.3   Lagrangian runs - including iodine chemistry

Three Lagrangian scenarios treating the calculation of iodine chemistry as well as air-sea exchange of iodine species explicitly were additionally simulated. In general the same setup is chosen as for scenario EXALL. The only difference between the three iodine scenarios is the iodide content in the Dead Sea water which is highest in scenario IOD_1 ($9.7\,\mu$mol/l) and lowest in scenario IOD_3 ($1\,\mu$mol/l). An intermediate value of initial iodide concentrations was chosen in scenario IOD_2 ($4\,\mu$mol/l). Initial I^- concentrations as chosen in scenario IOD_3 correspond with reported values from Zingler and Platt (2005). Both other scenarios were set up to investigate the sensitivity of gas phase iodine chemistry on a differing I^- content in the Dead Sea water.

Due to well known uncertainties regarding aqueous phase iodine chemistry and the related uncertainties in the air-sea exchange of iodine species, one scenario is calculated prescribing constant fluxes of I_2, IBr, ICl and HOI based on the explicitly calculated fluxes in scenario IOD_3. Fluxes of HOBr, Br_2, Cl_2 and BrCl are chosen to have the same strength as in scenario CONST, such that scenario ICON can be compared directly to scenario CONST. The strength of the fluxes out of the Dead Sea water is given in Table 8.3.

	Lagrange
NOEX	No air-sea exchange is calculated
EX	Air-Sea exchange of only BrCl, Br_2, Cl_2 is calculated
EXALL	The same setup as EX, but air-sea exchange of BrCl, Br_2, Cl_2, HOCl, HOBr, HCl, HBr is calculated
SUB	The same setup as EXALL, but strong subsidence is assumed leading to decreasing boundary layer height with time
EXLIM	The same setup as EXALL, but limited vertical transport for first 90 min, strong vertical mixing for rest of simulation time
CONST	The same setup as EXALL, but fluxes out of the water into the atmosphere are prescribed and are constant with time
NOSO	The same setup as EXALL, but model column crosses the Dead Sea from North to South
DRY	The same setup as EXALL, but heterogeneous reactions on non-deliquescent aerosols are calculated
ENH_1	The same setup as EXALL, but very strong hot spot emissions within the first 2 h
ENH_2	The same setup as EXALL, but strong hot spot emissions within the first 2 h, but less strong than in ENH_1
LOWBL	The same setup as EXALL, but Boundary layer height only 500 m
HIGHRH	The same setup as EXALL for chemistry but relative humidity higher in BL
CL_{HIGH}	The same setup as EXALL, but high Cl^- concentrations in the Dead Sea that stay constant with time
CL_{DECR}	The same setup as EXALL, but high Cl^- concentrations in the Dead Sea that decrease with time
	Stationary
STAT	The same initial conditions as EX, but model runs for 38 h over the same site at the South end of the Dead Sea
	Lagrange + Iodine
IOD_1	The same setup as EXALL, but including iodine chemistry, $I^-_{DeadSea}$ high (9.7 μmol/l initially)
IOD_2	The same setup as EXALL, but including iodine chemistry, $I^-_{DeadSea}$ middle (4 μmol/l initially)
IOD_3	The same setup as EXALL, but including iodine chemistry, $I^-_{DeadSea}$ low (1 μmol/l initially)
ICON	The same setup as CONST, but fluxes of iodine species (I_2, IBr, ICl, HOI) also prescribed

Table 8.4: Overview of all scenarios that are discussed in part II.

Chapter 9

Results

9.1 Lagrangian runs without iodine chemistry

9.1.1 Lagrangian runs without Air-Sea-Exchange

As mentioned in the introduction in Section 8.1, two other model study dealing with bromine and ozone chemistry at the Dead Sea already exists. However, the simple box model used by Stutz et al. (1999) does not include the explicit treatment of aerosol phase chemistry and the vertical extend of the ODE's could not be investigated either. Tas et al. (2006) also cannot calculate liquid phase and heterogeneous reactions. Furthermore, it is questionable whether the results presented by Tas et al. (2006) are reliable as their model was to a large extend constrained and reaction rates and advective fluxes were chosen arbitrarily.

Thus at first the scenario ignoring direct air-sea exchange (NOEX) is calculated as it only treats those chemical processes that according to Tas et al. (2006) should be responsible for the large BrO an low O_3 mixing ratios as measured at the Dead Sea: Emission of sea salt aerosol particles out of the Dead Sea water, degassing/uptake of bromine species out of aerosol particles and gas phase chemistry.

If not mentioned otherwise all line plots presented in this chapter show mixing ratios at two meters altitude as most measurements were taken at approximately this height. Only the time period when the model column moves over the Dead Sea (from 10:00 to 16:00) is shown in all plots.

Figure 9.1 shows mixing ratios for the gas phase species (a-f) and concentrations in sea salt aerosols (g-i) for scenario NOEX. The maximum BrO mixing ratio of 0.012 pmol/mol (Fig. 9.1 a) which is reached at 16:00, is up to four orders of magnitude lower than values reported from measurements. O_3 mixing ratios stay nearly stays constant at about 70 nmol/mol (Fig. 9.1 d) during the six hours of simulation time between 10:00 (South) and 16:00 (North) and thus the influence of bromine chemistry on ozone mixing ratios can be considered as negligible.

Without considering degassing out of the Dead Sea water the only source for gas phase chlorine and bromine species is the transfer of halogen precursor species out of sea salt aerosols. Even though sea salt aerosols contain high Br^- concentrations (around 3 mmol/l, Fig. 9.1 g) and have a high acidity (pH ≈ 1, Fig. 9.1 h),it is not possible to reproduce the measurements with model setup NOEX. As the sea salt production is low and aerosol chemistry is only effective in the lowest 2 meters above sea level due to the low rela-

a)

b)

c)

d)

e)

f)

g)

h)

i)
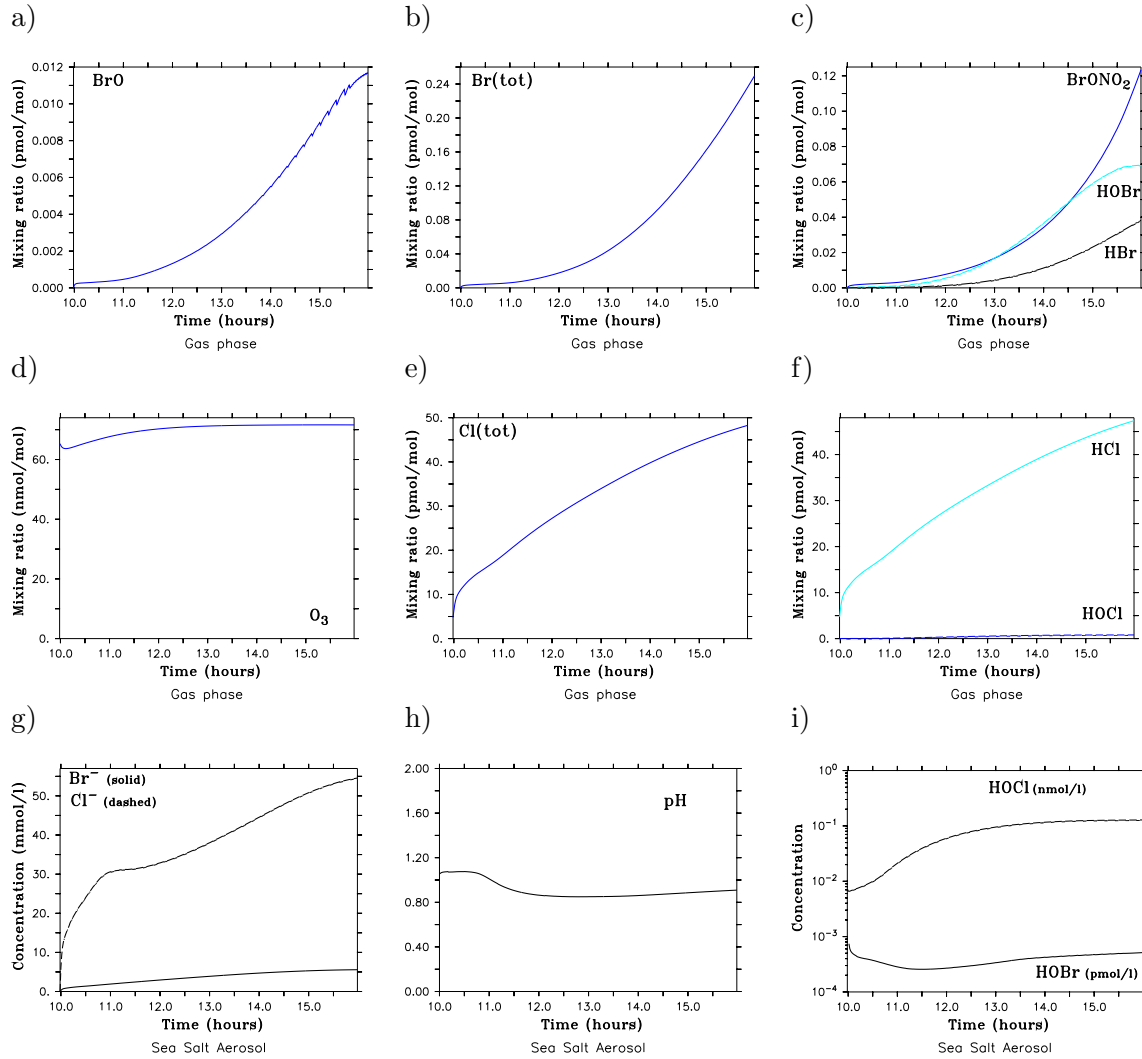
Figure 9.1: The plots show gas phase mixing ratios at $2\,\mathrm{m}$ altitude for scenario **NOEX** for BrO (a), Br_{tot} (b), HOBr, $BrONO_2$ and HBr (c), O_3 (d), Cl_{tot} (e), HOCl and HCl (f). Plots in the bottom row show aqueous phase concentrations in sea salt aerosols at the same height for Br^- (g), the pH (h) and HOBr and HOCl (i). Total gas phase chlorine (Cl(tot)) and bromine (Br(tot)) mixing ratios are the sum the mixing ratios of all chlorine and bromine containing species: (Br_{tot}=HBr+HOBr+$BrNO_2$+$BrNO_3$+2·Br_2+BrCl+Br+BrO Cl_{tot}=HCl+HOCl+$ClNO_2$+$ClNO_3$+2·Cl_2+Cl+ClO+OClO+ 2·Cl_2O_2+BrCl).

tive humidity (see explanation of activation of aerosol phase chemistry in Section 8.3.2 and vertical profile of relative humidity in Fig. 8.4), the Br_2 flux out of aerosol particles ($6 \cdot 10^{-7}$ - $2.8 \cdot 10^{-6}\,\mathrm{pmol/(m^3 s)}$) is too weak to produce significant bromine levels in the gas phase. Beside the vertical limitation of bromine production, vertical transport is another limiting factor for the accumulation of BrO in the lowest meters above ground as it leads to a quick vertical mixing of the anyway low concentrated tracers all over the boundary layer.

In general mixing ratios of gas phase halogen species increase with time (in terms of the Lagrangian model setup with space), e.g. total gas phase bromine mixing ratios rise steadily but reach only a maximum mixing ratio of $0.24\,\mathrm{pmol/mol}$ at 16:00 (Fig. 9.1 b). The in-

crease of gas phase bromine species is not a direct effect of changing the lower boundary conditions in the model during the six hours of simulation time i.e. decreasing the bromide content and pH in the Dead Sea water and thus changing the initial composition of freshly emitted sea salt particles. It is rather an effect of making the (idealised) assumption that air masses over the southern most end of the Dead Sea were not influenced in any way by halogen chemistry before the model crosses the lake but are mainly influenced by air masses that are advected from the desert. At the south end of the Dead Sea (10:00) halogen concentrations are close to zero, and the longer halogen chemistry is active (the closer the model column gets to the north end of the lake) the more the concentrations increase. The relative increase (for example in BrO mixing ratios) is thus large however, the absolute mixing ratios are very small.

The most abundant gas phase bromine species are HOBr (max: 0.07 pmol/mol), BrONO$_2$ (max: 0.12 pmol/mol) and HBr (max: 0.04 pmol/mol) as can be seen in Figure 9.1 c.

Total gas phase chlorine mixing ratios are much higher than total gas phase bromine mixing ratios with about 10 to 48 pmol/mol (Fig. 9.1 e). However, most of the chlorine is present in form of the hardly reactive hydrochloric acid (10 - 46 pmol/mol, Fig. 9.1 f).

Within sea salt particles, the most abundant chlorine species apart from Cl$^-$ (max: 55 mmol/l, Fig. 9.1 g) are HOCl (max: 0.12 nmol/l, Fig.9.1 i) and HCl (max: 1.4 nmol/l, not plotted). HCl has only two potential sources which is an equilibrium reaction with Cl$^-$ and H$^+$ and uptake from the gas phase. Due to the large Cl$^-$ concentrations and high aerosol acidity, HCl concentrations in the aerosol become high leading to the degassing out of the aerosol. Thus acid displacement is the key process leading to the release of chlorine from the aerosol into the gas phase. In contrast to HCl, HBr is not formed within the sea salt particles. Furthermore, HBr is more soluble than HCl and thus does not degas. Anyway, HBr would be of minor importance as it is relatively unreactive in the gas phase and it is in general taken up much faster into aerosols than it undergoes reaction to form reactive bromine species.

The production of Br$_2$ in the aerosol phase by the bromine explosion reaction is essential for the formation of significant gas phase BrO levels. However, in addition to the high acidity and salinity in the aerosol, significant HOBr levels would be required. As the total number of sea salt aerosols is small and aerosol chemistry is limited to only a few meters above sea level, halogen cycling between the gas phase and the aerosol phase is weak thus leading to the relatively small HOBr concentrations within sea salt particles ($\approx$ 5$\cdot$10^{-4} pmol/l, Fig. 9.1 i). HOBr concentrations are nearly four orders of magnitude lower than HOCl concentrations. Cl$^-$ mixing ratios are still about three orders of magnitude larger then Br$^-$ mixing ratios and due to the very high H$^+$ concentrations in sea salt aerosols, HOCl is produced more efficiently than HOBr. Furthermore, HOCl is slightly more soluble than HOBr and thus the cycling between the phases is potentially faster for chlorine than bromine species.

Generally, the low relative humidity and thus the very low liquid water content of sea salt aerosols (11$\cdot$10^{12} m$^3_{aq}$/m$^3_{gas}$) is the reason for the slow recycling of mainly bromine species on aerosol particles. The lower the liquid water content of an aerosol particle, the lower is the uptake rate of a gas phase species. Even though the bromide content of freshly emitted sea salt particles decreases with time (see description of model setup, Section 8.4.1), 'mean' Br$^-$ concentrations in sea salt aerosols increase with time (0.5 - 5.6 mmol/l, Fig. 9.1 g). The bromine explosion reaction - one of the most important Br$^-$ sink reactions in sea salt aerosols - gets slightly faster with time, however its reaction rate is very slow (4.7 - 3.8$\cdot$10^{-5} pmol/(m^{3}s)) leading to the increase of bromide concentrations

a)

b)

c)

d)

e)
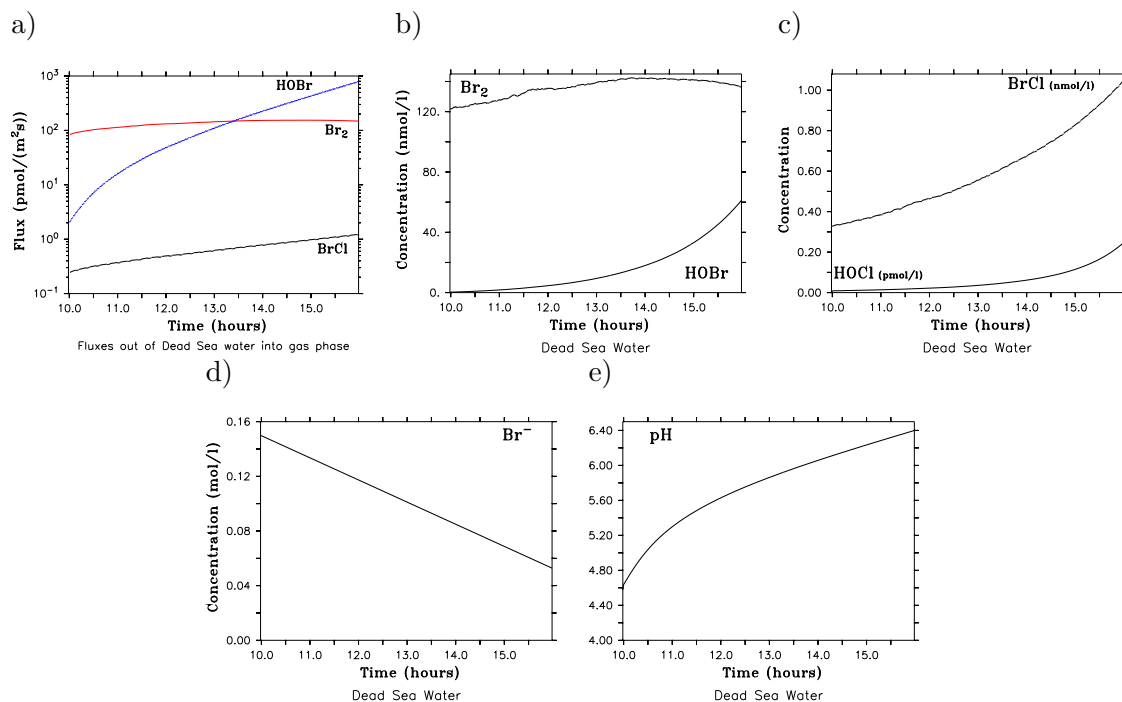
Figure 9.2: The fluxes of Br$_2$ (red solid line), BrCl (black dashed line) and HOBr (blue dotted line) out of the Dead Sea water are shown (a). Plots (b - d) show concentrations of several bromine containing species in the Dead Sea Water and Figure 9.2 (e) shows the pH of the Dead Sea water. All plots refer to scenario **EXALL**.

in the aerosol.

Clearly the model setup only including the interacting gas - and aerosol phase chemistry is not appropriate to simulate ozone depletion events and BrO levels in the range of 100 pmol/mol over the Dead Sea and air-sea exchange of halogen species is now also taken into account. Scenarios including the explicit treatment of air-sea exchange are now discussed in detail.

9.1.2   Lagrangian runs with Air-Sea-Exchange

9.1.2.1   Air-Sea Exchange and Water Chemistry

First of all the fluxes of bromine and chlorine species out of (into) the water of the Dead Sea and chemistry taking place in the Dead Sea water have to be investigated in detail. Only fluxes for scenario EXALL are discussed here as the magnitude of fluxes as well as aqueous phase concentrations in the water do not differ significantly between the scenarios. Figure 9.2 a shows fluxes (in pmol/(m^{2}s)) for Br$_2$ (red line), BrCl (black dashed line) and HOBr (blue dotted line) out of the Dead Sea water into the gas phase. Fluxes of all other halogen species are more than three orders of magnitude lower than the BrCl flux (which is the smallest flux shown) and thus of minor importance and not plotted in Figure 9.2 a. The strength of degassing of Br$_2$ (80 - 154 pmol/(m^{2}s)) stays on the same order of magnitude during the simulation time. It increases slightly until about 14:00 and then decreases slightly until 16:00. The change of order of magnitude with time for both other fluxes plotted in the same figure is much larger. BrCl and HOBr fluxes increase from 0.23 to

1.22 pmol/(m^{2}s) and 2 to 800 pmol/(m^{2}s), respectively. As explained in Section 8.4.1 describing the model setup, Br$^-$ and H$^+$ concentrations in the Dead Sea water are decreased during the six hours that the model column moves from the South to the North of the Dead Sea (Figures 9.2 d and e show Br$^-$ concentrations and the pH in the Dead Sea water). Regarding those background conditions it is surprising that Br$_2$ fluxes stay nearly constant and HOBr and BrCl fluxes even increase with time.

The direction and the strength of the tracer fluxes are driven by gas phase and aqueous phase concentrations as well as the tracers' solubility and the wind speed. Gas phase concentrations of all halogen species that are exchanged increase with time (Figure 9.4). Concentrations of HOBr in the water rise from 0.29 nmol/l to 61 nmol/l which is an increase by about 99% (Figure 9.2 b). Concentrations of Br$_2$ in the water slightly increase in the first three hours of simulation time from about 121 nmol/l to 142 nmol/l and then decrease slightly to about 136 nmol/l (Figure 9.2 b). As was explained in the introduction in Section 8.3.3, the same chemistry mechanism as used for sea salt aerosols is also applied to the chemistry taking place in the Dead Sea water. Thus, the most important reaction for activating bromine chemistry is the bromine explosion mechanism (red reaction path in Figure 9.3):

$$HOBr + Br^- + H^+ \rightleftharpoons Br_2 \tag{9.1}$$

Even though bromide concentrations and the acidity in the water are decrease with time in the model, they remain high enough so that the equilibrium reactions produce Br$_2$ throughout the simulation time (indicated through the larger red arrow in Figure 9.3 pointing at Br$_2$). The forward reaction (of Reaction 9.1) is getting only slightly slower in the last two hours between 14:00 and 16:00 as Br$^-$ and H$^+$ get less abundant with time, leading to the small decrease in Br$_2$ concentrations followed by a decrease in the Br$_2$ flux. Even though Br$^-$ concentrations decrease to about a third of their initial value after 6 hours of simulation time (from 0.15 to 0.05 mol/l, Fig. 9.2 d), the absolute concentrations at 16:00 are still very large. Furthermore, HOBr concentrations increase strongly with time, which will be explained below. Thus the ratio of the forward to the backward reaction of the equilibrium reaction (9.1) even increases slightly with time, but the absolute reaction rate slightly decreases with time. This explains why the bromine explosion reaction does not get significantly slower with time and the decrease in Br$_2$ concentrations in the Dead Sea water with time is negligibly small. Additionally the increase of the pH to a value of 6.4 (thus the water is still slightly acidic) at 16:00 does not yet limit Br$_2$ formation
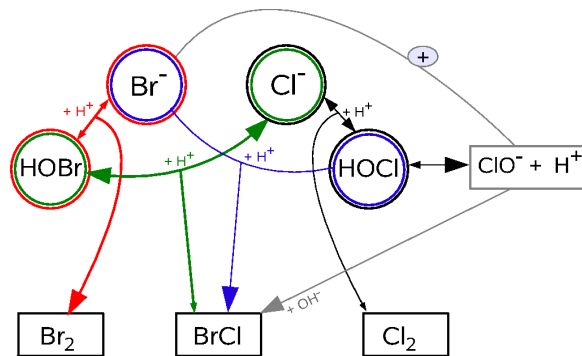

Figure 9.3: Chemical aqueous phase equilibria. Large arrows indicate whether the forward or backward reaction tends to dominate.

significantly compared to a value of 5 (Fickert et al., 1999).

In contrast to Br_2, HOBr concentrations increase nearly exponentially with time. Besides for the conversion of Br^- into Br_2, HOBr is needed to convert Cl^- into BrCl (green reaction path in Figure 9.3):

$$HOBr + Cl^- + H^+ \quad \rightleftharpoons \quad BrCl \tag{9.2}$$
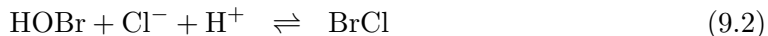
Due to the very high Cl^- and H^+ concentrations this reaction is very fast. Throughout the 6 hours of simulation time the backward reaction of the equilibrium reaction (9.2) is faster (indicated by large green arrows in Figure 9.3 pointing at HOBr and Cl^-) than the reverse reaction. Thus the backward reaction is a net source for HOBr in the Dead Sea water. In contrast, within aerosol particles, the forward reaction is in general faster than the backward reaction and BrCl is net produced. The explanation for the shift of the equilibria in the Dead Sea water can be found in the very high salt content and the very high and changing bromide content as well as the very low and changing pH of the Dead Sea water. Apart from reaction 9.2, BrCl is produced by other pH dependent but non-equilibrium reactions within the water of which the fastest two are shown in Figure 9.3 (blue and grey reaction path in Fig. 9.3):

$$HOCl + Br^- + H^+ \quad \longrightarrow \quad BrCl \tag{9.3}$$
$$Br^- + ClO^- + H^+ \quad \longrightarrow \quad BrCl + OH^-. \tag{9.4}$$
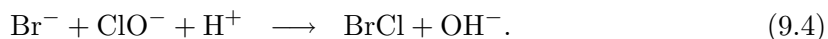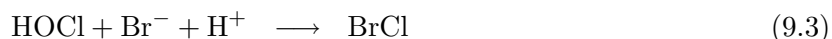
Exemplarily the increase of HOBr as well as of HOCl concentrations in the Dead Sea water from South to North can be seen as follows:

As both H^+ and Br^- concentrations decrease with time, less HOCl is consumed with time forming BrCl (via reaction 9.3, 'blue' reaction path in Fig. 9.3). This leads to an increase of HOCl concentrations followed by a stronger net production of ClO^- via the equilibrium reaction:

$$HOCl \rightleftharpoons ClO^- + H^+ \tag{9.5}$$

(black reaction path in Fig. 9.3) followed by a stronger production of BrCl (via reaction 9.4, grey reaction path in Fig.9.3). This now leads to an increase in BrCl concentrations followed by a stronger conversion to HOBr (via reaction 9.2, green reaction path in Fig. 9.3).

The strongly increasing HOBr concentrations in the water determine the strength of the HOBr flux into the atmosphere which exceeds the Br_2 flux (after 13:40) even though hypobromous acid is more soluble than Br_2.

Chemical reactions tend to push the coupled water - gas phase - aerosol phase chemistry system into a new steady state as the initial steady state of the gas phase-aerosol phase chemistry system (over the desert) gets destroyed as soon as the model column moves over the water.

9.1.2.2   Gas phase Chemistry

Figure 9.4 shows gas phase mixing ratios for scenarios EX (red dash-dotted line), EXALL (black line), SUB (blue dashed line) and EXLIM (green dotted line).

For scenario EX, EXALL and SUB, BrO mixing ratios increase rapidly within a few minutes up to 10 pmol/mol and increase further up to 102 pmol/mol for scenario EX, 151 pmol/mol for EXALL and 144 pmol/mol for scenario SUB indicating that the Dead
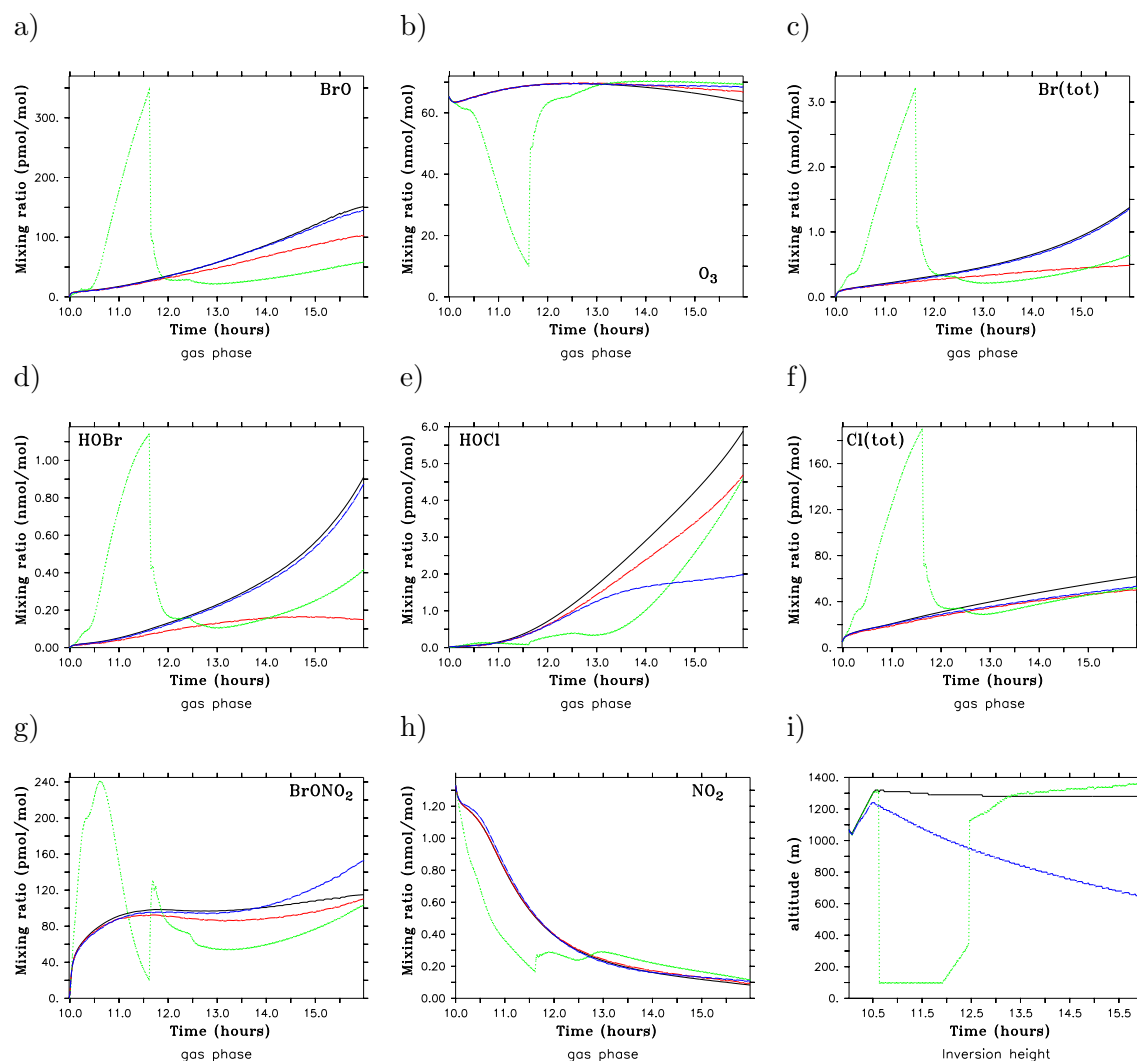
Figure 9.4: Plotted are gas phase mixing ratios at $2\,\mathrm{m}$ altitude for scenarios **EX** (red dash-dotted line), **EXALL** (black line), **SUB** (blue dashed line) and **EXLIM** (green dotted line) for the six hours model run time from the South (10:00) to the North end (16:00) of the Dead Sea. Plot (i) shows the boundary layer height for scenarios **EXALL**, **SUB** and **EXLIM**.

Sea water itself has to be considered as an important source for gas phase bromine species as the calculation of air-sea exchange is necessary in the model to simulate BrO mixing ratios on the same order of magnitude as field measurements show. The difference of about $50\,\mathrm{pmol/mol}$ BrO between scenario EX and EXALL can be explained with the very high gas phase HOBr mixing ratios in scenario EXALL (HOBr$_{(max)}$: $0.91\,\mathrm{nmol/mol}$ in EXALL compared to HOBr$_{(max)}$: $0.14\,\mathrm{nmol/mol}$ in EX) caused by the additional HOBr source due to direct degassing out of the Dead Sea water (Fig. 9.4 d). Hypobromous acid is under the prevailing circumstances an important precursor species for gas phase bromine as it is photolysed to form Br atoms (and OH radicals) which react with ozone to produce BrO. Under less dry atmospheric conditions, HOBr is taken up into sea salt aerosols quickly due to its high solubility. However, as the liquid water content of aerosol particles is very low, like mentioned above in Section 9.1.1 the uptake of gas phase species in aerosol particles

is not efficient. As additionally the source of HOBr due to degassing out of the Dead Sea water is large, a significant fraction of HOBr gets photolysed and provides an efficient source for Br atoms.

The steadily increasing BrO mixing ratios in scenarios EX, EXALL and SUB are caused by the constantly strong fluxes of bromine species out of the water. The most important source reaction of bromine atoms is photolysis of molecular bromine. Even though gas phase Br_2 gets quickly photolysed to Br (by reaction 9.6):

$$Br_2 + h\nu \quad \longrightarrow \quad 2Br \tag{9.6}$$

$$Br + O_3 \quad \longrightarrow \quad BrO + O_2 \tag{9.7}$$
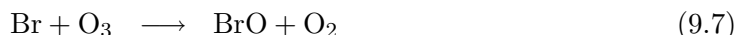
the reaction rate is in the range of $60\text{-}153\,\text{pmol}/(\text{m}^3\text{s})$ at $0.5\,\text{m}$ directly above the water surface and about $10\text{-}40\,\text{pmol}/(\text{m}^3\text{s})$ at $2\,\text{m}$ altitude. Regarding all Br_2 source and sink reactions, the large additional source of bromine compounds due to the air-sea exchange $(81\text{-}154\,\text{pmol}/(\text{m}^2\text{s}))$ leads to an accumulation of bromine in the air. Even though the largest source and sink reactions for Br_2 are in the same order of magnitude, the source of gas phase Br_2 due to air-sea exchange is slightly larger than the Br_2 photolysis throughout the simulation time. This leads indirectly also to the steady increase in BrO mixing ratios via reaction 9.7. The accumulation of HOBr due to air-sea exchange can be seen very well in Figure 9.4 d in the difference between the black line (EXALL) and the red dash-dotted line (EX). The increase in HOBr mixing ratios also indicates increasing BrO mixing ratios as HOBr is an indirect source of BrO as mentioned above.

The influence of those high bromine concentrations as simulated in scenarios EXALL, EX or SUB on O_3 chemistry is still small. The decrease from $69\,\text{nmol/mol}$ at 12:00 to $66\,\text{nmol/l}$ at 16:00 in scenario EX, as well as the decrease from 69 to $63\,\text{nmol/mol}$ (EX-ALL) is insignificant compared to the observed depletion events. The difference in O_3 mixing ratios in scenario EXALL means an O_3 reduction of only 9%. For scenario SUB O_3 does not decrease at all while the model is approaching the North shore of the Dead Sea. Subsidence, on the one hand side limits vertical transport of e.g. bromine species such that tracers might potentially accumulate stronger in the lower parts of the boundary layer. On the other hand O_3 and its precursor species like NO_2 subside from aloft. Thus the slightly larger sink of O_3 due to potentially slightly larger Br mixing ratios is ruled out by a slightly larger O_3 source potential. As was said while explaining the model setup in Section 8.4.1, subsidence gets intensified during the afternoon hours and as a consequence the boundary layer hight decreases within the six hours of simulation time (see Fig. 9.4 i). However, as the boundary layer height is larger than $800\,\text{m}$ until about 13:30, the effect of subsidence on bromine species at $2\,\text{m}$ altitude is negligible .

In Scenario EXLIM vertical transport is limited in the first two hours of simulation time leading to the sharp increase in BrO mixing ratios between 10:00 and 11:40 from below 1 up to $395\,\text{pmol/mol}$ and the likewise quick decrease to about $30\,\text{pmol/mol}$ between 11:40 and 13:00 (Fig. 9.4 a, green dotted line). After BrO mixing ratios reach a minimum value of $22\,\text{pmol/mol}$ at 12:50 they increase smoothly during the remaining three hours 'travel' time from South to North up to a value of $65\,\text{pmol/mol}$. Simultaneous to the very fast increase of BrO mixing ratios in the first 1.5 hours that the model crosses the Dead Sea, O_3 mixing ratios decrease until they reach a minimum of $9.3\,\text{nmol/mol}$ at 11:40 (Fig. 9.4 b, green dotted line). However, as soon as the low-level inversion is compensated, BrO mixing ratios start to decrease (very rapidly between 11:30 and 12:00) and O_3 quickly reaches background mixing ratio of about $69\,\text{nmol/mol}$ due to vertical mixing.

The limited O_3 destruction in scenarios EX, EXALL and SUB might be surprising on the first glance regarding the extraordinarily high BrO levels. Reaction 9.7 takes place roughly at a rate of $60\,\text{-}\,300\,\text{pmol}/(\text{m}^3\text{s})$ (at 2 m, EXALL). At the beginning (South) of the simulation time this reaction is much slower and at the end (North) it is much faster than the most efficient O_3 production reaction ($430\,\text{-}\,11\,\text{pmol}/(\text{m}^3\text{s})$):

$$NO_2 + h\nu \longrightarrow NO + O_3. \tag{9.8}$$

At the same time however, a large amount of BrO gets photolysed leading to the formation of O_3 and Br:

$$BrO + h\nu \longrightarrow Br + O_3. \tag{9.9}$$

Even though the net O_3 destruction is larger than the net O_3 production at 2 m altitude especially in the afternoon hours, the contribution of the strong O_3 sink due to reaction with halogens to the total O_3 mass balance is still not large enough to lead to a distinctive ODE and only leads to the slow (but steady) decrease of O_3 mixing ratios. As O_3 is distributed homogeneously within the boundary layer and mixing ratios of bromine species show a strong vertical gradient (see Fig. 9.5), the destruction of O_3 in the lower part of the boundary layer (due to bromine chemistry) is quickly compensated by the strong vertical transport.

The boundary layer height for scenarios EXALL, SUB and EXLIM is shown in Figure 9.4 i. For scenario EXALL it is almost constant at 1300 m altitude for the six hours of simulation time. As was stated out above in the introduction in Section 8.3.1, the boundary layer height in the model is calculated via buoyancy. Thus the high temperature at ground level ($\approx 34°$C, see Fig. 8.4) contributes strongly to the boundary layer height of 1300 m. Between 10:30 and 11:00 the inversion at 100 m altitude limits transport in scenario EXLIM. However, after the inversion is compensated, the boundary layer reaches the same height as in scenario EXALL (1300 m). As was said above, in scenario SUB the boundary layer height decreases from about 1200 m to 650 m at 16:00 due to subsidence. Figure 9.5 shows the vertical distribution of BrO and O_3 mixing ratios for scenarios EXALL, EXLIM and SUB up to an altitude of 1400 m (note the logarithmic scaling of the y-axis!).
BrO mixing ratios in scenario EXALL and SUB tend to increase with time throughout the boundary layer. From 13:00 on mixing ratios exceed 5 pmol/mol even at 1000 m altitude in scenario EXALL (Fig. 9.5 a) and increase further at this height up to 20 pmol/mol at 16:00, when it is supposed that the North shore of the Dead Sea is reached. It can nicely be seen that there is a delay of about one hour between the start of the model run at 10:00 when BrO surface values exceed 1 pmol/mol after a few minutes until BrO mixing ratios in 1000 m also exceed 1 pmol/mol at 11:00. As due to the subsidence the upward transport of tracers is slightly weaker in scenario SUB than in scenario EXALL, BrO mixing ratios at 700 m altitude at 12:00 are 2 pmol/mol in scenario EXALL and 1 pmol/mol in scenario SUB. In general the effect of the subsidence in scenario SUB and the resulting decrease in boundary layer height on the vertical distribution of BrO mixing ratios is small compared to scenario EXALL (Fig. 9.5 b). The limitation of vertical transport up to an altitude of 700 m between 15:00 and 16:00 in scenario SUB does not lead to a significant increase in BrO mixing ratios near ground level as was already stated out above.
Even though more than 10 pmol/mol BrO can be found in altitudes between 100 and
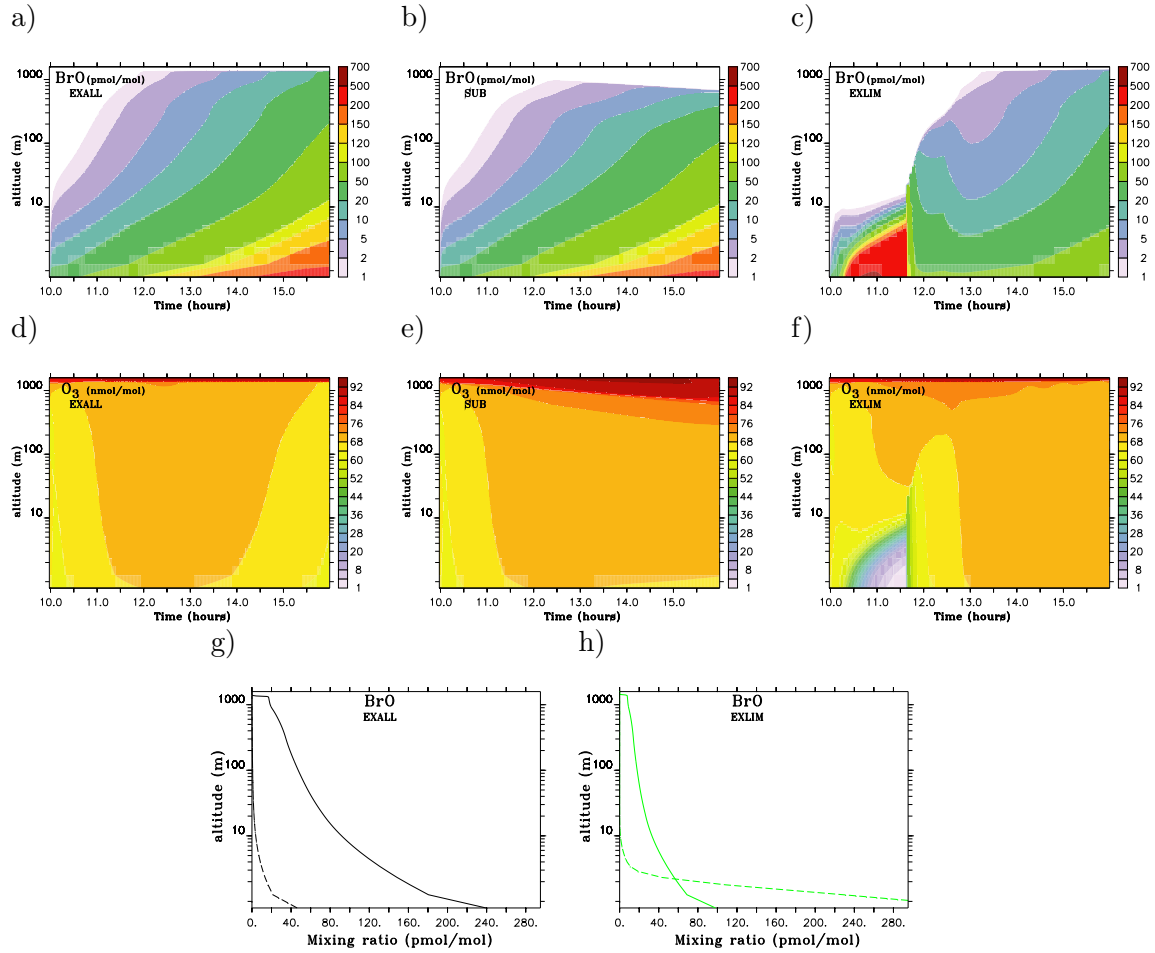
Figure 9.5: This figure (a-f) shows the vertical distribution of BrO (pmol/mol) and O_3 (nmol/mol) mixing ratios for the six hours model run time from the South (10:00) to the North end (16:00) of the Dead Sea for scenarios **EXALL**, **SUB** and **EXLIM**. Furthermore vertical BrO profiles of scenario EXALL (g) and EXLIM (h) are shown at 10:30 (dashed line) and 15:30 (solid line).

1000 m after 13:00 in scenarios EXALL and SUB, the strong vertical gradient in mixing ratios is striking (note the logarithmic scaling of the colour code in plots showing BrO mixing ratios!). To point out this aspect, Figure 9.5 g shows the vertical profiles of BrO mixing ratios at 10:30 (dashed lines) and 15:30 (solid lines) for scenario EXALL. Mixing ratios at 15:30 are only half the ground level values at 10 m altitude (180 pmol/mol $\longrightarrow$ 90 pmol/mol) and at 100 m altitude they are almost a factor of four smaller than mixing ratios directly above the Dead Sea water surface. At 10:30 the vertical gradient in BrO mixing ratios is even larger as the bromine load in the boundary layer is still lower than at 15:30 but the fluxes of bromine species out of the Dead Sea water are strong throughout the simulation time.

Regarding O_3 mixing ratios, the vertical distribution is nearly unaffected by bromine chemistry throughout the boundary layer for scenario EXALL (Fig. 9.5 d) as well as scenario SUB (Fig. 9.5 e). As bromine species are quickly distributed all over the boundary layer, mixing ratios are at the same time strongly diluted. Thus the O_3 destruction potential of halogen chemistry in altitudes larger than 100 m is not significant anymore. The net O_3

production is larger than the net O_3 destruction. Thus vertical mixing of O_3 compensates quickly the (net) O_3 destruction in the lowest parts of the boundary layer. However, in the last hour of simulation time more than 20 pmol/mol of BrO can be found even in heights exceeding 700 m. Under these conditions, O_3 loss processes get stronger also in the upper part of the boundary layer such that vertical transport cannot totally compensate the O_3 destruction in the lowest 10 m of the boundary layer anymore. As a consequence, O_3 mixing ratios decrease slowly with time.

As was discussed above O_3 is depleted strongly and quickly in scenario EXLIM between 10:30 and 11:30. As bromine mixing ratios are high only in the lowest meters above sea level due to the limited vertical transport (Fig. 9.5 c), O_3 destruction is also restricted to the lowest 10 - 20 m of the boundary layer (Fig. 9.5 f). Above this inversion layer O_3 mixing ratios are again hardly affected by bromine chemistry. As soon as the inversion is compensated, O_3 gets again rapidly well mixed throughout the whole boundary layer. After 13:30, when the boundary layer height quickly rises to 1300 m, BrO is also quickly distributed all over the boundary layer and mixing ratios are between 2 pmol/mol and 50 pmol/mol all over the boundary layer.

Figure 9.5 h shows in addition the vertical profiles of BrO mixing ratios in scenario EXLIM at 10:30 and 15:30. The vertical gradient is very large at 10:30 where mixing ratios decrease from 400 pmol/mol at 0.75 m above water level to 0.1 pmol/mol at 20 m altitude. At 15:30 the vertical gradient of BrO mixing ratios is similar to scenario EXALL.

As was mentioned in the model setup description in Section 8.4.1 all simulations were initialised with the same fields for chemistry. NO_2 mixing ratios were chosen such that they were roughly 1 nmol/mol in the morning (6:00) of the day that the model column is supposed to cross the Dead Sea between 10:00 and 16:00. NO_2 mixing ratios decrease stronger under the influence of the high bromine levels ($1.37 \rightarrow 0.09$ nmol/mol for EX, $1.37 \rightarrow 0.08$ nmol/mol for EXALL, $1.37 \rightarrow 0.11$ nmol/mol for SUB, Fig. 9.4 h) compared to scenario NOEX ($1.37 \rightarrow 0.22$ nmol/mol). Mixing ratios of $BrONO_2$ that is mainly formed by reaction between BrO and NO_2:

$$BrO + NO_2 \longrightarrow BrONO_2 \qquad (9.10)$$
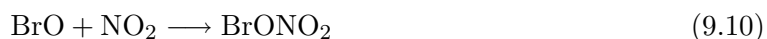
increase with time and have maximum values of 110 pmol/mol (EX), 115 pmol/mol (EX-ALL) and 153 pmol/mol (SUB) which can be seen in Figure 9.4 g. Thus bromine is a direct sink for O_3 (reaction 9.7) but it is also an indirect sink as BrO reacts efficiently with NO_2 therefore reducing photochemical O_3 production (reaction rates for Reaction 9.10 are: $7 \rightarrow 24$ pmol/(m³s) EXALL, $7 \rightarrow 18$ pmol/(m³s) EX, $7 \rightarrow 30$ pmol/(m³s) SUB). However, this latter indirect effect of bromine chemistry on O_3 mixing ratios is only a small contribution to the overall O_3 source/sink budget.

In general $BrONO_2$ reacts very efficiently on the surfaces of sulphate or sea salt aerosols. This sink reaction (starting the recycling of halogens in the liquid phase) is however very slow in the presented Lagrangian studies due to the low ambient humidity and due to the very low liquid water content of aerosol particles.

As the subsidence in scenario SUB influences the vertical NO_2 distribution leading to larger concentrations in the lowest two meters, $BrONO_2$ mixing ratios in this scenario are also higher than in all other presented scenarios.

In scenario EXLIM, $BrONO_2$ mixing ratios reach a maximum value of 241 pmol/mol at 10:40 which is about one hour before BrO reaches its maximum value of 395 pmol/mol. $BrONO_2$ mixing ratios in scenario EXLIM start to decrease before the limitation of verti-

cal transport stops, mainly because NO_2 mixing ratios decrease strongly due to the very fast reaction with BrO. The production of $BrONO_2$ is self-limited as one of the reactants, i.e. NO_2 gets very efficiently destroyed. However, it has to be noted that NO_2 mixing ratios stay always high enough such that O_3 can still be efficiently reproduced by NO_2 photolysis. However, quick vertical mixing controls O_3 mixing ratios in the lowest part of the atmosphere as soon as the boundary layer height is high and exceeds $1000\,m$ (see Fig. 9.4 b, h as well as Fig. 9.5 f).

In the following, the effect of the direct degassing of halogen species out of the Dead Sea water on other halogen species than BrO and HOBr is discussed.

If total gas phase bromine mixing ratios (Fig. 9.4 c) of scenarios EX (0.2 - 0.4 nmol/mol), EXALL (0.2 - 1.3 nmol/mol, similar to SUB) and EXLIM (2.1 - 0.2 nmol/mol) are compared to those of scenario NOEX (i.e. the scenario not including air-sea-exchange) it can be seen that they increased by two orders of magnitude due to the additional source by direct degassing out of the Dead Sea water and now also exceed total gas phase chlorine mixing ratios.

Apart from the flux of BrCl, no other fluxes of chlorine containing species out of the water into the gas phase were shown in Figure 9.2 a as they are very small and are obviously only of minor importance for the gas phase chlorine budget much in contrast to the importance of the air-sea exchange for the gas phase bromine budget. Acid displacement is still the dominant source for gas phase chlorine compounds despite the vertically limited calculation of aerosol phase chemistry in the model due to the low relative humidity. Thus it is not surprising that mixing ratios of chlorine species are very similar in all presented model runs (including scenario NOEX) as the initial conditions are always the same for all simulated scenarios and the composition of freshly emitted sea salt particles is the same ($Cltot_{max}$: 61 pmol/mol EXALL, $Cltot_{max}$: 50 pmol/mol EX, $Cltot_{max}$: 48 pmol/mol NOEX,).

The small difference in total gas phase chlorine mixing ratios between scenario EX (red dashed-dotted line, Fig. 9.2 f) and EXALL (black line, Fig. 9.2 f) is only an indirect effect of the degassing process. The flux of HOCl out of the Dead Sea water is very small in scenario EXALL. However, it leads to slightly larger HOCl gas phase mixing ratios compared to scenario EX. As a consequence the recycling on aerosol particles of chlorine compounds is slightly stronger in scenario EXALL compared to scenario EX. Thus the stronger aerosol recycling in scenario EXALL increases gas phase HOCl as well as HCl gas phase mixing ratios compared to scenario EX (EXALL: $HOCl_{(max)}$: 5.9 pmol/mol and EX: $HOCl_{(max)}$: 4.7 pmol/mol).

With respect to the absolute mixing ratios, this difference is small. The difference between HOCl mixing ratios in scenario EXALL and SUB is more striking as HOCl mixing ratios in scenario SUB only reaches a maximum value of 1.9 pmol/mol at 16:00 (blue dashed line, Fig. 9.4 e).

One effect caused by the strong subsidence assumed in scenario SUB, in especially the last two hours of simulation time is an enhanced particle sedimentation which affects mainly the larger particles, i.e. sea salt aerosols in the model terminology. Due to a stronger sedimentation also the deposition of particles is more efficient. Thus the number of sea salt particles decreases with time at 2 meters altitude. The total number of ('large') sea salt particles is small, however the decrease in number of particles is in the range of 22%. The difference in relative humidity in the lowest 2 meters of the atmosphere between scenarios SUB and EXALL is very small. As a consequence the available water in the atmosphere is distributed on fewer particles leading to an increase of their liquid water content. Related

to the increasing liquid water content is an increase in particle radius and thus a decrease in the mass transfer coefficient (see Fig. 4.1). As the liquid water content and the mass transfer coefficient (and the Henry's law coefficient) determine exchange rates of species between the aerosol and the gas phase (see chapter 4.1), these rates are comparatively smaller in scenario SUB than in scenario EXALL. This effect can mainly be seen in the difference in gas phase HOCl mixing ratios between scenarios EXALL and SUB. No other species are affected this strongly by the smaller mass transfer coefficient in scenario SUB, as in the presented Lagrangian scenarios HOCl is one of the few species that is predominantly controlled by aerosol-gas-phase exchange processes.

Even though it was mentioned several times above that aerosol phase chemistry is considered less important over the Dead Sea, it is still an important source for chlorine compounds as they do not efficiently degas out of the water itself. Again, it is obvious that mixing ratios of reactive chlorine compounds are not significantly large. Even though the effect of subsidence on total chlorine mixing ratios is small, a slight difference to scenario EXALL is still visible whereas hardly any difference can be seen for total bromine between those two scenarios. This shows again that with respect to bromine chemistry the effect of direct air-sea exchange obviously dominates the effect of subsidence.

9.1.3   Sensitivity of water chemistry

As was described while introducing the model setup in Section 8.4.1, the assumptions that were made for calculating chemistry in the Dead Sea water are simplified by not decreasing Cl^- concentrations in the water, as in reality Cl^- concentrations show a gradient in a similar way than Br^- concentrations do. To quantify that this simplification has no implications on the above presented results regarding gas phase chemistry, scenarios CL_{HIGH} (assuming Cl^- mixing ratios representing conditions in the evaporation ponds, i.e. even higher Cl^- concentrations than in scenario EXALL; Cl^- concentrations are not decreased in scenario CL_{HIGH}) and CL_{DECR} (Cl^- concentrations are initialised as in CL_{HIGH}, i.e. representing conditions in the South of the Dead Sea but Cl^- concentrations are decreased with time) are discussed and drawn in comparison to scenario EXALL.

Figure 9.6 shows fluxes of Br_2 (e), HOBr (d) and BrCl (f) out of the Dead Sea water into the atmosphere for cases EXALL (black solid line), CL_{HIGH} (purple dash-dotted line) and CL_{DECR} (green dotted line).

For scenario CL_{DECR}, Cl^- concentrations that are appropriate for the very southern part of the lake were chosen initially and are assumed to decrease towards the North (Fig.9.6 g). The flux of Br_2 in scenario CL_{DECR} (Fig. 9.6 e, green dotted line) increases up to a value that is almost twice as high as in scenario EXALL whereas it is always lower in scenario CL_{HIGH} than in scenario EXALL (max. flux in pmol/(m^{2}s) Br_2: 148 in EXALL, 102 in CL_{HIGH}, 242 in CL_{DECR}). Fluxes of HOBr are however largest in scenario CL_{HIGH} (max. flux in pmol/(m^{2}s) HOBr: 799 in EXALL, 3484 in CL_{HIGH}, 891 in CL_{DECR}).

To understand those model results, Figure 9.3, which gives an overview of the most important equilibrium reactions taking place in the Dead Sea water, has to be considered again. In case of constantly very high Cl^- concentrations (CL_{HIGH}), Br_2 concentrations in the water get lower with time than in case of initially very high, but decreasing Cl^- concentrations (CL_{DECR}). At the same time, HOBr concentrations in the water show an opposite behaviour, i.e. they are higher in scenario CL_{HIGH} than in CL_{DECR}. The explanation for the different time evolution of several species in the Dead Sea water as well as
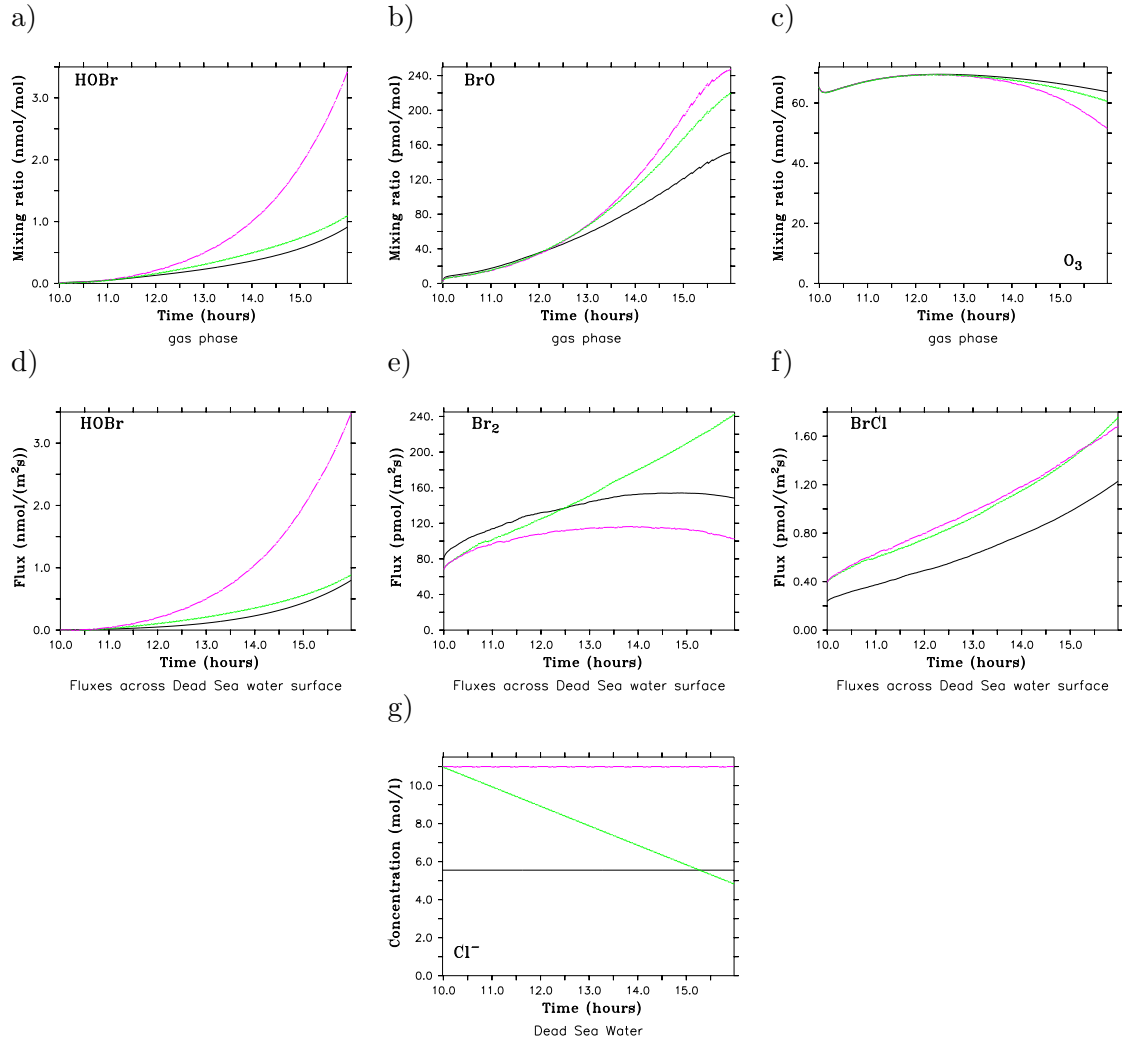
Figure 9.6: Shown are gas phase mixing ratios for HOBr (a), BrO (b) and O_3 (c). Plots (d - f) show fluxes out of the Dead Sea water for HOBr, Br_2 and BrCl. Plot (g) shows Cl^- concentrations in the Dead Sea water. All plots (apart from g) show the time evolution at $2\,m$ altitude and the colour code for all plots is as follows: scenario EXALL (black line), scenario CL_{HIGH} (purple dash-dotted line) and scenario CL_{DECR} (green dotted line).

in the gas phase in scenarios EXALL, CL_{HIGH} and CL_{DECR} is given in the following.

As Cl^- concentrations are constantly higher in the water in scenario CL_{HIGH} than in scenario CL_{DECR}, H^+ is more efficiently consumed by pH - dependant reactions involving Cl^-. Due to the very high Cl^- concentrations during the six hours of simulation time in scenario CL_{HIGH}, these reactions are very fast. Indeed they are much faster than Br^- equilibrium reactions. Thus the more the model approaches the North End of the lake and thus the smaller Cl^- concentrations in scenario CL_{DECR} become, the more H^+ can be consumed by equilibrium reactions involving Br^-, e.g. the bromine explosion reaction. As HOBr is converted into Br_2 by the latter named reaction, HOBr concentrations are lower in scenario CL_{DECR} than in scenario CL_{HIGH} at 16:00.

Br_2 concentrations in the water are also larger in scenario CL_{DECR} at 16:00 compared to

scenario EXALL. Due to the higher Cl^- concentrations at the beginning of the simulation time and related higher HOCl concentrations in scenario CL_{DECR}, the equilibrium reaction

$$HOCl + Br^- + H^+ \longrightarrow BrCl$$

(blue reaction path in Fig. 9.3) is significantly faster than in scenario EXALL. Thus BrCl concentrations in the water are about a factor of two higher in scenario CL_{DECR} than in scenario EXALL and more BrCl can be converted into HOBr via the backward reaction of:

$$HOBr + Cl^- + H^+ \rightleftharpoons BrCl$$
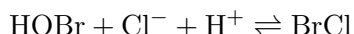
(green reaction path in Fig. 9.3) and more HOBr can be converted into Br_2 via the forward reaction of:

$$HOBr + Br^- + H^+ \rightleftharpoons Br_2$$
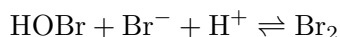
(red reaction path in Fig. 9.3) in scenario CL_{DECR} compared to scenario EXALL.

Comparing now gas phase HOBr mixing ratios between scenarios CL_{DECR} and EXALL, the differences are small ($HOBr_{(max)}$: 0.9 nmol/mol in EXALL and $HOBr_{(max)}$: 1 nmol/mol in CL_{DECR}, see Fig. 9.6 a) as the fluxes of HOBr out of the Dead Sea water are of same order of magnitude in both scenarios. As the strength of degassing is stronger in scenario CL_{HIGH}, gas phase HOBr mixing ratios are about a factor of three larger than in both other scenarios ($HOBr_{(max)}$: 3.4 nmol/mol in CL_{HIGH}).
Gas phase BrO mixing ratios are largest in scenario CL_{HIGH} ($BrO_{(max)}$: 247 pmol/mol) due to the very high HOBr mixing ratios. After 13:00, BrO mixing ratios are also comparatively higher in scenario CL_{DECR} ($BrO_{(max)}$: 219 pmol/mol) than in scenario EXALL ($BrO_{(max)}$: 151 pmol/mol) as the flux of Br_2 out of the Dead Sea water is larger (Fig. 9.6 b, e).
The influence of the higher initial Cl^- concentrations in the Dead Sea water in scenario CL_{DECR} compared to scenario EXALL on O_3 mixing ratios is small (Fig. 9.6 c). The relative decrease in mixing ratios in scenario CL_{DECR} is about 13 % whereas it is 9 % in scenario EXALL. For scenario CL_{HIGH} where Cl^- concentrations in the Dead Sea water are overestimated, the loss in O_3 mixing ratios is of more significance (ΔO_3: 26 %).
Thus initialising Cl^- concentrations in the Dead Sea water higher than in scenario EXALL and letting them decrease with time, leads to higher BrO mixing ratios, however, qualitatively the results do not differ from the results that were drawn from scenario EXALL.

9.1.4 Constant fluxes

As was pointed out above in Section 9.1.2.2, gas phase chemistry is very sensitive to the magnitude of fluxes out of the Dead Sea water. The strength of the fluxes, if calculated explicitly increases with time. The same holds for gas phase mixing ratios of bromine species (see Fig. 9.4).
To point out again that the increase in gas phase mixing ratios (e.g. BrO) with time is not an effect of increasing fluxes but of the intensity of the fluxes leading to an accumulation of bromine species in the gas phase, scenario EXALL was recalculated with constant fluxes
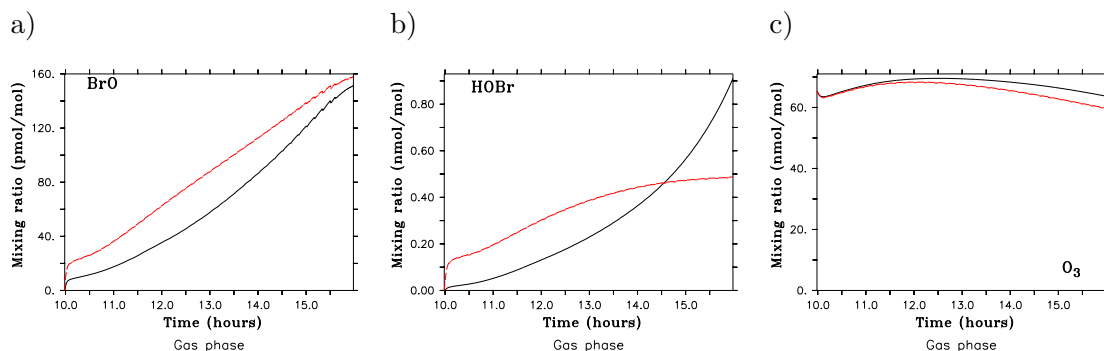
Figure 9.7: This figure shows BrO (a, in pmol/mol), HOBr (b, in pmol/mol) and O_3 (c, in nmol/mol) mixing ratios at 2 m altitude for scenarios **EXALL** (black solid line) and **CONST** (red dashed line).

for gas phase halogens like Br_2, BrCl or HOBr due to air-sea exchange. A mean value from the explicitly calculated fluxes is chosen (see Table 8.3 in Section 8.4 for flux strength).

Figure 9.7 shows gas phase mixing ratios for scenarios EXALL (black solid line) and CONST (red dashed line) at again 2 m altitude. In general gas phase mixing ratios of bromine species are on the same order of magnitude in both scenarios. Even though the fluxes stay constant with time in scenario CONST, BrO mixing ratios increase from 20 pmol/mol at 10:00 to 160 pmol/mol at 16:00 (Fig. 9.7 a). BrO mixing are larger during the six hours of model run time in scenario CONST compared to scenario EXALL. However, if the fluxes (of mainly HOBr and Br_2) in scenario CONST were set to slightly smaller values, BrO mixing ratios would be constantly smaller than in scenario EXALL but they would still increase with time.

The increase with time in HOBr mixing ratios is less strong in scenario CONST compared to scenario EXALL. As a mean value for the flux of HOBr from the explicitly calculated (and permanently increasing) fluxes in scenario EXALL is used in scenario CONST, HOBr mixing ratios are larger in scenario CONST than in scenario EXALL until 14:30 and afterwards they are significantly smaller (Fig. 9.7 b).

Figure. 9.7 c shows O_3 mixing ratios for scenario CONST and EXALL. As the bromide content at 2 m altitude is larger in scenario CONST than in scenario EXALL, i.e. more BrO is produced and thus more O_3 is consumed, O_3 mixing ratios decrease stronger with time in scenario CONST than in scenario EXALL. However, the relative decrease in O_3 mixing ratios in scenario CONST is in the range of 12 %. O_3 mixing ratios do not drop below 60 nmol/mol. Even though the loss in O_3 is larger in scenario CONST than in scenario EXALL, it is still much lower than the rapid and strong O_3 depletion events as observed along the Dead Sea.

9.1.5   Enhanced fluxes

With none of the Lagrangian scenarios presented above neither an ozone depletion event affecting the whole boundary layer could be simulated nor any O_3 depletion in case of a deep and well mixed boundary layer. It is possible that the fluxes of bromine species out of the very shallow and highly concentrated evaporation ponds are underestimated by the air-sea exchange parameterisation or even the bromide content of the water itself. Furthermore, heterogeneous reactions on salt deposits on the shore might be an additional bromine source especially over the southern part of the Dead Sea as the water level of the

a)

b)

c)

d)

e)

f)
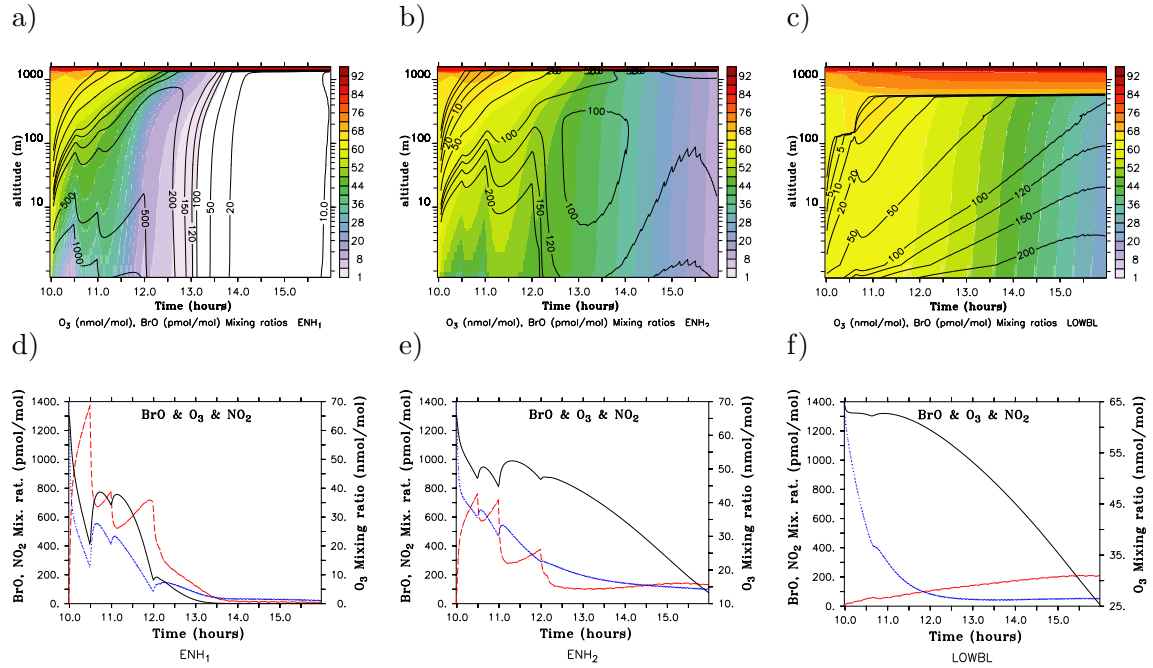
Figure 9.8: Figures in the top row show BrO (contour lines, in pmol/mol) and O_3 (shaded in nmol/mol) mixing ratios over the whole boundary layer for scenario ENH_1 (a), ENH_2 (b) and LOWBL (c) for the six hours that the model crosses the Dead Sea. Note the logarithmic scaling of the y-axis. Figures in the bottom row show BrO (red dashed lines, in pmol/mol), NO_2 (blue dotted lines, in pmol/mol) and O_3 (black solid lines, in nmol/mol) mixing ratios at 2 m altitude for the three scenarios ENH_1 (d), ENH_2 (e) and LOWBL (f).

evaporation ponds is frequently varied. For scenarios ENH_1 and ENH_2 the fluxes out of the water were enhanced for the first two hours of simulation time which is the time the model is roughly assumed to cross the evaporation ponds.

For scenario ENH_1 fluxes were enhanced by a factor of 50 for the first half hour, a factor of 20 until 11:00 and a factor of 10 until 12:00. Afterwards, the fluxes as calculated by the air-sea exchange parameterisation are not modified anymore. This leads to maximum BrO mixing ratios of nearly 1400 pmol/mol at 10:30 at 2 m altitude (red dotted line, Fig. 9.8 d). Between 10:30 and 12:00, mixing ratios stay around 700 pmol/mol and decrease rapidly afterwards and stay nearly zero between 14:00 and 16:00 . The strong decrease in BrO mixing ratios after 12:00 is not a consequence of the decreased out-gassing strength but of the strong loss in O_3. During the first half hour of extremely enhanced air-sea exchange, O_3 mixing ratios drop from 65 to 18 nmol/mol (black line, Fig. 9.8 f). As soon as the fluxes of Br_2, BrCl and HOBr are decreased after 10:30, O_3 mixing ratios even increase again up to 37 nmol/mol. However, after about 11:20 O_3 mixing ratios decrease steadily and stay below 1 nmol/mol after 13:00.

For scenario ENH_2 fluxes were 'only' enhanced by a factor of 30 during the first 30 minutes of simulation time. Afterwards, fluxes are treated in the same way as in scenario ENH_1. Between 10:00 and 11:00 BrO mixing ratios are between 600 and 750 pmol/mol (red dotted line, Fig. 9.8 e). Simultaneously O_3 mixing ratios decrease from 65 to 47 nmol/mol (black line, Fig. 9.8 e). As the strength of degassing is again decreased after 11:00, BrO mixing

ratios decrease quickly to about 300 pmol/mol. After 12:00, BrO mixing ratios drop further to about 100 pmol/mol and stay more or less constant around this value until 16:00. During the same time span O_3 mixing ratios decrease constantly, but not very fast and reach a minimum value of 13 nmol/mol at 16:00.

Photolysis of NO_2 is by far the most important O_3 source in the troposphere. In scenario ENH_1, NO_2 is quickly consumed by reaction with BrO (leading to the formation of $BrONO_2$) within the first two hours due to the very high BrO mixing ratios which are even larger than those of NO_2 (see Fig. 9.8 d). The efficient NO_2 sink via reaction with BrO is less strong in scenario ENH_2 as BrO mixing ratios are lower (see Fig. 9.8 e). Thus the process of O_3 reproduction via NO_2 photolysis is nearly totally inhibited in scenario ENH_1 after 12:00 whereas it is still productive to some extend in scenario ENH_2. The difference in NO_2 mixing ratios between both scenarios contributes to the different time evolution in O_3 mixing ratios. However, the ratio of O_3 destruction (by reaction with Br) to O_3 production in scenario ENH_1 is too large such that unrealistically high NO_2 mixing ratios would be required to produce significant O_3 mixing ratios purely by chemical reaction. The unregular features in mixing ratios in scenarios ENH_1 and ENH_2 are only artifacts of disrupting the model to run freely by changing the strength of the fluxes.

For both scenarios the 'afternoon' ozone depletion event affects the whole boundary layer up to an altitude of 1200 m (Fig. 9.8 a and b). Comparing the vertical distribution of BrO mixing ratios between scenarios EXALL and ENH_2, leads to the explanation why the depletion event affects the whole boundary layer in scenario ENH_2 but not in scenario EXALL. BrO mixing ratios are approximately 100 pmol/mol all over the boundary layer after 12:00 in scenario ENH_2 whereas mixing ratios never exceed 50 pmol/mol in altitudes larger than 100 m in scenario EXALL. Thus, due to the enhanced fluxes during the first two hours of simulation time the bromine load all over the boundary layer is significantly higher in scenario ENH_2 than in scenario EXALL during the whole simulation time. As a consequence, in scenario ENH_2 O_3 is destroyed all over the boundary layer by reaction with Br such that vertical mixing cannot compensate anymore the depletion as it happened in e.g. scenario EXALL. Surprising might still be the delayed decrease in O_3 mixing ratios especially in scenario ENH_2 compared to the times of maximum BrO mixing ratios. Only the formation of extremely high BrO mixing ratios in the first hour in scenario ENH_1 is followed by a strong *and* quick O_3 decrease. However, as bromine cannot be efficiently transported into the upper part of the boundary layer within minutes this 'morning' depletion event is restricted to the lowest 10 - 100 m (Fig. 9.8 a)

For scenario LOWBL background conditions were assumed leading to a constantly much lower boundary layer (500 m) than in all other by now presented Lagrangian studies. It has to be reminded that therefore the temperature in the atmosphere had to be decreased by more than 5°C compared to the other scenarios and thus relative humidity in scenario LOWBL is higher than in other scenarios all over the boundary layer (see Fig. 8.4). This also indicates that aerosol phase chemistry gains in importance as it is not only calculated in the lowest 2 - 4 meters but also constantly in altitudes exceeding 300 meters. BrO gas phase mixing ratios increase with time as it was seen before (see Fig. 9.8 f). Compared to scenario EXALL, they increase stronger with time ($BrO_{(max)}$: 207 pmol/mol (LOWBL) versus $BrO_{(max)}$: 151 pmol/mol (EXALL)). Simultaneously to the increase in BrO mixing ratios, O_3 mixing ratios decrease from 65 to 25 nmol/mol at 2 m altitude. As in scenarios ENH_1 and ENH_2 the depletion of O_3 affects the whole boundary layer (see Fig. 9.8 c). Even though O_3 mixing ratios never drop below 25 nmol/mol, the simulated depletion event shows a similar spacial evolution and strength as a depletion event over the Dead
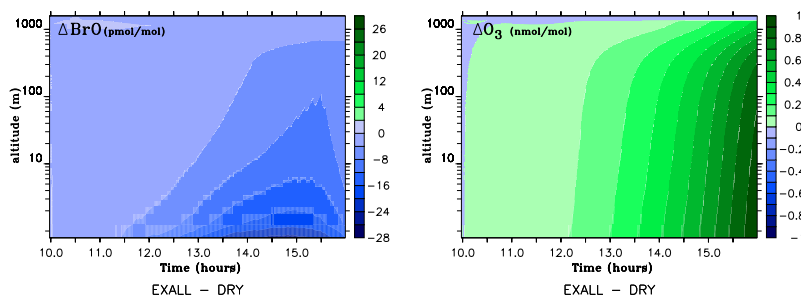
Figure 9.9: The difference of gas phase mixing ratios between scenarios **EXALL** and **DRY** all over the boundary layer is plotted for the six hours model run time over the Dead Sea for BrO (in pmol/mol) and O_3 (in nmol/mol) (EXALL - DRY)

Sea that was observed while flight measurements were performed, i.e. a depletion event affecting only the northern part of the Dead Sea. Very similar to scenario LOWBL or ENH_1 the decrease in O_3 was not only restricted to ground levels (Matveev et al., 2001). Although BrO mixing ratios at 2 m altitude are lower in scenario LOWBL than in scenario ENH_2, NO_2 mixing ratios are lower (see Fig. 9.8 f). Even though BrO reacts efficiently with NO_2, this reaction is significantly slower in the upper parts of the boundary layer, especially during the first two hours of simulation time in scenario ENH_2. Vertical transport can compensate the stronger NO_2 destruction in the lower parts of the boundary layer in scenario ENH_2. As the boundary layer is more than 600 m higher in scenario ENH_2, compared to scenario LOWBL, vertical transport of NO_2 is less efficient in the latter named scenario. Note, that NO_2 mixing ratios at 2 m altitude are higher in scenario ENH_2 than in scenario LOWBL but lower than in scenario EXALL.

9.1.6 Heterogeneous reactions on dry aerosol particles

With respect to the Lagrangian model scenarios presented above, it was found that varying the boundary layer height or varying the flux strength out of the water enhances the strength as well as the vertical extent of ozone depletion events. In scenario DRY the boundary layer is again high (1300 m) and well mixed but the recycling potential of halogen species on aerosol particles is amplified. Above the lowest two meters of the atmosphere where the ambient humidity is so low that aerosol phase chemistry is not activated in the model anymore, heterogeneous uptake of $BrONO_2$ and $ClONO_2$ on dry particles is additionally calculated. This might enhance the importance of bromine chemistry as the recycling of halogen species on aerosol surfaces is now calculated throughout the boundary layer.

Figure 9.9 shows the difference for gas phase BrO (in pmol/mol) and O_3 (in nmol/mol) mixing ratios between scenarios DRY and EXALL. Until 14:30 the difference in BrO mixing ratios between both scenarios is in the range of only 1 pmol/mol. Between 14:30 and 16:00 this difference increases in the lowest 200 m whereas above it stays as low as before. The difference between both scenarios is largest in the lowest part of the boundary layer and gets less with increasing height. In the last minutes before the model column is supposed to reach again the desert North of the Dead Sea, BrO mixing ratios in scenario DRY exceed those in EXALL by nearly 40 pmol/mol at about 2 m altitude. Bringing back to mind, that the maximum BrO mixing ratio at 2 m altitude for scenario EXALL was roughly 150 pmol/mol it is about 200 pmol/mol for scenario DRY. However,

in altitudes above 100 m the difference between both simulations is still only approximately 4 pmol/mol (note the logarithmic scaling in Fig. 9.9). The influence of bromine chemistry on O_3 mixing ratios is still very small and the maximum difference between both scenarios is only 1.8 nmol/mol at about 2 m when the model column nearly has reached the North shore of the Dead Sea (16:00).

The extension of heterogeneous chemistry all over the boundary layer leads to an increase in aqueous phase concentrations within the lowest meters of the boundary layer where the full aqueous phase chemistry mechanism is calculated. This is mainly because of transport effects. The total load of aqueous phase halogen species within the boundary layer gets increased due to the uptake on dry particles. This effects the vertical distribution and leads also to an increase of aqueous phase bromine concentrations in the lowest 2 meters. This leads to a stronger degassing of Br_2 out of aerosol particles followed by a stronger increase in BrO mixing ratios in scenario DRY, especially in the lowest part of the boundary layer.

9.1.7   North to South

For all scenarios presented above it was assumed that the wind direction was South to North and that the model column moves from an area where the water has the highest acidity and highest bromide content to an area where acidity and Br^- concentrations decrease with time (and with space in reality). Therefore a scenario analogous to EXALL was calculated, assuming that the model column moves over the Dead Sea from North to South and that H^+ concentrations as well as Br^- concentrations in the water increase with time (scenario NOSO). Both scenarios are compared and results are presented in the following.

Figure 9.10 shows gas phase mixing ratios of BrO (a), HOBr (b) and O_3 (c) for scenarios EXALL (black solid line) and NOSO (red dash-dotted line) together with aqueous phase concentrations in the water of the Dead Sea (e - i) and fluxes out of the water into the atmosphere (d).

Like it was done for scenario EXALL in Section 9.1.2.1, at first the chemistry taking place in the Dead Sea water is discussed. Very striking is the reverse time evolution of HOBr, BrCl and HOCl concentrations in the water in scenario EXALL and NOSO (Fig. 9.10 e,f). HOBr concentrations in the Dead Sea water in scenario EXALL increase from 0.3 nmol/l up to 61 nmol/l whereas HOBr mixing ratios decrease from 107 nmol/l to 0.8 nmol/l in scenario NOSO (Fig. 9.10 e).

In Section 8.4.1 where the model setup was described, it was explained that chemistry in the Dead Sea water for scenario EXALL was initialised such that chemistry in the water was calculated for three days under conditions valid for the South (pH of 4.9, Br^- concentrations of 0.15 mol/l) without allowing any exchange with the atmosphere in order to have a spin up for the model. Chemistry in the Dead Sea water in scenario NOSO is now initialised with a model run representing conditions in the North (pH of 6, Br^- concentrations of 0.05 mol/l) (see Fig. 9.10 h, i). Thus initial concentrations of bromine species in the water at 10:00 differ between scenario EXALL and NOSO. Due to this model setup concentrations at 10:00 in scenario NOSO are almost the same as at 16:00 in scenario EXALL and vice versa.

In order to explain the decrease in HOBr and BrCl concentrations with time in scenario NOSO it is referred to the same example that was used to explain the increasing HOBr and BrCl concentrations in scenario EXALL in Section 9.1.2.1. All references to reaction pathways in the following refer to Figure 9.3.
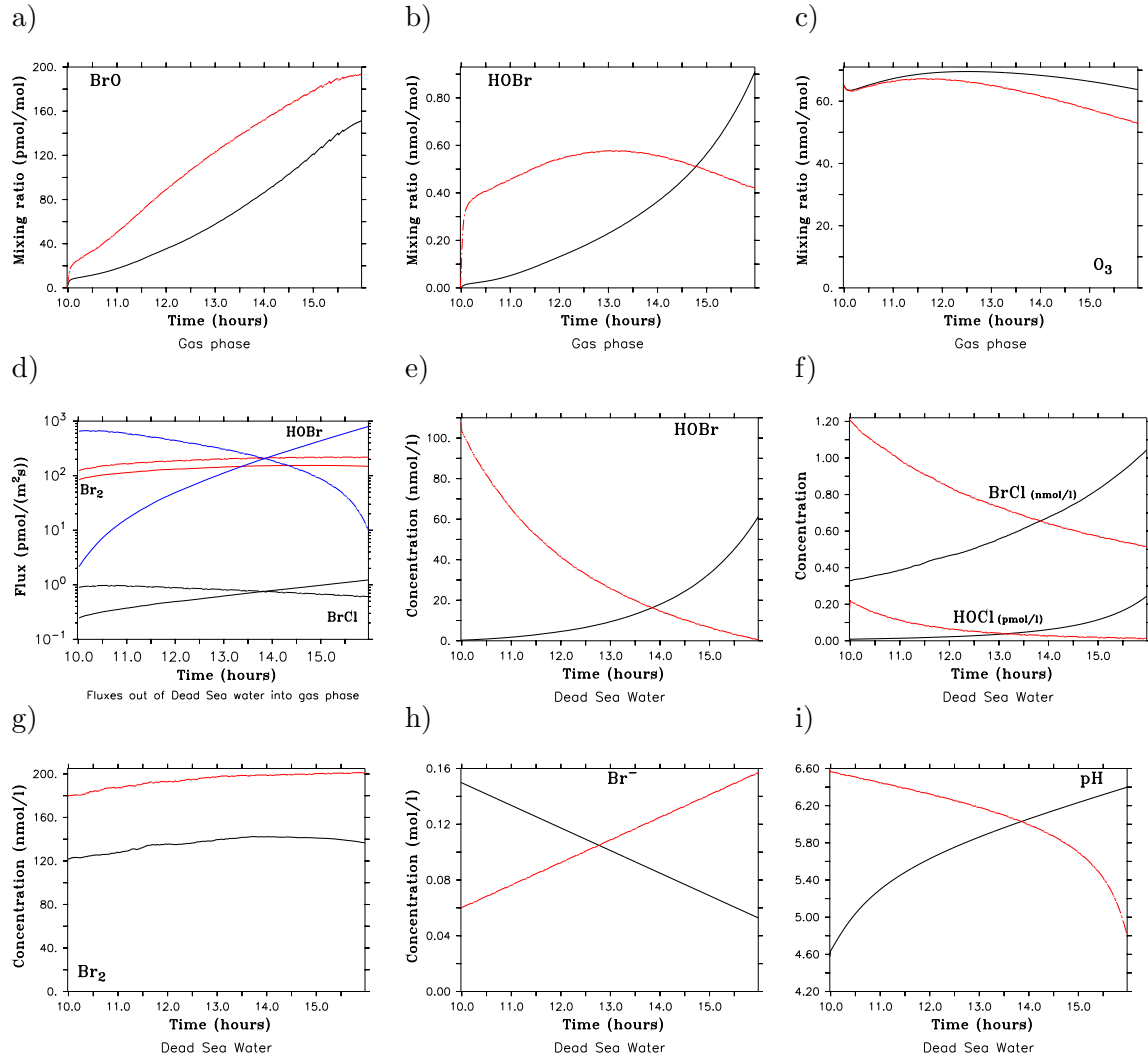
Figure 9.10: Plots in the top row show BrO (a) in pmol/mol), HOBr (b) in nmol/mol) and O_3 (c) in nmol/mol) mixing ratios at 2 m altitude. Figures (e - i) show concentrations in the Dead Sea water for the following species: HOBr (e), BrCl, HOCl (f), Br_2 (g), Br^- (h) and the pH (i). Black solid lines refer to scenario **EXALL** and red dash-dotted lines refer to scenario **NOSO**. Figure (d) shows fluxes out of the Dead Sea water into the gas phase for scenario EXALL (solid lines) and NOSO (dash-dotted lines) for Br_2 (red), HOBr (blue) and BrCl (black).

For scenario EXALL, the following example was given to explain the time evolution of halogen species in the Dead Sea water:

As both H^+ and Br^- concentrations *decrease* with time, less HOCl is consumed with time forming BrCl via reaction

$$HOCl + Br^- + H^+ \longrightarrow BrCl \tag{9.11}$$

(blue reaction path). This leads to an *increase* in HOCl concentrations followed by a *stronger* net production of ClO^- via reaction

$$HOCl \rightleftharpoons ClO^- + H^+ \tag{9.12}$$

(black reaction path) followed by a *stronger* production of BrCl via reaction

$$Br^- + ClO^- + H^+ \longrightarrow BrCl + OH^- \tag{9.13}$$

(grey reaction path). This now leads to an *increase* in BrCl concentrations followed by a *stronger* conversion of BrCl to HOBr via the backward reaction of:

$$HOBr + Cl^- + H^+ \rightleftharpoons BrCl \tag{9.14}$$

(green reaction path).

Going now from North to South in scenario NOSO, the opposite happens:

As both H^+ and Br^- concentrations *increase* with time, more HOCl is consumed with time forming BrCl (via reaction 9.11, blue reaction path). This leads to a *decrease* of HOCl concentrations followed by a *weaker* net production of ClO^- (via reaction 9.12, black reaction path) followed by a *weaker* production of BrCl (via reaction 9.13, grey reaction path). This now leads to a *decrease* in BrCl concentrations followed by a *weaker* conversion of BrCl to HOBr (via reaction 9.14, green reaction path) (see Fig. 9.10 e, f, g).

Br_2 concentrations in the Dead Sea water are higher in scenario NOSO than in scenario EXALL throughout the simulation time. It was mentioned before in Section 9.1.2.1, that even though Br^- and H^+ concentrations vary with time, the absolute concentrations are comparatively high at all times. HOBr concentrations in scenario NOSO are larger than in scenario EXALL until about 14:00. Absolute maximum values of HOBr are also higher in scenario NOSO (at 10:00) than in scenario EXALL (at 16:00) leading to a stronger production of Br_2 in the Dead Sea water in scenario NOSO compared to scenario EXALL. However, this is only an indirect effect as the bromide content as well as the pH at 16:00 in scenario EXALL and at 10:00 in scenario NOSO are not absolutely equivalent (Fig. 9.10 h, i).

Additionally, HOBr is in an aqueous phase equilibrium with BrO^- and H^+. However, the influence of this strongly pH-dependant equilibrium on HOBr concentrations in the Dead Sea water is of minor importance.

When comparing the fluxes out of the Dead Sea water into the gas phase between scenarios EXALL and NOSO, they show the same opposite behaviour as concentrations of bromine species in the water show. The flux of HOBr in scenario NOSO (Fig. 9.10 d, blue dash-dotted line) decreases from $645 \, pmol/(m^2s)$ at 10:00 to $9 \, pmol/(m^2s)$ at 16:00 and the flux of BrCl (Fig. 9.10 d, black dash-dotted line) from $0.87 \, pmol/(m^2s)$ to $0.61 \, pmol/(m^2s)$. The flux of Br_2 out of the water (Fig. 9.10 d, red dash-dotted line) increases from $120 \, pmol/(m^2s)$ to $218 \, pmol/(m^2s)$.

The effect on gas phase chemistry of letting the model run from either South to North (EXALL) or from North to South (NOSO) is discussed in the following.

In both scenarios BrO mixing ratios increase with time leading to BrO maximum mixing ratios of about $192 \, pmol/mol$ at 16:00 in scenario NOSO and $151 \, pmol/mol$ in scenario EXALL (Fig. 9.10 a). As the flux of Br_2 is on the same order of magnitude in both scenarios and as the flux of HOBr is stronger in scenario NOSO than in scenario EXALL until 14:00, bromine species accumulate even stronger in scenario NOSO than in scenario EXALL, explaining the higher BrO mixing ratios throughout the six hours of simulation time.

The time evolution of HOBr mixing ratios differs stronger between both scenarios. As the flux strength of HOBr decreases with time, less HOBr accumulates in the lowest part of the boundary layer and mixing ratios slightly decrease with time. Thus after 14:00 HOBr
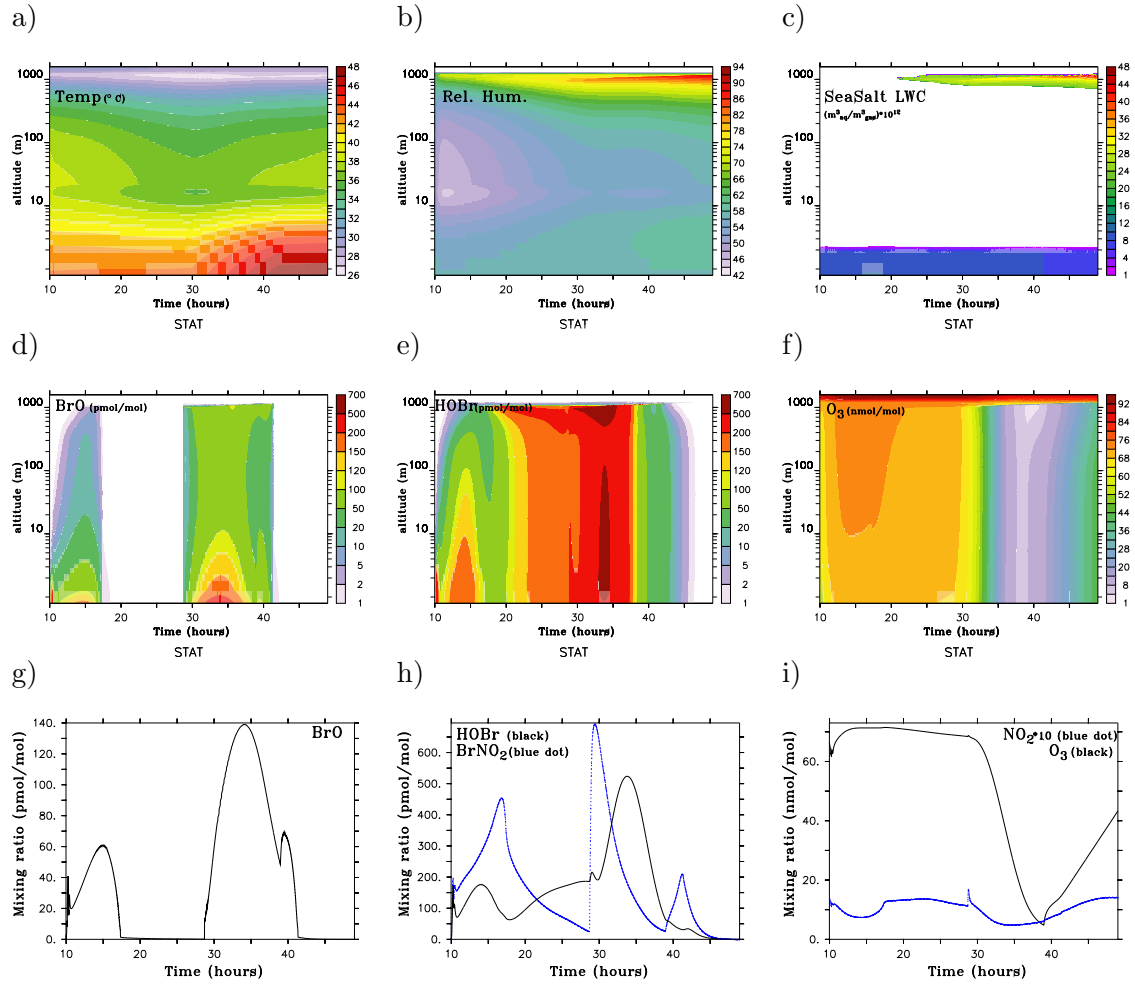
Figure 9.11: All plots in this figure refer to scenario **STAT**. Plots in the top row show the vertical distribution of temperature (°C), relative humidity (%) and the liquid water content of sea salt aerosols as an indicator where aerosol phase is active in the model. Plots in the middle row show the vertical distribution of gas phase mixing ratios of BrO (d, in pmol/mol), HOBr (e, in pmol/mol) and O_3 (f, in nmol/mol). Plots in the bottom row show the time evolution at 2 m altitude of gas phase mixing ratios of BrO (g, in pmol/mol), HOBr (black solid line) and $BrONO_2$ (blue dotted line, h, in pmol/mol) as well as O_3 (black solid line) and NO_2 (blue dotted line, i, in nmol/mol)

mixing ratios in scenario EXALL exceed those in scenario NOSO. As constantly more O_3 is consumed by reaction with bromine due to a higher gas phase bromine content in scenario NOSO, the O_3 loss is stronger than in scenario EXALL ($67 \longrightarrow 53$ nmol/mol ΔO_3 $\approx 21\%$). However, the O_3 destruction process is still slow and it is still weaker than O_3 depletion events observed along the Dead Sea.

9.2 Stationary runs

To study the time evolution of trace gases within two days at one single site at the Dead Sea and to study the influence of changing meteorological background conditions on tracer

mixing ratios, scenario STAT was calculated (see Section 8.4.2 for a more detailed description of the model setup). Plots in the top row of Figure 9.11 show the vertical distribution with time of the temperature (a, in °C), the relative humidity (b, in %) as well as the liquid water content of sea salt aerosols (c, in $m_{aq}^3/m_g^3 \times 10^{12}$) for the two days of simulation time (10:00 day 1 until 24:00 day 2). The liquid water content serves as an indicator for those levels where sea salt aerosol phase as well as sulphate aerosol phase chemistry is calculated in the model. Figure 9.11 further shows the vertical distributions (middle row) of gas phase mixing ratios of BrO (d, in pmol/mol), HOBr (e, in pmol/mol) and O_3 (f, in nmol/mol) for scenario STAT. Note the logarithmic scaling of the y-axis in plots (a) - (f). Plots in the bottom row show in addition the time evolution of BrO (g, in pmol/mol), HOBr and $BrONO_2$ (h, in pmol/mol) as well as O_3 and NO_2 (i, in nmol/mol, note the scaling factor in the plot for NO_2) at 2 m altitude.

In comparison to scenario EX, BrO mixing ratios on day 1 in scenario STAT are slightly lower: $BrO_{max(EX)}$: 100 pmol/mol, $BrO_{max(STAT)}$: 60 pmol/mol (Fig. 9.11 g). NO_2 mixing ratios are higher during the whole day in scenario STAT compared to scenario EX (mixing ratios at 15:00 day 1: $NO_2 = 0.8$ nmol/mol in STAT, $NO_2 = 0.3$ nmol/mol in EX). Thus comparatively more BrO is consumed via the reaction

$$BrO + NO_2 \longrightarrow BrONO_2 \tag{9.15}$$

leading mainly to the difference in BrO mixing ratios at day 1 between scenarios STAT and EX (day 1: $BrONO_{2max(EX)}$: 110 pmol/mol, $BrONO_{2max(STAT)}$: 454 pmol/mol, Fig. 9.11 h). On the second day of simulation time, BrO mixing ratios in scenario STAT increase stronger than on day 1 and reach a maximum value of 140 pmol/mol at 2 m altitude at about 10:00 in the morning. Mixing ratios decrease again after 10:00 but are always larger than on day 1. BrO Mixing ratios exceed 50 pmol/mol almost the whole day all over the boundary layer up to an altitude of about 1200 m whereas on day 1 they were always lower than 12 pmol/mol in heights larger than 100 m (Fig. 9.11 d).

Maximum HOBr mixing ratios at 2 m altitude on day 1 of the simulation time are of similar order of magnitude in scenarios STAT and EX. However, on the second day of simulation time, HOBr mixing ratios also increase to larger values than on day 1 and exceed maximum values from scenario EX by a factor of three (day 1: $HOBr_{max(STAT)}$: 174 pmol/mol, day 2: $HOBr_{max(STAT)}$: 523 pmol/mol, $HOBr_{max(EX)}$: 165 pmol/mol, Fig. 9.11 h).

Comparing the results from scenario STAT and the Lagrangian studies, the vertical distribution and the time evolution of O_3 mixing ratios is surprising. On the first day of simulation time, O_3 mixing ratios stay constant at around 70 nmol/mol and are not affected at all by halogen chemistry. On the second day (30 hours in Fig. 9.11 = 6:00 day 2) O_3 mixing ratios start to decrease immediately after sunrise, when photochemistry and thus bromine chemistry starts getting activated. At 14:00, O_3 mixing ratios at 2 m altitude reach a minimum value of 5 nmol/mol and increase again afterwards mainly because of the prescribed O_3 flux and because mixing ratios of bromine species decrease in the afternoon.

In contrast to the Lagrangian scenarios EXLIM or $ENH_{1,2}$, needing a low level inversion or enhanced fluxes to simulate an ozone depletion event, O_3 is strongly depleted up to an altitude of about 1200 m in scenario STAT where the boundary layer is high and well mixed throughout the simulation time. However, O_3 mixing ratios reach their minimum value at 14:00, (Fig. 9.11 i) four hours after BrO mixing ratios had reached their maximum value at 10:00 (Fig. 9.11 g). Even though BrO mixing ratios are on the same order of magnitude as in some of the Lagrangian studies where no influence on O_3 chemistry could

be found, the bromine oxide production in scenario STAT is sufficiently large to lead to a significant O_3 depletion event.

The magnitude of NO_2 mixing ratios which is crucial for the O_3 budget is controlled by the inflow into the model domain. NO_2 mixing ratios are almost of identical order of magnitude on day 1 and day 2 such that O_3 production by the most efficient source reaction ($NO_2 + h\nu \longrightarrow O_3 + NO$) has the same strength on both days (Fig. 9.11 i, note again the scaling factor).

The explanation for the strong O_3 depletion is related to slightly changing meteorological background conditions from day 1 to day 2. Air masses cool down during the night in the boundary layer (Fig. 9.11 a), relative humidity increases during the night and stays higher during the second day of simulation time than the first day (Fig. 9.11 b). Under the very hot and dry conditions prevailing along the Dead Sea, sea salt particles dry out quickly after they have been injected into the atmosphere. It was explained in the model description in Section 8.3.2 that the ambient relative humidity has to exceed the aerosol's deliquescence humidity of 75 % (70 % for sulphate aerosols) to reactivate the calculation of sea salt (and respectively sulphate) chemistry in the model. On day 1 of the simulation time the relative humidity is below this threshold value all over the boundary layer but on day 2 it exceeds 75% in altitudes above about 800 m (and 70 % in altitudes above 650 m) and thus aerosol phase (sulphate and sea salt) chemistry is activated. As a result, aqueous phase chemistry and the cycling of halogens on aerosol particles gains in importance. As stated out above the liquid water content of sea salt aerosols that is plotted in Figure 9.11 c) is an indicator for levels where aerosol phase chemistry (on sea salt and sulphate aerosols) is calculated. Within all levels having a LWC of 0 in Figure 9.11 c), liquid phase chemistry is not activated (note again the logarithmic scaling of the y-axis in all plots showing vertical distributions!). The most efficient recycling process is the heterogeneous decomposition of $BrONO_2$ on sulphate aerosols and the subsequent release of HOBr out of aerosol particles:

$$BrONO_2 \quad \longrightarrow \quad HOBr_{aq} + HNO3_{aq} \qquad (9.16)$$
$$HOBr_{aq} \quad \longrightarrow \quad HOBr_g$$
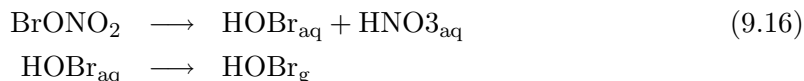
Through strong vertical transport, also the lower part of the boundary layer is indirectly influenced by the enhanced halogen chemistry in the upper parts of the boundary layer. This can be seen very well in the vertical distribution of gas phase HOBr mixing ratios(Fig. 9.11 e). As the total halogen recycling capacity all over the boundary layer is enhanced, O_3 is depleted even though BrO mixing ratios do not exceed 200 pmol/mol as they did e.g. in the Lagrangian scenario EXLIM.

Even though the cycling of halogen species between the aerosol phase and the gas phase contributes to the increase in the gas phase halogen mixing ratios, the air-sea exchange of Br_2 and BrCl is still the dominant source for BrO especially in the lowest part of the boundary layer. BrO mixing ratios still show a strong vertical gradient on day 2 of the simulation time. In addition to the above discussed changes in meteorological background conditions between day 1 and day 2, the idealised model setup has also to be considered: In contrast to the assumptions made for the Lagrangian studies, for scenario STAT it is assumed that one particular site is influenced strongly by halogen chemistry for two days. Background halogen mixing ratios are higher in the morning of the second day of simulation than on the first day. Br_2 mixing ratios before sunrise at day 2 are 470 pmol/mol whereas they increase from 0 at 10:00 on day 1 when the model simulations start (Br_2: 100 pmol/mol at 10:00 day 2 in STAT).

While explaining the model setup in Section 8.4.2 it was mentioned that the inflow of O_3

into the model domain was increased in the afternoon hours of day 2 of simulation time. This was done as otherwise O_3 mixing ratios did not increase anymore. The advective flux was chosen such, that the model results agree well with the measurements which show all an increase of O_3 mixing ratios in the late afternoon / early evening hours. However, a flux of 6.8 pmol/(mol s) of O_3 (see Table 8.2) was necessary to reach mixing ratios of at least 40 nmol/mol at 20:00 day 2.

To be better able to assess the effect of the different assumptions that were made to set up scenario STAT, a Lagrangian scenario (HIGHRH) was calculated, which was initialised with the same fields for chemistry as all other Lagrangian scenarios, but with meteorological fields taken from scenario STAT at 10:00 day 2. Thus the relative humidity is higher than in the other Lagrangian scenarios and aerosol phase chemistry is calculated in altitudes exceeding 800 m. This scenario was mainly performed to investigate whether it is more important to enhance aqueous phase chemistry or whether the higher Br_2 mixing ratios in the morning of day 2 in scenario STAT are of the same importance for the quick development of the O_3 depletion event.

O_3 and BrO mixing ratios at 2 m altitude as well as the vertical distribution of O_3 and BrO for scenario HIGHRH is shown in Figure 9.12. Maximum mixing ratios of BrO (81 pmol/mol) are even lower in scenario HIGHRH than in scenario EXALL (151 pmol/mol). Under the prevailing conditions, the most efficient sink reaction for BrO (apart from photolysis) is reaction with NO_2 leading to the formation of $BrONO_2$. In scenario EXALL, $BrONO_2$ sink reactions are weak whereas it is taken up on aerosol particles in scenario HIGHRH. Thus the active recycling of halogen species leads to a faster conversion of species. Again it has to be stated out that aerosol phase chemistry is only active in the lowest and upper most part of the boundary layer. However, as vertical mixing is strong, the whole boundary layer is affected by those layers where aerosol phase chemistry is calculated.

Compared to scenario EXALL ($\Delta O_3 = 9\%$), O_3 mixing ratios decrease stronger ($\Delta O_3 = 13\%$) and have a minimum value of 57 nmol/mol at 16:00 ($O_{3(min)}$: 63 nmol/mol in EXALL). Even though aerosol phase chemistry is active in the upper parts of the boundary layer, the area of maximum O_3 loss is still the lowest part of the boundary layer that is dominated by the fluxes out of the Dead Sea water. However, O_3 mixing ratios do never drop below 56 nmol/mol and thus the depletion event is still insignificant compared to
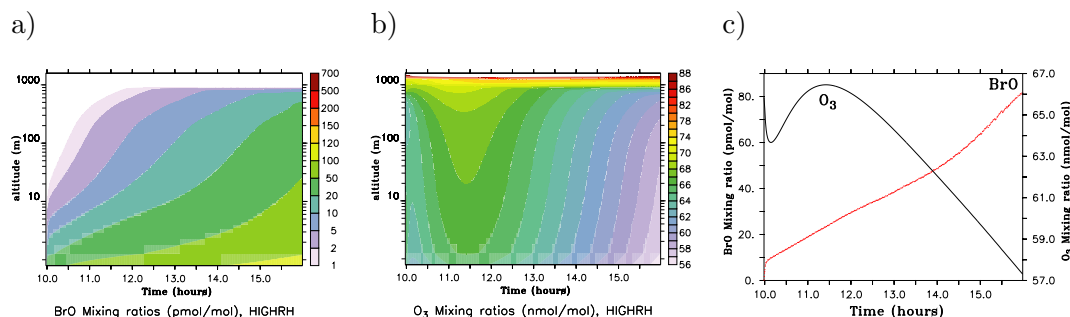
Figure 9.12: Shown is the vertical distribution of BrO (a) in pmol/mol) and O_3 (b) in nmol/mol for scenario HIGHRH (shaded) and EXLIM (contoured). Figure (c) shows BrO (red dotted line, pmol/mol) and O_3 (black solid line, nmol/mol) mixing ratios at 2 m altitude for scenario HIGHRH.

observed ones.

This model run showed that only the combined effect of enhanced aqueous phase chemistry as well as the larger 'background' gas phase halogen load on day 2 in scenario STAT leads to the strong and especially strongly vertically extended ozone depletion event.

9.3   Lagrangian runs including Iodine chemistry

In correspondence to the Lagrangian scenario EXALL, scenarios were performed including the calculation of iodine chemistry and explicitly treating air-sea exchange of iodine species between the Dead Sea water and the atmosphere.

9.3.1   Chemistry in the Dead Sea water

Figure 9.13 a) shows aqueous phase concentrations of iodide for the three scenarios IOD_1, IOD_2 and IOD_3 to visualise the different model setups for those three scenarios, i.e. the differing I^- concentrations in the Dead Sea water.

As was explained in the introduction in Section 8.4.3, iodide concentrations were initialised based on values published by Zingler and Platt (2005). In general, scenarios IOD_1 and IOD_2 give very similar results regarding chemistry in the Dead Sea water and in the following discussion regarding aqueous phase equilibria it is only referred to scenario IOD_2 for comprehensiveness. Thus Figure 9.13 b) shows representatively only concentrations in the Dead Sea water for scenario IOD_2.

Again, the primary focus is on the chemistry taking place in the Dead Sea water and the fluxes of species across the water surface which highly influence gas phase concentrations of halogen species.

Of the species that are explicitly exchanged between the Dead Sea and the atmosphere, I_2 is the most efficiently produced iodine species in the water in scenario IOD_2 (red line Fig. 9.13 b). I_2 concentrations increase to a maximum value of 148 nmol/l at 13:15 and decrease afterwards to 121 nmol/l at 16:00. The time evolution of I_2 concentrations is similar to the time evolution of Br_2 concentrations in the Dead Sea water in scenario EXALL (i.e. a slight decrease after 14:00, but concentrations stay in the same order of magnitude, see Fig. 9.2 b). The decrease after 13:15 is related to the decreasing H^+ concentrations in the Dead Sea water.

The strongest net source of I_2 in the water is the reaction:

$$I^- + ICl \longrightarrow I_2 + Cl^- \tag{9.17}$$
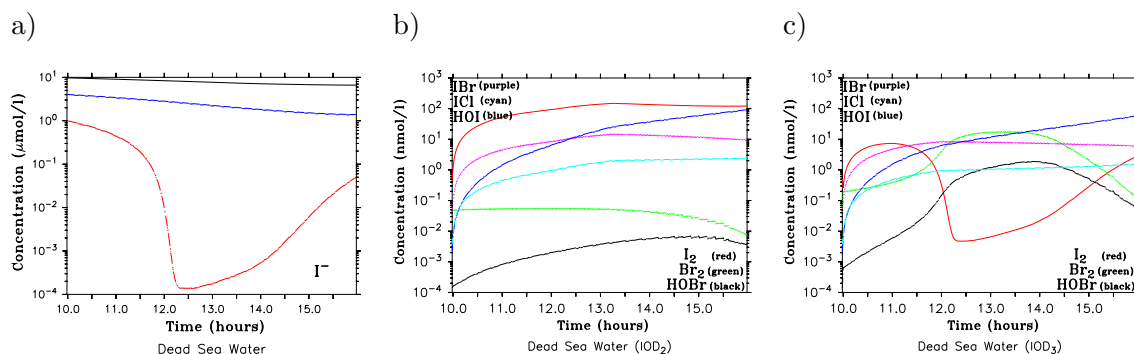
Figure 9.13: Plotted are concentrations of iodide **(a)** in the Dead Sea water for scenarios IOD_1 (black line), IOD_2 (blue dashed line) and IOD_3 (red dash-dotted line). Furthermore, Dead Sea water concentrations of IBr (purple dotted line), ICl (cyan dashed line), HOI (blue dash-dotted line), HOBr (black dash-dotted line), Br_2 (green dotted line) and I_2 (red line) for scenarios IOD_2 **(b)** and IOD_3 **(c)**.
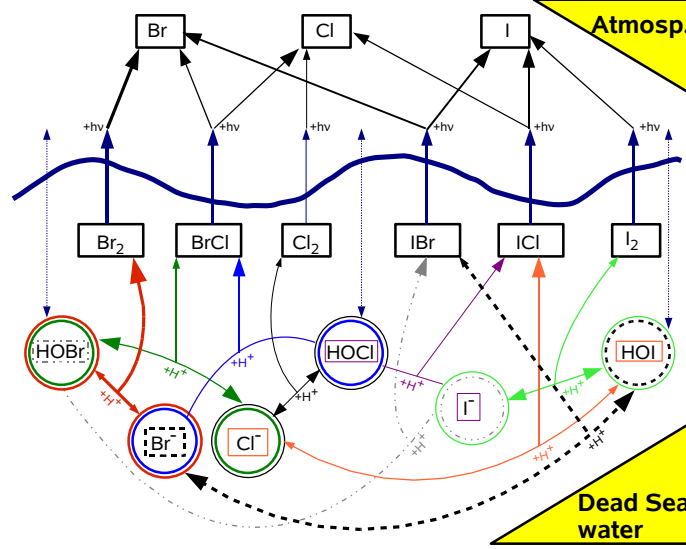
Figure 9.14: Schematic overview of the most important aqueous phase equilibria including iodine species.

The reaction proceeds with a rate of about $4\,\mathrm{mmol/(m^3 s)}$ in scenario IOD_2. The equilibrium reaction:

$$HOI + I^- + H^+ \rightleftharpoons I_2 \tag{9.18}$$

that is shown in Figure 9.14 as the light green reaction pathway has a reaction rate of approximately $400\,\mu\mathrm{mol/(m^3 s)}$ and tends to produce HOI, which is indicated in Figure 9.14 by the larger arrows pointing at HOI and I^-. Furthermore, I_2 and Br^- are in an aqueous phase equilibrium with I^- and IBr where the latter named two species are net produced $(I_2 + Br^- \rightleftharpoons I^- + IBr)$. This source for IBr, together with the production via HOBr (grey dotted reaction path in Fig. 9.14):

$$HOBr + H^+ + I^- \longrightarrow IBr \tag{9.19}$$

is sufficient to press the equilibrium reaction:

$$HOI + Br^- + H^+ \rightleftharpoons IBr \tag{9.20}$$

into the direction to produce HOI (black dashed reaction path in Fig. 9.14). HOI concentrations in the water steadily increase with time (up to $92.18\,\mathrm{nmol/l}$ in IOD_2, Fig. 9.13 b). The time evolution of HOI concentrations in scenario IOD_2 is very similar to the time evolution of HOBr concentrations in the Dead Sea water in scenario EXALL, i.e. concentrations increase constantly with time (Fig. 9.2 b). HOI is net produced by the equilibrium reactions with IBr (see equation 9.20, black dashed reaction path in Fig. 9.14) and with I_2 (see equation 9.18, light green reaction path in Fig. 9.14). HOBr is produced on analogous reaction pathways by the equilibrium reaction with BrCl (green reaction path in Fig. 9.14):

$$HOBr + Cl^- + H^+ \rightleftharpoons BrCl \tag{9.21}$$

as was explained above in detail in Section 9.1.2.1.
As ICl does not have significant other sources, it is mainly produced via the equilibrium

reaction:

$$HOI + Cl^- + H^+ \rightleftharpoons ICl \tag{9.22}$$

(orange reaction path in Fig. 9.14). ICl concentrations show a similar increase during the first three hours of simulation time as I_2 or IBr concentrations. However, after 13:15 ICl concentrations increases further but less strong whereas concentrations of IBr as well as I_2 slightly decrease (all numbers refer again to scenario IOD_2):

I_2:	148 nmol/l	at 13:15	$\longrightarrow$	121 nmol/l	at 16:00
IBr:	14.95 nmol/l	at 13:15	$\longrightarrow$	9.67 nmol/l	at 16:00
ICl:	2 nmol/l	at 13:15	$\longrightarrow$	2.39 nmol/l	at 16:00

It is somewhat difficult to see those different time evolutions in Figure 9.13 b (red line (I_2), purple dotted line (IBr), cyan dashed line (ICl)) as it is drawn on a logarithmic axis. As was said above, the strongest net source of ICl is the pH-dependant equilibrium reaction with Cl^- and HOI (see equation 9.22, orange reaction path in Fig. 9.14) whereas IBr concentrations strongly depend on Br^- concentrations via the equilibrium reaction: $I_2 + Br^- \rightleftharpoons I^- + IBr$. As Br^- concentrations decrease with time in this model setup, but Cl^- concentrations stay constant, ICl concentrations can increase steadily with time but IBr concentrations decrease in the last two hours of simulation time after Br^- concentrations subside below a threshold value such that the production of IBr gets significantly smaller. As was stated at the beginning of this section, scenarios IOD_1 and IOD_2 give very similar results and thus only scenario IOD_2 was discussed above. However, concentrations of I_2 in the water differ significantly between these two scenarios ($I_{2(max)}$ (IOD_1): 535 nmol/l, $I_{2(max)}$ (IOD_2): 148 nmol/l) whereas e.g. HOI concentrations are almost the same in both scenarios and are even slightly larger in scenario IOD_2. This is mainly because I_2 concentrations are more or less directly proportional to I^- concentrations in the water, as their by far strongest source is reaction 9.17. HOI concentrations in all presented scenarios depend strongly on Br^- concentrations in addition to I^- concentrations (e.g. via reaction 9.20, black dashed reaction path in Fig. 9.14). As Br^- concentrations are almost the same in scenario IOD_1 and IOD_2 the influence of the different I^- concentrations on e.g. HOI concentrations is less strong than on I_2 concentrations.

Figure 9.13 b shows in addition to iodine species also concentrations of bromine species in the Dead Sea water (Br_2: green dotted line, HOBr: black dash-dotted line). Obviously concentrations of bromine species are significantly smaller if iodine chemistry is additionally calculated Br_2 (40 pmol/l IOD_2, 21 pmol/l IOD_1), HOBr (6.4 pmol/l IOD_2, 1.5 pmol/l IOD_1) and BrCl (not plotted, 0.2 pmol/l IOD_2, 0.06 pmol/l IOD_1) compared to scenario EXALL ($Br_2 \approx 134$ nmol/l, HOBr ≈ 30 nmol/l, BrCl ≈ 0.7 nmol/l).

In the chemical mechanism calculating aqueous phase chemistry including iodine chemistry as implemented in MISTRA and as described in detail in Pechtl et al. (2007), iodine equilibria are kinetically preferred compared to bromine equilibria. Thus, H^+ as well as Cl^- and Br^- are efficiently consumed by iodine involving reactions leading to a less efficient production of the main bromine species like HOBr and Br_2.

Taking again a closer look, at iodide concentrations in the water, it can be seen in Figure 9.13 a that they decrease slightly with time. This decrease is an effect of the decreasing H^+ and Br^- in the Dead Sea water. It was mentioned above that reaction is fast and produces HOI as well as I^-. However, as I_2 concentrations decrease slightly in the last two
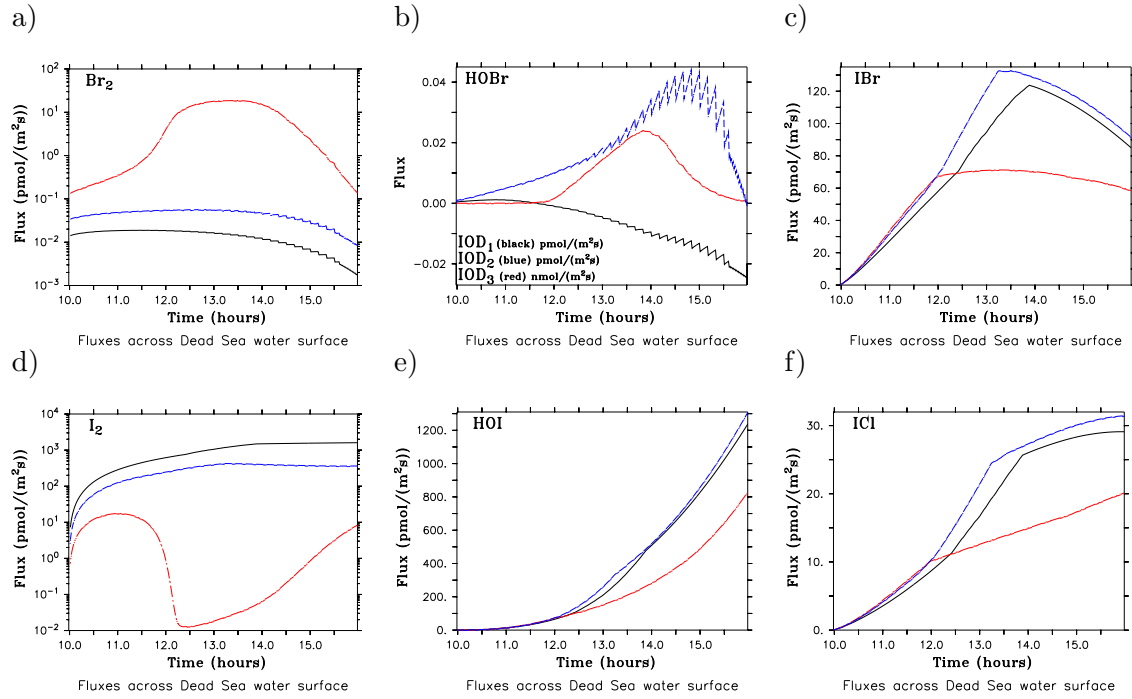
Figure 9.15: Figures **(a - d)** show fluxes across the Dead Sea water interface for scenarios IOD_1 (black line), IOD_2 (blue dashed line) and IOD_3 (red dash-dotted line)

.

hours of simulation time as explained above, less I^- is formed via reaction. Additionally, one of the fastest reactions including iodine compounds, i.e. the reaction (I_2 + Br^- $\rightleftharpoons$ I^- + IBr) that is a net source for I^- gets also slower with time, as Br^- concentrations decrease with time.

9.3.2   Fluxes across Dead Sea water surface

As was shown in Section 9.1.2.1 explaining the chemistry taking place in the Dead Sea water as well as the calculation of the fluxes out of the Dead Sea water into the atmosphere of scenario EXALL, the fluxes of bromine containing species are mainly driven by the extremely high bromide and chloride (and iodide) content as well as the low pH in the water. Regarding the absolute flux strength as well as the photostability in the gas phase, I_2 should be the most important source for gas phase iodine compounds with respect to iodine species that can degas directly out of the Dead Sea. The time evolution of all fluxes follows that of the corresponding aqueous phase species.

The flux of I_2 reaches a maximum value of up to 1602 pmol/(m^2s) in scenario IOD_1 (black solid line Fig. 9.13 e) and 424 pmol/(m^2s) in scenario IOD_2 (blue dashed line Fig. 9.13 e). On the same order of magnitude are maximum HOI fluxes with a value of up to 1237 pmol/(m^2s) in scenario IOD_1 and 1307pmol/(m^2s) in scenario IOD_2 at 16:00 (Fig. 9.13 e). Fluxes of IBr (Fig. 9.13 c) and ICl (Fig. 9.13 f) are lower, but still of a significant strength (ICl_{max}: 29 pmol/(m^2s) IOD_1, 31 pmol/(m^2s) IOD_2, IBr_{max}: 123 pmol/(m^2s) IOD_1, 132 pmol/(m^2s) IOD_2). With a maximum value of about 0.1 pmol/(m^2s) in scenario IOD_1 and 0.05 pmol/(m^2s) in scenario IOD_2, fluxes of Br_2 are about three orders of magnitude lower than in scenario EXALL (Fig. 9.13 a). The flux of

HOBr in scenario IOD_1 is even of opposite direction as in all other scenarios leading from the gas phase into the water. In scenario IOD_2 HOBr degasses again out of the water into the gas phase but the strength of the flux is very low $(0.04 \, pmol/(m^2s))$, blue dashed-line in Fig. 9.13 b, note the different units for scenarios IOD_1, IOD_2 $(pmol/(m^2s))$ and scenario IOD_3 $(nmol/(m^2s))$.

9.3.3   Scenario IOD_3

Before discussing the effect of air-sea exchange of iodine species on gas phase chemistry, scenario IOD_3 has to be discussed.

Initial I^- concentrations in the Dead Sea water in scenario IOD_3 at 10:00 (South of Dead Sea) are a factor of four lower than in scenario IOD_2 and are in the same order of magnitude as concentrations of iodide in the Dead Sea water as reported by Zingler and Platt (2005). However, I^- concentrations in the Dead Sea water in the model decrease strongly within the first two hours of simulation time. They are about four orders of magnitude lower at 12:00 compared to 10:00. They increase again after 12:00 but are still more than one order of magnitude lower at 16:00 compared to the initial value. It is rather unrealistic that the iodide content in the Dead Sea water varies by more than three orders of magnitude between the South and the North end of the lake. However, these oscillations can again be explained with equilibrium chemistry taking place in the Dead Sea water in the model:

I^- concentrations drop below some kind of 'threshold' value such that bromine chemistry gains in importance compared to iodine chemistry. As was explained above, in scenario IOD_1 and IOD_2 iodine equilibria are faster than 'pure' bromine equilibria that are also calculated if iodine chemistry is excluded. While especially the bromine explosion reaction (red reaction path in Fig. 9.14) gains in importance in scenario IOD_3, much more H^+ and Br^- but also Cl^- is consumed by non-iodine reactions leading to the formation of bromine containing species like HOBr and Br_2. As H^+ and Br^- concentrations in the water decrease with time, bromine equilibria get again less kinetically preferred compared to iodine equilibria and thus I^- concentrations increase again. This shift of equilibria can best be seen in the counteractive behaviour of I_2 (red solid line Fig. 9.13 c) and Br_2 concentrations (green dotted line Fig. 9.13 c). The time evolution of I_2 concentrations follows the one of I^- and decreases strongly after 11:00 whereas Br_2 concentrations increase at the same time by about two orders of magnitude. As was said above the most efficient and fastest source reaction for I_2 is reaction 9.17. However, at the same time I_2 is in equilibrium with HOI, I^- and H^+ (see equation 9.18). The latter named reaction is a strong source for I^-. Thus the decrease of I^- concentrations is directly followed by a strong decrease in I_2 concentrations which intensifies the effect of decreasing I^- concentrations via equilibrium reactions.

HOBr concentrations in the water increase strongly in scenario IOD_3 until the afternoon hours but never exceed values of Br_2 concentrations. As significantly more Br_2 and HOBr are produced in the water in scenario IOD_3 compared to both other iodine-scenarios, the corresponding fluxes out of the water are about two orders of magnitude faster. However, IBr is still the strongest emitted bromine containing species in scenario IOD_3 $(70 \, pmol/(m^2s)$, red dash-dotted line Fig. 9.15 c).

In contrast to I_2, concentrations of inter-halogen compounds like IBr, ICl as well as HOI strongly depend on Br^- and Cl^- concentrations. Thus these compounds do not show a strong decrease with time in scenario IOD_3 but have concentrations in the same order of
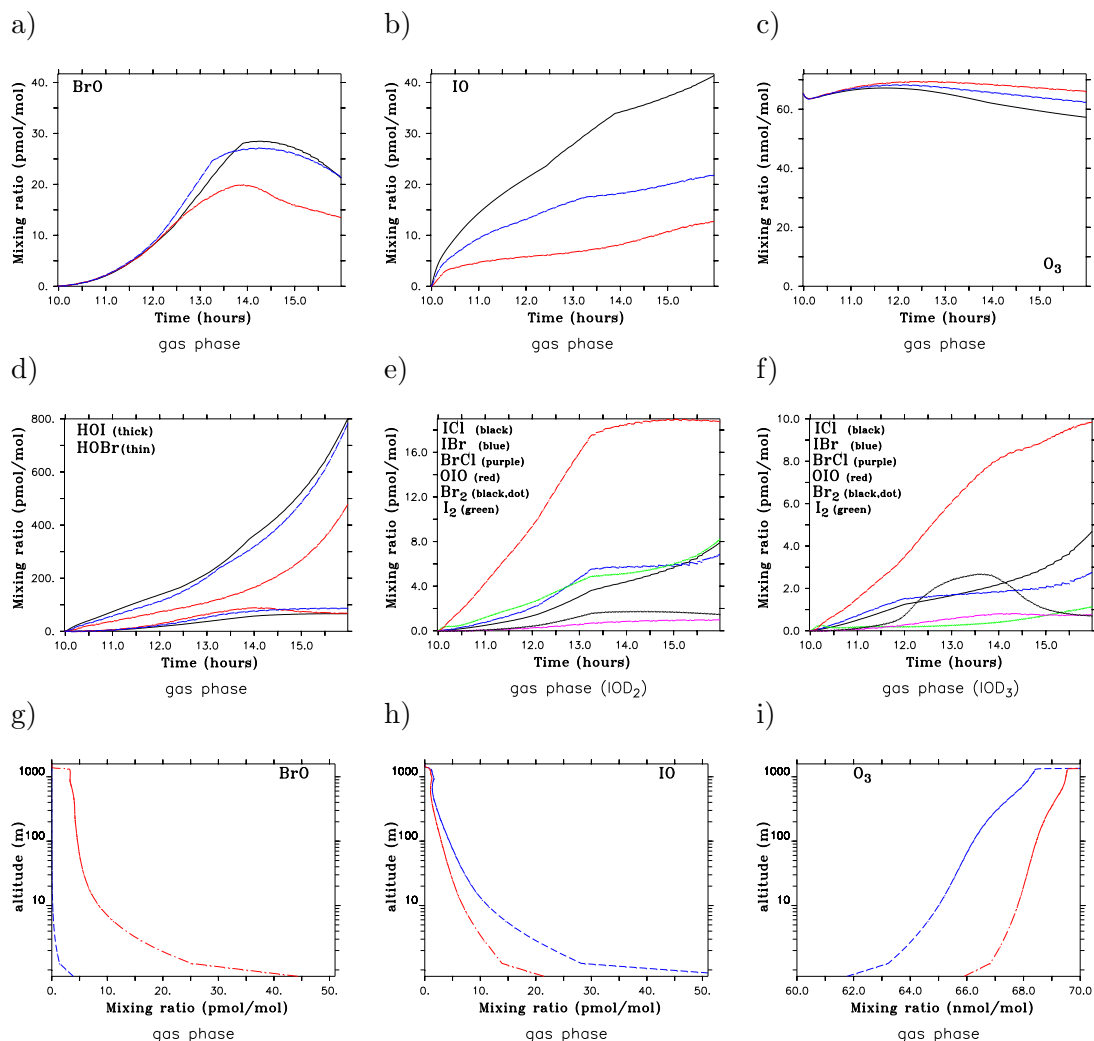
Figure 9.16: Gas phase mixing ratios at $2\,m$ altitude are shown for BrO (a, in pmol/mol), IO (b, in pmol/mol), O_3 (c, in nmol/mol) and HOI,HOBr (d, in pmol/mol) for scenarios IOD_1 (black line), IOD_2 (blue dashed line) and IOD_3 (red dash-dotted line). Figures (e, IOD_2) and (f, IOD_3) show gas phase mixing ratios (in pmol/mol) for ICl (black continuous line), IBr (blue dash-dotted line), BrCl (purple dash-dotted line), OIO (red dashed line), Br_2 (black dotted line) and I_2 (green dotted line).

Vertical profiles at 15:00 of BrO (g), IO (h) and O_3 (i) are further plotted for scenarios IOD_2 (blue dashed line) and IOD_3 (red dash-dotted line).

magnitude as in scenario IOD_2.

Summarising it can be said that even though I^- concentrations show variations in the range of more than three orders of magnitude, only I_2 concentrations in the water and the flux of I_2 out of the water are affected to that same extent. All other iodine species in the water are influenced less strongly by the decrease of I^- concentrations.

9.3.4   Gas Phase Chemistry

Of main interest in general is the influence of the varying I^- concentrations in the Dead
Sea water on gas phase iodine oxide mixing ratios. Thus, the results of the different sce-
narios for gas phase chemistry are now discussed in detail.
IO mixing ratios in all of the three scenarios IOD_1, IOD_2 as well as IOD_3 quickly exceed
5 pmol/mol (Fig 9.16 b) and increase further with time. The time evolution of IO mixing
ratios at 2 m altitude is very similar to the one of BrO mixing ratios in scenario EXALL.
For scenario IOD_1, IO mixing ratios even reach a maximum mixing ratio of 41 pmol/mol
at 16:00 which is a factor of 4 higher than the maximum measured value. In scenario
IOD_2 the maximum mixing ratio also still reaches 22 pmol/mol when the model column is
assumed to reach the North end of the Dead Sea at 16:00. Even though precursor species
of IO are lowest concentrated in scenario IOD_3, mixing ratios still reach a maximum value
of 12 pmol/mol at 16:00.
BrO mixing ratios are in all three scenarios much lower than in those scenarios excluding
iodine chemistry, e.g. scenario EXALL. Hardly any difference can be seen between scenar-
ios IOD_1 and IOD_2 where the maximum BrO mixing ratio of about 27 pmol/mol is reached
at about 14:00 (black solid and blue dashed line in Fig. 9.16 a). Regarding the strength of
fluxes of bromine containing species out of the Dead Sea water in scenarios IOD_1, IOD_2
or IOD_3, this result is not surprising. In all three scenarios the flux of IBr out of the Dead
Sea water is the strongest gas phase bromine source. This flux is largest in scenario IOD_1
and IOD_2. As the flux of IBr is almost the same in these two scenarios, mixing ratios of
gas phase bromine species are also very similar in scenarioIOD_1 and IOD_2.
It was stated out above in Section 9.3.2 that fluxes of Br_2, HOBr or BrCl are very small in
the iodine scenario compared to scenario EXALL. This explains, why BrO mixing ratios
are by far lower than than in the Lagrangian scenarios without calculating iodine chem-
istry.
Even though the fluxes of Br_2 and HOBr are much stronger in scenario IOD_3 than in
scenarios IOD_1 and IOD_2, gas phase BrO mixing ratios are roughly 12 pmol/mol lower
than in both other iodine scenarios. This is mainly because in scenario IOD_3, IBr is still
the largest flux of a bromine containing species out of the Dead Sea water.
In contrast to scenario EXALL, BrO mixing ratios decrease in all three scenarios after
14:00 as the flux of IBr gets weaker in the last two hours of simulation time.

With regard to O_3 chemistry, the same effect can be seen as in most of the Lagrangian
scenarios presented above: O_3 mixing ratios are hardly affected by halogen chemistry.
The effect is strongest in scenario IOD_1 as the fluxes of iodine containing species out of
the Dead Sea water is strongest. The decrease from 67.19 nmol/mol to 57.26 nmol/mol
corresponds to an O_3 loss of 14.8% within the six hours of 'travel' time. The amount of
O_3 that is destroyed in scenario IOD_1 is significant, however it is very likely that iodine
concentrations are overestimated in this scenario. The relative loss in O_3 mixing ratios in
scenario IOD_2 is about 8 % and in scenario IOD_3 it is only 4.7 % (see Fig. 9.16 c).
Figure 9.16 g, h, i show the vertical profiles of BrO, IO and O_3 mixing ratios at 15:00 for
scenarios IOD_2 and IOD_3 (note the logarithmic scaling of the y-axis). BrO and especially
IO mixing ratios decrease rapidly with altitude. At a height of only 10 m mixing ratios
of both species have less than half the values they have directly above the water surface.
Thus the surface loss in O_3 mixing ratios can be quickly compensated by vertical transport
as the O_3 destruction potential of halogens is weak in the upper parts of the boundary

a)

b)

c)

d)

e)
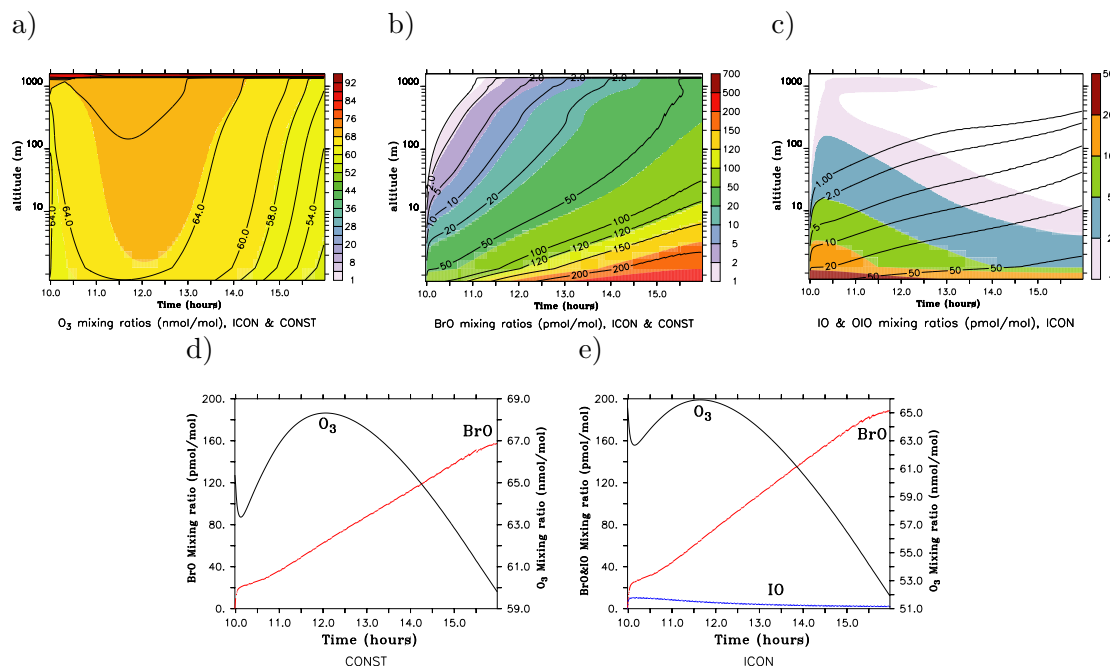
Figure 9.17: Plots in the upper row show the vertical distribution of O_3 and BrO for scenarios **CONST** (shaded) and **ICON** (contoured). Plot (c) shows the vertical distributions of IO (shaded) and OIO (contoured) for scenario ICON. Note the logarithmic scaling of the y-axis.
The contour lines in (c) have the same scaling as the colour code, i.e. the lowest line stands for 50 pmol/mol and the upper most contour line for 1 pmol/mol.
Plots in the bottom row show BrO (red dashed line), O_3 (black line) and IO (only ICON) mixing ratios at 2 m altitude for scenarios CONST and ICON.

layer.
OIO (red dashed line in Fig. 9.16 e,f) is one of the iodine species with the highest gas phase mixing ratios in scenario IOD_2 as well as in scenario IOD_3. The difference in OIO mixing ratios at 2 m altitude between these two scenarios is about 8 pmol/mol. The relative difference in I_2 (green dotted line in Fig. 9.16 e,f) and Br_2 (black dotted line in Fig. 9.16 e,f) mixing ratios between scenarios IOD_2 and IOD_3 is larger, due to the different flux strength of these two species both scenarios. Also very similar are mixing ratios of IBr (blue dash-dotted line), ICl (black line) and BrCl (purple dash-dotted line) in scenarios IOD_2 and IOD_3 (Fig. 9.16 e,f).

9.3.5 Iodine 'prescribed fluxes'

Due to the potential uncertainties especially with respect to aqueous phase iodine chemistry one Lagrangian 'iodine' scenario (ICON) was set up prescribing constant fluxes of I_2, IBr, ICl, HOI as well as fluxes of Br_2, Cl_2, HOBr and BrCl as was explained in the introductory part of this chapter in Section 8.4.3. Now, it is compared with the scenario CONST.
Figures 9.17 a and b show the vertical distribution of O_3 and respectively BrO mixing ratios for scenario CONST (shaded) and scenario ICON (contoured). Figure 9.17 c) shows IO mixing ratios (shaded) and OIO mixing ratios (contoured) for scenario ICON. Further-

more, BrO (red dashed line), O_3 (black line) (and IO for scenario ICON, blue dashed line) at 2 m altitude are shown for scenarios CONST (d) and ICON (e).

Comparing scenarios CONST and ICON, BrO mixing ratios are of the same order of magnitude all over the boundary layer. It was explained several times above, that the order of magnitude of BrO mixing ratios is strongly controlled by HOBr as well as Br_2 fluxes out of the Dead Sea water. These fluxes have the same strength in both scenarios. However, taking a closer look, BrO mixing ratios at 2 m altitude are about 30 pmol/mol larger at 16:00 in scenario ICON than in scenario CONST (BrO_{max}: 188 pmol/mol in ICON versus BrO_{max}: 157 pmol/mol in CONST, see Fig. 9.17 d, e). The difference in BrO mixing ratios that can be seen all over the boundary layer (Fig. 9.17 b) between these two scenarios arises, as in scenario ICON the flux of IBr out of the Dead Sea water into the atmosphere and the subsequent photolysis of IBr provides an additional source for bromine atoms and thus for BrO in scenario ICON.

O_3 mixing ratios decrease stronger in the presence of iodine, i.e. in scenario ICON compared to scenario CONST. At 2 m altitude O_3 mixing ratios in scenario ICON decrease from 66 nmol/mol to 52 nmol/mol which is a decrease by 22%. The reduction of O_3 mixing ratios in scenario CONST is only in the range of 14 % and the minimum O_3 mixing ratios at 2 m altitude are still 59 nmol/mol. The O_3 depletion event in scenario ICON is strongest in the lowest 10 meters of the boundary layer as bromine as well as iodine mixing ratios are largest there. However, between 15:00 and 16:00 more than 10% of the initially present O_3 is depleted all over the boundary layer. Still the strength of the depletion event is weaker than observed depletion events.

IO mixing ratios at 2 m altitude decrease from 10.6 pmol/mol at 10:00 to 2.5 pmol/mol at 16:00 (blue dotted line, Fig. 9.17 e). IO is transported quickly into upper parts of the boundary layer and even though the vertical gradient in mixing ratios is large, IO mixing ratios of 1 pmol/mol can be found all over the boundary layer between 10:00 and 11:00 (Fig. 9.17 c). However, mixing ratios decrease in the whole boundary layer with time. At the same time OIO mixing ratios increase with time all over the boundary layer. Mixing ratios of OIO, which is formed to a large extent by self - reaction of IO increase at 2 m altitude from 4.7 up to 41.4 pmol/mol. Due to the high total load of particles at the Dead Sea, the OIO nucleation rate is relatively low. Although OIO condenses on existing particles the source by IO self reaction is strong, which explains the high mixing ratios of up to 41.4 pmol/mol.

Thus, IO is quickly distributed all over the boundary layer but mixing ratios decrease due to reactions. Among the fastest reactions is the IO self reaction leading to the formation of OIO as well as the reaction between IO and BrO.

Even though, the fluxes of all iodine containing species stay constant over time, IO mixing ratios at 2 m altitude decrease with time. Thus in contrast to the prescribed fluxes of bromine containing species, fluxes for iodine species are not sufficient to lead to an accumulation of iodine in the lowest part of the boundary layer as it happens for bromine species. Indeed ICl mixing ratios at 2 m altitude increases only from 1.4 to 2.9 pmol/mol, those for IBr from 1.6 to 6.4 pmol/mol and those for HOI increase in the first hour between from 42 to 132 pmol/mol but decrease afterwards to 93 pmol/mol.

	$BrO_{(max)}$ [pmol/mol]	$O_{3(min)}$ [nmol/mol]	ΔO_3	**Lagrangian**
NOEX	0.012	const 69	0%	No air-sea-exchange, BrO $<$ 1 pmol/mol, O_3 not affected
EX	102	66	4%	High BrO, No ODE
EXALL	151	63	9%	High BrO, No ODE
SUB	144	const 68	0%	Subsidence has no effect on BrO and O_3
EXLIM	347	10	84%	ODE affects only lowest 20 m
CONST	157	59	14%	Constant fluxes out of D.S. water still lead to accumulation and increase with time of bromine species
NOSO	192	53	20%	Fluxes of HOBr decrease with time whereas they increased in EXALL
DRY	142	64	7%	Inclusion of heterogeneous reactions on dry aerosols lead to larger BrO but have no effect on O_3
ENH_1	717	0.02	99%	ODE affects whole BL, O_3 totally destroyed after 3 h
ENH_2	375	13	80%	ODE affects whole BL, O_3 decrease still slow but steady
LOWBL	207	25	63%	ODE affects whole BL, less strong than when enhancing fluxes
HIGHRH	81	57	13%	Aerosol chem. active in upper part of BL, no ODE
CL_{HIGH}	247	51	26%	Overestimation of Cl^- in D.S. water $\longrightarrow$ much higher BrO but still no strong ODE
CL_{DECR}	219	60	13%	$BrO > BrO_{EXALL}$ but O_3 decrease on same order of magnitude as in EXALL
				Stationary
STAT	61 day1 / 139 day2	70 day1 / 5 day2	0% / 92%	No ODE on day1 but ODE on day2 affecting the whole BL due to slightly differing meteorological background conditions

	$BrO_{(max)}$ [pmol/mol]	$IO_{(max)}$ [pmol/mol]	ΔO_3	**Lagrangian + Iodine**
IOD_1	28	41	14%	I^- in D.S. $\approx$ 10 $\times$ too large $\longrightarrow$ IO $\approx$ 4 $\times$ larger than max. measurement
IOD_2	27	21	8%	I^- in D.S. $\approx$ 4 $\times$ too large $\longrightarrow$ IO $\approx$ 2 $\times$ larger than max. measurement
IOD_3	19	12	4%	I^- as in D.S. $\longrightarrow$ IO on order of magnitude as in measurements, BrO lower
ICON	188	10	21%	I_2, Br_2, HOI, HOBr fluxes $\approx 10^{10}$ molec/(cm^{s}s) $\longrightarrow$ BrO $>$ 100 pmol/mol and IO $\approx$ 10 pmol/mol

Table 9.1: Summary of Results of scenarios calculated for the Dead Sea. BrO, IO and O_3 mixing ratios refer to values at 2 m altitude.

Chapter 10

Discussion and Conclusions

Numerous measurements taken along the Dead Sea show high bromine oxide mixing ratios and correlated ozone depletion events. However, the spacial extent as well as the strength of the ODEs differ significantly. Bromine oxide mixing ratios of about 60 to 100 pmol/mol can be, but are not necessarily followed by an extraordinary fast decrease in O_3 mixing ratios (Tas et al., 2005, see Fig. 10.1). The strong spacial and temporal variablity of ODE's and the comparatively large range ($\Delta \approx 40$ pmol/mol) of corresponding BrO mixing ratios complicates the finding of an overall explanation of the occurring processes.

The knowledge about the gradient of Br^- and H^+ concentrations between the southern part (evaporation ponds) and the northern part of the Dead Sea and the analysis of measurements let several scientists (Hebestreit et al., 1999; Matveev et al., 2001; Tas et al., 2003) conclude that BrO production over the southern evaporation ponds has to be stronger than over the northern more alkaline part of the Dead Sea. However, this hypothesis has to be at least extended regarding the data from the latest measurement campaigns. During a long term campaign, Tas et al. (2005) detected the absolute maximum BrO mixing ratio of 220 pmol/mol at the mid-site measurements station and not at the South-site. Tas et al. (2003) also found larger mean BrO mixing ratios in the North compared to the South end of the lake (see Fig. 10.1). The Lagrangian scenarios presented in this model study indicate, that the gradient in Br^- and Cl^- concentrations as well as of the pH within the water cannot be the reason for more pronounced O_3 depletion events and correlated high BrO mixing ratios at the South end of the Dead Sea.

Tas et al. (2005) further present measurements for one single day where at all three measurement sites along the Dead Sea - in the South (on the peninsula), a site at the middle part of the lake and on the North shore of the Dead Sea - BrO mixing ratios were high ($>$ 60 pmol/mol), with maximum values in the South (120 pmol/mol). Ozone was depleted only in the South. At both other sites O_3 levels decreased only slightly (see Fig. 10.1, left). With the Lagrangian scenario EXLIM it was possible to reproduce these measurements with good agreement regarding the strength of the ODE as well as the spacial distribution of O_3 and BrO as well as the temporal distribution meaning a very quick decrease when air masses are assumed to reach the Dead Sea from the South (see Fig. 9.5). Nevertheless, the production of maximum BrO mixing ratios of 395 pmol/mol (at 2 m altitude) are necessary to destroy a significant amount of O_3 in the model. This value is a factor of two to four larger than the largest ever measured BrO mixing ratio at the Dead Sea. However, it is very likely that the effect of a potential low level inversion is overestimated in the model in scenario EXLIM. It is assumed that vertical transport is strongly limited for two hours until the mixing of air masses compensates the inversion. These two hours are roughly
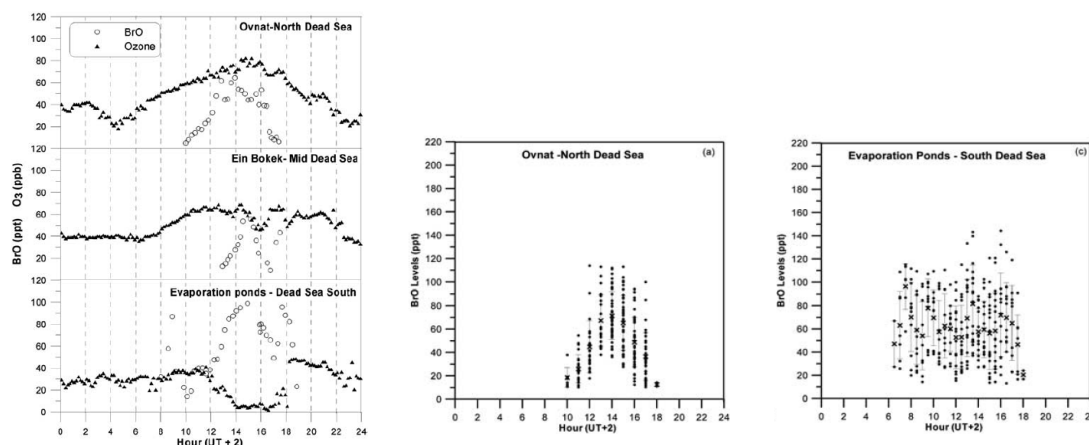
119

Figure 10.1: The plot on the left shows BrO and O_3 mixing ratios as measured simultaneously at three different sites along the Dead Sea, 3 August 2001. On the right, mean BrO mixing ratios from a long term campaign are plotted (Summer 2001). Both plots are taken from Tas et al. (2005).

needed to transport an air parcel across the evaporation ponds at the average occurring wind speed. However, it can be assumed that the compensation of the low-level inversion could happen much faster in reality. As a consequence BrO mixing ratios would not become as high as in scenario EXLIM and O_3 mixing ratios would still decrease rapidly, even though not as strong as in this model scenario.

In order to test this, scenario EXLIM was recalculated only allowing the exchange of Br_2 and BrCl. In that case BrO mixing ratios reached a maximum mixing ratio of 290 pmol/mol (in contrast to 395 pmol/mol in EXLIM) and O_3 still decreased quickly to 13 nmol/mol (in contrast to 10 nmol/mol in EXLIM).

With regard to the reaction rates it can be seen that such a large BrO production rate by the reaction $Br + O_3$ as in scenario EXLIM (or at least its modified version) is necessary to simulate the temporal as well as spacial development of an ODE as measurements show it occurring. With respect to the total O_3 balance, the maximum destruction of O_3 by reaction with Br at about 11:30 in scenario EXLIM is 0.6 pmol/(mol·s). However, in scenario EXLIM only the lowest 10 to 20 meters are affected by the depletion event. Again it has to be reminded that a similar scenario might develop in reality affecting not only the lowest 10, but maybe 100 or 300 meters. It is not possible to evaluate those model results, as the above mentioned measurements (see Fig. 10.1) were only taken at one level at approximately 2 m height and no information about the vertical extent of the real depletion event in the South is available.

10.1   Influence of transportation time over the Dead Sea

With regard to the steadily increasing halogen gas phase concentrations in the Lagrangian scenarios EX, EXALL and SUB (as well as the scenarios CONST, NOEX and NOSO) the influence of transportation time and wind direction on trace gas concentrations has to be discussed.

A summary of the current understanding about the wind pattern over the Dead Sea was given in the introduction in Section 8.1. For all scenarios apart from scenario NOSO it

was assumed that the wind direction all over the lake is southerly. With respect to the measurements this is an idealised assumption as the wind direction in the North and South might be in opposite directions with the North shore being mainly influenced by southerly and the South shore being very often influenced by northerly winds (potentially caused by the lake breeze, see Fig. 10.2 c). However, even under such circumstances an air parcel reaching the northern (or southern) end of the Dead Sea has been transported roughly across half the length of the lake.

Regarding the modelled Lagrangian scenarios, it is assumed that the southern most edge of the Dead Sea is strongly influenced by air masses that crossed the desert before they reach the lake (apart from scenario NOSO). In all these scenarios, bromine mixing ratios increase rapidly within the first minutes that the model starts to cross the lake (ΔBrO $\approx 50\,\%$ between minute 1 and minute 10 of the simulation time). As was already said in Section 9.1.1, the constant increase in gas phase mixing ratios is an effect of making the (idealised) assumption that air masses over the southern most end of the Dead Sea were not influenced in any way by halogen chemistry before the model crosses the lake. The longer halogen chemistry is active (the closer the model column gets to the north end of the lake) the more the concentrations increase.

Comparing the results of the Lagrangian model runs and the measurements, the wind direction and the transportation time of an air mass over the Dead Sea water seems to be crucial for the order of magnitude of bromine mixing ratios. Figure 10.1 b and c show mean BrO mixing ratios at a North and South site at the Dead Sea. At the north site the time evolution of BrO mixing ratios during the day seems to be very similar on all measurement days with a maximum in mixing ratios at around noon. Data taken at the south site show strong fluctuations and no regular time evolution during day time. The time of maximum mixing ratios varies strongly between the different measurement days. Thus the regular wind direction from South to North in the North seems to contribute to the regular time evolution of BrO mixing ratios.

As the wind direction over the southern end of the lake is very often northerly, this might change the initial conditions in the Lagrangian model runs compared to the simulated scenarios as it might be possible that even air masses over the desert South of the Dead Sea can contain bromine levels significantly exceeding background concentrations as was shown by Tas et al. (2005). Meteorological conditions can be assumed leading to northerly winds over the South end of the Dead Sea for several hours. If the wind direction changes afterwards it is very likely that air masses reaching the Dead Sea from the desert already contain a significant load of halogens. For such cases the Lagrangian setup underestimates initial bromine and chlorine concentrations. However, with respect to the measurements taken at Ein Tamar south of the Dead Sea which show average BrO mixing ratios of $20\,\text{pmol/mol}$, it is unlikely that the potential additional halogen load of this order of magnitude in air masses that reach the Dead Sea would lead to a much faster and much stronger O_3 decrease than in the modelled cases. The exchange of halogen species out of the Dead Sea water was increased by more than one order of magnitude in scenario $ENH_{1,2}$ leading to BrO mixing ratios of more than $300\,\text{pmol/mol}$. However, the timescale of the simulated O_3 depletion events still did not agree with the measurements, i.e. it took more than three hours until background O_3 mixing ratios decreased by about $50\,\%$.

Due to the very low relative humidity the recycling capacity in the air over the desert with respect to bromine chemistry should be very small. Potentially BrO can react with NO_2 and the resulting $BrONO_2$ can be taken up onto aerosol particles and is converted to reactive halogen species. However, as it was shown in this thesis this recycling pathway

as well as e.g. the recycling pathway via uptake of HOBr onto aerosol particles is not very efficient over the dry desert. Thus the additional amount of Br-atoms (based on the measurements of mean BrO concentrations of 20 pmol/mol) in air masses arriving at the Dead Sea from the desert which are neglected in the model scenarios should not be responsible for the strong depletion events over the South end of the lake.

Furthermore, the way measurements of BrO mixing ratios and wind data are presented by Tas et al. (2003) (Figure 6 and 7 in their paper) does not account for the wind direction changes during the day. As the wind pattern in the South seems to vary during the day it might be possible, that a correlation plot between BrO or O_3 mixing ratios and the wind direction might look significantly different an hour later or earlier than presented in Tas et al. (2003). Thus knowing the time evolution of the wind direction in correlation with the mixing ratios of chemical tracers at the South end of the Dead Sea might help to understand the unregular pattern in measured BrO mixing ratios.

From the Lagrangian scenarios (EX, EXALL, SUB) treating air-sea exchange explicitly it can be concluded: Under the considered circumstances the transportation time of an air parcel over the water seems to be more important for BrO mixing ratios than the actual source strength of the degassing species which differs insignificantly between the South compared to the North. Furthermore, such scenarios would represent conditions where high BrO levels build up but O_3 would not be depleted necessarily.

Meteorological background conditions highly determine whether an O_3 depletion event develops over the southern end of the Dead Sea in the model or not. If southerly winds are present (i) air masses in the lowest meters of the boundary layer are much warmer over the land surface than the water surface and a low level inversion might develop leading to a limited vertical transportation leading to an ODE. (ii) air masses get well mixed over the water, vertical transport leads to a distribution of halogen species all over the boundary layer leading to high BrO levels near the water surface which are however not sufficient to destroy significant amounts of O_3.

10.2   Stationary Model Run

Scenario STAT is the only scenario presented, where it was possible to simulate an ODE affecting quickly the whole boundary layer even though air masses in the boundary layer are well mixed and air - sea exchange of tracers was not enhanced. Considering it from a more technical point of view, the ODE is an effect of several combined assumptions: The strongly idealised character of this scenario regarding the advection of environmental air masses into the model domain was discussed while describing the model setup in Section 8.4.2. This first assumption simplifies the problem of mixing of air masses to the most simple regime - only the two most important 'background' species (NO_2 and O_3) are advected and the strength of the inflow is chosen more or less arbitrary. The advantage of this approach is the exact knowledge of the additional source strength of NO_2 and O_3. The second assumption - horizontal mixing for halogen species is negligible - is more realistic. It was shown in the Lagrangian scenarios, that the fluxes of bromine containing species out of the Dead Sea water are very large all over the Dead Sea and even though their strength differs slightly between the South and the North in the model, air-sea exchange is however the dominant source for gas phase bromine species. Thus horizontal mixing of halogen compounds should not significantly change the order of absolute concentrations. Furthermore, scenario STAT represents two days where air masses in the Dead Sea valley are not influenced by mixing with air masses from aloft. The boundary layer height is constantly

very high (about 1200 m). However, these assumptions considered individually have only a smaller effect on the development of the ODE. The two, most important factors leading to the depletion event affecting the whole boundary layer are the changing meteorological background conditions and the allowance of Br_2 and $BrCl$ as well, building a night time reservoir. Furthermore, it is worth mentioning, that the ODE occurs simultaneously to the production of BrO mixing ratios exceeding 100 pmol/mol even though a limited source strength for the degassing of the halogens out of the Dead Sea water was assumed as only the exchange of Br_2 and $BrCl$ was allowed. In none of the Lagrangian scenarios, this setup lead to BrO mixing ratios of that order of magnitude and O_3 was least affected.

Again, one of the main conclusions which can be drawn from scenario STAT is that it is important not only to consider chemistry as an isolated system as apparently very small changes in the meteorological background conditions (namely temperature and humidity) gives a large feedback to chemistry.

10.3 Measurements at an elevated site 400 m above Dead Sea

As mentioned in the introduction some of the measurements took place at an elevated site 400 m above water level. At 3 out of 22 days average BrO mixing ratios of 20 pmol/mol were detected. BrO mixing ratios as simulated in scenario EX or EXALL are in the same order of magnitude at this height. Tas et al. (2003) assumed that on those three days where high BrO mixing ratios were detected, the boundary layer height was very low (they assume that it was approximately 300 m above the measurement site, i.e. 700 m above the lake surface). However, in scenario EXALL the boundary layer height as calculated in the model is about 1300 m and BrO is transported very efficiently with high concentrations into altitudes around 400 m. This let the question arise, what kind of local wind and transport pattern is responsible for the *lack* of BrO on the other days.

The explanation might be found in the potentially very complicated local flow patterns. Measurements show that even the surface wind direction is highly variable and no comprehensive three dimensional wind data set exists which would be crucial to understand the extent of vertical transport over the Dead Sea as well as of subsiding air (as was mentioned in the introduction).

Potentially two kinds of flow systems might develop which could explain the contradictory measurements at the 400 m site as well as easterly winds at this site as detected by Bitan (1977).

For the first scenario it is assumed that the general weather situation is such that the air masses in the valley are more or less uninfluenced by larger scale weather systems and the local flow pattern is dominated by the lake breeze and the mountain breeze (see Fig. 10.2 a). The measurement site at 400 m above the Dead Sea should then mainly be influenced by ascending air masses from the bottom of the valley (containing the large bromine contents) and from the mountain ridges due to thermal heating. Such a weather situation should also be accompanied with a high (partially due to the dryness) and well mixed boundary layer as simulated e.g. in scenario EXALL leading to potentially detectable BrO mixing ratios at a height of 400 m (Fig. 10.2 a).

The second supposed wind pattern includes an overlaying westerly flow. Air masses are lifted west of the mountain ridge and descend into the valley. They get well mixed with local air masses. Under such circumstances the measurement site would be more influ-

enced by air masses originated over the Mediterranean rather than over the Dead Sea and BrO mixing ratios would probably not exceed the detection limit of an instrument at the measurement site 400 m above the Dead Sea. Furthermore, the comparatively cooler, descending air masses might turn over and their flow might direct towards the western mountains due to the thermal depression over the relatively warm mountain ridges as indicated in Figure 10.2 b. An anemometer might then determine the wind direction as easterly as observed by Bitan (1977). It is known that such a flow pattern occurs often in the late afternoon and early evening hours as explained in the introduction (Bitan, 1977). However, it is not unrealistic that weather situations develop where such an overlying flow might influence the valley during large parts of the day. One additional effect of the subsiding air might be a lower boundary layer height which would enhance the potential for the occurrence of well pronounced ozone depletion events as the vertical transport of bromine species would be limited. This might lead to an accumulation of the emitted species in lower parts of the boundary layer. However, as scenario SUB has shown, this effect is either negligible or the boundary layer height has to be low constantly during the day as in scenario LOWBL.

Again it has to be concluded: it is not possible to conclusively assess how representative the model scenarios are as apparently meteorological conditions determine the vertical extend of bromine levels and important information regarding the measurements are missing. The knowledge about the boundary layer height on the measurement days is crucial as well as the knowledge about the temperature and relative humidity.

For all presented studies the same background concentrations for NO_x and O_3 were assumed. With respect to the measurements a background O_3 mixing ratio of about 70 nmol/mol like chosen for all simulations might slightly overestimate the actual values whereas a morning mixing ratio for NO_2 of about 1 nmol/mol might underestimate actual values. Theoretically, lower background O_3 mixing ratios could lead to a faster depletion event. Therefore one model run (same set up as scenario EXALL) was performed with an O_3 background mixing ratio of about 50 nmol/mol and NO_2 morning-mixing ratios of
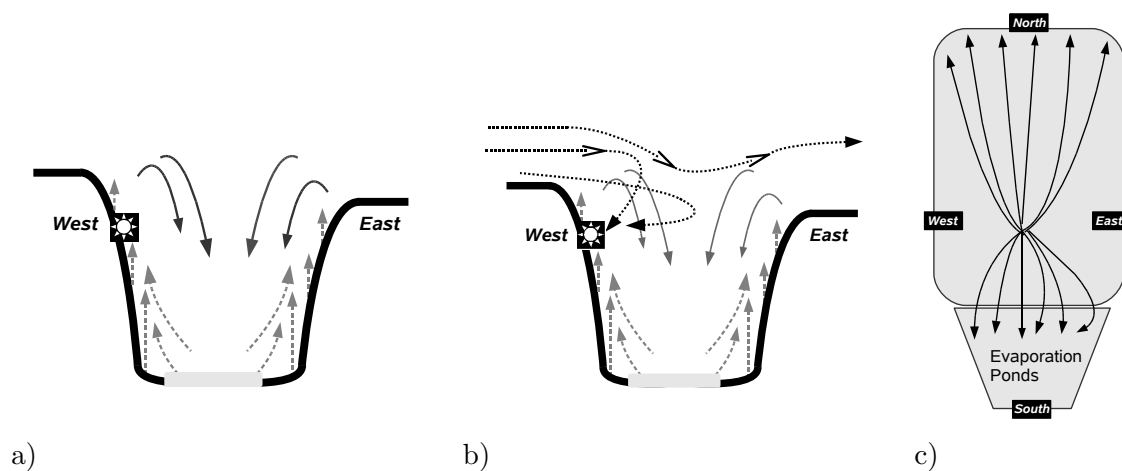

Figure 10.2: Potential flow patterns over the Dead Sea (a,b). The stars mark the measurement site 400 m above the Dead Sea water level. The horizontal flow pattern due to the lake breeze is shown in (c).

2 nmol/mol, based on measurements for one day presented by Tas et al. (2005) (Fig. 7). BrO mixing ratios increase up to 114 pmol/mol at 16:00 which are about 40 pmol/mol less than in scenario EXALL. However, the order of magnitude agrees well with measured values. As the source strength for O_3 via NO_2 photolysis is even stronger than in the scenarios discussed above, O_3 mixing ratios do not decrease significantly and the loss is less than 5%. Again, no new conclusions in general could be drawn from this model setup and thus it was not discussed in detail in Section 9.

10.4 Potential additional bromine sources

It was discussed above in great detail that strict assumptions to the meteorological background conditions have to be made to simulate fast and strong O_3 depletion events like a low level inversion or restrictions to horizontal mixing have to be made. Furthermore, the source strength of the halogen species by direct degassing was increased leading to extremely high BrO mixing ratios but leading at the same time to a quick decrease in O_3 mixing ratios. Regarding the uncertainties of the parameterisation of the air-sea exchange of tracers, the order of magnitude by which the fluxes had to be enhanced (a factor of 30 to 50) to initialise a depletion event exceeds the potential error of the parameterisation. The more likely explanation for a larger total source strength compared to the direct degassing is a missing source.

Like mentioned in the introduction, Stutz et al. (2002) detected up to 6 pmol/mol BrO at the Great Salt Lake and Hönninger et al. (2004a) detect up to 20 pmol/mol BrO at the Salar de Uyuni. Especially the Great Salt Lake has a much lower salinity ($Br^-/Cl^- \approx$ 0.07 % for the Great Salt Lake, 0.34 % for the ocean, 2.5 % for the Dead Sea, Stutz et al. (2002) and references therein) and acidity (pH $\approx$ 8, Stutz et al. (2002) and references therein) than the Dead Sea. The pH of the Salar de Uyuni varies from below 5 in highly concentrated brines to 7.5 in diluted brines and the bromide content varies between 30 and 300 mg/l (Hönninger et al. (2004a) and references therein) compared to 6 - 11 g/l in the Dead Sea water. For both lakes it is very unlikely that bromine, chlorine or iodine species can directly degas out of the water of the lakes because of the pH of the water as well as the lower bromide content of the water. However, for both measurement sites an anticorrelation between BrO (as well as ClO at the Great Salt Lake) and O_3 was observed. The depletion of O_3 at the Great Salt Lake is only in the range of about 12 % but it is much larger at the Salar de Uyuni. Hönninger et al. (2004a) assume that the bromine sources are *concentrated acidic brines supporting the bromine explosion mechanism*. Stutz et al. (2002) have a similar source suggestion for the observed reactive bromine and chlorine mixing ratios at the Great Salt Lake. They assume that crystallised salt deposits at the shore of the lake get acidified by deposited pollutants and act as a reaction surface for heterogeneous reactions that release halogens by mechanisms similar to those observed in the Arctic. Furthermore they assume that due to the relatively high wind speed (5 - 7 m/s) salt particles might be lifted up into the atmosphere and provide a reaction surface for halogen chemistry.

The latter process is unlikely to occur at the Dead Sea due to the very low wind speed. Furthermore the relative humidity at the Great Salt Lake as reported by Stutz et al. (2002) is slightly higher than reported for the Dead Sea. The effect of calculating heterogeneous chemistry on dried aerosol particles in the atmosphere has shown no big effect on O_3 chemistry (see Section 9.1.6). It might be possible that there are uncertainties on the reaction kinetics for those reactions. It is however more likely, that the number of

those particles being able to act as a halogen reaction body are too few and the yield of reactive gas phase bromine species is too low to contribute significantly to the total gas phase bromine budget.

Matveev et al. (2001) also suggest a similar additional bromine source as Stutz et al. (2002): *The shores of the Dead Sea are periodically covered by water. During those periods that the shore is free of water the top layer of the soil contains very high concentrations of bromine-rich sea salt providing a highly reactive surface.* Even though the wind speed is in general very low, it is imaginable that shallow waves might frequently wash parts of the shore. Thus the wet soil might potentially be even a larger source than the water itself.

As the evaporation ponds are very shallow and the depth of each pond is different and is varied regularly, the parameterisation used to calculate air-sea exchange might underestimate the bromine source strength over the evaporation ponds. However, it is difficult to say quantitatively how large this potential error might be. It is likely that the bromine source strength of the various ponds is variable. In addition to the variable wind direction over the southern part of the Dead Sea, this might explain the unregular pattern of BrO mixing ratios as detected at the Evaporation Ponds (see Fig. 10.1).

Matveev et al. (2001) further suggest that heterogeneous reactions on the water surface might take place similar to the reaction between O_3 and iodide that is supposed to take place at the sea surface microlayer and contributes to gas phase iodine mixing ratios. As the potential yields of Br atoms from such kind of reaction is much smaller (mainly because of the limited uptake of O_3 due to it's low solubility) than the calculated fluxes out of the water by the air-sea exchange parameterisation, it can be assumed that this process is of minor importance.

In order to test the effect of an additional bromine source over the southern part of the Dead Sea, scenarios ENH_1 and ENH_2 were calculated (see Section 9.1.5). Even though the depletion events in both scenarios affect the whole boundary layer, both scenarios do not seem to represent the situation along the Dead Sea properly. The quick and strong O_3 depletion in the first hour as simulated in scenario ENH_1 agrees very well with measurements (e.g. Fig. 10.1). However, the total load of bromine in the atmosphere is so large that O_3 is destroyed completely in the following hours. In such a case a strong inflow of ozone rich air would be necessary for again building up O_3 background mixing ratios of at least 40 nmol/mol. Scenario ENH_2 is much more realistic in terms of minimum O_3 mixing ratios. Even though more than 800 pmol/mol BrO are formed between 10:00 and 11:00 it takes about five hours until O_3 mixing ratios drop below 20 nmol/mol. This scenario is in good agreement with flight measurements taken along the Dead Sea. Matveev et al. (2001) present data for for one day showing an ozone depletion only over the northern part of the Dead Sea. Especially with regard to scenario ENH_1 the question arises again what kind of local transport pattern might influence the spacial distribution of chemical tracers along the Dead Sea valley that cannot be captured in the model simulations.

It was mentioned several times above, that the boundary layer height strongly influences the order of magnitude of bromine species. The above discussed scenario SUB where the boundary layer hight decreased from about 1400 to 700 m did not show a significant impact on ozone mixing ratios. Indeed the loss of 61.5% (65→25 nmol/mol, see Fig. 9.8 c) in O_3 mixing ratios during the six hours simulation time in scenario LOWBL is much more striking. As no data regarding the boundary layer height during sampling days is published, it is purely speculative in which way those model results represent conditions

really occurring at the Dead Sea.

10.5 Comparison of results from this thesis with results from Tas et al. (2006)

In the introduction of part II of this thesis, the model studies by Stutz et al. (1999) and Tas et al. (2006) were already mentioned. Stutz et al. (1999) concluded that the production of about 500 pmol/mol BrO would be essential to simulate a significant loss in O_3 after three hours of simulation time. This result agrees well with results from this thesis as discussed above. However, as the results recently published by Tas et al. (2006) significantly differ from those results presented in this thesis, both works are drawn in comparison. In the following, it is explained why the chemical mechanism suggested by Tas et al. (2006) is not correct to explain the measurements as several questions arise regarding the robustness of their approach.

Similar to the approach chosen in this thesis, Tas et al. (2006) use a one-dimensional numerical model. However, Tas et al. (2006) do not calculate chemistry in the aqueous phase explicitly but treat only gas phase chemistry explicitly. Tas et al. (2006) use a parametrisation to determine the yield of Br_2 as formed by the bromine explosion mechanism. They further parameterise the heterogeneous decomposition of $BrONO_2$ on sulphate aerosols. Tas et al. (2006) conclude that Br^- concentrations in sea salt aerosols are sufficiently large to produce about 120 pmol/mol of BrO via the bromine explosion mechanism. Further they assume that the most important - and only considered - recycling process for gas phase bromine is the heterogeneous reaction of $BrONO_2$ on sulphate aerosols leading in their parameterised approach directly to the formation of gas phase HOBr.

Considering only these two bromine sink/source reactions is 'dangerous'. As halogen concentrations strongly depend and are controlled by the cycling between the phases, only considering the most important sink and source reaction disrupts this sensitive system. The heterogeneous reaction of $BrONO_2$ leads to the formation of gas phase HOBr. In general, HOBr is taken up efficiently on sea salt particles due to its high solubility. Assuming that aerosol phase chemistry is of importance even though the relative humidity is extremely low but ignoring e.g. the sink for HOBr due to uptake increases mixing ratios in the gas phase and the potential of HOBr to photolyse and form Br atoms. However, the general question regarding the importance of aerosol phase chemistry under the very dry conditions along the Dead Sea arises again.

Furthermore, Tas et al. (2006) chose an unrealistically high reaction rate for the bromine explosion reaction ($1.35 \cdot 10^{-6}$ nmol/s). Under the prevailing circumstances the first order reaction rate as calculated in scenario NOEX (see Section 9.1.1) in MISTRA is about two orders of magnitude slower at 2 m altitude (1-$3 \cdot 10^{-8}$ nmol/(m^{3}s)). In general the way Tas et al. (2006) determined this reaction rate is not the appropriate way how to implement the bromine explosion reaction into a numerical model. Tas et al. (2006) *obtained the reaction rate for the bromine explosion reaction as the only degree of freedom in the structure of the model. A range of values for the reaction rate was tested and the value giving the best agreement between simulations and measurements was then chosen as the reaction rate used for all model simulations.* At first, obtaining a reaction rate that has been measured (Liu and Margerum, 2001) as a degree of freedom in a numerical model is inappropriate. Secondly, choosing the rate until results from the model simulations agree best with measurements, casts doubt on all results presented by Tas et al. (2006).

In general the setup as chosen for scenario NOEX corresponds to the simulations done by Tas et al. (2006) and should give similar results. However, as the source strength for Br atoms is highly overestimated by Tas et al. (2006), the amount of produced BrO is much larger in their studies (up to 120 pmol/mol) compared to scenario NOEX (BrO$_{max}$: 0.012 pmol/mol).

The dryness of the atmosphere above the Dead Sea has to be discussed again in this context: A relative humidity between 45 and 50 % in the lowest 100 m as used in almost all model runs in this thesis (see Section 8.4.1) represents the conditions at the Dead Sea well (Tas, personal communication, on some days the relative humidity was as low as 40 % only a few meters above the water surface). Tas et al. (2006) do not give any information about meteorological parameters as used for their model simulations. They state out that the heterogeneous decomposition of BrONO$_2$ is fast even under dry conditions. However, a value of 0.75 that Tas et al. (2006) have chosen for the uptake coefficient might be too high for the extremely dry conditions at the Dead Sea. A value of 0.3 (Aguzzi and Rossi, 1999) as chosen in the model scenario including heterogeneous reactions on dry aerosol particles (see Section 9.1.6) is maybe more appropriate.

In all of the above presented model runs apart from scenario EXLIM, the O$_3$ depletion process is much slower than observations show it happen. In the model simulations presented by Tas et al. (2006), O$_3$ is destroyed quickly - however, Tas et al. (2006) do not provide any information about the boundary layer height or the vertical distribution of BrO and O$_3$ mixing ratios. Whenever a one dimensional model is used the question arises, how horizontal advection into the model domain has to be treated if not a Lagrangian setup is chosen as was done in most of the simulations presented in this study. Tas et al. (2006) chose the strength of fluxes into the model domain again such, that their simulations agree best with measurements. A problem in their line of argument occurs as their results strongly depend on the ('manually') varied O$_3$ inflow. Measurements show a quick decrease but also a quick increase in O$_3$ mixing ratios. Tas et al. (2006) argument that *the decrease in* O$_3$ *concentrations beneath a threshold value of 1 - 2 nmol/mol acts as a motive force for fresh* O$_3$ *fluxes to move into the evaporation ponds.* Indeed, the inflow of O$_3$ is controlled by the wind speed (although it is low) and wind direction and not by the gradient in O$_3$ concentrations itself.

Even though the Dead Sea water is highly enriched in bromide compared to ocean water, again it is unlikely that bromide content in sea salt aerosols and the related degassing of Br$_2$ can explain observed levels of BrO. In an earlier work Matveev et al. (2001) analysed the bromide content of the aerosol phase at the Dead Sea and came to the conclusion that the concentrations of bromine compounds within aerosols are too low to be considered as a significant source for the observed gas phase BrO mixing ratios. They found filterable Cl$^-$ in the range of 100 to 1000 pmol/mol and filterable Br$^-$ in the range of 10 to 60 pmol/mol. Regarding the bromide ($\approx$ 5 pmol/mol) and chloride ($\approx$ 40 pmol/mol) content of sea salt particles at 2 m altitude in scenario NOEX (see Section 9.1.1 and Figure 9.1), the salt content of the aerosol is slightly lower than in the samples. However, the difference between the model and the measurements should not be significant enough so that the bromide and chloride contents in aerosol particles in the model are too low to produce sufficient amounts of Br$_2$ that can degas and finally lead to the formation of BrO mixing ratios in the range of 100 pmol/mol but that this process should be of more importance in reality.

10.6 Discussion including Iodine chemistry

Zingler and Platt (2005) report the largest ever published IO mixing ratios in midlatitudes which were detected during a measurement campaign at the Dead Sea. Due to the very high salinity of the Dead Sea water and the extreme hot and dry ambient conditions they conclude that algae and organic precursors which are of crucial importance for the detection of significant gas phase iodine levels in polar as well as coastal regions cannot be the reason for the high IO mixing ratios at the Dead Sea. The first release mechanism they suggest, i.e. the uptake of O_3 and the subsequent release of I_2 out of the Dead Sea water is of no significance mainly because of the low solubility and thus low uptake rate of O_3. Zingler and Platt (2005) suggest further a similar iodine release process out of aerosol particles (or the Dead Sea water directly) as it is known to be responsible for activating bromine chemistry (bromine explosion reaction). Such a process should be possible to happen at the Dead Sea due to the low pH of the water. In general this idea gets supported by the herein presented model results - with the restriction that it is not the aerosol phase chemistry that is important but the chemistry taking place in the Dead Sea water itself and the air-sea exchange of iodine containing species. However, due to the general uncertainties that were already discussed above and due to the known uncertainties regarding aqueous phase iodine reaction kinetics, the potential sources for gas phase IO have to be discussed.

The model was able to simulate even more than $10\,\mathrm{pmol/mol}$ gas phase IO just by using the 'standard' chemistry mechanism as discussed in Pechtl et al. (2007) and initialising chemistry in the Dead Sea water with iodide concentrations as appropriate for the Dead Sea. However, one of the largest known uncertainties regarding aqueous phase iodine chemistry is the obvious inability of models to simulate the iodide-iodate speciation in aerosol particles. Thus we need to have in mind that potentially unknown aqueous phase iodine reactions exist or the reaction kinetics are insufficiently understood.

A slight discrepancy between model results and measurements was found regarding the [IO]/[BrO] ratio. Zingler and Platt (2005) present data for one day, showing IO mixing ratios of about $3\,\mathrm{pmol/mol}$ and at the same time BrO mixing ratios of about $60\,\mathrm{pmol/mol}$ (and no O_3 depletion!). Even though in all presented Lagrangian studies treating air-sea exchange explicitly, IO mixing ratios were even overestimated, BrO mixing ratios only reach a maximum value of about $40\,\mathrm{pmol/mol}$. In all cases IBr was the highest concentrated precursor species for gas phase bromine. Thus assuming lower initial iodide concentrations for the Dead Sea water than in scenario IOD_3 ($1\,\mu\mathrm{mol/l}$), would lead to the formation of higher Br_2 concentrations in the Dead Sea water in the model (due to a shift in equilibria) and consequently to higher fluxes of Br_2 out of the water into the gas phase. However, at the same time, decreasing the iodide content would lead to smaller concentrations of iodine species like I_2 and HOI in the Dead Sea water in the model and smaller fluxes of these species out of the Dead Sea water and thus it would lead to lower gas phase IO mixing ratios.

A further potential discrepancy between the model results and measurements has to be addressed: Zingler and Platt (2005) and Tas et al. (2006) mention days where large amounts of BrO could be detected but no IO. If the calculation of aqueous phase iodine chemistry is totally appropriate as implemented in MISTRA, it can be assumed that the iodide content of the water as well as the flux strength of iodine species out of the Dead Sea water should stay more or less constant. This would however mean that gas phase IO mixing ratios over the Dead Sea should nearly always exceed at least $1\,\mathrm{pmol/mol}$. Thus the question is

again: do we understand aqueous phase iodine chemistry complete enough? Or is the local wind pattern responsible for days with detectable and days without detectable amounts of IO? However, why should BrO be detected with extraordinary high mixing ratios if local transport inhibits the detection of IO?

In scenario IOD_3 initial I^- concentrations are $1\,\mu$mol/l which is very close to the value published in Zingler and Platt (2005) ($2 \cdot 10^{-4}$g/l). However, the chemical mechanism in MISTRA predicts a strong decrease in iodide mixing ratios with time. When remembering again that those Lagrangian scenarios should represent a variation with space it is very difficult to imagine that iodide concentrations should vary by more than three orders of magnitude within the Dead Sea.

The only place on earth where ozone depletion events have been observed as strong and sometimes even as quick as along the Dead Sea are polar regions. Even though the meteorological background conditions cannot be more contrarious as between those two areas, the chemical reactions taking place are the same. Jones et al. (2006) report long term measurements of O_3 at Antarctica. They observe several extremely rapid and strong depletion events (maximum of $16\,$nmol/mol depletion in 1 min) which were always correlated with a certain type of wind pattern as well as weaker O_3 depletion events during periods of a very stable boundary layer letting chemical reactions dominate meteorological processes. The measurements done by Jones et al. (2006) give further indications that chemical reactions alone (under stable boundary conditions) are unlikely to lead to a very quick and strong ozone depletion. Saiz-Lopez et al. (2007b) and Saiz-Lopez et al. (2007c) did similar measurements in Antarctica but also collected data regarding IO and BrO mixing ratios. On several days they observe only little O_3 depletion in the presence of high BrO as well as IO mixing ratios. To explain those measurements they assume a fast entrainment of O_3 from the free troposphere.

In general one of the most important differences between ozone depletion events over the Dead Sea and Antarctica/the Arctic is the period of time during which O_3 decreases from background mixing ratios to significant lower values. The fast depletion events such as mentioned by Jones et al. (2006) are always dominated by regional transport and not by local chemistry however, it is questionable in which way transport could directly explain the fast ozone destruction over the Dead Sea. Horizontal advection of O_3-low air can be almost certainly ruled out and subsidence of O_3-low air is also unlikely. NO_x mixing ratios in central Israel are almost always several nmol/mol high (Matvev et al., 2002; Tas et al., 2005) and thus O_3 can be efficiently produced. Furthermore, the boundary layer height in Antarctica is almost always lower (Saiz-Lopez et al., 2007c, $\approx 200\,$m) than it can be assumed for the Dead Sea. Thus vertical mixing is limited and bromine can accumulate stronger in the boundary layer. Additionally, NO_2 and thus the most important source for re-production of tropospheric O_3 is much less concentrated in Antarctica than along the Dead Sea so that the re-formation of O_3 is slower than over the Dead Sea.

10.7   Future Research Needs

As was mentioned several times above, it is difficult to evaluate the model results properly due to missing information regarding background conditions at the measurement days. To improve the understanding of ozone and halogen chemistry along the Dead Sea the following aspects have to be regarded:

1. It would be very interesting to have a data set describing the vertical distribution of BrO, IO as well as the vertical extent of the depletion events.

   - Model simulations indicate that the vertical gradient in BrO mixing ratios is very strong in the lowest 10 to 20 m above the water surface. All published measurements were done with the DOAS technique at an altitude of approximately 2 m. According to the model results it would even make a great difference whether measurements are taken at 1.50 m or 2.30 m or 10 m. The only information available about the spacial extent of the O_3 depletion events are the flight measurements taken at about 300 m above ground by Matveev et al. (2001) and measurements taken at the elevated site at Metzoke Dragot. As only on 3 out of 22 days BrO was detected at this site the question arises whether this site and the measurements taken their are representative for the whole Dead Sea valley? It is not known on how many days that an ODE occurs it influences also higher levels of the boundary layer or not.

2. The time evolution of the wind direction might be of importance to understand the unregular pattern in BrO mixing ratios at the Evaporation Ponds.

   - As was said several times above it is possible that the air-sea exchange parameterisation is slightly inaccurate to describe the degassing of bromine, chlorine and iodine species out of the highly concentrated and shallow evaporation ponds. Furthermore, as the water level differs between the different ponds the source strength for bromine species is highly variable on a very small area. In addition the wind direction over the Southern End of the Dead Sea seems to vary regularly during day time. Thus to be better able to differentiate between transport and emission effects it might be helpful to present the time evolution of the wind direction as well.

3. Absolutely crucial is the knowledge of the following meteorological parameters for every single measurement day.

   - Temperature
   - Relative Humidity
   - Boundary layer height

Overall local, small scale transport is as important as chemistry itself. Chemical processes lead to the formation of BrO and IO and the destruction of O_3. However the strength and spacial extend of the O_3 depletion events as well as the distribution of halogen species within the boundary layer strongly depends on the horizontal wind pattern as well as on vertical transport and likewise subsidence.

Appendix

Appendix A - Acronyms and Abbrevations

Abbreviation	Meaning
BL	Boundary Layer
CCN	Cloud Condensation Nuclei
CFC	ChloroFluoroCarbon
DFG	Deutsche ForschungsGemeinschaft
DMS	DiMethylSulfide
DOAS	Differential Optical Absorption Spectroscopy
FFC	Film Forming Compound
KPP	Kinetic Preprocessor
LFA	Long Chain Fatty Acids
LWC	Liquid Water Content
MarHal	Marine Halogen modeling group
MBL	Marine Boundary Layer
MISTRA	MIcrophysical STRAtus model
ODE	Ozone Depletion Event
RH	Relative Humidity
RHS	Reactive Halogen Species
ROS3	Third-order Rosenbrock method
SOA	Secondary Organic Aerosol
TC	Total Carbon
TKE	Turbulent Kinetic Energy
VOC	Volatile Organic Compound
WIOC	Water Insoluble Organic Compound
WSOC	Water Soluble Organic Compound

Table 10.1:

Appendix B - Symbols

Table 10.2: Symbols used in this discussion.

Symbol	Meaning
a	dry aerosol radius (μm)
A/r	curvature term in Köler equation
α	accomodation coefficient (or "sticking" coefficient)
$B/(r^3)$	solution term in Köler equation
C	condensation rate
c_i	concentration of a gas phase species i (mol/l/m^3)
$c_{a,i}$	concentration of aqueous phase species (mol m$_{air}^{-3}$)
c_g	concentration of gas phase species (mol m$_{air}^{-3}$)
c_p	specific heat of dry air at constant pressure
c_w	specific heat capacity of water (J g^{-1} K^{-1})
c_w	concentration of an aqueous phase tracer (mol/m^3)
D	diffusion coefficient
$D_d ep$	deposition on the ocean surface
$D_v^{\star}$	diffusivity of air corrected for gas kinetic effects
δ_i	ratio between actual actinic flux and actinic flux of this purely absorbing atmosphere
e	turbulence kinetic energy
ϵ	dissipation of TKE
E	emission of the chemical species
E_r	net radiative flux density
f	Coriolis parameter
$f(a,r)$	two-dimensional particle size distribution function
F	Flux of tracers across a water surface (mol/(m^{2}s))
F_p	flux of particles per unit area of sea surface, per increment of droplet radius dr and time dt (part. m^{-2} s^{-1} μm^{-1})
$F_r(a,r)$	net flux of radiation absorbed by a droplet with dry radius a and total radius r
$F_a ct(\lambda_w)$	spectral actinic flux
$F^a(\lambda_{w,i})$	actinic flux of this purely absorbing atmosphere
$h\nu$	dissociation energy
$H^{\star}$	effective Henry's law constant (M atm^{-1}) for gas i
H	Henry's law coefficient (mol/(m^{3}Pa))
I	photochemical active spectral interval
$J_{i,X}^a$	photolysis rate for a purely absorbing atmosphere
J_X	photolysis rate coefficient of a species X
k	thermal conductivity
k_H^{cc}	dimensionless Henry constant
k_H	Henry's law coefficient (mol/(m^{3}Pa))
$k_{t,i}$	transfer coefficient for bin i

Table 10.2: Continued.

Symbol	Meaning
K_e	turbulent exchange coefficient for energy
K_g	exchange constatant for gas phase (m/s)
K_h	turbulent exchange coefficient for heat
K_m	turbulent exchange coefficient for momentum
K_{tot}	transfer (piston) velocity (m/s)
K_w	exchange constatant for aqueous phase (m/s)
κ	Von Kàrmàn constant
l_{12}	latent heat of condensation
l_{21}	latent heat of evaporation
l	mixing length
L	Loss term
L	Monin-Obukhov length
LWC	liquid water content of the particle
λ_w	wavelength (nm)
λ	mean free path length
M	used to name a third-body reactant in chemical equations
m_s	mass of solute
m_w	mass of water
M	molar mass
M_s	molecular weight of solute
M_w	molecular weight of water
μ	Ratio applied on Monahan aerosol source function
n_{kc}	total number of aqueous classes
ν	number of ions that one sal tmolecule dissociates into
ν	dynamic viscosity of air
p	air pressure
p_0	air pressure at the surface
p_g	partial pressure of a gas phase species directly above a water surfac (pa)
P	Production term
P_{pc}	transport of tracers from aerosol to cloud regime or vice versa
$\phi_x(\lambda_w)$	quantum yield for wavelength λ_w
Φ	potential temperature gradient calculated from similarity theory
Ψ_h	stability correction function for heat transfer
Ψ_m	stability correction function for momentum exchange
$\Psi_s(z, L)$	stability function
R	gas constant for dry air (J/(mol·K))
r	total particle radius (nm)
r_c	critical radius (μm)
R_a	aerodynamic resistance

Table 10.2: Continued.

Symbol	Meaning
R_c	surface resistance
R_g	gas phase resistance
R_m	molecular diffusion resistance
R_v	gas constant for water vapour
R_w	aqueous phase resistance
ρ	density (kg m^{-3})
ρ_s	saturation vapor density (kg m^{-3})
ρ_w	density of water (kg m^{-3})
R_v	specific gas constant for water vapor
S_a	ambient supersaturation ratio
Sc	dimensionless Schmidt number
Sc	critical saturation ratio
$S_h G_h$	dimensionless buoyancy production
Si	photochemically active spectral interval
$Sliq$	dimensionless Schmidt number for liquid phase
$S_m G_m$	dimensionless shear production
S_p	particle sedimentation term
S_r	saturation ratio required for equilibrium at surface of droplet
St	dimensionless Stokes number
σ	surface tension
σ_X	absorption cross section
θ	potential temperature (K)
T	temperature (K)
u, v	horizontal wind components (m/s)
u_g, v_g	geostrophic wind components (m/s)
u_{10}	10 m wind speed (m/s)
$u_\star$	friction velocity
v_g^{dry}	dry deposition velocity
w	vertical wind component (m/s)
z	height above surfacd (m)
z_0	surface roughness length

Gas phase
O^1D, O_2, O_3, OH, HO_2, H_2O_2, H_2O
NO, NO_2, NO_3, N_2O_5, HONO, HNO_3, HNO_4, PAN, NH_3, $RONO_2$
CO, CO_2, CH_4, C_2H_6, C_2H_4, HCHO, HCOOH, ALD (i.e., CH_3CHO), CH_2O_2, $HOCH_2O_2$, CH_3CO_3, CH_3O_2, $C_2H_5O_2$, H_3CO_2, EO_2 (i.e., $H_2C(OH)CH_2OO$), CH_2O_2, ROOH (i.e., alkylhydroperoxides), DOM
SO_2, SO_3, $HOSO_2$, H_2SO_4, DMS, CH_3SCH_2OO, DMSO, $DMSO_2$, CH_3S, CH_3SO, CH_3SO_2, CH_3SO_3, CH_3SO_2H, CH_3SO_3H
Cl, ClO, OClO, HCl, HOCl, Cl_2, Cl_2O_2 $ClNO_2$, $ClNO_3$
Br, BrO, HBr, HOBr, Br_2, $BrNO_2$, $BrNO_3$, BrCl, $CHBr_3$, CH_3Br
I, IO, OIO, HI, HOI, INO_2, INO_3, I_2, ICl, IBr, HIO_3, CH_3I, C_2H_5I, C_3H_7I, CH_2ClI, CH_2BrI, CH_2I_2
Liquid phase (neutral)
O_2, O_3, OH, HO_2, H_2O_2, H_2O
NO, NO_2, NO_3, HONO, HNO_3, HNO_4, NH_3
CO_2, HCHO, HCOOH, CH_3OH, CH_3OO, CH_3OOH, OA, ORG
SO_2, H_2SO_4, DMSO, $DMSO_2$, CH_3SO_2H, CH_3SO_3H
Cl, HCl, HOCl, Cl_2
Br, HBr, HOBr, Br_2, BrCl
IO, HI, HOI, I_2, ICl, IBr
Liquid phase (ions)
H^+, OH^-, O_2^-
NO_2^-, NO_3^-, NO_4^-, NH_4^+
HCO_3^-, CO_3^-, $HCOO^-$
HSO_3^-, SO_3^{2-}, HSO_4^-, SO_4^{2-}, HSO_5^-, SO_3^-, SO_4^-, SO_5^-, $CH_3SO_3^-$, $CH_2OHSO_2^-$, $CH_2OHSO_3^-$
Cl^-, Cl_2^-, ClO^-, $ClOH^-$
Br^-, Br_2^-, BrO^-, $BrCl_2^-$, Br_2Cl^-, $BrOH^-$
I^-, IO_2^-, IO_3^-, ICl_2^-, IBr_2^-, $IClBr^-$

Table 10.3: This table gives a complete listing of all gas and aqueous phase species in MISTRA.

no	reaction	n	A $[(\text{cm}^{-3})^{1-n}\text{s}^{-1}]$	$-E_a / R$ [K]	reference
O 1	$O^1D + O_2 \longrightarrow O_3$	2	3.2×10^{-11}	70	Atkinson et al. (2004)
O 2	$O^1D + N_2 \longrightarrow O_3$	2	1.8×10^{-11}	110	Atkinson et al. (2004)
O 3	$O^1D + H_2O \longrightarrow 2\,OH$	2	2.2×10^{-10}		Atkinson et al. (2004)
O 4	$OH + O_3 \longrightarrow HO_2 + O_2$	2	1.7×10^{-12}	-940	Atkinson et al. (2004)
O 5	$OH + HO_2 \longrightarrow H_2O + O_2$	2	4.8×10^{-11}	250	Atkinson et al. (2004)
O 6	$OH + H_2O_2 \longrightarrow HO_2 + H_2O$	2	2.9×10^{-12}	-160	Atkinson et al. (2004)
O 7	$HO_2 + O_3 \longrightarrow OH + 2O_2$	2	1.0×10^{-14}	-490	Atkinson et al. (2004)
O 8	$HO_2 + HO_2 \longrightarrow H_2O_2 + O_2$	2	2.3×10^{-13}	600	Atkinson et al. (2004)
O 9	$O_3 + h\nu \longrightarrow O_2 + O^1D$	1	1		DeMore et al. (1997)
O 10	$H_2O_2 + h\nu \longrightarrow 2OH$	1	1		DeMore et al. (1997)
N 1	$NO + OH \xrightarrow{M} HONO$	3	2		Sander et al. (2003)
N 2	$NO + HO_2 \longrightarrow NO_2 + OH$	2	3.5×10^{-12}	250	Atkinson et al. (2004)
N 3	$NO + O_3 \longrightarrow NO_2 + O_2$	2	3.0×10^{-12}	-1500	Sander et al. (2003)
N 4	$NO + NO_3 \longrightarrow 2NO_2$	2	1.5×10^{-11}	170	Sander et al. (2003)
N 5	$NO_2 + OH \xrightarrow{M} HNO_3$	3	2		Sander et al. (2003)
N 6	$NO_2 + HO_2 \xrightarrow{M} HNO_4$	3	2		Atkinson et al. (2004)
N 7	$NO_2 + O_3 \longrightarrow NO_3 + O_2$	2	1.2×10^{-13}	-2450	Sander et al. (2003)
N 8	$NO_2 + h\nu \longrightarrow NO + O_3$	1	1		DeMore et al. (1997)
N 9	$NO_2 + NO_3 \xrightarrow{M} N_2O_5$	3	2		Sander et al. (2003)
N 10	$NO_3 + h\nu \longrightarrow NO + O_2$	1	1		Wayne et al. (1991)
N 11	$NO_3 + HO_2 \longrightarrow 0.3\,HNO_3 + 0.7\,OH + 0.7\,NO_2 + O_2$	2	4.0×10^{-12}		Atkinson et al. (2004)
N 12	$NO_3 + NO_3 \longrightarrow NO_2 + NO_2 + O_2$	2	8.5×10^{-13}	-2450	Sander et al. (2003)
N 13	$NO_3 + h\nu \longrightarrow NO_2 + O_3$	1	1		Wayne et al. (1991)
N 14	$N_2O_5 \xrightarrow{M} NO_2 + NO_3$	2	2		Sander et al. (2003)
N 15	$N_2O_5 + H_2O \longrightarrow 2HNO_3$	2	2.6×10^{-22}		Atkinson et al. (2004)
N 16	$N_2O_5 + h\nu \longrightarrow NO_2 + NO_3$	1	1		DeMore et al. (1997)
N 17	$HONO + OH \longrightarrow NO_2$	2	1.8×10^{-11}	-390	Sander et al. (2003)
N 18	$HONO + h\nu \longrightarrow NO + OH$	1	1		DeMore et al. (1997)
N 19	$HNO_3 + h\nu \longrightarrow NO_2 + OH$	1	1		DeMore et al. (1997)

Table 10.4:

no	reaction	n	A $[(cm^{-3})^{1-n}s^{-1}]$	$-E_a/R$ [K]	reference
N 20	$HNO_3 + OH \longrightarrow NO_3 + H_2O$	2	2		Atkinson et al. (2004)
N 21	$HNO_4 \overset{M}{\longrightarrow} NO_2 + HO_2$	2	2		Sander et al. (2003)
N 22	$HNO_4 + OH \longrightarrow NO_2 + H_2O + O_2$	2	1.3×10^{-12}	380	Haggerstone et al. (2005)
N 23	$HNO_4 + h\nu \longrightarrow NO_2 + HO_2$	1	1		DeMore et al. (1997)
N 24	$HNO_4 + h\nu \longrightarrow OH + NO_3$	1	1		DeMore et al. (1997)
C 1	$CO + OH \overset{O_2}{\longrightarrow} HO_2 + CO_2$	2	2		Sander et al. (2003)
C 2	$CH_4 + OH \overset{O_2}{\longrightarrow} CH_3OO + H_2O$	2	2.4×10^{-12}	-1775	Sander et al. (2003)
C 3	$C_2H_6 + OH \longrightarrow C_2H_5O_2 + H_2O$	2	1.7×10^{-11}	-1232	Lurmann et al. (1986)
C 4	$C_2H_4 + OH \longrightarrow EO_2$	2	1.66×10^{-12}	474	Lurmann et al. (1986), see note
C 5	$C_2H_4 + O_3 \longrightarrow HCHO + 0.4CH_2O_2 + 0.12HO_2 + 0.42CO + 0.06CH_4$	2	1.2×10^{-14}	-2633	Lurmann et al. (1986), see note
C 6	$HO_2 + CH_3OO \longrightarrow ROOH + O_2$	2	4.1×10^{-13}	750	Sander et al. (2003)
C 7	$HO_2 + C_2H_5O_2 \longrightarrow ROOH + O_2$	2	7.5×10^{-13}	700	Sander et al. (2003)
C 8	$HO_2 + CH_3CO_3 \longrightarrow ROOH + O_2$	2	4.5×10^{-13}	1000	DeMore et al. (1997)
C 9	$CH_3OO + CH_3OO \longrightarrow 1.4HCHO + 0.8HO_2 + O_2$	2	1.5×10^{-13}	220	Lurmann et al. (1986)
C 10	$C_2H_5O_2 + NO \longrightarrow ALD + HO_2 + NO_2$	2	4.2×10^{-12}	180	Lurmann et al. (1986)
C 11	$2C_2H_5O_2 \longrightarrow 1.6ALD + 1.2HO_2$	2	5.00×10^{-14}		Lurmann et al. (1986)
C 12	$EO_2 + NO \longrightarrow NO_2 + 2.0HCHO + HO_2$	2	4.2×10^{-12}	180	Lurmann et al. (1986)
C 13	$EO_2 + EO_2 \longrightarrow 2.4HCHO + 1.2HO_2 + 0.4ALD$	2	5.00×10^{-14}		Lurmann et al. (1986)
C 14	$HO_2 + EO_2 \longrightarrow ROOH + O_2$	2	3.00×10^{-12}		Lurmann et al. (1986)
C 15	$HCHO + h\nu \longrightarrow 2HO_2 + CO$	1	1		DeMore et al. (1997)
C 16	$HCHO + h\nu \longrightarrow CO + H_2$	1	1		DeMore et al. (1997)
C 17	$HCHO + OH \overset{O_2}{\longrightarrow} HO_2 + CO + H_2O$	2	1.00×10^{-11}		DeMore et al. (1997)
C 18	$HCHO + HO_2 \longrightarrow HOCH_2O_2$	2	6.7×10^{-15}	600	Sander et al. (2003)
C 19	$HCHO + NO_3 \overset{O_2}{\longrightarrow} HNO_3 + HO_2 + CO$	2	5.8×10^{-16}		DeMore et al. (1997)
C 20	$ALD + OH \longrightarrow CH_3CO_3 + H_2O$	2	6.9×10^{-12}	250	Lurmann et al. (1986)
C 21	$ALD + NO_3 \longrightarrow HNO_3 + CH_3CO_3$	2	1.40×10^{-15}		DeMore et al. (1997)
C 22	$ALD + h\nu \longrightarrow CH_3OO + HO_2 + CO$	1	1		Lurmann et al. (1986)
C 23	$ALD + h\nu \longrightarrow CH_4 + CO$	1	1		Lurmann et al. (1986)

Table 10.4: Continued

no	reaction	n	A [(cm^{-3})$^{1-n}$s^{-1}]	$-E_a/R$ [K]	reference
C 24	$HOCH_2O_2 + NO \longrightarrow HCOOH + HO_2 + NO_2$	2	4.2×10^{-12}	180	Lurmann et al. (1986)
C 25	$HOCH_2O_2 + HO_2 \longrightarrow HCOOH + H_2O + O_2$	2	2.00×10^{-12}		Lurmann et al. (1986)
C 26	$2\ HOCH_2O_2 \longrightarrow 2HCOOH + 2HO_2 + 2O_2$	2	1.00×10^{-13}		Lurmann et al. (1986)
C 27	$HCOOH + OH \overset{O_2}{\longrightarrow} HO_2 + H_2O + CO_2$	2	4.0×10^{-13}		DeMore et al. (1997)
C 28	$CH_3CO_3 + NO_2 \longrightarrow PAN$	2	4.70×10^{-12}		Lurmann et al. (1986)
C 29	$PAN \longrightarrow CH_3CO_3 + NO_2$	1	1.9×10^{16}	-13543	DeMore et al. (1997)
C 30	$CH_3CO_3 + NO \longrightarrow CH_3OO + NO_2 + CO_2$	2	4.2×10^{-12}	180	Lurmann et al. (1986)
C 31	$CH_3OO + NO \overset{O_2}{\longrightarrow} HCHO + NO_2 + HO_2$	2	3.0×10^{-12}	280	DeMore et al. (1997)
C 32	$ROOH + OH \longrightarrow 0.7\ CH_3OO + 0.3\ HCHO + 0.3\ OH$	2	3.8×10^{-12}	200	DeMore et al. (1997), see note
C 33	$ROOH + h\nu \longrightarrow HCHO + OH + HO_2$	1	1		DeMore et al. (1997), see note
S 1	$SO_2 + OH \overset{M}{\longrightarrow} HOSO_2$	3	2		Atkinson et al. (2004)
S 2	$HOSO_2 + O_2 \longrightarrow HO_2 + SO_3$	2	1.3×10^{-12}	330	Atkinson et al. (2004)
S 3	$SO_3 \overset{H_2O}{\longrightarrow} H_2SO_4$	1	2		Blanchard (1964)
S 4	$CH_3SCH_3 + OH \longrightarrow CH_3SCH_2OO + H_2O$	2	2		Atkinson et al. (1997)
S 5	$CH_3SCH_3 + OH \overset{O_2}{\longrightarrow} CH_3SOCH_3 + HO_2$	2	2		Atkinson et al. (1997)
S 6	$CH_3SCH_3 + NO_3 \overset{O_2}{\longrightarrow} CH_3SCH_2OO + HNO_3$	2	1.9×10^{-13}	520	Atkinson et al. (1999)
S 7	$CH_3SCH_3 + Cl \overset{O_2}{\longrightarrow} CH_3SCH_2OO + HCl$	2	3.3×10^{-10}		Atkinson et al. (1999)
S 8	$CH_3SCH_3 + Br \overset{O_2}{\longrightarrow} CH_3SCH_2OO + HBr$	2	9.0×10^{-11}	-2386	Jefferson et al. (1994)
S 9	$CH_3SCH_3 + BrO \longrightarrow CH_3SOCH_3 + Br$	2	2.54×10^{-14}	850	Ingham et al. (1999)
S 10	$CH_3SCH_3 + ClO \longrightarrow CH_3SOCH_3 + Cl$	2	9.5×10^{-15}		Barnes et al. (1991)
S 11	$CH_3SCH_3 + IO \longrightarrow CH_3SOCH_3 + I$	2	1.4×10^{-14}		THALOZ (2005)
S 12	$CH_3SCH_2OO + NO \longrightarrow HCHO + CH_3S + NO_2$	2	4.9×10^{-12}	263	Urbanski et al. (1997)
S 13	$CH_3SCH_2OO + CH_3SCH_2OO \overset{O_2}{\longrightarrow} 2\ HCHO + 2\ CH_3S$	2	1.0×10^{-11}		Urbanski et al. (1997); Atkinson et al. (2004)
S 14	$CH_3S + O_3 \longrightarrow CH_3SO + O_2$	2	1.15×10^{-12}	432	Atkinson et al. (2004)

Table 10.4: Continued

no	reaction	n	A $[(cm^{-3})^{1-n}s^{-1}]$	$-E_a/R$ [K]	reference
S 15	$CH_3S + NO_2 \longrightarrow CH_3SO + NO$	2	3.0×10^{-11}	210	Atkinson et al. (2004)
S 16	$CH_3SO + NO_2 \xrightarrow{O_2} 0.82\ CH_3SO_2 + 0.18\ SO_2 + 0.18\ H_3CO_2 + NO$	2	1.2×10^{-11}		Atkinson et al. (2004); Kukui et al. (2000), product ratios from van Dingenen et al. (1994)
S 17	$CH_3SO + O_3 \xrightarrow{O_2} CH_3SO_2$	2	6.0×10^{-13}		Atkinson et al. (2004)
S 18	$CH_3SO_2 \longrightarrow SO_2 + CH_3OO$	1	1.9×10^{13}	-8661	Barone et al. (1995)
S 19	$CH_3SO_2 + NO_2 \longrightarrow CH_3SO_3 + NO$	2	2.2×10^{-12}		Ray et al. (1996)
S 20	$CH_3SO_2 + O_3 \longrightarrow CH_3SO_3$	2	$3.\times10^{-13}$		Barone et al. (1995)
S 21	$CH_3SO_3 + HO_2 \longrightarrow CH_3SO_3H$	2	$5.\times10^{-11}$		Barone et al. (1995)
S 22	$CH_3SO_3 \xrightarrow{H_2O,O_2} CH_3OO + H_2SO_4$	1	1.36×10^{14}	-11071	Barone et al. (1995)
S 23	$CH_3SOCH_3 + OH \longrightarrow 0.95\ CH_3SO_2H + 0.95\ CH_3OO + 0.05\ DMSO_2$	2	8.7×10^{-11}		Urbanski et al. (1998)
S 24	$CH_3SO_2H + OH \longrightarrow 0.95\ CH_3SO_2 + 0.05\ CH_3SO_3H + 0.05\ HO_2 + H_2O$	2	$9.\times10^{-11}$		Kukui et al. (2003)
S 25	$CH_3SO_2H + NO_3 \longrightarrow CH_3SO_2 + HNO_3$	2	1.0×10^{-13}		Yin et al. (1990)
Cl 1	$Cl + O_3 \longrightarrow ClO + O_2$	2	2.8×10^{-11}	-250	Atkinson et al. (2004)
Cl 2	$Cl + HO_2 \longrightarrow HCl + O_2$	2	1.8×10^{-11}	170	Sander et al. (2003)
Cl 3	$Cl + HO_2 \longrightarrow ClO + OH$	2	4.1×10^{-11}	-450	Sander et al. (2003)
Cl 4	$Cl + H_2O_2 \longrightarrow HCl + HO_2$	2	1.1×10^{-11}	-980	Atkinson et al. (2004)
Cl 5	$Cl + CH_3OO \longrightarrow 0.5\ ClO + 0.5\ HCHO + 0.5\ HO_2 + 0.5\ HCl + 0.5\ CO + 0.5\ H_2O$	2	1.6×10^{-10}		Sander et al. (2003)
Cl 6	$Cl + CH_4 \xrightarrow{O_2} HCl + CH_3OO$	2	9.6×10^{-12}	-1360	Sander et al. (2003)
Cl 7	$Cl + C_2H_6 \xrightarrow{O_2} HCl + C_2H_5O_2$	2	7.7×10^{-11}	-90	Sander et al. (2003)
Cl 8	$Cl + C_2H_4 \xrightarrow{O_2} HCl + C_2H_5O_2$	2	$1.\times10^{-10}$		see note
Cl 9	$Cl + HCHO \xrightarrow{O_2} HCl + HO_2 + CO$	2	8.1×10^{-11}	-30	Sander et al. (2003)
Cl 10	$Cl + ROOH \longrightarrow CH_3OO + HCl$	2	5.7×10^{-11}		Wallington et al. (1990), see note
Cl 11	$Cl + OClO \longrightarrow ClO + ClO$	2	3.2×10^{-11}	170	Atkinson et al. (2004)
Cl 12	$Cl + ClNO_3 \longrightarrow Cl_2 + NO_3$	2	6.5×10^{-12}	135	Sander et al. (2003)
Cl 13	$ClO + OH \longrightarrow Cl + HO_2$	2	7.4×10^{-12}	-270	Sander et al. (2003)

Table 10.4: Continued

no	reaction	n	$A\ [(\mathrm{cm}^{-3})^{1-n}\mathrm{s}^{-1}]$	$-E_a\ /\ R$ [K]	reference
Cl 14	ClO + OH $\longrightarrow$ HCl + O$_2$	2	6.0×10^{-13}	-230	Sander et al. (2003)
Cl 15	ClO + HO$_2$ $\longrightarrow$ HOCl + O$_2$	2	2.2×10^{-12}	340	Atkinson et al. (2004)
Cl 16	ClO + CH$_3$OO $\longrightarrow$ Cl + HCHO + HO$_2$	2	3.3×10^{-12}	-115	Sander et al. (2003)
Cl 17	ClO + NO $\longrightarrow$ Cl + NO$_2$	2	6.2×10^{-12}	295	Atkinson et al. (2004)
Cl 18	ClO + NO$_2$ $\overset{M}{\longrightarrow}$ ClNO$_3$	3	2		Atkinson et al. (2004)
Cl 19	ClO + ClO $\longrightarrow$ Cl$_2$O$_2$	2	2		Atkinson et al. (2004)
Cl 20	ClO + ClO $\longrightarrow$ Cl$_2$ + O$_2$	2	1.0×10^{-12}	-1590	Atkinson et al. (2004)
Cl 21	ClO + ClO $\longrightarrow$ Cl$_2$O$_2$	2	3.0×10^{-11}	-2450	Atkinson et al. (2004)
Cl 22	ClO + ClO $\longrightarrow$ Cl + OClO	2	3.5×10^{-13}	-1370	Atkinson et al. (2004)
Cl 23	OClO + OH $\longrightarrow$ HOCl + O$_2$	2	4.5×10^{-13}	800	Atkinson et al. (2004)
Cl 24	OClO + NO $\longrightarrow$ ClO + NO$_2$	2	1.1×10^{-13}	350	Atkinson et al. (2004)
Cl 25	Cl$_2$O$_2$ $\longrightarrow$ ClO + ClO	1	2		Atkinson et al. (2004)
Cl 26	HOCL + OH $\longrightarrow$ ClO + H$_2$O	2	3.0×10^{-12}	-500	Sander et al. (2003)
Cl 27	HCl + OH $\longrightarrow$ H$_2$O + Cl	2	1.8×10^{-12}	-240	Atkinson et al. (2004)
Cl 28	ClNO$_2$ + OH $\longrightarrow$ HOCl + NO$_2$	2	2.4×10^{-12}	-1250	Atkinson et al. (2004)
Cl 29	ClNO$_3$ + OH $\longrightarrow$ 0.5 ClO + 0.5 HNO$_3$ + 0.5 HOCl + 0.5 NO$_3$	2	1.2×10^{-12}	-330	Atkinson et al. (2004)
Cl 30	ClNO$_3$ $\longrightarrow$ ClO + NO$_2$	1	2		Anderson and Fahey (1990)
Cl 31	OClO + $h\nu$ $\overset{O_2,O_3}{\longrightarrow}$ O$_3$ + ClO	1	1		DeMore et al. (1997)
Cl 32	Cl$_2$O$_2$ + $h\nu$ $\longrightarrow$ Cl + Cl + O$_2$	1	1		DeMore et al. (1997)
Cl 33	Cl$_2$ + $h\nu$ $\longrightarrow$ 2 Cl	1	1		DeMore et al. (1997)
Cl 34	HOCl + $h\nu$ $\longrightarrow$ Cl + OH	1	1		DeMore et al. (1997)
Cl 35	ClNO$_2$ + $h\nu$ $\longrightarrow$ Cl + NO$_2$	1	1		DeMore et al. (1997)
Cl 36	ClNO$_3$ + $h\nu$ $\longrightarrow$ Cl + NO$_3$	1	1		DeMore et al. (1997)
Br 1	Br + O$_3$ $\longrightarrow$ BrO + O$_2$	2	1.7×10^{-11}	-800	Atkinson et al. (2004)
Br 2	Br + HO$_2$ $\longrightarrow$ HBr + O$_2$	2	7.7×10^{-12}	-450	Atkinson et al. (2004)
Br 3	Br + C$_2$H$_4$ $\overset{O_2}{\longrightarrow}$ HBr + C$_2$H$_5$O$_2$	2	$5.\times10^{-14}$		see note
Br 4	Br + HCHO $\overset{O_2}{\longrightarrow}$ HBr + CO + HO$_2$	2	1.7×10^{-11}	-800	Sander et al. (2003)
Br 5	Br + ROOH $\longrightarrow$ CH$_3$OO + HBr	2	2.66×10^{-12}	-1610	Mallard et al. (1993), see note

Table 10.4: Continued

no	reaction	n	$A\ [(cm^{-3})^{1-n} s^{-1}]$	$-E_a / R$ [K]	reference
Br 6	$Br + NO_2 \longrightarrow BrNO_2$	2	2		Sander et al. (2003)
Br 7	$Br + BrNO_3 \longrightarrow Br_2 + NO_3$	2	4.9×10^{-11}		Orlando and Tyndall (1996)
Br 8	$BrO + OH \longrightarrow Br + HO_2$	2	1.8×10^{-11}	250	Atkinson et al. (2004)
Br 9	$BrO + HO_2 \longrightarrow HOBr + O_2$	2	4.5×10^{-12}	500	Atkinson et al. (2004)
Br 10	$BrO + CH_3OO \longrightarrow HOBr + HCHO$	2	4.1×10^{-12}		Aranda et al. (1997)
Br 11	$BrO + CH_3OO \longrightarrow Br + HCHO + HO_2$	2	1.6×10^{-12}		Aranda et al. (1997)
Br 12	$BrO + HCHO \overset{O_2}{\longrightarrow} HOBr + CO + HO_2$	2	1.5×10^{-14}		Hansen et al. (1999)
Br 13	$BrO + NO \longrightarrow Br + NO_2$	2	8.7×10^{-12}	260	Atkinson et al. (2004)
Br 14	$BrO + NO_2 \overset{M}{\longrightarrow} BrNO_3$	3	2		Atkinson et al. (2004)
Br 15	$BrO + BrO \longrightarrow 2\ Br + O_2$	2	2.4×10^{-12}	40	Sander et al. (2003)
Br 16	$BrO + BrO \longrightarrow Br_2 + O_2$	2	2.9×10^{-14}	860	Sander et al. (2003)
Br 17	$HBr + OH \longrightarrow Br + H_2O$	2	5.5×10^{-12}	205	Atkinson et al. (2004)
Br 18	$BrNO_3 \longrightarrow BrO + NO_2$	1	2		Orlando and Tyndall (1996)
Br 19	$BrO + h\nu \overset{O_2}{\longrightarrow} Br + O_3$	1	1		DeMore et al. (1997)
Br 20	$Br_2 + h\nu \longrightarrow 2\ Br$	1	1		Hubinger and Nee (1995)
Br 21	$HOBr + h\nu \longrightarrow Br + OH$	1	1		Ingham et al. (1999)
Br 22	$BrNO_2 + h\nu \longrightarrow Br + NO_2$	1	1		Scheffler et al. (1997)
Br 23	$BrNO_3 + h\nu \longrightarrow Br + NO_3$	1	1		DeMore et al. (1997)
I 1	$I + O_3 \longrightarrow IO + O_2$	2	1.9×10^{-11}	-830	Atkinson et al. (2004)
I 2	$I + HO_2 \longrightarrow HI + O_2$	2	1.5×10^{-11}	-1090	Atkinson et al. (2004)
I 3	$I + NO_2 \overset{M}{\longrightarrow} INO_2$	3	2		Atkinson et al. (2004)
I 4	$I + NO_3 \longrightarrow IO + NO_2$	2	4.5×10^{-10}		Chambers et al. (1992)
I 5	$I + I \longrightarrow I_2$	2	2.99×10^{-11}		Hippler et al. (1973)
I 6	$IO + HO_2 \longrightarrow HOI + O_2$	2	1.4×10^{-11}	540	Atkinson et al. (2004)
I 7	$IO + NO \longrightarrow I + NO_2$	2	7.15×10^{-12}	300	Atkinson et al. (2004)
I 8	$IO + NO_2 \overset{M}{\longrightarrow} INO_3$	3	2		Atkinson et al. (2004)
I 9	$IO + IO \longrightarrow OIO + I$	2	5.4×10^{-11}	180	Atkinson et al. (2004), for product ratios see text

Table 10.4: Continued

no	reaction	n	A [$(cm^{-3})^{1-n} s^{-1}$]	$-E_a / R$ [K]	reference
I 10	$OIO + OH \longrightarrow 0.5\ HIO_3 + 0.5\ HOI$	2	2.0×10^{-10}		assumed, see von Glasow et al. (2002c)
I 11	$OIO + NO \longrightarrow NO_2 + IO$	2	5.1×10^{-13}	712	THALOZ (2005)
I 12	$HI + OH \longrightarrow I + H_2O$	2	1.6×10^{-11}	440	Atkinson et al. (2004)
I 13	$HI + NO_3 \longrightarrow I + HNO_3$	2	1.3×10^{-12}	-1830	Atkinson et al. (2004)
I 14	$INO_2 \overset{M}{\longrightarrow} I + NO_2$	2	2.4		estimated from data in Jenkin et al. (1985)
I 15	$INO_3 \overset{M}{\longrightarrow} IO + NO_2$	2	1.1×10^{15}	-12060	Atkinson et al. (2005)
I 16	$I_2 + OH \longrightarrow I + HOI$	2	2.1×10^{-10}		Atkinson et al. (2004)
I 17	$I_2 + NO_3 \longrightarrow I + INO_3$	2	1.5×10^{-12}		Chambers et al. (1992)
I 18	$CH_3I + OH \longrightarrow HCHO + I$	2	4.3×10^{-12}	-1120	Atkinson et al. (2004)
I 19	$C_3H_7I + OH \longrightarrow CH_3OO + I$	2	1.2×10^{-12}		J. Crowley, pers. comm.
I 20	$IO + h\nu \overset{O_2}{\longrightarrow} I + O_3$	1	1		Laszlo et al. (1995)
I 21	$OIO + h\nu \longrightarrow I + O_2$	1	1		THALOZ (2005), for sensitivity studies see text
I 22	$HOI + h\nu \longrightarrow I + OH$	1	1		Bauer et al. (1998)
I 23	$INO_2 + h\nu \longrightarrow I + NO_2$	1	1		Bröske and Zabel (1998) , R. Bröske, pers. comm.
I 24	$INO_3 + h\nu \longrightarrow I + NO_3$	1	1		same as $BrNO_3$, but redshifted by 50 nm
I 25	$I_2 + h\nu \longrightarrow 2\ I$	1	1		Wesely (1989b)
I 26	$CH_3I + h\nu \longrightarrow I + CH_3OO$	1	1		Roehl et al. (1997)
I 27	$C_2H_5I + h\nu \longrightarrow I + ROOH$	1	1		$= CH_3I$
I 28	$C_3H_7I + h\nu \longrightarrow I + ROOH$	1	1		Roehl et al. (1997)
I 29	$CH_2ClI + h\nu \longrightarrow I + Cl + 2\ HO_2 + CO$	1	1		Roehl et al. (1997)
I 30	$CH_2BrI + h\nu \longrightarrow I + Br + 2\ HO_2 + CO$	1	1		Mössinger et al. (1998)
I 31	$CH_2I_2 + h\nu \longrightarrow I + IO + HCHO$	1	1		Roehl et al. (1997)
Hx 1	$Cl + CH_3I \longrightarrow HCl + HCHO + I$	2	2.9×10^{-11}	-1000	Sander et al. (2003), products simplified
Hx 2	$Cl + BrCl \longrightarrow Br + Cl_2$	2	1.5×10^{-11}		Mallard et al. (1993)
Hx 3	$Cl + Br_2 \longrightarrow BrCl + Br$	2	1.2×10^{-10}		Mallard et al. (1993)

Table 10.4: Continued

no	reaction	n	$A\ [(\mathrm{cm}^{-3})^{1-n}\mathrm{s}^{-1}]$	$-E_a\ /\ R$ [K]	reference
Hx 4	$I_2 + Cl \longrightarrow I + ICl$	2	2.09×10^{-10}		Bedjanian et al. (1996)
Hx 5	$Br + OClO \longrightarrow BrO + ClO$	2	2.6×10^{-11}	-1300	Atkinson et al. (2004)
Hx 6	$Br + Cl_2 \longrightarrow BrCl + Cl$	2	1.1×10^{-15}		Mallard et al. (1993)
Hx 7	$Br + BrCl \longrightarrow Br_2 + Cl$	2	3.3×10^{-15}		Mallard et al. (1993)
Hx 8	$I_2 + Br \longrightarrow I + IBr$	2	1.2×10^{-10}		Bedjanian et al. (1997)
Hx 9	$I + BrO \longrightarrow IO + Br$	2	1.2×10^{-11}		Sander et al. (2003)
Hx 10	$BrO + ClO \longrightarrow Br + OClO$	2	1.6×10^{-12}	430	Atkinson et al. (2004)
Hx 11	$BrO + ClO \longrightarrow Br + Cl + O_2$	2	2.9×10^{-12}	220	Atkinson et al. (2004)
Hx 12	$BrO + ClO \longrightarrow BrCl + O_2$	2	5.8×10^{-13}	170	Atkinson et al. (2004)
Hx 13	$IO + ClO \longrightarrow 0.8\ I + 0.55\ OClO + 0.45\ O_2 + 0.25\ Cl$ $+ 0.2\ ICl$	2	4.7×10^{-12}	280	Atkinson et al. (2004)
Hx 14	$IO + BrO \longrightarrow Br + 0.8\ OIO + 0.2\ I + 0.2\ O_2$	2	1.5×10^{-11}	510	Atkinson et al. (2004)
Hx 15	$BrCl + h\nu \longrightarrow Br + Cl$	1	1		DeMore et al. (1997)
Hx 16	$ICl + h\nu \longrightarrow I + Cl$	1	1		Seery and Britton (1964)
Hx 17	$IBr + h\nu \longrightarrow I + Br$	1	1		Seery and Britton (1964)

Table 10.4: Continued

[a] n is the order of the reaction. [1] photolysis rates calculated online, [2] special rate functions (pressure dependent and/or humidity dependent). Notes: The rates for ROOH were assumed as that of CH_3OOH; C_2H_4 is used as generic alkene as in the Lurmann et al. (1986) mechanism. The rate coefficients are calculated with $k = A \times \exp(\frac{-E_a}{RT})$.

no	reaction	n	k_0 [$(M^{1-n})s^{-1}$]	$-E_a / R$ [K]	reference
O 1	$O_3 + OH \longrightarrow HO_2$	2	1.1×10^8		Sehested et al. (1984)
O 2	$O_3 + O_2^- \longrightarrow OH + OH^-$	2	1.5×10^9		Sehested et al. (1983)
O 3	$OH + OH \longrightarrow H_2O_2$	2	5.5×10^9		Buxton et al. (1988)
O 4	$OH + HO_2 \longrightarrow H_2O$	2	7.1×10^9		Sehested et al. (1968)
O 5	$OH + O_2^- \longrightarrow OH^-$	2	1.0×10^{10}		Sehested et al. (1968)
O 6	$OH + H_2O_2 \longrightarrow HO_2$	2	2.7×10^7	-1684	Christensen et al. (1982)
O 7	$HO_2 + HO_2 \longrightarrow H_2O_2$	2	9.7×10^5	-2500	Christensen and Sehested (1988)
O 8	$HO_2 + O_2^- \xrightarrow{H^+} H_2O_2$	2	1.0×10^8	-900	Christensen and Sehested (1988)
N 1	$HONO + OH \longrightarrow NO_2$	2	1.0×10^{10}		assumed $=$N7 Barker et al. (1970)
N 2	$HONO + H_2O_2 \xrightarrow{H^+} HNO_3$	3	4.6×10^3	-6800	Damschen and Martin (1983)
N 3	$NO_3^- + OH^- \longrightarrow NO_3^- + OH$	2	8.2×10^7	-2700	Exner et al. (1992)
N 4	$NO_2 + NO_2 \longrightarrow HNO_3 + HONO$	2	1.0×10^8		Lee and Schwartz (1981)
N 5	$NO_2 + HO_2 \longrightarrow HNO_4$	2	1.8×10^9		Warneck (1999)
N 6	$NO_2^- + O_3 \longrightarrow NO_3^- + O_2$	2	5.0×10^5	-6950	Damschen and Martin (1983)
N 7	$NO_2^- + OH \longrightarrow NO_2 + OH^-$	2	1.0×10^{10}		Barker et al. (1970)
N 8	$NO_4^- \longrightarrow NO_2^- + O_2$	1	8.0×10^{-1}		Warneck (1999)
C 1	$HCHO + OH \longrightarrow HCOOH + HO_2$	2	7.7×10^8	-1020	Chin and Wine (1994)
C 2	$HCOOH + OH \longrightarrow HO_2 + CO_2$	2	1.1×10^8	-991	Chin and Wine (1994)
C 3	$HCOO^- + OH \longrightarrow OH^- + HO_2 + CO_2$	2	3.1×10^9	-1240	Chin and Wine (1994)
C 4	$CH_3OO + HO_2 \longrightarrow CH_3OOH$	2	4.3×10^5		estimated by Jacob (1986)
C 5	$CH_3OO + O_2^- \longrightarrow CH_3OOH + OH^-$	2	5.0×10^7		estimated by Jacob (1986)
C 6	$CH_3OH + OH \longrightarrow HCHO + HO_2$	2	9.7×10^8		Buxton et al. (1988)
C 7	$CH_3OOH + OH \longrightarrow CH_3OO$	2	2.7×10^7	-1715	estimated by Jacob (1986)
C 8	$CH_3OOH + OH \longrightarrow HCHO + OH$	2	1.1×10^7	-1715	estimated by Jacob (1986)
C 9	$CO_3^- + O_2^- \longrightarrow HCO_3^- + OH^-$	2	6.5×10^8		Ross et al. (1992)
C 10	$CO_3^- + H_2O_2 \longrightarrow HCO_3^- + HO_2$	2	4.3×10^5		Ross et al. (1992)
C 11	$CO_3^- + HCOO^- \longrightarrow HCO_3^- + HCO_3^- + HO_2$	2	1.5×10^5		Ross et al. (1992)
C 12	$HCO_3^- + OH \longrightarrow CO_3^-$	2	8.5×10^6		Ross et al. (1992)
C 13	$DOM + OH \longrightarrow HO_2$	2	5.0×10^9		estimated by (C. Anastasio, pers. comm.) from Ross et al. (1998)

Table 10.5: Aqueous phase reactions.

no	reaction	n	k_0 [$(M^{1-n})s^{-1}$]	$-E_a / R$ [K]	reference
S 1	$SO_3^- + O_2 \rightarrow SO_5^-$	2	1.5×10^9		Huie and Neta (1987)
S 2	$HSO_3^- + O_3 \rightarrow SO_4^{2-} + H^+ + O_2$	2	3.7×10^5	-5500	Hoffmann (1986)
S 3	$SO_3^{2-} + O_3 \rightarrow SO_4^{2-} + O_2$	2	1.5×10^9	-5300	Hoffmann (1986)
S 4	$HSO_3^- + OH \rightarrow SO_3^-$	2	4.5×10^9		Buxton et al. (1988)
S 5	$SO_3^{2-} + OH \rightarrow SO_3^- + OH^-$	2	5.5×10^9		Buxton et al. (1988)
S 6	$HSO_3^- + HO_2 \rightarrow SO_4^{2-} + OH + H^+$	2	3.0×10^3		upper limit D. Sedlak pers. comm. with R. Sander
S 7	$HSO_3^- + O_2^- \rightarrow SO_4^{2-} + OH$	2	3.0×10^3		upper limit D. Sedlak pers. comm. with R. Sander
S 8	$HSO_3^- + H_2O_2 \rightarrow SO_4^{2-} + H^+$	2	$5.2 \times 10^6 \times \frac{[H^+]}{[H^+] + 0.1M}$	-3650	Damschen and Martin (1983)
S 9	$HSO_3^- + NO_2 \xrightarrow{NO_2} HSO_4^- + HONO + HONO$	2	2.0×10^7		Clifton et al. (1988)
S 10	$SO_3^{2-} + NO_2 \xrightarrow{NO_2} SO_4^{2-} + HONO + HONO$	2	2.0×10^7		Clifton et al. (1988)
S 11	$HSO_3^- + NO_3 \rightarrow SO_3^- + NO_3^- + H^+$	2	1.4×10^9	-2000	Exner et al. (1992)
S 12	$HSO_3^- + HNO_4 \rightarrow HSO_4^- + NO_3^- + H^+$	2	3.1×10^5		Warneck (1999)
S 13	$HSO_3^- + CH_3OOH \xrightarrow{H^+} SO_4^{2-} + H^+ + CH_3OH$	3	1.6×10^7	-3800	Lind et al. (1987)
S 14	$SO_3^{2-} + CH_3OOH \xrightarrow{H^+} SO_4^{2-} + CH_3OH$	3	1.6×10^7	-3800	Lind et al. (1987)
S 15	$HSO_3^- + HCHO \rightarrow CH_2OHSO_3^-$	2	4.3×10^{-1}		Boyce and Hoffmann (1984)
S 16	$SO_3^{2-} + HCHO \xrightarrow{H^+} CH_2OHSO_3^-$	2	1.4×10^4		Boyce and Hoffmann (1984)
S 17	$CH_2OHSO_3^- + OH^- \rightarrow SO_3^{2-} + HCHO$	2	3.6×10^3		Seinfeld and Pandis (1998)
S 18	$HSO_3^- + HSO_5^- \xrightarrow{H^+} SO_4^{2-} + SO_4^{2-} + H^+ + H^+$	3	7.1×10^6		Betterton and Hoffmann (1988)
S 19	$SO_4^- + OH \rightarrow HSO_5^-$	2	1.0×10^9		Jiang et al. (1992)
S 20	$SO_4^- + HO_2 \rightarrow SO_4^{2-} + H^+$	2	3.5×10^9		Jiang et al. (1992)
S 21	$SO_4^- + O_2^- \rightarrow SO_4^{2-}$	2	3.5×10^9		assumed =S20
S 22	$SO_4^- + H_2O \rightarrow SO_4^{2-} + H^+ + OH$	2	1.1×10^1		Herrmann et al. (1995)
S 23	$SO_4^- + H_2O_2 \rightarrow SO_4^{2-} + H^+ + HO_2$	2	1.2×10^7		Wine et al. (1989)
S 24	$SO_4^- + NO_3^- \rightarrow SO_4^{2-} + NO_3$	2	5.0×10^4	-1110	Exner et al. (1992)
S 25	$SO_4^- + HSO_3^- \rightarrow SO_3^- + SO_4^{2-} + H^+$	2	8.0×10^8		Huie and Neta (1987)
S 26	$SO_4^- + SO_3^{2-} \rightarrow SO_3^- + SO_4^{2-}$	2	4.6×10^8		Huie and Neta (1987)

Table 10.5: Continued

no	reaction	n	k_0 [$(M^{1-n})s^{-1}$]	$-E_a / R$ [K]	reference
S 27	$SO_4^{2-} + NO_3 \longrightarrow NO_3^- + SO_4^-$	2	1.0×10^5		Logager et al. (1993)
S 28	$SO_5^- + HSO_3^- \longrightarrow SO_4^- + SO_4^{2-} + H^+$	2	7.5×10^4		Huie and Neta (1987)
S 29	$SO_5^- + SO_3^{2-} \longrightarrow SO_4^- + SO_4^{2-}$	2	9.4×10^6		Huie and Neta (1987)
S 30	$SO_5^- + HSO_3^- \longrightarrow SO_3^- + HSO_5^-$	2	2.5×10^4		Huie and Neta (1987); Deister and Warneck (1990)
S 31	$SO_5^- + SO_3^{2-} \overset{H^+}{\longrightarrow} SO_3^- + HSO_5^-$	2	3.6×10^6		Huie and Neta (1987); Deister and Warneck (1990)
S 32	$SO_5^- + O_2^- \overset{H^+}{\longrightarrow} HSO_5^- + O_2$	2	2.3×10^8		Buxton et al. (1996)
S 33	$SO_5^- + SO_5^- \longrightarrow H_2O$	2	1.0×10^8		Ross et al. (1992)
S 34	$DMS + O_3 \longrightarrow O_2 + DMSO$	2	8.6×10^8	-2600	Gershenzon et al. (2001)
S 35	$DMS + OH \longrightarrow 0.5\ CH_3SO_3^- + 0.5\ CH_3OO + 0.5\ HSO_4^- + HCHO + H^+$	2	1.9×10^{10}		Ross et al. (1998)
S 36	$DMSO + OH \longrightarrow CH_3SO_2^- + CH_3OO + H^+$	2	4.5×10^9		Bardouki et al. (2002)
S 37	$CH_3SO_2^- + OH \longrightarrow CH_3SO_3^- + H2O - O2$	2	1.2×10^{10}		Bardouki et al. (2002)
S 38	$CH_3SO_3^- + OH \longrightarrow SO_4^{2-} + H^+ + CH_3OO$	2	1.2×10^7		Bonsang et al. (1991)
Cl 1	$Cl + H_2O_2 \longrightarrow HO_2 + Cl^- + H^+$	2	2.0×10^9		Yu (2001)
Cl 2	$Cl + H_2O \longrightarrow H^+ + ClOH^-$	2	1.8×10^5		Yu (2001)
Cl 3	$Cl + NO_3^- \longrightarrow NO_3 + Cl^-$	2	1.0×10^8		Buxton et al. (1999b)
Cl 4	$Cl + DOM \longrightarrow Cl^- + HO_2$	2	5.0×10^9		estimated (C. Anastasio, pers. comm.) from Ross et al. (1998)
Cl 5	$Cl + SO_4^{2-} \longrightarrow SO_4^- + Cl^-$	2	2.1×10^8		Buxton et al. (1999a)
Cl 6	$Cl + Cl \longrightarrow Cl_2$	2	8.8×10^7		Wu et al. (1980)
Cl 7	$Cl^- + OH \longrightarrow ClOH^-$	2	4.2×10^9		Yu (2001)
Cl 8	$Cl^- + O_3 \longrightarrow ClO^- + O_2$	2	3.0×10^{-3}		Hoigné et al. (1985)
Cl 9	$Cl^- + NO_3 \longrightarrow NO_3^- + Cl$	2	9.3×10^6	-4330	Exner et al. (1992)
Cl 10	$Cl^- + SO_4^- \longrightarrow SO_4^{2-} + Cl$	2	2.5×10^8		Buxton et al. (1999a)
Cl 11	$Cl^- + HSO_5^- \longrightarrow HOCl + SO_4^{2-}$	2	1.8×10^{-3}	-7352	Fortnum et al. (1960)
Cl 12	$Cl^- + HOCl + H^+ \longrightarrow Cl_2$	3	2.2×10^4	-3508	Ayers et al. (1996)
Cl 13	$Cl_2 \longrightarrow Cl^- + HOCl + H^+$	1	2.2×10^1	-8012	Ayers et al. (1996)

Table 10.5: Continued

no	reaction	n	k_0 [(M^{1-n})s^{-1}]	$-E_a / R$ [K]	reference
Cl 14	$Cl_2^- + OH \rightarrow HOCl + Cl^-$	2	1.0×10^9		Ross et al. (1998)
Cl 15	$Cl_2^- + OH^- \rightarrow Cl^- + Cl^- + OH$	2	4.0×10^6		Jacobi (1996)
Cl 16	$Cl_2^- + HO_2 \rightarrow Cl^- + Cl^- + H^+ + O_2$	2	3.1×10^9		Yu (2001)
Cl 17	$Cl_2^- + O_2^- \rightarrow Cl^- + Cl^- + O_2$	2	6.0×10^9		Jacobi (1996)
Cl 18	$Cl_2^- + H_2O_2 \rightarrow Cl^- + Cl^- + H^+ + HO_2$	2	7.0×10^5	-3340	Jacobi (1996)
Cl 19	$Cl_2^- + NO_2^- \rightarrow Cl^- + Cl^- + NO_2$	2	6.0×10^7		Jacobi (1996)
Cl 20	$Cl_2^- + CH_3OOH \rightarrow Cl^- + Cl^- + H^+ + CH_3OO$	2	7.0×10^5	-3340	assumed by Jacobi (1996)
Cl 21	$Cl_2^- + DOM \rightarrow Cl^- + Cl^- + HO_2$	2	1.0×10^6		estimated (C. Anastasio, pers. comm.) from Ross et al. (1998)
Cl 22	$Cl_2^- + HSO_3^- \rightarrow SO_3^- + Cl^- + Cl^- + H^+$	2	4.7×10^8	-1082	Shoute et al. (1991)
Cl 23	$Cl_2^- + SO_3^{2-} \rightarrow SO_3^- + Cl^- + Cl^-$	2	6.2×10^7		Jacobi et al. (1996)
Cl 24	$Cl_2^- + Cl_2^- \rightarrow Cl_2 + 2Cl^-$	2	6.2×10^9		Yu (2001)
Cl 25	$Cl_2^- + Cl \rightarrow Cl^- + Cl_2$	2	2.7×10^9		Yu (2001)
Cl 26	$Cl_2^- + DMS \rightarrow 0.5\ CH_3SO_3^- + 0.5\ CH_3OO + 0.5\ HSO_4^- + HCHO + 2\ Cl^- + 2\ H^+$	2	3.0×10^9		rate from Ross et al. (1998)
Cl 27	$ClOH^- \rightarrow Cl^- + OH$	1	6.0×10^9		Yu (2001)
Cl 28	$ClOH^- + H^+ \rightarrow Cl$	2	4.0×10^{10}		Yu (2001)
Cl 29	$HOCl + HO_2 \rightarrow Cl + O_2$	2	7.5×10^6		assumed = Cl30 Long and Bielski (1980)
Cl 30	$HOCl + O_2^- \rightarrow Cl + OH^- + O_2$	2	7.5×10^6		Long and Bielski (1980)
Cl 31	$HOCl + SO_3^{2-} \rightarrow Cl^- + HSO_4^-$	2	7.6×10^8		Fogelman et al. (1989)
Cl 32	$HOCl + HSO_3^- \rightarrow Cl^- + HSO_4^- + H^+$	2	7.6×10^8		assumed = Cl31 Fogelman et al. (1989)
Cl 33	$Cl_2 + HO_2 \rightarrow Cl_2^- + H^+ + O_2$	2	1.0×10^9		Bjergbakke et al. (1981)
Cl 34	$Cl_2 + O_2^- \rightarrow Cl_2^- + O_2$	2	1.0×10^9		assumed = Cl33 Bjergbakke et al. (1981)
Br 1	$Br + OH^- \rightarrow BrOH^-$	2	1.3×10^{10}		Zehavi and Rabani (1972)
Br 2	$Br + DOM \rightarrow Br^- + HO_2$	2	2.0×10^8		estimated (C. Anastasio, pers. comm.) from Ross et al. (1998)
Br 3	$Br^- + OH \rightarrow BrOH^-$	2	1.1×10^{10}		Zehavi and Rabani (1972)
Br 4	$Br^- + O_3 \rightarrow BrO^-$	2	2.1×10^2	-4450	Haag and Hoigné (1983)

Table 10.5: Continued

no	reaction	n	k_0 [$(M^{1-n})s^{-1}$]	$-E_a / R$ [K]	reference
Br 5	$Br^- + NO_3 \longrightarrow Br + NO_3^-$	2	3.8×10^9		Zellner et al. 1996 in Herrmann et al. (2000)
Br 6	$Br^- + SO_4^- \longrightarrow Br + SO_4^{2-}$	2	2.1×10^9		Jacobi (1996)
Br 7	$Br^- + HSO_5^- \longrightarrow HOBr + SO_4^{2-}$	2	1.0	-5338	Fortnum et al. (1960)
Br 8	$Br^- + HOBr + H^+ \longrightarrow Br_2$	3	1.6×10^{10}		Liu and Margerum (2001)
Br 9	$Br_2 \longrightarrow Br^- + HOBr + H^+$	1	9.7×10^1	7457	Liu and Margerum (2001)
Br 10	$Br_2^- + O_2^- \longrightarrow Br^- + Br^-$	2	1.7×10^8		Wagner and Strehlow (1987)
Br 11	$Br_2^- + HO_2 \longrightarrow Br_2 + H_2O_2 - H^+$	2	4.4×10^9		Matthew et al. (2003)
Br 12	$Br_2^- + H_2O_2 \longrightarrow Br^- + Br^- + H^+ + HO_2$	2	5.0×10^2		Chameides and Stelson (1992)
Br 13	$Br_2^- + Br_2^- \longrightarrow Br^- + Br^- + Br_2$	2	1.9×10^9		Ross et al. (1992)
Br 14	$Br_2^- + CH_3OOH \longrightarrow Br^- + Br^- + H^+ + CH_3OO$	2	1.0×10^5		assumed by Jacobi (1996)
Br 15	$Br_2^- + DOM \longrightarrow Br^- + Br^- + HO_2$	2	1.0×10^5		estimated (C. Anastasio, pers. comm.) from Ross et al. (1998)
Br 16	$Br_2^- + NO_2^- \longrightarrow Br^- + Br^- + NO_2$	2	1.7×10^7	-1720	Shoute et al. (1991)
Br 17	$Br_2^- + HSO_3^- \longrightarrow Br^- + Br^- + H^+ + SO_3^-$	2	6.3×10^7	-782	Shoute et al. (1991)
Br 18	$Br_2^- + SO_3^{2-} \longrightarrow Br^- + Br^- + SO_3^-$	2	2.2×10^8	-650	Shoute et al. (1991)
Br 19	$Br_2^- + DMS \longrightarrow 0.5 \ CH_3SO_3 + 0.5 \ CH_3OO + 0.5$ $HSO_4^- + HCHO + 2 \ Br^- + 2 \ H^+$	2	3.2×10^9		rate from Ross et al. (1998)
Br 20	$BrOH^- \longrightarrow Br^- + OH$	1	3.3×10^7		Zehavi and Rabani (1972)
Br 21	$BrOH^- \longrightarrow Br + OH^-$	1	4.2×10^6		Zehavi and Rabani (1972)
Br 22	$BrOH^- + H^+ \longrightarrow Br$	2	4.4×10^{10}		Zehavi and Rabani (1972)
Br 23	$BrOH^- + Br^- \longrightarrow Br_2^- + OH^-$	2	1.9×10^8		Zehavi and Rabani (1972)
Br 24	$BrO^- + SO_3^{2-} \longrightarrow Br^- + SO_4^{2-}$	2	1.0×10^8		Troy and Margerum (1991)
Br 25	$HOBr + HO_2 \longrightarrow Br + O_2$	2	1.0×10^9		Herrmann et al. (1999)
Br 26	$HOBr + O_2^- \longrightarrow Br + OH^- + O_2$	2	3.5×10^9		Schwarz and Bielski (1986)
Br 27	$HOBr + H_2O_2 \longrightarrow Br^- + H^+ + O_2$	2	1.2×10^6		von Gunten and Oliveras (1998)
Br 28	$HOBr + SO_3^{2-} \longrightarrow Br^- + HSO_4^-$	2	5.0×10^9		Troy and Margerum (1991)
Br 29	$HOBr + HSO_3^- \longrightarrow Br^- + HSO_4^- + H^+$	2	5.0×10^9		assumed = Br28
Br 30	$Br_2 + HO_2 \longrightarrow Br_2^- + H^+ + O_2$	2	1.1×10^8		Ross et al. (1998)
Br 31	$Br_2 + O_2^- \longrightarrow Br_2^- + O_2$	2	5.6×10^9		Ross et al. (1998)

Table 10.5: Continued

no	reaction	n	k_0 [$(M^{1-n})s^{-1}$]	$-E_a/R$ [K]	reference
I 1	$HOI + I^- + H^+ \longrightarrow I_2$	3	4.4×10^{12}		Eigen and Kustin (1962)
I 2	$HOI + Cl^- + H^+ \longrightarrow ICl$	3	2.9×10^{10}		Wang et al. (1989)
I 3	$ICl \longrightarrow HOI + Cl^- + H^+$	1	2.4×10^{6}		Wang et al. (1989)
I 4	$HOI + Br^- + H^+ \longrightarrow IBr$	3	3.3×10^{12}		Troy et al. (1991)
I 5	$IBr \longrightarrow HOI + H^+ + Br^-$	1	8.0×10^{5}		Troy et al. (1991)
I 6	$HOCl + I^- + H^+ \longrightarrow ICl$	3	3.5×10^{11}		Nagy et al. (1988)
I 7	$HOBr + I^- \longrightarrow IBr + OH^-$	2	5.0×10^{9}		Troy and Margerum (1991)
I 9	$IO_2^- + H_2O_2 \longrightarrow IO_3^-$	2	6.0×10^{1}		Furrow (1987)
I 10	$IO + IO \longrightarrow HOI + IO_2^- + H^+$	2	1.5×10^{9}		Buxton et al. (1986)
I 11	$I^- + O_3 \xrightarrow{H^+} HOI$	2	4.2×10^{9}	-9311	Magi et al. (1997)
I 12	$HOI + Cl_2 \longrightarrow IO_2^- + 2Cl^- + 3H^+$	2	1.0×10^{6}		Lengyel et al. (1996)
I 13	$HOI + HOCl \longrightarrow IO_2^- + Cl^- + 2H^+$	2	5.0×10^{5}		Citri and Epstein (1988)
I 14	$HOI + HOBr \longrightarrow IO_2^- + Br^- + 2H^+$	2	1.0×10^{6}		Chinake and Simoyi (1996)
I 15	$IO_2^- + HOCl \longrightarrow IO_3^- + Cl^- + H^+$	2	1.5×10^{3}		Lengyel et al. (1996)
I 16	$IO_2^- + HOBr \longrightarrow IO_3^- + Br^- + H^+$	2	1.0×10^{6}		Chinake and Simoyi (1996)
I 17	$IO_2^- + HOI \longrightarrow IO_3^- + I^- + H^+$	2	6.0×10^{2}		Chinake and Simoyi (1996)
I 18	$I_2 + HSO_3^- \longrightarrow 2\,I^- + HSO_4^- + 2\,H^+$	2	1.0×10^{6}		Olsen and Epstein (1991)
Hx 1	$Br^- + HOCl + H^+ \longrightarrow BrCl$	3	1.3×10^{6}		Liu and Margerum (2001)
Hx 2	$Cl^- + HOBr + H^+ \longrightarrow BrCl$	3	2.3×10^{10}		Liu and Margerum (2001)
Hx 3	$BrCl \longrightarrow Cl^- + HOBr + H^+$	1	3.0×10^{6}		Liu and Margerum (2001)
Hx 4	$Br^- + ClO^- + H^+ \longrightarrow BrCl + OH^-$	3	3.7×10^{10}		Kumar and Margerum (1987)
Hx 5	$Cl_2 + Br^- \longrightarrow BrCl_2^-$	2	7.7×10^{9}		Liu and Margerum (2001)
Hx 6	$BrCl_2^- \longrightarrow Cl_2 + Br^-$	1	1.83×10^{3}		Liu and Margerum (2001)

Table 10.5: Continued

no	reaction	n	k_0 [$(\text{M}^{1-n})\text{s}^{-1}$]	$-E_a / R$ [K]	reference
hv 1	$O_3 + hv \longrightarrow OH + OH + O_2$	1	1		assumed 2x gas phase
hv 2	$H_2O_2 + hv \longrightarrow OH + OH$	1	1		assumed 2x gas phase
hv 3	$NO_3^- + hv \xrightarrow{H^+} NO_2 + OH$	1	1		Zellner et al. (1990)
hv 4	$NO_2^- + hv \xrightarrow{H^+} NO + OH$	1	1		Zellner et al. (1990); Burley and Johnston (1992)
hv 5	$HOCl + hv \longrightarrow OH + Cl$	1	1		assumed 2x gas phase
hv 6	$Cl_2 + hv \longrightarrow Cl + Cl$	1	1		assumed 2x gas phase
hv 7	$HOBr + hv \longrightarrow OH + Br$	1	1		assumed 2x gas phase
hv 8	$Br_2 + hv \longrightarrow Br + Br$	1	1		assumed 2x gas phase
hv 9	$BrCl + hv \longrightarrow Cl + Br$	1	1		assumed 2x gas phase

[a] n is the order of the reaction. [1] photolysis rates calculated online. The temperature dependence is $k = k_0 \times \exp(\frac{-E_a}{R}(\frac{1}{T} - \frac{1}{T_0}))$, $T_0 = 298$ K.

Table 10.5: Continued

no	reaction	$\overline{k}$	reference
H 1	$N_2O_5 \xrightarrow{H_2O} HNO_{3aq} + HNO_{3aq}$	$\overline{k_t}(N_2O_5)w_{l,i}[H_2O]/Het_T$	Behnke et al. (1994), Behnke et al. (1997)
H 2	$N_2O_5 \xrightarrow{Cl^-} ClNO_2 + NO_3^-$	$\overline{k_t}(N_2O_5)w_{l,i}f(Cl^-)[Cl^-]/Het_T$	Behnke et al. (1994), Behnke et al. (1997)
H 3	$N_2O_5 \xrightarrow{Br^-} BrNO_2 + NO_3^-$	$\overline{k_t}(N_2O_5)w_{l,i}f(Br^-)[Br^-]/Het_T$	Behnke et al. (1994), Behnke et al. (1997)
H 4	$ClNO_3 \xrightarrow{H_2O} HOCl_{aq} + HNO_{3aq}$	$\overline{k_t}(ClNO_3)w_{l,i}[H_2O]/Het_T$	see note
H 5	$ClNO_3 \xrightarrow{Cl^-} Cl_{2aq} + NO_3^-$	$\overline{k_t}(ClNO_3)w_{l,i}f(Cl^-)[Cl^-]/Het_T$	see note
H 6	$ClNO_3 \xrightarrow{Br^-} BrCl_{aq} + NO_3^-$	$\overline{k_t}(ClNO_3)w_{l,i}f(Br^-)[Br^-]/Het_T$	see note
H 7	$BrNO_3 \xrightarrow{H_2O} HOBr_{aq} + HNO_{3aq}$	$\overline{k_t}(BrNO_3)w_{l,i}[H_2O]/Het_T$	see note
H 8	$BrNO_3 \xrightarrow{Cl^-} BrCl_{aq} + NO_3^-$	$\overline{k_t}(BrNO_3)w_{l,i}f(Cl^-)[Cl^-]/Het_T$	see note
H 9	$BrNO_3 \xrightarrow{Br^-} Br_{2aq} + NO_3^-$	$\overline{k_t}(BrNO_3)w_{l,i}f(Br^-)[Br^-]/Het_T$	see note
H 10	$HOBr \xrightarrow{HOBr_{aq}} Br_{2aq} + H_2O + 0.5\ O_2$	$\overline{k_t}(HOBr)w_{l,i}[H_2O]/Het_T$	Mochida et al. (1998) see note[a,b]
H 11	$HOBr \xrightarrow{Cl^-} BrCl_{aq} + OH^-$	$\overline{k_t}(HOBr)w_{l,i}f(Cl^-)[Cl^-]/Het_T$	Mochida et al. (1998) see note[a,b]
H 12	$HOBr \xrightarrow{Br^-} Br_{2aq} + OH^-$	$\overline{k_t}(HOBr)w_{l,i}f(Br^-)[Br^-]/Het_T$	Mochida et al. (1998) see note[a,b]
H 13	$INO_3 \xrightarrow{H_2O} HOI_{aq} + HNO_{3aq}$	$\overline{k_t}(INO_3)w_{l,i}$	
H 14	$HI \xrightarrow{H_2O} H^+ + I^-$	$\overline{k_t}(HI)w_{l,i}$	
H 15	$INO_2 \xrightarrow{H_2O} HOI_{aq} + HONO_{aq}$	$\overline{k_t}(INO_2)w_{l,i}$	
H 16	$OIO \xrightarrow{H_2O} HOI_{aq} + HO_{2aq}$	$\overline{k_t}(OIO)w_{l,i}$	assumed, see von Glasow et al. (2002c)
H 17	$HIO_3 \xrightarrow{H_2O} IO_3^- + H^+$	$\overline{k_t}(HIO_3)w_{l,i}$	assumed, see von Glasow et al. (2002c)

[a] For a definition of $\overline{k_t}$ and $w_{l,i}$ see von Glasow et al. (2002c) or von Glasow (2000). $Het_T = [H_2O + f(Cl^-)[Cl^-] + f(Br^-)[Br^-]$, with $f(Cl^-) = 5.0 \times 10^2$ and $f(Br^-) = 3.0 \times 10^5$. H4 - H9: the total rate is determined by $\overline{k_t}$, the distribution among the different reaction paths was assumed to be the same as for reactions H1 - H3.

[b] Reactions H10 - H12 are only calculated on 'dry' aerosol particles.

Table 10.6: Heterogeneous Reactions

no	reaction	m	n	K_0 [M^{n-m}]	$-\Delta H/R$ [K]	reference
EQ 1	$CO_{2aq} \longleftrightarrow H^+ + HCO_3^-$	1	2	4.3×10^{-7}	-913	Chameides (1984)
EQ 2	$NH_{3aq} \longleftrightarrow OH^- + NH_4^+$	1	2	1.7×10^{-5}	-4325	Chameides (1984)
EQ 3	$H_2O_{aq} \longleftrightarrow H^+ + OH^-$	1	2	1.0×10^{-14}	-6716	Chameides (1984)
EQ 4	$HCOOH_{aq} \longleftrightarrow H^+ + HCOO^-$	1	2	1.8×10^{-4}		Weast (1980)
EQ 5	$HSO_3^- \longleftrightarrow H^+ + SO_3^{2-}$	1	2	6.0×10^{-8}	1120	Chameides (1984)
EQ 6	$H_2SO_{4aq} \longleftrightarrow H^+ + HSO_4^-$	1	2	1.0×10^{3}		Seinfeld and Pandis (1998)
EQ 7	$HSO_4^- \longleftrightarrow H^+ + SO_4^{2-}$	1	2	1.2×10^{-2}	1120	Weast (1980)
EQ 8	$HO_{2aq} \longleftrightarrow O_2^- + H^+$	1	2	1.6×10^{-5}		Weinstein-Lloyd and Schwartz (1991)
EQ 9	$SO_{2aq} \longleftrightarrow H^+ + HSO_3^-$	1	2	1.7×10^{-2}	2090	Chameides (1984)
EQ 10	$Cl_2^- \longleftrightarrow Cl_{aq} + Cl^-$	1	2	5.2×10^{-6}		Jayson et al. (1973)
EQ 11	$HOCl_{aq} \longleftrightarrow H^+ + ClO^-$	1	2	3.2×10^{-8}		Lax (1969)
EQ 12	$HBr_{aq} \longleftrightarrow H^+ + Br^-$	1	2	1.0×10^{9}		Lax (1969)
EQ 13	$Br_2^- \longleftrightarrow Br_{aq} + Br^-$	1	2	9.1×10^{-6}		Mamou et al. (1977)
EQ 14	$HOBr_{aq} \longleftrightarrow H^+ + BrO^-$	1	2	2.3×10^{-9}	-3091	Kelley and Tartar (1956)
EQ 15	$BrCl_{aq} + Cl^- \longleftrightarrow BrCl_2^-$	2	1	3.8		Wang et al. (1994)
EQ 16	$BrCl_{aq} + Br^- \longleftrightarrow Br_2Cl^-$	2	1	1.8×10^{4}	1143	Wang et al. (1994)
EQ 17	$Br_{2aq} + Cl^- \longleftrightarrow Br_2Cl^-$	2	1	1.3		Wang et al. (1994)
EQ 18	$HNO_{3aq} \longleftrightarrow H^+ + NO_3^-$	1	2	1.5×10^{1}		Davis and de Bruin (1964)
EQ 19	$HCl_{aq} \longleftrightarrow H^+ + Cl^-$	1	2	1.7×10^{6}		Marsh and McElroy (1985)
EQ 20	$HONO_{aq} \longleftrightarrow H^+ + NO_2^-$	1	2	5.1×10^{-4}	-1260	Schwartz and White (1981)
EQ 21	$HNO_{4aq} \longleftrightarrow NO_4^- + H^+$	1	2	1.0×10^{-5}	8700	Warneck (1999)
EQ 22	$ICl_{aq} + Cl^- \longleftrightarrow ICl_2^-$	2	1	7.7×10^{1}		Wang et al. (1989)
EQ 23	$IBr_{aq} + Br^- \longleftrightarrow IBr_2^-$	2	1	2.9×10^{2}		Troy et al. (1991)
EQ 24	$ICl_{aq} + Br^- \longleftrightarrow IClBr^-$	2	1	1.8×10^{4}		assumed = EQ 16
EQ 25	$IBr_{aq} + Cl^- \longleftrightarrow IClBr^-$	2	1	1.3		assumed = EQ 17

[a] The temperature dependence is $K = K_0 \times \exp(\frac{-\Delta H}{R}(\frac{1}{T} - \frac{1}{T_0}))$, $T_0 = 298$ K.

Table 10.7: Aqueous phase equilibrium constants.

Table 10.8: Henry constants and accommodation coefficients.

specie	K_H^0 [M/atm]	$-\Delta_{soln}H/R$ [K]	reference	α^0	$-\Delta_{obs}H/R$ [K]	reference
O_3	1.2×10^{-2}	2560	Chameides (1984)	0.002	(at 292 K)	DeMore et al. (1997)
O_2	1.3×10^{-3}	1500	Wilhelm et al. (1977)	0.01	2000	estimated
OH	3.0×10^{1}	4300	Hanson et al. (1992)	0.01	(at 293 K)	Takami et al. (1998)
HO_2	3.9×10^{3}	5900	Hanson et al. (1992)	0.2	(at 293 K)	DeMore et al. (1997)
H_2O_2	1.0×10^{5}	6338	Lind and Kok (1994)	0.077	2769	Worsnop et al. (1989)
NO_2	6.4×10^{-3}	2500	Lelieveld and Crutzen (1991)	0.0015	(at 298 K)	Ponche et al. (1993)
NO_3	2.0	2000	Thomas et al. (1993)	0.04	(at 273? K)	Rudich et al. (1996)
N_2O_5	∞	—		0.1	(at 195-300 K)	DeMore et al. (1997)
HONO	4.9×10^{1}	4780	Schwartz and White (1981)	0.04	(at 247-297 K)	DeMore et al. (1997)
HNO_3	1.7×10^{5}	8694	Lelieveld and Crutzen (1991)	0.5	(at RT)	Abbatt and Waschewsky (1998)
HNO_4	1.2×10^{4}	6900	Régimbal and Mozurkewich (1997)	0.1	(at 200 K)	DeMore et al. (1997)
NH_3	5.8×10^{1}	4085	Chameides (1984)	0.06	(at 295 K)	DeMore et al. (1997)
CH_3OO	6.0	$=HO_2$	Pandis and Seinfeld (1989)	0.01	2000	estimated
ROOH	3.0×10^{2}	5322	Lind and Kok (1994)	0.0046	3273	Magi et al. (1997)
HCHO	7.0×10^{3}	6425	Chameides (1984)	0.04	(at 260-270 K)	DeMore et al. (1997)
HCOOH	3.7×10^{3}	5700	Chameides (1984)	0.014	3978	DeMore et al. (1997)
CO_2	3.1×10^{-2}	2423	Chameides (1984)	0.01	2000	estimated
HCl	1.2	9001	Brimblecombe and Clegg (1989)	0.074	3072	Schweitzer et al. (2000)
HOCl	6.7×10^{2}	5862	Huthwelker et al. (1995)	$=HOBr$	$=HOBr$	estimated
$ClNO_3$	∞	—		0.1	(at RT)	Koch and Rossi (1998)
Cl_2	9.1×10^{-2}	2500	Wilhelm et al. (1977)	0.038	6546	Hu et al. (1995)
HBr	1.3	10239	Brimblecombe and Clegg (1989)	0.031	3940	Schweitzer et al. (2000)
HOBr	9.3×10^{1}	$=HOCl$	Vogt et al. (1996b)	0.5	(at RT)	Abbatt and Waschewsky (1998)
$BrNO_3$	∞	—		0.8	0	Hanson et al. (1996)
Br_2	7.6×10^{-1}	4094	Dean (1992)	0.038	6546	Hu et al. (1995)
BrCl	9.4×10^{-1}	5600	Bartlett and Margerum (1999)	$=Cl_2$	$=Cl_2$	estimated
DMSO	5.0×10^{4}	$=HCHO$	De Bruyn et al. (1994)	0.048	2578	De Bruyn et al. (1994)

Table 10.8: Continued

specie	K_H^0 [M/atm]	$-\Delta_{soln}H/R$ [K]	reference	α^0	$-\Delta_{obs}H/R$ [K]	reference
DMSO$_2$	∞	—	assumed	0.03	5388	De Bruyn et al. (1994)
SO$_2$	1.2	3120	Chameides (1984)	0.11	0	DeMore et al. (1997)
H$_2$SO$_4$	∞	—		0.65	(at 303 K)	Pöschl et al. (1998)
CH$_3$SO$_2$H	∞	—	assumed	0.0002	0	Lucas and Primm (2002)
CH$_3$SO$_3$H	∞	—	assumed	0.076	1762	De Bruyn et al. (1994)
HI	∞	—		0.036	4130	Schweitzer et al. (2000)
IO	4.5×10^2	=HOI	estimated by Vogt et al. (1999b)	0.5	2000	estimated by Vogt et al. (1999b)
HOI	4.5×10^2	=HOCl	Chatfield and Crutzen (1990)	=HOBr	=HOBr	estimated
INO$_2$	∞	—		0.1	2000	estimated by Vogt et al. (1999b)
INO$_3$	∞	—		0.1	2000	estimated by Vogt et al. (1999b)
I$_2$	3.0	4431	Palmer et al. (1985)	0.01	2000	estimated by Vogt et al. (1999b)
ICl	1.1×10^2	=BrCl	Wagman et al. (1982)	0.01	2000	estimated by Vogt et al. (1999b)
IBr	2.4×10^1	=BrCl	Wagman et al. (1982)	0.01	2000	estimated by Vogt et al. (1999b)
OIO	∞	—		1		estimated
HIO$_3$	∞	—		0.01	2000	estimated

[a] For ROOH the values of CH$_3$OOH have been assumed. The temperature dependence is for the Henry constants is $K_H = K_H^0 \times \exp(\frac{-\Delta_{soln}H}{R}(\frac{1}{T} - \frac{1}{T_0}))$, $T_0 = 298$ K and for the accommodation coefficients $dln(\frac{\alpha}{1-\alpha})/d(\frac{1}{T}) = \frac{-\Delta_{obs}H}{R}$. RT stands for "room temperature".
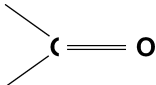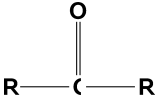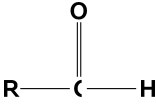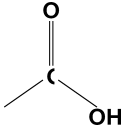
Carbonyl group	$C = O$
Ketone	$R - C(=O) - R$
Aldehyde	$R - C(=O) - H$
Formaldehyde (Methanal)	H - CHO
Acetaldehyde (Ethanal)	CH_3 - CHO
Propionaldehyde (Propanal)	CH_3 - (CH_2) - CHO
Butyraldehyde (Butanal)	CH_3 - $(CH_2)_2$ - CHO
Valeraldehyde (Pentanal)	CH_3 - $(CH_2)_3$ - CHO
Capronaldehyde (Hexanal)	CH_3 - $(CH_2)_4$ - CHO
Heptanaldehyde (Heptantal)	CH_3 - $(CH_2)_5$ - CHO
Caprylicaldehyde (Octanal)	CH_3 - $(CH_2)_6$ - CHO
Nonylaldehyde (Nonanal)	CH_3 - $(CH_2)_7$ - CHO
Carboxy group	$C(=O)OH$
Dicarboxylic acids	HOOC - $(CH_2)_n$ - COOH
oxalic acid (ethanedioic acid)	$n=0$
malonic acid (propanedioic acid)	$n=1$
succinic acid (butanedioic acid)	$n=2$
glutaric acid (pentanedioic acid)	$n=3$
adipic acid (hexanedioic acid)	$n=4$
pimelic acid (heptanedioic acid)	$n=5$
suberic acid (octanedioic acid)	$n=6$
azelaic acid (nonanedioic acid)	$n=7$
sebacic acid (decanedioic acid)	$n=8$

Table 10.9: This table gives an overview of the most important organic functional groups that are mentioned in this thesis. Exemplarily some of the species belonging to the different funtional groups are additionally listed.
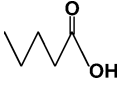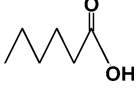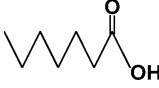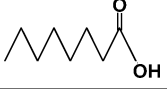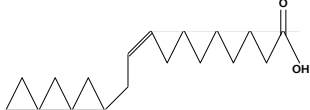
Formal name	IUPAC name	Sum formula	
formic acid	methanoic acid	$C_1H_2O_2$	
acetic acid	ethanoic acid	$C_2H_4O_2$	
butyric acid	butanoic acid	$C_4H_8O_2$	
valeric acid	pentanoic acid	$C_5H_{10}O_2$	
caproic acid	hexanoic acid	$C_6H_{12}O_2$	
enanthic acid	heptanoic acid	$C_7H_{14}O_2$	
caprylic acid	octanoic acid	$C_8H_{16}O_2$	
pelargonic acid	nonanoic acid	$C_9H_{18}O_2$	
capric acid	decanoic acid	$C_{10}H_{20}O_2$	
lauric acid	dodecanoic acid	$C_{12}H_{24}O_2$	
myristic acid	tetradecanoic acid	$C_{14}H_{28}O_2$	
palmitic acid	hexadecanoic acid	$C_{16}H_{32}O_2$	
stearic acid	octadecanoic acid	$C_{18}H_{36}O_2$	
oleic acid	octadecenoic acid	$C_{18}H_{36}O_2$	

Table 10.10: Overview of several fatty acids.

Bibliography

Abbatt, J. P. D. and Waschewsky, G. C. G.: Heterogeneous interactions of HOBr, HNO$_3$, O$_3$ and NO$_2$ with deliquescent NaCl aerosols at room temperature, J. Phys. Chem. A, 102, 3719 – 3725, 1998.

Aguzzi, A. and Rossi, M.: The kinetics of the heterogeneous reaction of BrONO$_2$ with solid alkali halides at ambient temperature. A comparison with the interaction of ClONO$_2$ on NaCl and KBr, Phys. Chem. Chem. Phys., 1, 4337–4346, 1999.

Alfonso, L. and Raga, G.: The influence of organic compounds in the development of precipitation acidity in maritime clouds, Atmos. Chem. Phys., 4, 1097–1111, 2004.

Alicke, B., Hebestreit, K., Stutz, J., and Platt, U.: Iodine oxide in the marine boundary layer, Nature, 397, 572 – 573, 1999.

Allan, B. J., McFiggans, G., Plane, J. M. C., and Coe, H.: Observation of Iodine monoxide in the Remote Marine Boundary Layer, J. Geophys. Res., 105, 14 363 – 14 370, 2000.

Allan, B. J., Plane, J. M. C., and McFiggans, G.: Observations of OIO in the remote marine boundary layer, Geophys. Res. Lett., 28, 1945 – 1948, 2001a.

Allan, W., Lowe, D. C., and Cainey, J. M.: Active chlorine in the remote marine boundary layer: Modeling anomalous measurements of ^{13}C in methane, Geophys. Res. Lett., 28, 3239 – 3242, 2001b.

Alpert, P., Shafir, H., and Issahary, D.: Recent changes in the climate at the Dead Sea - A Preliminary Study, Climate Change, 37, 513–537, 1997.

Anati, D. and Shasha, S.: Dead Sea surface-level changes, Isr. J. Earth Sci., 38, 29–32, 1989.

Anderson, L. C. and Fahey, D. W.: Studies with ClONO$_2$: Thermal dissociation rate and catalytic conversion to NO using an NO/O$_3$ chemiluminescence detector, J. Phys. Chem., 94, 644 – 652, 1990.

Anttila, T. and Kerminen, V.: Influence of organic compounds on the cloud drolet activation: A model investigation considering the volatility, water soubility and surface activity of organic matter, J. Geophys. Res., 107(D22), doi:10.1029/2001JD001 482, 2002.

Aranda, A., Le Bras, G., La Verdet, G., and Poulet, G.: The BrO + CH$_3$O$_2$ reaction: Kinetics and role in the atmospheric ozone budget, Geophys. Res. Lett., 24 (22), 2745–2748, doi:10.1029/97GL02 686, 1997.

Asad, A., Mmereki, B., and Donaldson, D.: Enhanced uptake of water by oxidatively processed oleic acid, Atmos. Chem. Phys., 4, 2083–2089, 2004.

Ashworth, S., Allan, B., and Plane, J.: High resolution spectroscopy of the OIO radical: implications for the ozone-depletion potential of iodine in the marine boundary layer, Geophys. Res. Lett., 29, doi:10.1029/2001GL013 851, 2002.

Atkinson, R., Baulch, D. L., Cox, R. A., Hampson, Jr., R. F., Kerr, J. A., Rossi, M. J., and Troe, J.: Evaluated Kinetic and Photochemical Data for Atmospheric Chemistry: Supplement VI, J. Phys. Chem. Ref. Data, 26, 1329 – 1499, 1997.

Atkinson, R., Baulch, D. L., Cox, R. A., Hampson, Jr., R. F., Kerr, J. A., Rossi, M. J., and Troe, J.: Summary of Evaluated Kinetic and Photochemical Data for Atmospheric Chemistry, Web Version, http://www.iupac-kinetic.ch.cam.ac.uk, 1999.

Atkinson, R., Baulch, D. L., Cox, R. A., Crowley, J. N., Hampson, R. F., Jenkin, R. G. H. M. E., Kerr, J. A., Rossi, M. J., and Troe, J.: Summary of Evaluated Kinetic and Photochemical Data for Atmospheric Chemistry, Web Version, Jul. 2004, http://www.iupac-kinetic.ch.cam.ac.uk, 2004.

Atkinson, R., Baulch, D. L., Cox, R. A., Crowley, J. N., Hampson, R. F., Hynes, R. G., Jenkin, M. E., Kerr, J. A., Rossi, M. J., and Troe, J.: Summary of Evaluated Kinetic and Photochemical Data for Atmospheric Chemistry, Web Version, Mar. 2005, http://www.iupac-kinetic.ch.cam.ac.uk, 2005.

Avallone, L. M., Toohey, D. W., Fortin, T. J., McKinney, K. A., and Fuentes, J. D.: In situ measurements of bromine oxide at two high-latitude boundary layer sites: Implications of variability, J. Geophys. Res., 108, 4089, doi: 10.1029/2002JD002 843, 2003.

Ayers, G. P., Penkett, S. A., Gillett, R. W., Bandy, B., Galbally, I. E., Meyer, C. P., Elsworth, C. M., Bentle, S. T., and Forgan, B. W.: The Annual Cycle of Peroxides and Ozone in Marine Air at Cape Grim, Tasmania, J. Atmos. Chem., 23, 221 – 252, 1996.

Badger, C. L., Griffiths, P. T., George, I., Abbatt, J. P. D., and Cox, R. A.: Reactive Uptake of (N_2O_5) by Aerosol Particles Containing Mixtures of Humic Acid and Ammonium Sulfate, J. Phys. Chem. A, 110(21), 6986–6994, 2006.

Baker, A.: Inorganic Iodine Speciation in Tropical Atlantic Aerosol, Geophys. Res. Lett., 31, L23S02, doi:10.1029/2004GL020 144, 2004.

Baker, A. R.: Marine Aerosol Iodine Chemistry: The Importance of Soluble Organic Iodine, Env. Chem., 2, 295–298, 2005.

Bardouki, H., da Rosa, M. B., Mihalopoulos, N., Palm, W.-U., and Zetzsch, C.: Kinetics and mechanism of the oxidation of dimethylsulfoxide (DMSO) and methanesulfinate (MSI^-) in aqueous medium, Atmos. Environ., 36, 4627 – 4634, 2002.

Barger, W. and Garrett, W.: Surface active organic material in the air over the mediterranean and over the eastern equatorial Pacific, J. Geophys. Res., 81, 3151–3157, 1976.

Barker, G. C., Fowles, P., and Stringer, B.: Pulse radiolytic induced transient electrical conductance in liquid solutions, Trans. Faraday Soc., 66, 1509–1519, 1970.

Barnes, I., Bastian, V., Becker, K. H., and Overrath, R. D.: Kinetic studies of the reactions of IO, BrO and ClO with DMS, Int. J. Chem. Kinet., 23, 579–591, 1991.

Barone, S. B., Turnipseed, A. A., and Ravishankara, A. R.: Role of adducts in the atmospheric oxidation of dimethyl sulfide, Faraday Discuss., 100, 39 – 54, 1995.

Barrie, L. A., Bottenheim, J. W., Schnell, R. C., Crutzen, P. J., and Rasmussen, R. A.: Ozone destruction and photochemical reactions at polar sunrise in the lower Arctic atmosphere, Nature, 334, 138 – 141, 1988.

Barrie, L. A., den Hartog, G., Bottenheim, J. W., and Landsberger, S.: Anthropogenic aerosols and gases in the lower troposphere at Alert, Canada in April 1986, J. Atmos. Chem., 9, 101 – 127, 1989.

Bartlett, W. P. and Margerum, D. W.: Temperature dependencies of the Henry's law constant and the aqueous phase dissociation constant of bromine chloride, Environ. Sci. Technol., 33, 3410–3414, 1999.

Bauer, D., Ingham, T., Carl, S. A., Moortgat, G. K., and Crowley, J. N.: Ultraviolet-visible absorption cross sections of gaseous HOI and its photolysis at 355 nm, J. Phys. Chem. A, 102, 2857–2864, 1998.

Bedjanian, Y., Bras, G. L., and Poulet, G.: Rate constants for the reactions of I + OClO, I + ClO, Cl + I_2, and Cl + IO and heat formation of IO radicals, J. Phys. Chem., 100, 15 130 – 15 136, 1996.

Bedjanian, Y., Bras, G. L., and Poulet, G.: Kinetic study of the Br + IO, I + BrO and Br + I_2 reactions. Heat formation of the BrO radical, Chem. Phys. Lett., 266, 233 – 238, 1997.

Behnke, W., Scheer, V., and Zetzsch, C.: Production of $BrNO_2$, Br_2 and $ClNO_2$ from the Reaction between Sea Spray Aerosol and N_2O_5, J. Aerosol Sci., 25, Suppl.1, S277–S278, 1994.

Behnke, W., George, C., Scheer, V., and Zetzsch, C.: Production and decay of $ClNO_2$ from the reaction of gaseous N_2O_5 with NaCl solution: Bulk and aerosol experiments, J. Geophys. Res., 102 (D3), 3795–3804, doi:10.1029/96JD03 057, 1997.

Bertram, A. K., Ivanov, A. V., Hunter, M., Molina, L. T., and Molina, M. J.: The Reaction Probability of OH on Organic Surfaces of Tropospheric Interest, J. Phys. Chem. A, 105, 9415 – 9421, 2001.

Betterton, E. A. and Hoffmann, M. R.: Oxidation of aqueous SO_2 by peroxymonosulfate, J. Phys. Chem., 92, 5962–5965, 1988.

Bigg, E., Brownscombe, J., and Thompson, W.: Fog Modification with Long-Chain Alcohols, J. Appl. Met., 8, 75–82, 1969.

Bilde, M. and Svenningsson, B.: CCN activation of slightly soluble organics: The importance of small amounts of inorganic salt and particle phase, Tellus, 56B, 128–134, 2004.

Bill, M., Rhew, R. C., Weiss, R. F., and Goldstein, A. H.: Carbon isotope ratios of methyl bromide and methyl chloride emitted from a coastal salt marsh, Geophys. Res. Lett., 29, doi: 10.1029/2001GL012 946, 2002.

BinAbas, M., Simoneit, B., Elias, V., Cabral, J., and Cardoso, J.: Composition of higher molecular weight organic matter in smoke aerosol from biomass combustion in amazonien, Chemosphere, 30, 995–1015, 1995.

Bitan, A.: The Influence of the Special Shape of the Dead-Sea and Its Environment on the Local Wind System, Arch. Met. Geoph. Bioklim., 24, 283–301, 1977.

Bjergbakke, E., Navartnam, S., Parsons, B. J., and Swallow, A. J.: Reaction between $HO_2\cdot$ and chlorine in aqueous solution, J. Am. Chem. Soc., 103, 5926–5928, 1981.

Blanchard, D. C.: Sea-to-Air Transport of Surface Active Material, Science, 146, 396 – 397, 1964.

Bloss, W. J., Lee, J. D., Johnson, G. P., Sommariva, R., Heard, D. E., Saiz-Lopez, A., Plane, J. M. C., McFiggans, G., Coe, H., Flynn, M., Williams, P., Rickard, A. R., and Fleming, Z. L.: Impact of halogen monoxide chemistry upon boundary layer OH and HO_2 concentrations at a coastal site, Geophys. Res. Lett., 32, L06 814, doi:10.1029/2004GL022 084, 2005.

Bobrowski, N., Hönninger, G., Galle, B., and Platt, U.: Detection of bromine monoxide in a volcanic plume, Nature, 423, 273 – 276, 2003.

Bobrowski, N., von Glasow, R., Aiuppa, A., Inguaggiato, S., Louan, I., Ibrahim, O., and Platt, U.: Reactive halogen chemistry in volcanic plumes, J. Geophys. Res., 112, D06 311, doi:10.1029/2006JD007 206, 2007.

Bonsang, B., Martin, D., Lambert, G., Kanakidou, M., de Roulley, J., and Sennequir, G.: Vertical distribution of nonmethane hydrocarbons in the remote marine boundary layer, J. Geophys. Res., 96, 7313 – 7324, 1991.

Bott, A., Trautmann, T., and Zdunkowski, W.: A numerical model of the cloud-topped planetary boundary-layer: Radiation, turbulence and spectral microphysics in marine stratus, Q. J. R. Meteorol. Soc., 122, 635–667, 1996.

Bottenheim, J. W., Gallant, A. J., and Brice, K. A.: Measurements of NO_y species and O_3 at 82°N latitude, Geophys. Res. Lett., 13, 113 – 116, 1986.

Bottenheim, J. W., Barrie, L. A., Atlas, E., Heidt, L. E., Niki, H., Rasmussen, R. A., and Shepson, P. B.: Depletion of lower tropospheric ozone during Arctic spring: The polar sunrise experiment 1988, J. Geophys. Res., 95, 18 555 – 18 568, 1990.

Bowman, J., Dennis J. Barket j., and Shepson, P. B.: Atmospheric Chemistry of Nonanal, Environ. Sci. Technol., 37, 2218–2225, 2003.

Boyce, S. D. and Hoffmann, M. R.: Kinetics and mechanism of the formation of hydroxymethanesulfonic acid at low pH, J. Phys. Chem., 88, 4740–4746, 1984.

Brimblecombe, P. and Clegg, S. L.: Erratum, J. Atmos. Chem., 8, 95, 1989.

Bröske, R. and Zabel, F.: Spectroscopic and kinet = Br, I), Ann. Geophys. Suppl. II, 16, C717, 1998.

Brown, S. S., Ryerson, T. B., Wollny, A. G., Brock, C. A., Peltier, R., Sullivan, A. P., Weber, R. J., Dube, W. P., Trainer, M., Meanher, J. F., Fehsenfeld, F. C., and Ravishankara, A. R.: Variability in Nocturnal Nitrogen Oxide Processing and Its Role in Regional Air Quality, Science, 311, 69–70, 2006.

Burkholder, J., Curtius, J., Ravishankara, A., and Lovejoy, E.: Laboratory studies of the homogeneous nucleation of iodine oxides, Atmos. Chem. Phys., 4, 19–34, 2004.

Burley, J. D. and Johnston, H. S.: Ionic mechanisms for heterogeneous stratospheric reactions and ultraviolet photoabsorption cross-sections for NO_2^+, HNO_3, and NO_3^- in sulfuric-acid, Geophys. Res. Lett., 19, 1359 – 1362, 1992.

Buxton, G. V., Kilner, C., and Sellers, R. M.: Pulse radiolysis of HOI and IO^- in aqueous solution, formation and characterization of I^{II}, in 6th. Symp. on Radiation Chemistry, pp. 155 – 159, 1986.

Buxton, G. V., Greenstock, C. L., Helman, W. P., and Ross, A. B.: Critical review of rate constants for reactions of hydrated electrons, hydrogen atoms and hydroxyl radicals ($\cdot OH/\cdot O^-$) in aqueous solution, J. Phys. Chem. Ref. Data, 17, 513–886, 1988.

Buxton, G. V., McGowan, S., Salmon, G. S., Williams, J. E., and Wood, N. D.: A study of the spectra and reactivity of oxysulphur-radical anions involved in the chain oxidation of S(IV): A pulse and γ-radiolysis study, Atmos. Environ., 30, 2483–2493, 1996.

Buxton, G. V., Bydder, M., and Salmon, G. A.: The reactivity of chlorine atoms in aqueous solution Part II: The equilibrium $SO_4^- + Cl^- \longleftrightarrow Cl + SO_4^{2-}$, Phys. Chem. Chem. Phys., 1, 269 – 273, 1999a.

Buxton, G. V., Salmon, G. A., and Wang, J.: The equilibrium $NO_3 + Cl^- \longleftrightarrow NO_3^- + Cl$: A laser flash photolysis and pulse radiolysis study of the reactivity of NO_3 with chloride ion in aqueous solution, Phys. Chem. Chem. Phys., 1, 3589 – 3593, 1999b.

Carpenter, L., Malin, G., Liss, P., and Kuepper, F.: Novel biogenic iodine-containing trihalomethanes and other short-lived halocarbons in the coastal East Atlantic, Global Biogeochem. Cycles, 14, 1191–1204, 2000.

Carpenter, L. J., Sturges, W. T., Penkett, S. A., Liss, P. S., Alicke, B., Hebestreit, K., and Platt, U.: Short-lived alkyl iodides and bromides at Mace Head, Ireland: Links to biogenic sources and halogen oxide production, J. Geophys. Res., 104, 1679 – 1689, 1999.

Cavalli, F., Facchini, M., Decesari, S., Mircea, M., Emblico, L., Fuzzi, S., Ceburnis, D., Yoon, Y., O'Dowd, C., Putaud, J.-P., and Dell'Acqua, A.: Advances in characterization of size-resolved organic matter in marine aerosol over the North Atlantic, J. Geophys. Res., 109, D24 215, doi:10.1029/2004JD005 137, 2004.

Chambers, R. M., Heard, A. C., and Wayne, R. P.: Inorganic gas-phase reactions of the nitrate radical: $I_2 + NO_3$ and $I + NO_3$, J. Phys. Chem., 96, 3321–3331, 1992.

Chameides, W. L.: The Photochemistry of a Remote Marine Stratiform Cloud, J. Geophys. Res., 89, 4739 – 4755, 1984.

Chameides, W. L. and Stelson, A. W.: Aqueous-Phase Chemical Processes in Deliquescent Sea-Salt Aerosols: A Mechanism That Couples the Atmospheric Cycles of S and Sea Salt, J. Geophys. Res., 97, 20 565 – 20 580, 1992.

Chatfield, R. B. and Crutzen, P. J.: Are There Interactions of Iodine and Sulfur Species in Marine Air Photochemistry?, J. Geophys. Res., 95 (D13), 22 319–22 341, 1990.

Cheng, Y., Li, S.-M., Leithead, A., Brickell, P., and Leaitch, W.: Characterizations of cis-pionic acid and n-fatty acids on fine aerosols in the Lower Fraser Valley during Pacific 2001 Air Quality Study, Atmos. Environ., 38, 5789–5800, 2004.

Chin, M. and Wine, P. H.: A temperature-dependent competitive kinetics study of the aqueous-phase reactions of OH radicals with formate, formic acid, acetate, acetic acid, and hydrated formaldehyde, in Aquatic and Surface Photochemistry, edited by G. R. Helz, R. G. Zepp, and D. G. Crosby, pp. 85–96, A. F. Lewis, NY, 1994.

Chinake, C. R. and Simoyi, R. H.: Kinetics and mechanism of the complex bromate-iodine reaction, J. Phys. Chem., 100, 1643 – 1656, 1996.

Christensen, H. and Sehested, K.: HO_2 and O_2^- radicals at elevated temperatures, J. Phys. Chem., 92, 3007–3011, 1988.

Christensen, H., Sehested, K., and Corfitzen, H.: Reactions of hydroxyl radicals with hydrogen peroxide at ambient and elevated temperatures, J. Phys. Chem., 86, 1588–1590, 1982.

Chuang, P.: Measurement of the timescale of hygroscopic growth for atmospheric aerosols, J. Geophys. Res., 108, doi:10.1029/2002JD002 757, 2003.

Chuang, P. Y.: Sensitivity of cloud condensation nuclei activation processes to kinetic parameters, J. Geophys. Res., 111, doi:10.1029/2005JD006 529, 2006.

Citri, O. and Epstein, I. R.: Mechanistic study of a coupled chemical oscillator: the bromate-chlorite-iodide reaction, J. Phys. Chem., 92, 1865 – 1871, 1988.

Clarke, R. H.: Recommended methods for the treatment of the boundary layer in numerical models, Austr. Meteor. Mag., 18, 51 – 73, 1970.

Clifton, C. L., Altstein, N., and Huie, R. E.: Rate constant for the reaction of NO_2 with sulfur(IV) over the pH range 5.3–13, Environ. Sci. Technol., 22, 586–589, 1988.

Damian, V., Sandu, A., Damian, M., Potra, F., and R.Carmichael, G.: The kinetic pre-processor KPP - a software environment for solving chemical kinetics, Comp Chem Eng, 26, 1567–1579, 2002.

Damschen, D. E. and Martin, L. R.: Aqueous aerosol oxidation of nitrous acid by O_2, O_3 and H_2O_2, Atmos. Environ., 17, 2005–2011, 1983.

Davies, R.: Response of Cloud Supersaturation to Radiative Forcing, J. Atmos. Sci., 42, 2820–2825, 1985.

Davis, Jr., W. and de Bruin, H. J.: New activity coefficients of 0-100 per cent aqueous nitric acid, J. Inorg. Nucl. Chem., 26, 1069 – 1083, 1964.

De Bruyn, W. J., Shorter, J. A., Davidovits, P., Worsnop, D. R., Zahniser, M. S., and Kolb, C. E.: Uptake of gas phase sulfur species methanesulfonic acid, dimethylsulfoxide, and dimethyl sulfone by aqueous surface, J. Geophys. Res., 99, 16 927 – 16 932, 1994.

de Gouw, J. A. and Lovejoy, E. R.: Reactive uptake of ozone by liquid organic compounds, Geophys. Res. Lett., 25, 931–934, 1998.

de Ridder, K. and Gallee, H.: Land Surface-Induced Regional climate Change in Southern Israel, J. Appl. Met., 37, 1470–1485, 1998.

Dean, J. A.: Lange's Handbook of Chemistry, McGraw-Hill, Inc., 1992.

Deister, U. and Warneck, P.: Photooxidation of SO_3^{2-} in aqueous solution, J. Phys. Chem., 94, 2191–2198, 1990.

DeMore, W. B., Sander, S. P., Golden, D. M., Hampson, R. F., Kurylo, M. J., Howard, C. J., Ravishankara, A. R., Kolb, C. E., and Molina, M. J.: Chemical Kinetics and Photochemical Data for Use in Stratospheric Modeling, Tech. Rep. JPL Publication 97-4, Jet Propulsion Laboratory, Pasadena, CA, 1997.

Eigen, M. and Kustin, K.: The kinetics of halogen hydrolysis, J. Am. Chem. Soc., 84, 1355 – 1361, 1962.

Ellison, G., Tuck, A., and Vaida, V.: Atmospheric processing of organic aerosol, J. Geophys. Res., 104, 11 633 – 11 641, 1999.

Ervens, B., Feingold, G., Clegg, S. L., and Kreidenweis, S. M.: A modeling study of aqueous production of dicarboxylic acids: 2. Implications for cloud microphysics, J. Geophys. Res., 109, D15 206, doi:10.1029/2004JD004 575, 2004.

Ervens, B., Feingold, G., and Kreidenweis, S. M.: Influence of water-soluble organic carbon on cloud drop number concentration, J. Geophys. Res., 110, D18 211, doi:10.1029/2004JD005 634, 2005.

Exner, M., Herrmann, H., and Zellner, R.: Laser-based studies of reactions of the nitrate radical in aqueous solution, Ber. Bunsenges. Phys. Chem., 96, 470 – 477, 1992.

Facchini, M., Mircea, M., Fuzzi, S., and Charlson, R.: Cloud albedo enhancement by surface-active organic solutes in growing droplets, Nature, 401, 257 – 259, 1999.

Fan, S.-M. and Jacob, D. J.: Surface ozone depletion in Arctic spring sustained by bromine reactions on aerosols, Nature, 359, 522 – 524, 1992.

Fang, J., Kawamura, K., Ishimura, Y., and Matsumoto, K.: Carbon isotope composition of fatty acids in the marine aerosols from the Western North Pacific: Implication for the source and atmospheric transport, Environ. Sci. Technol., 36, 2598–2604, 2002.

Farman, J. C., Gardiner, B. G., and Shanklin, J. D.: Large losses of total ozone in Antarctica reveal seasonal ClO_x/NO_x interaction, Nature, 315, 207 – 210, 1985.

Feingold, G. and Chuang, P.: Analysis of the Influence of Film-Forming Compounds on Droplet Growth: Implications for Cloud Microphysical Processes and Climate, J. Atmos. Sci., 12, 2006–2018, 2002.

Fickert, S., Adams, J. W., and Crowley, J. N.: Activation of Br_2 and BrCl via uptake of HOBr onto aqueous salt solutions, J. Geophys. Res., 104, 23 719 – 23 727, 1999.

Fogelman, K. D., Walker, D. M., and Margerum, D. W.: Non-metal redox kinetics: Hypochlorite and hypochlorous acid reactions with sulfite, Inorg. Chem., 28, 986 – 993, 1989.

Fortnum, D. H., Battaglia, C. J., Cohen, S. R., and Edwards, J. O.: The kinetics of the oxidation of halide ions by monosubstituted peroxides, J. Am. Chem. Soc., 82, 778–782, 1960.

Foster, K. L., Plastridge, R. A., Bottenheim, J. W., Shepson, P. B., Finlayson-Pitts, B. J., and Spicer, C. W.: The Role of Br_2 and BrCl in Surface Ozone Destruction at Polar Sunrise, Science, 291, 471 – 474, 2001.

Frieß, U., Wagner, T., Pundt, I., Pfeilsticker, K., and Platt, U.: Spectroscopic Measurements of Tropospheric Iodine Oxide at Neumayer Station, Antarctica, Geophys. Res. Lett., 28, 1941 – 1944, 2001.

Frieß, U., Hollwedel, J., König-Langlo, G., Wagner, T., and Platt, U.: Dynamics and chemistry of tropospheric bromine explosion events in the Antarctic coastal region, J. Geophys. Res., 109, D06 305, doi:10.1029/2003JD004 133, 2004.

Furrow, S.: Reactions of iodine intermediates in iodate-hydrogen peroxide oscillators, J. Phys. Chem., 91, 2129 – 2135, 1987.

Fuzzi, S., M.O.Andreae, Huebert, B., M.Kulmala, Bond, T., Boy, M., Doherty, S., Guenther, A., Kanakidou, M., Kawamura, K., Kerminen, V.-M., Lohmann, U., Russel, L., and Pöschl, U.: Critical assessment of the current stat of scientific knowledge, terminology, and research needs concerning the role of organic aerosols in the atmosphere, climate, and global change, Atmos. Chem. Phys., 5, 11 729–11 780, 2006.

Garland, J. A. and Curtis, H.: Emission of Iodine From the Sea Surface in the Presence of Ozone, J. Geophys. Res., 86, 3183 – 3186, 1981.

Garland, R. M., Wise, M. E., Beaver, M. R., DeWitt, H. L., Aiken, A. C., Jimenez, J. L., and Tolbert, M. A.: Impact of palmitic acid coating on the water uptake and loss of ammonium sulfate particles, Atmos. Chem. Phys., 5, 1951–1961, 2005.

Garrett, W. D.: Retardation of Water Drop Evaporation with Monomolecular Surface Films, J. Atmos. Chem., 28, 816–819, 1971.

Gershenzon, M., Davidovits, P., Jayne, J. T., Kolb, C. E., and Worsnop, D. R.: Simultaneous Uptake of DMS and Ozone on Water, J. Phys. Chem. A, 105, 7031 – 7036, 2001.

Giebl, H., Berner, A., Reichl, G., Puxbaum, H., Kasper-Giebl, A., and Hitzenberger, R.: CCN activation of oxalic and malonic acid test aerosols with the University of Vienna cloud condensation nuclei counter, J. Aerosol Sci., 33, 1623–1634, 2002.

Gilfedder, B., Petri, M., and Biester, H.: Iodine and bromine speciation in snow and the effect of orographically induced precipitation, Atmos. Chem. Phys., 7, 2661–2669, 2007.

Gill, P. S., Graedel, T. E., and Weschler, C. J.: Organic films on atmospheric aerosol particles, fog droplets, cloud droplets, raindrops, and snowflakes, Rev. Geoph. Space Ph., 21, 903 – 920, 1983.

Haag, W. R. and Hoigné, J.: Ozonation of bromide-containing waters: Kinetics of formation of hypobromous acid and bromate, Environ. Sci. Technol., 17, 261 – 267, 1983.

Haggerstone, A.-L., Carpenter, L. J., Carslaw, N., and McFiggans, G.: Improved model predictions of HO_2 with gas to particle mass transfer rates calculated using aerosol number size distributions, J. Geophys. Res., 110, D04 303, doi: 10.1029/2004JD005 282, 2005.

Hansen, J. C., Li, Y., Francisco, J. S., and Li, Z.: On the Mechanism of the $BrO + CH_2O$ Reaction, J. Phys. Chem. A, 103, 8543 – 8546, 1999.

Hanson, D. R., Burkholder, J. B., Howard, C. J., and Ravishankara, A. R.: Measurement of OH and HO_2 radical uptake coefficients on water and sulfuric acid surfaces, J. Phys. Chem., 96, 4979–4985, 1992.

Hanson, D. R., Ravishankara, A. R., and Lovejoy, E. R.: Reaction of $BrONO_2$ with H_2O on submicron sulfuric acid aerosol and the implications for the lower stratosphere, J. Geophys. Res., 101D, 9063–9069, 1996.

Hausmann, M. and Platt, U.: Spectroscopic measurement of bromine oxide and ozone in the high Arctic during Polar Sunrise Experiment 1992, J. Geophys. Res., 99, 25 399 – 25 413, 1994.

Heald, C., Jacob, D., Park, R., Russell, L., Huebert, B., Seinfeld, J., Liao, H., and Weber, R.: A large organic aerosol source in the free troposhphere missing from current models, Geophys. Res. Lett., 32, doi:10.1029/2005GL023 831, 2005.

Hearn, J. D. and Smith, G. D.: Kinetics and Product Studies for Ozonolysis Reactions of Organic Particles using Aerosol CMIS, J. Phys. Chem., 108, 10 019–10 029, 2004.

Hearn, J. D., Lovett, A. J., and Smith, G. D.: Ozonolysis of oleic acid particles: evidence for a surface reaction and secondary reactions involving Crigee intermediates, Phys. Chem. Chem. Phys., 7, 501–511, 2005.

Hebestreit, K., Stutz, J., Rosen, D., Matveev, V., Peleg, M., Luria, M., and Platt, U.: DOAS Measurements of Tropospheric Bromine Oxide in Mid-Latitudes, Science, 283, 55 – 57, 1999.

Hegg, D. A., Gao, S., Hoppel, W., Frick, F., Caffrey, P., Leaitch, W., Shantz, N., Ambrusko, J., and Albrechcinski, R.: Laboratory studies of the efficiency of selected organic aerosols as CCN, Atmos. Res., 58, 155–166, 2001.

Herrmann, H., Reese, A., and Zellner, R.: Time resolved UV/VIS diode array absorption spectroscopy of SO_x^- (x=3, 4, 5) radical anions in aqueous solution, J. Mol. Struct., 348, 183–186, 1995.

Herrmann, H., Ervens, B., Nowacki, P., Wolke, R., and Zellner, R.: A chemical aqueous phase radical mechanism for tropospheric chemistry, Chemosphere, 38, 1223 – 1232, 1999.

Herrmann, H., Ervens, B., Jacobi, H.-W., Wolke, R., Nowacki, P., and Zellner, R.: CAPRAM2.3: A Chemical Aqueous Phase Radical Mechanism for Tropospheric Chemistry, J. Atmos. Chem., 36, 231 – 284, 2000.

Hippler, H., Luther, K., and Troe, J.: Untersuchung der Rekombination von Jodatomen in stark komprimierten Gasen und Flüssigkeiten, Ber. Bunsenges. Phys. Chem., 77, 1104 – 1114, 1973.

Hoffmann, M. R.: On the kinetics and mechanism of oxidation of aquated sulfur dioxide by ozone, Atmos. Environ., 20, 1145 – 1154, 1986.

Hoffmann, T., O'Dowd, C., and Seinfeld, J.: Iodine oxide homogeneous nucleation: An explanation for coastal new particle production, Geophys. Res. Lett., 28, 1949–1952, 2001.

Hoigné, J., Bader, H., Haag, W. R., and Staehelin, J.: Rate constants of reactions of ozone with organic and inorganic compounds in water — III Inorganic compounds and radicals, Wat. Res., 19, 993–1004, 1985.

Hollwedel, J., Wenig, M., Beirle, S., Kraus, S., Kühl, S., Wilms-Grabe, W., Platt, U., and Wagner, T.: Year-to- Year Variability of Polar Tropospheric BrO as seen by GOME, Adv. Space Res., 34, 804 – 808, 2004.

Hönninger, G. and Platt, U.: Observations of BrO and its vertical distribution during surface ozone depletion at Alert, Atmos. Environ., 36, 2481 – 2489, 2002.

Hönninger, G., Bobrowski, N., Palenque, E. R., Torrez, R., and Platt, U.: Reactive bromine and sulfur emissions at Salar de Uyuni, Bolivia, Geophys. Res. Lett., 31, L04 101, doi: 10.1029/2003GL018 818, 2004a.

Hönninger, G., Leser, H., Sebastián, O., and Platt, U.: Ground-based measurements of halogen oxides at the Hudson Bay by longpath DOAS and passive MAX-DOAS, Geophys. Res. Lett., 31, L04 111, doi: 10.1029/2003GL018 982, 2004b.

Hoppel, W. A. and Frick, G. M.: Submicron aerosol size distributions measured over the tropical and south Pacific, Atmos. Environ., 24A, 645 – 659, 1990.

Hu, J. H., Shi, Q., Davidovits, P., Worsnop, D. R., Zahniser, M. S., and Kolb, C. E.: Reactive uptake of Cl_2 and Br_2 by aqueous surfaces as a function of Br^- and I^- ion concentration: The effect of chemical reaction at the interface, J. Phys. Chem., 99, 8768 – 8776, 1995.

Hubinger, S. and Nee, J. B.: Absorption spectra of Cl_2, Br_2 and BrCl between 190 and 600 nm, J. Photochem. Photobiol. A: Chem., 86, 1–7, 1995.

Huie, R. E. and Neta, P.: Rate constants for some oxidations of S(IV) by radicals in aqueous solutions, Atmos. Environ., 21, 1743–1747, 1987.

Hung, H. and Ariya, P.: Oxidation of oleic acid and oleic acid/sodium chloride(aq) mixture droplets with ozone: Changes of hygroscopicity and role of secondary reactions, J. Phys. Chem., A, 111, 620–632, 2007.

Hung, H.-M., Katrib, Y., and Martin, S.: Products and mechanisms of the Reaction of Oleic Acid with Ozone and Nitrate Radical, J. Phys. Chem., 109, 4517–4530, 2005.

Huthwelker, T., Clegg, S. L., Peter, T., Carslaw, K., Luo, B. P., and Brimblecombe, P.: Solubility of HOCl in water and aqueous H_2SO_4 to stratospheric temperatures, J. Atmos. Chem., 21, 81–95, 1995.

Ingham, T., Bauer, D., Sander, R., Crutzen, P. J., and Crowley, J. N.: Kinetics and Products of the Reactions BrO + DMS and Br + DMS at 298 K, J. Phys. Chem. A, 103, 7199–7209, 1999.

Jacob, D. J.: Chemistry of OH in Remote Clouds and Its Role in the Production of Formic Acid and Peroxymonosulfate, J. Geophys. Res., 91, 9807 – 9826, 1986.

Jacobi, H.-W.: Kinetische Untersuchungen und Modellrechnungen zur troposphärischen Chemie von Radikalanionen und Ozon in wässriger Phase, Ph.D. thesis, Universität Essen, Germany, 1996.

Jacobi, H.-W., Herrmann, H., and Zellner, R.: Kinetic investigation of the Cl_2^- radical in the aqueous phase, in Air Pollution Research Report 57: Homogenous and hetrogenous chemical Processes in the Troposphere, edited by P. Mirabel, pp. 172–176, Office for official Publications of the European Communities, Luxembourg, 1996.

Jacobson, M., Hansson, H.-C., Noone, K., and Charlson, R.: Organic atmospheric aerosols: Review and state of the science, Rev. Geoph., 38, 267 – 294, 2000.

Jaenicke, R.: Aerosol Physics and Chemistry, in Landolt-Börnstein "'Zahlenwerte und Funktionen aus Naturwissenschaften und Technik"', V 4b, pp. 391–457, Springer, 1988.

Jayson, G. G., Parsons, B. J., and Swallow, A. J.: Some simple, highly reactive, inorganic chlorine derivatives in aqueous solution, J. Chem. Soc. Faraday Trans., 69, 1597–1607, 1973.

Jefferson, A., Nicovich, J. M., and Wine, P. H.: Temperature-dependent kinetics studies of the reactions $Br(^2P_{3/2})$ + CH_3SCH_3 ↔ CH_3SCH_2 + HBr. Heat of formation of the CH_3SCH_2 radical, J. Phys. Chem., 98, 7128 – 7135, 1994.

Jenkin, M. E., Cox, R. A., and Candeland, D. E.: Photochemical Aspects of Tropospheric Iodine behaviour, J. Atmos. Chem., 2, 359 – 375, 1985.

Jiang, P.-Y., Katsumura, Y., Nagaishi, R., Domae, M., Ishikawa, K., Ishigure, K., and Yoshida, Y.: Pulse radiolysis study of concentrated sulfuric acid solutions. Formation mechanism, yield and reactivity of sulfate radicals, J. Chem. Soc. Faraday Trans., 88, 1653–1658, 1992.

Jimenez, J. L., Cocker, D. R., Bahreini, R., Zhuang, H., Varutbangkul, V., Flagan, R. C., Seinfeld, J. H., O'Dowd, C., and Hoffmann, T.: New Particle Formation from Photooxidation of Diiodomethane (CH_2I_2), J. Geophys. Res., 108, 4318, 10.1029/2002 JD002 452, 2003.

Jones, A., Anderson, P., Wolff, E., Turner, J., Rankin, A., and Colwell, S.: A role for newly forming sea ice in springtime polar tropospheric ozone loss?, J. Geophys. Res., doi:10.1029/2005JD006566, 2006.

Kaku, K. C., Hegg, D. A., Covert, D. S., Santarpia, J. L., Jonsson, H., Buzorius, G., and Collins, D.: Organics in the Northeastern Pacific and their impacts on aerosol hygroscopicity in the subsaturated and supersaturated regimes, Atmos. Chem. Phys., 6, 4101–4115, 2006.

Kanakidou, M., Seinfeld, J., Pandis, S., Barnes, I., Dentener, F., Facchini, M., Dingenen, R. V., Ervens, B., Nenes, A., Nielson, C., Swietlicki, E., Putaud, J., Balkanski, Y., Fuzzi, S., Horth, J., Moortgat, G., Winterhalter, R., Myhre, C., Tsigaridis, K., Bignati, E., Stephanou, E., and Wilson, J.: Organic aerosol and global climate modelling: a review, Atmos. Chem. Phys., 5, 1053–1123, 2005.

Katrib, Y., Martin, S., Hung, H.-M., Rudich, Y., Zhang, H., Slowik, J., Dividovits, P., Jayne, J., and Worsnop, D.: Products and Mechanisms of Ozone Reactions with Oleic Acid for Aerosol particles Having Core-Shell Morphologies, J. Phys. Chem., 108, 6686–6695, 2004.

Katrib, Y., Biskos, G., Buseck, P. R., Davidovits, P., Jayne, J. T., Mochida, M., Wise, M. E., Worsnop, D. R., and Martin, S. T.: Ozonolysis of Mixed Oleic-Acid/Stearic-Acid Particles: Reaction Kinetics and Chemical Morphology, J. Phys. Chem., 109, 10 910–10 919, 2005a.

Katrib, Y., Martin, S., Rudich, Y., P.Davidovits, Jayne, J., and Worsnop, D.: Density changes of aerosol particles as a reesult of chemical reaction, Atmos. Chem. Phys., 5, 275–291, 2005b.

Kawamura, K. and Gagosian, R.: Implications of ω-oxocarboxylic acids in the remote marine atmosphere for photo-oxidation of unsaturated fatty acids, Nature, 325, 330–332, 1987.

Keene, W., Pszenny, A., Maben, J., OHalloran, T., Wall, A., Kerkweg, A., and Sander, R.: Latitudinal variation in volatile and particulate inorganic halogens over the eastern North and South Atlantic Oceans, Geophys. Res. Abs., 7, 05 337, 2005.

Keene, W. C., Maben, J. R., Pszenny, A. A. P., and Galloway, J. N.: Measurement Technique for Inorganic Chlorine Gases in the Marine Boundary Layer, Environ. Sci. Technol., 27, 866 – 874, 1993.

Keene, W. C., Sander, R., Pszenny, A. A. P., Vogt, R., Crutzen, P. J., and Galloway, J. N.: Aerosol pH in the marine boundary layer: A review and model evaluation., J. Aerosol Sci., 29, 339 – 356, 1998.

Kelley, C. M. and Tartar, H. V.: On the system: bromine-water, J. Am. Chem. Soc., 78, 5752–5756, 1956.

Knopf, D. A., Anthony, L. M., and Bertram, A. K.: Reactive Uptake of O_3 by Multicomponent and Multiphase Mixtures Containing Oleic Acid, J. Phys. Chem., 109, 5579–5589, 2005.

Knopf, D. A., Mark, J., Gross, S., and Bertram, A.: Does atmospheric processing of saturated hydrocarbon surfaces by NO_3 lead to volatilization, Geophys. Res. Lett., 33, L17 816, doi:10.1029/2006GL026 884, 2006.

Koch, T. G. and Rossi, M. J.: Direct measurement of surface residence times: Nitryl chloride and chlorine nitrate on alkali halides at room temperature, J. Phys. Chem. A, 102, 9193–9201, 1998.

Kocmond, W., Garrett, W., and Mack, E.: Modification of laboratory fog with organic surface filnms, J. Geophys. Res., 77, 3221–3231, 1972.

Kreher, K., Johnston, P. V., Wood, S. W., Nardi, B., and Platt, U.: Ground-based measurements of tropospheric and stratospheric BrO at Arrival Heights, Antarctica, Geophys. Res. Lett., 24, 3021 – 3024, 1997.

Kukui, A., Bossoutrot, V., Laverdet, G., and Bras, G. L.: Mechanism of the Reaction of CH_3SO with NO_2 in Relation to Atmospheric Oxidation of Dimethyl Sulfide: Experimental and Theoretical Study, J. Phys. Chem. A, 104, 935 – 946, 2000.

Kukui, A., Borissenko, D., Laverdet, G., and Bras, G. L.: Gas phase reactions of OH radicals with dimethyl sulfoxide and methane sulfonic acid using turbulent flow reactor and chemical ionization mass spectrometry, J. Phys. Chem. A, 107, 5732 – 5742, 2003.

Kumar, K. and Margerum, D. W.: Kinetics and mechanism of general-acid-assisted oxidation of bromide by hypochlorite and hypochlorous acid, Inorg. Chem., 26, 2706 – 2711, 1987.

Landgraf, J. and Crutzen, P.: An Efficient Method for 'On-Line' Calculations of Photolysis and Heating Rates, J. Atmos. Sci., 55, 863–878, 1998.

Laszlo, B., Kurylo, M. J., and Huie, R. E.: Absorption cross sections, kinetics of formation, and self-reaction of the IO radical produced via the laser photolysis of $N_2O/I_2/N_2$ mixtures, J. Phys. Chem., 99, 11 701 – 11 707, 1995.

Lax, E.: Taschenbuch für Chemiker und Physiker, Springer Verlag, Berlin, 1969.

Lee, C., Kim, Y. J., Tanimoto, H., Bobrowski, N., Platt, U., Mori, T., Yamamoto, K., and Hong, C. S.: High ClO and ozone depletion observed in the plume of Sakurajima volcano, Japan, Geophys. Res. Lett., 32, 21 809, doi:10.1029/2005GL023 785, 2005.

Lee, Y.-N. and Schwartz, S. E.: Reaction kinetics of nitrogen dioxide with liquid water at low partial pressure, J. Phys. Chem., 85, 840–848, 1981.

Lehrer, E., Wagenbach, D., and Platt, U.: Aerosol chemical composition during tropospheric ozone depletion at Ny Ålesund/Svalbard, Tellus, 49B, 486 – 495, 1997.

Lelieveld, J. and Crutzen, P. J.: The Role of Clouds in Tropospheric Photochemistry, J. Atmos. Chem., 12, 229 – 267, 1991.

Lengyel, I., Li, J., Kustin, K., and Epstein, I. R.: Rate constants for reactions between iodine- and chlorine-containing species: A detailed mechanism of the chlorine dioxine/chlorite reaction, J. Am. Chem. Soc., 118, 3708 – 3719, 1996.

Leser, H., Hönninger, G., and Platt, U.: MAX-DOAS Measurements of BrO and NO_2 in the Marine Boundary Layer, Geophys. Res. Lett., 30, 1537, doi:10.1029/2002GL015 811, 2003.

Li, Z., Williams, A. L., and Rood, M. J.: Influence of Soluble Surfactant Properties on the Activation of Aerosol Particles Containing Inorganic Solute, J. Atmos. Sci., 55, 1859–1866, 1998.

Lind, J. A. and Kok, G. L.: Correction to "Henry's law determinations for aqueous solutions of hydrogen peroxide, methylhydroperoxide, and peroxyacetic acid" by John A. Lind and Gregory L. Kok, J. Geophys. Res., 99D, 21 119, 1994.

Lind, J. A., Lazrus, A. L., and Kok, G. L.: Aqueous phase oxidation of sulfur(IV) by hydrogen peroxide, methylhydroperoxide, and peroxyacetic acid, J. Geophys. Res., 92D, 4171–4177, 1987.

Liss, P. S. and Slater, P. G.: Flux of Gases across the Air-Sea Interface, Nature, 147, 181–184, 1974.

Liu, Q. and Margerum, D. W.: Equilibrium and Kinetics of Bromine Chloride Hydrolysis, est, 35, 1127 – 1133, 2001.

Logager, T., Sehested, K., and Holcman, J.: Rate constants of the equilibrium reactions $SO_4 + HNO_3 \longleftrightarrow HSO_4^- + NO_3$ and $SO_4 + NO_3 \longleftrightarrow SO_4^{2-} + NO_3$., Radiat. Phys. Chem., 41, 539 – 543, 1993.

Lohmann, U., Broekhuizen, K., Leaitch, R., and Shantz, N.: How effective is cloud droplet formation of organic aerosols?, J. Geophys. Res., 31, doi:10.1029/2003GL018 999, 2004.

Long, C. A. and Bielski, B. H. J.: Rate of reaction of superoxide radical with chloride-containing species, J. Phys. Chem., 84, 555–557, 1980.

Lucas, D. D. and Prinn, R. G.: Mechanistic studies of dimethylsulfide oxidation products using an observationally constrained model, J. Geophys. Res., 107, doi: 10.1029/2001JD000 843, 2002.

Lurmann, F. W., Lloyd, A. C., and Atkinson, R.: A Chemical Mechanism for Use in Long-Range Transport/Acid Deposition Computer Modeling, J. Geophys. Res., 91, 10 905 – 10 936, 1986.

Magi, L., Schweitzer, F., Pallares, C., Cherif, S., , Mirabel, P., and George, C.: Investigation of the uptake rate of ozone and methyl hydroperoxide by water surfaces, J. Phys. Chem. A, 101, 4943 – 4949, 1997.

Mallard, W. G., Westley, F., Herron, J. T., Hampson, R. F., and Frizzel, D. H.: NIST Chemical Kinetics Database: Version 5.0, National Institute of Standards and Technology, Gaithersburg, MD, 1993.

Mamou, A., Rabani, J., and Behar, D.: On the oxidation of aqueous Br^- by OH radicals, studied by pulse radiolysis, J. Phys. Chem., 81, 1447–1448, 1977.

Marsh, A. R. W. and McElroy, W. J.: The dissociation constant and Henry's law constant of HCl in aqueous solution, Atmos. Environ., 19, 1075 – 1080, 1985.

Martinez, M., Arnold, T., and Perner, D.: The role of bromine and chlorine chemistry for arctic ozone depletion events in Ny Ålesund and comparison with model calculations, Ann. Geoph., 17, 941–956, 1999.

Marty, J., Saliot, A., Buat-Menard, P., Chesselet, R., and Hunter, K.: Relationship between the lipid compositions of marine aerosols, the sea surface microlayer, and subsurface water, J. Geophys. Res., 84, 5707–5716, 1979.

Masslinger, A., Wiedensohler, A., Busch, B., C, N., Quinn, P., Bates, T., and Covert, D.: Hygroscopic properties of different aerosol types over the Atlantic and Indian Oceans, Atmos. Chem. Phys., 3, 1377–1397, 2003.

Matthew, B. M., George, I., and Anastasio, C.: Hydroperoxyl radical (HO_2) oxidizes dibromide radical anion (Br_2^-) to bromine (Br_2) in aqueous solution: Implications for the formation of Br_2 in the marine boundary layer, Geophys. Res. Lett., 30 (24), 2297, doi: 10.1029/2003GL018 572, 2003.

Matveev, V., Peleg, M., Rosen, D., Tov-Alper, D. S., Hebestreit, K., Stutz, J., Platt, U., Blake, D., and Luria, M.: Bromine oxide - ozone interaction over the Dead Sea, J. Geophys. Res., 106, 10,375–10,387, 2001.

Matvev, V., Dayan, U., Tass, E., and Peleg, M.: Atmospheric sulfur flux rates to and from Israel, Sci. Tot. Env., 291, 143–154, 2002.

Mc Figgans, G., Coe, H., Burgess, R., Allan, J., cubision, M., Alfarra, M., Saunders, R., Saiz-Lopez, A., Plane, J., Webvill, D., Carpenter, L., Rickard, A., and Monks, P.: Direct evidence for coastal iodine particles from laminaria macroalgae - linkage to emissions of molecular iodine, Atmos. Chem. Phys., 4, 701–713, 2004.

McConnell, J. C., Henderson, G. S., Barrie, L., Bottenheim, J., Niki, H., Langford, C. H., and Templeton, E. M. J.: Photochemical bromine production implicated in Arctic boundary-layer ozone depletion, Nature, 1992.

McElroy, C. T., McLinden, C. A., and McConnell, J. C.: Evidence for bromine monoxide in the free troposphere during the Arctic polar sunrise, Nature, 397, 338 – 341, 1999.

McFiggans, G., Plane, J., Allan, B., Carpenter, L., Coe, H., and O'Dowd, C.: A modeling study of iodine chemistry in the marine boundary layer, J. Geophys. Res., 105, 14,374–14,385, 2000.

Mellor, G. and Yamada, T.: Development of a Turbulence Closure Model for Geophysical Fluid Problems, Rev. Geoph. Space Ph., 20, 851–875, 1982.

Middlebrook, A., Murphy, D., and Thomson, D.: Observations of organic material in individual marine particles at Cape Grim during the First Aerosol Characterization Experiment (ACE 1), J. Geophys. Res., 103, 16 475 – 16 483, 1998.

Ming, Y. and Russell, L.: Organic aerosol effects of fog droplet spectra, J. Geophys. Res., 109, D10206, doi:10.1029/2003JD004 427, 2004.

Mircea, M., Facchini, M., Decesari, S., Fuzzi, S., and Charlson, R.: The influence of the organic aerosol component on CCN supersaturation spectra for different aerosol types, Tellus, 54B, 74–81, 2002.

Mochida, M., Hirokawa, J., Kajii, Y., and Akimoto, H.: Geophys. Res. Lett., 25, 3927–3930, 1998.

Mochida, M., Kitamori, Y., Kawamura, K., Nojiri, Y., and Suzuki, K.: Fatty acids in the marine atmosphere: Factors governing their concentrations and evaluation of organic films on sea-salt particles, J. Geophys. Res., 107, 4325,doi:10.1029/2001JD001 278, 2002.

Mochida, M., Katrib, Y., Jayne, J. T., Worsnop, D., and Martin, S. T.: The relative importance of competing pathways for the formation of high-molecular-weight peroxides in the ozonolysis of organic aerosol particles, Atmos. Chem. Phys. Discuss., 6, 7137–7176, 2006.

Moise, T. and Rudich, Y.: Uptake of Cl and Br by organic surfaces - a perspective on organic aerosols processing by tropospheric oxidants, Geophys. Res. Lett., 28, 4083 – 4086, 2001.

Moise, T. and Rudich, Y.: Reactive Uptake of Ozone by Aerosol-Associated Unsaturated Fatty Acids: Kinetics, Mechanism, and Products, J. Phys. Chem. A, 106, 6469 – 6476, 2002.

Molina, M. J. and Rowland, F. S.: Stratospheric sink for chlorofluoromethanes: Chlorine-atom catalysed destruction of ozone, Nature, 249, 810 – 812, 1974.

Monahan, E. C., Spiel, D. E., and Davidson, K. L.: A model of marine aerosol generation via whitecaps and wave disruption, in Oceanic Whitecaps, edited by E. C. Monahan and G. M. Niocaill, pp. 167 – 174, D. Reidel, Norwell, Mass, 1986.

Morris, J., Davidovits, P., Jayne, J., Jiminez, J., Shi, Q., Kolb, C., Worsnop, D., Barney, W., and Cass, G.: Kinetics of submicron oleic acid aerosols with ozone: A novel aerosol mass spectrometric technique, Geophys. Res. Lett., 29, doi: 10.1029/2002GL014 692, 2002.

Mössinger, J., Shallcross, D. E., and Cox, R. A.: UV-VIS absorption cross-sections and atmospheric lifetimes if CH_2Br_2, CH_2I_2 and CH_2BrI, J. Chem. Soc. Faraday Trans., 94, 1391 – 1396, 1998.

Murayama, S., Nakazawa, T., Tanka, M., Aoki, S., and Kawaguchi, S.: Variations of tropospheric ozone concentrations over Syowa Station Antarcitca, Tellus, 44B, 262–272, 1992.

Murphy, D., Thomson, D., and Mahoney, M.: In Situ Measurements of Organics, Meteoritic Material, Mercury, and Other Elements in Aerosols at 5 to 19 Kilometers, 27, 1664–1669, 1998.

Nagao, I., Matsumoto, K., and Tanaka, H.: Sunrise ozone destruction found in the subtropical marine boundary layer, Geophys. Res. Lett., 26, 3377 – 3380, 1999.

Nagy, J. C., Kumar, K., and Margerum, D. W.: Non-metal redox kinetics: Oxidation of iodide by hypochlorous acid and by nitrogen trichloride measured by the pulsed-accelerated-flow method, Inorg. Chem., 27, 2773–2780, 1988.

Neill, V. M., Patterson, J., Wolfe, M., and Thornton, J. A.: The effect of varying levels of surfactant on the reactive uptake of (N_2O_5) to aqueous aerosol, Atmos. Chem. Phys., 6, 1635–1644, 2006.

Nenes, A., Ghan, S., Abdul-Razzak, H., Chuang, P., and Seinfeld, J.: Kinetic limitations on cloud droplet formation and impact on cloud albedo, Tellus, 53B, 133–149, 2001.

Nenes, A., Charlson, R., Facchini, M. C., Kulmala, M., Laaksonen, A., and Seinfeld, J.: Can chemical effects on cloud droplet number rival the first indirect effect?, 29(17),1848, doi:10.1029/2002GL015 295, 2002.

Niemi, T., Ben-Avrahem, Z., and Gat, J.: The Dead Sea: The Lake and Its Setting, Oxford Monogr. Geol. Geophys., vol. 36, Oxford Univ. Press, New York, 1997.

Novakov, T. and Penner, J.: Large contribution of organic aerosols to cloud-condensation-nuclei concentrations, Nature, 365, 823–826, 1993.

Novakov, T., Corrigan, C., Penner, J., Chuang, C., Rosario, O., and Bracero, O. M.: Organic aerosols in the Caribbean trade winds: A natural source?, J. Geophys. Res., 20, 21,307–21,313, 1997.

O'Dowd, C., Jimenez, J., Bahreini, R., Flagan, R., Seinfeld, J., Hämeri, K., Pirjola, L., Kulmala, M., Jennings, S., and Hoffmann, T.: Marine particle formation by biogenic iodine emissions, Nature, 417, 632 – 636, 2002.

O'Dowd, C., Facchini, M., Cavalli, F., Ceburnis, D., Mircea, M., Descari, S., Fuzzi, S., Yoon, Y., and Rutaud, J.-P.: Biogenically driven organic contribution to marine aerosol, Nature, 431, 676–677, 2004.

Olsen, R. J. and Epstein, I. R.: Bifurcation analysis of chemical reaction mechanisms. I. Steady state bifurcation structure, J. Chem. Phys., 94, 3083–3095, 1991.

Oltmans, S. J. and Komhyr, W.: Surface ozone distributions and variations from 1973 - 1984 measurements at the NOAA Geophysical Monitoring for Climate Change Baseline observatories, J. Geophys. Res., 91, 5229 – 5236, 1986.

Oppenheimer, C., Tsanev, V. I., Braban, C. F., Cox, R. A., Adams, J. W., Aiuppa, A., Bobrowski, N., Delmelle, P., Barclay, J., and McGonigle, A. J.: BrO formation in volcanic plumes, Geochim. Cosmochim. Acta, 70, 2935 – 2941, 2006.

Orlando, J. J. and Tyndall, G. S.: Rate coefficients for the thermal decomposition of $BrONO_2$ and the heat of formation of $BrONO_2$, J. Phys. Chem., 100, 19 398 – 19 405, 1996.

Oros, D. and Simoneit, B.: Identification and emission rates of molecular tracers in coal smoke particulate matter, 79, 515–536, 2000.

Oros, D. and Simoneit, B.: Identification and emission factors of molecular tracers in organic aerosols from biomass burning part 1. Temperate climate conifers, Appl. Geochem., 16, 1513–1544, 2001.

Otani, Y. and Wang, C. S.: Growth and Deposition of Saline Droplets Covered with a Monolayer of Surfactants, Aerosol Sci. Technol., 3, 155–166, 1984.

Palmer, D. A., Ramette, R. W., and Mesmer, R. E.: The hydrolysis of iodine: Equilibria at high temperatures, J. Nucl. Mater., 130, 280–286, 1985.

Pandis, S. N. and Seinfeld, J. H.: Sensitivity Analysis of a Chemical Mechanism for Aqueous-Phase Atmospheric Chemistry, J. Geophys. Res., 94, 1105 – 1126, 1989.

Pechtl, S., Lovejoy, E. R., Burkholder, J. B., and von Glasow, R.: Modeling the possible role of iodine oxides in atmospheric new particle formation, Atmos. Chem. Phys., 6, 505–523, 2006.

Pechtl, S., Schmitz, G., and von Glasow, R.: Modelling iodine - iodate speciation in atmospheric aerosol: Contributions of inorganic and organic iodine chemistry, Atmos. Chem. Phys., 7, 1381–1393, 2007.

Peters, C., Pechtl, S., Stutz, J., Hebestreit, K., Hönninger, G., Heumann, K. G., Schwarz, A., Winterlik, J., and Platt, U.: Reactive and organic halogen species in three different European coastal environments, Atmos. Chem. Phys., 5, 3357 – 3375, 2005.

Pio, C., Alves, C., and Duarte, A.: Organic components of aerosols in a forested area of central Greece, Atmos. Environ., 5, 389–401, 2001.

Piot, M. and von Glasow, R.: The potential importance of frost flowers, recycling on snow, and open leads for Ozone Depletion Events, Atmos. Chem. Phys. Discuss., 7, 4521–4595, 2007.

Platt, U. and Janssen, C.: Observation and Role of the Free Radicals NO_3, ClO, BrO and IO in the Troposphere, Faraday Discuss., 100, 175 – 198, 1995.

Ponche, J. L., George, C., and Mirabel, P.: Mass transfer at the air/water interface: Mass accommodation coefficients of SO_2, HNO_3, NO_2 and NH_3, J. Atmos. Chem., 16, 1–21, 1993.

Pope, F., Hansen, J., Bayes, K., Friedl, R., and Sander, S.: The Ultraviolett Absorption Spectrum of Chlorine Peroxide, ClOOCl, J. Phys. Chem., A,111(20), 4322–4332, 2007.

Pöschl, U., Canagaratna, M., Jayne, J. T., Molina, L. T., Worsnop, D. R., Kolb, C. E., and Molina, M. J.: Mass accommodation coefficient of H_2SO_4 vapor on aqueous sulfuric acid surfaces and gaseous diffusion coefficient of H_2SO_4 in N_2/H_2O, J. Phys. Chem. A, 102, 10 082–10 089, 1998.

Pöschl, U., Letzel, T., Schauer, C., and Niessner, R.: Interaction of Ozone and Water Vapor with Spark Discharge Soot Aerosol Particles Coated with Benzo[a]pyrene: O_3 and H_2O Adsorption, Benzo[a]pyrene Degradation, and Atmospheric Implications, J. Phys. Chem. A, 105, 4029–4041, 2001.

Pöschl, U., Rudich, Y., and Amman, M.: Kinetic model framework for aerosol and cloud surface chemistry and gas-particle interactions: Part 1 - general equations, parameters, and terminology, Atmos. Chem. Phys. Discuss., 5, 2111–2191, 2005.

Pozzer, A., Jöckel, P., Sander, R., Ganzeveld, L., and Lelieveld, J.: Technical Note: The MESSy-submodel AIRSEA calculating the air-sea exchange of chemical species, Atmos. Chem. Phys., 6, 5435–5444, 2006.

Pruppacher, H. R. and Klett, J. D.: Microphysics of Clouds and Precipitation, Kluwer Academic Pub., Dordrecht/Boston/London, 1997.

Pszenny, A. A. P., Keene, W. C., Jacob, D. J., Fan, S., Maben, J. R., Zetwo, M. P., Springer-Young, M., and Galloway, J. N.: Evidence of inorganic chlorine gases other hydrogen chloride in marine surface air, Geophys. Res. Lett., 20, 699 – 702, 1993.

Pszenny, A. A. P., Moldanova, J., Keene, W. C., Sander, R., Maben, J. R., Martinez, M., Crutzen, P. J., Perner, D., and Prinn, R. G.: Halogen cycling and aerosol pH in the Hawaiian marine boundary layer, Atmos. Chem. Phys., 4, 147 – 168, 2004.

Putaud, J.-P., Dingenen, R. V., Mangoni, M., Virkkula, A., Raes, F., Maring, H., Prospero, J., Swietlicki, E., Berg, O., Hilamo, R., and Mkel, T.: Chemical mass closure and assessment of the origin of the submicron aerosol in the marine boundary layer and the free troposphere at Tenerife during ACE-2, Tellus, 52B, 141–168, 2000.

Quack, B. and Wallace, D. W. R.: The air-sea flux of bromoform: controls, rates and implication, Global Biogeochem. Cycles, 17, 1023, doi:10.1029/2002GB001 890, 2003.

Ray, A., Vassalli, I., G.Laverdet, and Bras, G. L.: Kinetics of the Thermal Decomposition of the CH_3SO_2 Radical and Its Reaction with NO_2 at 1 Torr and 298 K, J. Phys. Chem., 100, 8895 – 8900, 1996.

Régimbal, J.-M. and Mozurkewich, M.: Peroxynitric acid decay mechanisms and kinetics at low pH, J. Phys. Chem. A, 101, 8822–8829, 1997.

Rhew, R. C., Miller, B. R., Bill, M., Goldstein, A. H., and Weiss, R. F.: Environmental and biological controls on methyl halide emissions from southern California saltmarshes, Biogeochemistry, 60, 141 – 161, 2002.

Richter, A., Wittrock, F., Eisinger, M., and Burrows, J. P.: GOME Observations of Tropospheric BrO in Northern Hemispheric Spring and Summer 1997, Geophys. Res. Lett., 25, 2683 – 2686, 1998.

Richter, A., Wittrock, F., Ladstätter-Weißenmayer, A., and Burrows, J. P.: GOME measurements of stratospheric and tropospheric BrO, Adv. Space Res., 29, 1667 – 1672, 2002.

Rideal, E.: On the influence of thin surface films on the evaporation of water, J. Phys. Chem., 38, 1244–1248, 1924.

Rissman, T., Nenes, A., and Seinfeld, J.: Chemical amplification (of damping) of the Twomey effect: Conditions derived from droplet activation theory, J. Atmos. Sci., 61, 919–930, 2004.

Robinson, A., Donahue, N., and Rogge, W.: Photochemical oxidation and changes in molecular composition of organic aerosol in the regional context, J. Geophys. Res., 111, D03 302, doi:10.1029/2005JD006 265, 2006.

Roehl, C. M., Burkholder, J. B., Moortgat, G. K., Ravishankara, A. R., and Crutzen, P. J.: The temperature dependence of the UV absorption cross sections and the atmospheric implications of several alkyl iodides, J. Geophys. Res., 102D, 12 819–12 829, 1997.

Rogge, W., Hildemann, L., Mazurek, M., Cass, G., and Simoneit, B.: Sources of fine organic aerosol. 1. Charbroilers and Meat Cooking Operations, Environ. Sci. Technol., 25, 1112–1125, 1991.

Rogge, W., Hildemann, L., Mazurek, M., Cass, G., and Simoneit, B.: Sources of fine organic aerosol. 2. noncatalyst and catalyst-equipped automobiles and heavy-duty diesel trucks, Environ. Sci. Technol., 27, 636–651, 1993.

Ross, A. B., Mallard, W. G., Helman, W. P., Bielski, B. H. J., Buxton, G. V., Cabelli, D. E., Greenstock, C. L., Huie, R. E., and Neta, P.: NDRL-NIST Solution Kinetics Database: - Ver. 1, National Institute of Standards and Technology, Gaithersburg, MD, 1992.

Ross, A. B., Mallard, W. G., Helman, W. P., Buxton, G. V., Huie, R. E., and Neta, P.: NDRL-NIST Solution kinetics database: Version 3.0, Notre Dame Radiation Laboratory, Notre Dame, and National Institut of Standards and Technology, Gaithersburg, 1998.

Rubel, G. and Gentry, J. W.: Measurement of the Kinetics of Solution Droplets in the Presence of Adsorbed Monolayers: Determination of Water Accommodation Coefficients, J. Chem. Phys., 88, 3142–3148, 1984.

Rudich, Y., Talukdar, R. K., Imamura, T., Fox, R. W., and Ravishankara, A. R.: Uptake of NO_3 on KI solutions: Rate coefficient for the $NO_3 + I^-$ reaction and gas-phase diffusion coefficients for NO_3, Chem. Phys. Lett., 261, 467–473, 1996.

Ruehl, C., Chuang, P., and Nenes, A.: How quickly do cloud droplets form on atmospheric particles, Atmos. Chem. Phys., 8, 1043–1055, 2008.

Russell, L., Maria, S., and Myneni, S.: Mapping organic coatings on atmospheric particles, Geophys. Res. Lett., 29, doi:10.1029/2002GL014 874, 2002.

Saiz-Lopez, A. and Boxe, C.: A mechanism for biologically-induced iodine emissions from sea-ice, Atmos. Chem. Phys. Discuss., 8, 2953–2976, 2008.

Saiz-Lopez, A. and Plane, J. M. C.: Novel iodine chemistry in the marine boundary layer, Geophys. Res. Lett., 31, L04 112, doi: 10.1029/2003GL019 215, 2004.

Saiz-Lopez, A., Plane, J. M. C., and Shillito, J. A.: Bromine oxide in the mid-latitude marine boundary layer, Geophys. Res. Lett., 31, L03 111, doi: 10.1029/2003GL018 956, 2004.

Saiz-Lopez, A., Chance, K., Liu, X., Kurosu, T., and Sander, S.: First observations of iodine oxide from space, Geophys. Res. Lett., 34, L12 812,doi:10.1029/2007GL030 111, 2007a.

Saiz-Lopez, A., Mahajan, A., Salmon, R., Bauguitte, S.-B., Jones, A., Roscoe, H., and Plane, J.: Boundary Layer Halogens in Coastal Antarctica, Science, 317, 348–351, 2007b.

Saiz-Lopez, A., Plane, J. M. C., Mahajan, A. S., Anderson, P. S., Bauguitte, S.-B., Jones, A., Roscoe, H., Salmon, R., Bloss, W., Lee, J., and Heard, D.: On the vertical distribution of boundary layer halogens over coastal Antarctica: implications for O_3, HO_X, NO_X and the Hg lifetime, Atmos. Chem. Phys. Discuss., 7, 9385–9417, 2007c.

Saiz-Lopez, A. a. d. S., Coe, H., and Plane, J.: Measurements and modelling of I_2, IO, OIO, BrO and NO_3 in the mid-latitude marine boundary layer, Atmos. Chem. Phys., 6, 1512–1528, 2006a.

Saiz-Lopez, A. J. M. C. P., McFiggans, G., Williams, P. I., Ball, S. M., Bitter, M., Jones, R. L., Hongwei, C., and Hoffmann, T.: Modelling molecular iodine emissions in a coastal marine environment: the link to new particle formation, Atmos. Chem. Phys., 6, 883 – 895, 2006b.

Sander, R.: Modeling Atmospheric Chemistry: Interactions between Gas-Phase Species and Liquid Cloud/Aerosol Particles, Surv. Geophys., 20, 1 – 31, 1999.

Sander, R., Rudich, Y., von Glasow, R., and Crutzen, P. J.: The role of $BrNO_3$ in marine tropospheric chemistry: A model study, Geophys. Res. Lett., 26, 2857 – 2860, 1999.

Sander, S. P., Friedl, R. R., Golden, D. M., Kurylo, M. J., Huie, R. E., Orkin, V. L., Moortgat, G. K., Ravishankara, A. R., Kolb, C. E., Molina, M. J., and Finlayson-Pitts, B. J.: Chemical Kinetics and Photochemical Data for Use in Atmospheric Studies, Tech. Rep. JPL Publication 02-25, Jet Propulsion Laboratory, Pasadena, CA, 2003.

Sandu, A., Verwer, J. G., Blom, J. G., Spee, E. J., Carmichael, G. R., and Potra, F. A.: Benchmarking stiff ODE solvers for atmospheric chmistry problems - II. Rosenbrock Solvers, Atmos. Environ., 31, 3459–3472, 1997.

Schauer, J., Kleeman, M., Cass, G., and Simoneit, B.: Measurement of Emissions from Air Pollution Sources. 1. C_1 through C_{29} Organic Compounds from Meat Charbroiling, Environ. Sci. Technol., 33, 1566–1577, 1999a.

Schauer, J., Kleeman, M., Cass, G., and Simoneit, B.: Measurement of Emissions from Air Pollution Sources. 2.C_1 through C_{30} Organic Compounds from Medium Duty Diesel Trucks, Environ. Sci. Technol., 33, 1578–1587, 1999b.

Scheffler, D., Grothe, H., Willner, H., Frenzel, A., and Zetzsch, C.: Properties of Pure Nitryl Bromide. Thermal Behaviour, UV/Vis and FTIR Spectra, and Photoisomerization to *trans*-BrONO in an Argon Matrix, Inorg. Chem., 36, 335 – 338, 1997.

Schönhardt, A., Richter, A., Wittrock, F., Kirk, H., Oetjen, H., Roscoe, H., and Burrows, J.: Observations of iodine monoxide columns from satellite, Atmos. Chem. Phys., 8, 637–653, 2008.

Schwartz, S. E.: Mass-Transport Considerations Pertinent to Aqueous Phase Reactions of Gases in Liquid-Water Clouds, in Chemistry of Multiphase Atmospheric Systems, edited by W. Jaeschke, pp. 415 – 471, NATO ASI Series, Vol. G6, 1986.

Schwartz, S. E. and White, W. H.: Solubility equilibria of the nitrogen oxides and oxyacids in dilute aqueous solution, in Advances in Environmental Science and Engineering, edited by J. R. Pfafflin and E. N. Ziegler, vol. 4, pp. 1–45, Gordon and Breach Science Publishers, NY, 1981.

Schwarz, H. A. and Bielski, B. H. J.: Reactions of HO_2 and O_2^- with iodine and bromine and the I_2^- and I atom reduction potentials, J. Phys. Chem., 90, 1445–1448, 1986.

Schweitzer, F., Mirabel, P., and George, C.: Uptake of hydrogen halides by water droplets, J. Phys. Chem. A, 104, 72–76, 2000.

Seaver, M., Peele, J., Manuccia, T., Rubel, G., and Ritchie, G.: Evaporation Kinetics of Ventilated Waterdrops Coated with Octadecanol Monolayers, J. Phys. Chem., 96, 6389–6394, 1992.

Seery, D. J. and Britton, D.: The continous absorption spectra of chlorine, bromine, bromine chloride, iodine chloride, and iodine bromide, J. Phys. Chem., 68, 2263–2266, 1964.

Sehested, K., Rasmussen, O. L., and Fricke, H.: Rate constants of OH with HO_2, O_2^-, and $H_2O_2^+$ from hydrogen peroxide formation in pulse-irradiated oxygenated water, J. Phys. Chem., 72, 626–631, 1968.

Sehested, K., Holcman, J., and Hart, E. J.: Rate constants and products of the reactions of e_{aq}^-, O_2^- and H with ozone in aqueous solutions, J. Phys. Chem., 87, 1951–1954, 1983.

Sehested, K., Holcman, J., Bjergbakke, E., and Hart, E. J.: A pulse radiolytic study of the reaction $OH + O_3$ in aqueous medium, J. Phys. Chem., 88, 4144–4147, 1984.

Seidl, W.: Model for a surface film of fatty acids on rain water and aerosol particles, Atmos. Environ., 34, 4917 – 4932, 2000.

Seinfeld, J. H. and Pandis, S. N.: Atmospheric Chemistry and Physics, John Wiley & Sons, New York, Chichester, Weinheim, 1998.

Sempere, R. and Kawamura, K.: Trans-hemispheric contribution of C2-C10 alpha omega-dicarboxylic acids and related polar compounds to water-soluble organic carbon in the western Pacific aerosols in relation to photochemical oxidation reactions, Global Biogeochem. Cycles, 17, 1069,doi:10.1029/2002GB001 980, 2003.

Shantz, N. C., Leaitch, W. R., and Caffrey, P. F.: Effect of organics of low solubility on the growth rate of cloud droplets, J. Geophys. Res., 108, 20–50, 2003.

Shoute, L. C. T., Alfassi, Z. B., Neta, P., and Huie, R. E.: Temperature dependence of the rate constants for reaction of dihalide and azide radicals with inorganic reductants, J. Phys. Chem., 95, 3238 – 3242, 1991.

Shulman, M. L., Jacobson, M. C., Charlson, R. J., Synovec, R. E., and Young, T. E.: Dissolution behaviour and surface tension effects of organic compounds in nucleating cloud droplets, Geophys. Res. Lett., 23, 277 – 280, 1996.

Simoneit, B. and Mazurek, M.: Organic matter of the troposphere - II. Natural background of biogenic lipid matter in aerosols over the rural western United States, Atmos. Environ., 16, 2139–2159, 1982.

Smith, G., WoodsIII, E., DeForest, C., Baer, T., and Miller, R.: Reactive Uptake of Ozone by Oleic Acid Aerosol Particles: Application of Single-Particle Mass Spectrometry by Heterogeneous Reaction Kinetics, J. Phys. Chem., 106, 8085–8095, 2002.

Smith, M. H., Park, P. M., and Consterdine, I. E.: Marine aerosol concentrations and estimated fluxes over the sea, Q. J. R. Meteorol. Soc., 119, 809 – 824, 1993.

Snead, C. C. and Zung, J.: The effects of insoluble films upon the evaporation kinetics of liquid droplets, J. Colloid Interface Sci., 27, 25–31, 1968.

Solberg, S., Schmidbauer, N., Semb, A., and Stordal, F.: Boundary-layer ozone depletion as seen in the Norwegian arctic in spring, J. Atmos. Chem., 23, 301 – 332, 1996.

Solomon, S.: Progress towards a quantitative understanding of Antarctic ozone depletion, Nature, 347, 347 – 354, 1990.

Spicer, C. W., Chapman, E. G., Finlayson-Pitts, B. J., Plastridge, R. A., Hubbe, J. M., Fast, J. D., and Berkowitz, C. M.: Unexpectedly high concentrations of molecular chlorine in coastal air, Nature, 394, 353 – 356, 1998.

Spicer, C. W., Plastridge, R. A., Foster, K. L., Finlayson-Pitts, B. J., Bottenheim, J. W., Grannas, A. M., and Shepson, P. B.: Molecular halogens before and during ozone depletion events in the Arctic at polar sunrise: concentrations and sources, Atmos. Environ., 36, 2721 – 2731, 2002.

Stutz, J., Hebestreit, K., Alicke, B., and Platt, U.: Chemistry of Halogen Oxides in the Troposphere: Comparison of Model Calculations with Recent Field Data, J. Atmos. Chem., 34, 65 – 85, 1999.

Stutz, J., Ackermann, R., Fast, J. D., and Barrie, L.: Atmospheric Reactive Chlorine and Bromine at the Great Salt Lake, Utah, Geophys. Res. Lett., 29, doi: 10.1029/2002GL014 812, 2002.

Stutz, J., Pikelnaya, O., Hurlock, S., Trick, S., Pechtl, S., and von Glasow, R.: Daytime OIO in the Gulf of Maine, Geophys. Res. Lett., 34, doi: 10.1029/2007GL031 332, 2007.

Sverdrup, H., Johnson, M., and Fleming, R.: The Oceans, Their Physics, Chemistry and General Biology, Prentice-Hall, Englewood Cliffd, N.J., 1942.

Takami, A., Kato, S., Shimono, A., and Koda, S.: Uptake coefficient of OH radical on aqueous surface, Chem. Phys., 231, 215–227, 1998.

Tas, E., Matveeva, V., Zingler, J., Luria, M., and Peleg, M.: Frequency and extent of ozone destruction episodes over the Dead Sea, Israel, Atmos. Environ., 37, 4769 – 4780, 2003.

Tas, E., Peleg, M., Matveev, V., Zingler, J., and Luria, M.: Frequency and extent of bromine oxide formation over the Dead Sea, J. Geophys. Res., 110, D11 304, doi:10.1029/2004JD005 665, 2005.

Tas, E., Peleg, M., Pedersen, D. U., Matveev, V., Biazar, A. P., and Luria, M.: Measurement-based modeling of bromine chemistry in the boundary layer: 1. Bromine chemistry at the Dead Sea, Atmos. Chem. Phys., 6, 5589 – 5604, 2006.

Tervahattu, H., Hartonen, K., Kerminen, V.-M., Kupiainen, K., Aarnio, P., Koskentalo, T., Tuck, A., and Vaida, V.: New evidence of an organic layer on marine aerosols, J. Geophys. Res., 107, doi: 10.1029/2000JD000 282, 2002a.

Tervahattu, H., Juhanoja, J., and Kupiainen, K.: Identification of an organic coating on marine aerosol particles by TOF-SIMS, J. Geophys. Res., 107, 4319,10.1029/2001JD001 403, 2002b.

Tervahattu, H., Juhanoja, J., Vaida, V., Tuck, A. F., Niemi, J., Kupiainen, K., Kulmala, M., and Vehkamki, H.: Fatty acids on continental sulfate aerosol particles, J. Geophys. Res., 110, doi:10.1029/2004JD005 400, 2005.

THALOZ: Final report of the EU project THALOZ: Tropospheric Halogens - effect on ozone, coordinated by R. A. Cox, University of Cambridge, U.K., 2005.

Thomas, E. R., Frost, G. J., and Rudich, Y.: Reactive uptake of ozone by proxies for organic aerosols: Surface-bound and gas-phase products, J. Geophys. Res., 106, 3045–3056, 2001.

Thomas, K., Volz-Thomas, A., and Kley, D.: Zur Wechselwirkung von NO_3-Radikalen mit wässrigen Lösungen: Bestimmung des Henry- und des Massenakkomodationskoeffizienten, Ph.D. thesis, Institut für Chemie und Dynamik der Geosphäre 2, Forschungszentrum Jülich GmbH, FRG, 1993.

Thornberry, T. and Abbatt, J.: Heterogeneous reaction of ozone with liquid unsaturated fatty acids: Detailed kinetics and gas-phase product studies, Phys. Chem. Chem. Phys., 6, 84–93, 2004.

Thornton, J. A. and Abbatt, J. P. D.: (N_2O_5) Reaction on Submicron Sea Salt Aerosol: Kinetics, Products, and the Effect of Surface Active Organics, J. Phys. Chem., 109, 10 004–10 012, 2005.

Troy, R. C. and Margerum, D. W.: Non-metal redox kinetics: Hypobromite and hypobromous acid reactions with iodide and with sulfite and the hydrolysis of bromosulfate, Inorg. Chem., 30, 3538 – 3543, 1991.

Troy, R. C., Kelley, M. D., Nagy, J. C., and Margerum, D. W.: Non-metal redox kinetics: Iodine monobromide reaction with iodide ion and the hydrolysis of IBr, Inorg. Chem., 30, 4838–484, 1991.

Tuckermann, M., Ackermann, R., Golz, C., Lorenzen-Schmidt, H., Senne, T., Stutz, J., Trost, B., Unold, W., and Platt, U.: DOAS-observation of halogen radical-catalysed arctic boundary layer ozone destruction during the ARCTOC-campaigns 1995 and 1996 in Ny-Alesund, Spitsbergen, Tellus, 49B, 533 – 555, 1997.

Urbanski, S., Stickel, R. E., Zhao, Z. Z., and Wine, P. H.: Mechanistic and kinetic study of formaldehyde production in the atmospheric oxidation of dimethyl sulfide, J. Chem. Soc. Faraday Trans., 93, 2813 – 2819, 1997.

Urbanski, S., Stickel, R. E., and Wine, P. H.: Mechanistic and kinetic study of the gas-phase reaction of hydroxyl radical with dimethyl sulfoxide, J. Phys. Chem. A, 102, 10 522 – 10 529, 1998.

van Dingenen, R., Jensen, N. R., Hjorth, J., and Raes, F.: Peroxynitrate Formation During the Night-Time Oxidation of Dimethylsulfide: Its Role as a Reservoir Species for Aerosol Formation, J. Atmos. Chem., 18, 211 – 237, 1994.

Vesna, O., Sjogren, S., Weingartner, E., Samburova, V., Kalberer, M., Gaeggeler, H., and Ammann, M.: Changes of fatty acid aerosol hygroscopicity induced by ozonolysis under humid conditions, Atmos. Chem. Phys. Discuss., 7, 15 651–15 668, 2007.

Vogt, R., Crutzen, P. J., and Sander, R.: A mechanism for halogen release from sea-salt aerosol in the remote marine boundary layer, Nature, 383, 327 – 330, 1996a.

Vogt, R., Crutzen, P. J., and Sander, R.: A mechanism for halogen release from sea-salt aerosol in the remote marine boundary layer, Nature, 383, 327–330, doi:10.1038/383 327a0, 1996b.

Vogt, R., Sander, R., von Glasow, R., and Crutzen, P.: Iodine Chemistry and its Role in Halogen Activation and Ozone Loss in the Marine Boundary Layer: A Model Study, J. Atmos. Chem., 32, 375 – 395, 1999a.

Vogt, R., Sander, R., von Glasow, R., and Crutzen, P.: Iodine Chemistry and its Role in Halogen Activation and Ozone Loss in the Marine Boundary Layer: A Model Study, J. Atmos. Chem., 32, 375–395, 1999b.

von Glasow, R.: Modeling the gas and aqueous phase chemistry of the marine boundary layer, Ph.D. thesis, Universität Mainz, Germany, http://www.rolandvonglasow.de, 2000.

von Glasow, R. and Crutzen, P.: Troposheric Halogen Chemistry, in Vol. 4.02 *Treatise on Geochemistry Update 1* (eds. H. D. Holland and K. K. Turekian), pp. 1–67, Elsevier-Pergamon, Oxford, 2007.

von Glasow, R. and Crutzen, P. J.: Model study of multiphase DMS oxidation with a focus on halogens, Atmos. Chem. Phys., 4, 589–608, 2004.

von Glasow, R., Sander, R., Bott, A., and Crutzen, P.: Modeling halogen chemistry in the marine boundary layer 1. Cloud-free MBL, J. Geophys. Res., 107, 4341, doi:10.1029/2001JD000 942, 2002a.

von Glasow, R., Sander, R., Bott, A., and Crutzen, P. J.: Modeling halogen chemistry in the marine boudary layer 2. Interactions with sulfur and cloud-covered MBL, J. Geophys. Res., 107, 4323, doi:10.1029/2001JD000 943, 2002b.

von Glasow, R., Sander, R., Bott, A., and Crutzen, P. J.: Modeling halogen chemistry in the marine boundary layer 1. Cloud-free MBL, J. Geophys. Res., 107 (D17), 4341, doi:10.1029/2001JD000 942, 2002c.

von Gunten, U. and Oliveras, Y.: Advanced oxidation of bromide-containing waters: Bromate formation mechanisms, Environ. Sci. Technol., 32, 63 – 70, 1998.

von Hobe, M., Salawitch, R., Cantry, T., Keller-Rudek, H., Moortgat, G., Grooss, J.-U., Mueller, R., and Stroh, F.: Understanding the kinetics of the ClO dimer cycle, Atmos. Chem. Phys., 7, 3055–3069, 2007.

Wagman, D. D., Evans, W. H., Parker, V. B., Schummm, V. B., Halow, I., Bailey, S. M., Churney, K. L., and Nuttall, R. L.: The NBS tables of chemical thermodynamic properties; selected values for inorganic and C1 and C2 organic substances in SI units, J. Phys. Chem. Ref. Data, 11, Suppl. 2, 1982.

Wagner, I. and Strehlow, H.: On the flash photolysis of bromide ions in aqueous solution, Ber. Bunsenges. Phys. Chem., 91, 1317 – 1321, 1987.

Wagner, T. and Platt, U.: Satellite mapping of enhanced BrO concentrations in the troposphere, Nature, 395, 486 – 490, 1998.

Wagner, T., Leue, C., Wenig, M., Pfeilsticker, K., and Platt, U.: Spatial and temporal distribution of enhanced boundary layer BrO concentrations measured by the GOME instrument aboard ERS-2, J. Geophys. Res., 106, 24 225 – 24 235, 2001.

Wallington, T. J., Andino, J. M., Ball, J. C., and Japar, S. M.: Fourier transform infrared studies of the reaction of Cl atoms with PAN, PPN, CH_3OOH, HCOOH, CH_3COCH_3 and $CH_3COC_2H_5$ at 295±2 K, J. Atmos. Chem., 10, 301 – 313, 1990.

Wang, T. X., Kelley, M. D., Cooper, J. N., Beckwith, R. C., and Margerum, D. W.: Equilibrium, kinetic, and UV-spectral characteristics of aqueous bromine chloride, bromine, and chlorine species, Inorg. Chem., 33, 5872 – 5878, 1994.

Wang, Y. L., Nagy, J. C., and Margerum, D. W.: Kinetics of hydrolysis of iodine monochloride measured by the pulsed-accelerated-flow method, J. Am. Chem. Soc., 111, 7838–7844, 1989.

Wanninkhof, R.: Relationship between wind speed and gas exchange over the ocean, J. Geophys. Res., 97, 7373–7382, 1992.

Warneck, P.: The relative importance of various pathways for the oxidation of sulfur dioxide and nitrogen dioxide in sunlit continental fair weather clouds, Phys. Chem. Chem. Phys., 1, 5471 – 5483, 1999.

Warwick, N. J., Pyle, J. A., Carver, G. D., Yang, X., Savage, N. H., O'Connor, F. M., and Cox, R. A.: Global modelling of natural bromocarbons, J. Geophys. Res., 111, 24 305,doi:10.1029/2006JD007 264, 2006.

Wayne, R. P., Barnes, I., Biggs, P., Burrows, J. P., Canosa-Mas, C. E., Hjorth, J., Le Bras, G., Moortgat, G. K., Perner, D., Poulet, G., Restelli, G., and Sidebottom, H.: The nitrate radical: Physics, chemistry, and the atmosphere, Atmos. Environ., 25A, 1–203, 1991.

Weast, R. C., ed.: CRC Handbook of Chemistry and Physics, 61st Edition, CRC Press, Inc., Boca Raton, FL, 1980.

Weinstein-Lloyd, J. and Schwartz, S. E.: Low-intensity radiolysis study of free-radical reactions in cloudwater: H_2O_2 production and destruction, Environ. Sci. Technol., 25, 791–800, 1991.

Wesely, M. L.: Parameterization of surface resistances to gaseous deposition in regional-scale numerical models, Atmos. Environ., 23, 1293 – 1304, 1989a.

Wesely, M. L.: Parameterization of surface resistances to gaseous deposition in regional-scale numerical models, Atmos. Environ., 23, 1293–1304, 1989b.

Wessel, S., Aoki, S., Winkler, P., Weller, R., Herber, A., Gernandt, H., and Schrems, O.: Tropospheric ozone depletion in polar regions. A comparison of observations in the Arctic and Antarctic, Tellus, 50B, 34 – 50, 1998.

Wilhelm, E., Battino, R., and Wilcock, R. J.: Low-pressure solubility of gases in liquid water, Chem. Rev., 77, 219–262, 1977.

Wine, P. H., Tang, Y., Thorn, R. P., Wells, J. R., and Davis, D. D.: Kinetics of aqueous phase reactions of the SO_4^- radical with potential importance in cloud chemistry, J. Geophys. Res., 94D, 1085–1094, 1989.

Wingenter, O. W., Kubo, M. K., Blake, N. J., Smith Jr., T. W., Blake, D. R., and Rowland, F. S.: Hydrocarbon and halocarbon measurements as photochemical and dynamical indicators of atmospheric hydroxyl, atomic chlorine, and vertical mixing obtained during Lagrangian flights, J. Geophys. Res., 101, 4331 – 4340, 1996.

Wingenter, O. W., Sive, B. C., Blake, N. J., Blake, D. R., and Rowland, F. S.: Atomic chlorine concentrations derived from ethane and hydroxyl measurements over the Equatorial Pacific Ocean: Implication for dimethyl sulfide and bromine monoxide, J. Geophys. Res., 110, D20 308, doi:10.1029/2005JD005 875, 2005.

Worsnop, D. R., Zahniser, M. S., Kolb, C. E., Gardner, J. A., Watson, L. R., van Doren, J. M., Jayne, J. T., and Davidovits, P.: The temperature dependence of mass accommodation of SO_2 and H_2O_2 on aqueous surfaces, J. Phys. Chem., 93, 1159–1172, 1989.

Wu, D., Wong, D., and Di Bartolo, B.: Evolution of Cl_2^- in aqueous NaCl solutions, J. Photochem., 14, 303–310, 1980.

Yang, H., Xu, J., Wu, W.-S., Wan, C. H., and Yu, J. Z.: Chemical Characterization of Water-Soluble Organic Aerosols at Jeju Island Collected During ACE-Asia, Atmos. Environ., 1, 13–17, 2004.

Yang, X., Cox, R. A., Warwick, N., Pyle, J. A., Carver, G. D., O'Connor, F. M., and Savage, N. H.: Tropospheric bromine chemistry and its impacts on ozone: A model study, J. Geophys. Res., 110, D23 311, doi:10.1029/2005JD006 244, 2005.

Yin, F., Grosjean, D., and Seinfeld, J. H.: Photooxidation of Dimethyl Sulfide and Dimethyl Disulfide. I: Mechanism Development, J. Atmos. Chem., 11, 309 – 364, 1990.

Yoon, Y., Ceburnis, D., Cavalli, F., Jourdan, O., Putaud, J., Facchini, M., Decesari, S., Fuzzi, S., Sellegri, K., Jennings, S., and O'Dowd, C.: Seasonal characteristics of the physicochemical properties of North Atlantic marine atmospheric aerosols, J. Geophys. Res., 112, D04 206, doi:10.1029/2005JD007 044, 2007.

Yu, X.-Y.: Kinetics of free radical reactions generated by laser flash photolysis of $OH + Cl^-$ and $SO_4^- + Cl^-$ in the aqueous phase – Chemical mechanism, kinetics data and their implications, Ph.D. thesis, University of Michigan, Ann Arbor, 2001.

Zahardis, J. and Petrucci, G. A.: The oleic acid-ozone heterogeneous reaction system: products, kinetics, secondary chemistry, and atmospheric implications of a model system -a review, Atmos. Chem. Phys., 7, 1237–1247, 2007.

Zahardis, J., LaFranchi, B. W., and Petrucci, G. A.: Photoelectron resonance capture ionization-aerosol mass spectrometry of the ozonolysis products of oleic acid particles: Direct measure of higher molecular weight oxygenates, J. Geophys. Res., 110, D08 307, doi:10.1029/2004JD005 336, 2005.

Zahardis, J., LaFranchi, B. W., and Petrucci, G. A.: Direct observation of polymerization in the oleic acid-ozone heterogeneous reaction system by photoelectron resonance capture ionization aerosol mass spectrometry, Atmos. Environ., 40, 1661–1670, 2006.

Zehavi, D. and Rabani, J.: Oxidation of aqueous bromide ions by hydroxyl radicals. Pulse radiolytic investigation, J. Phys. Chem., 76, 312 – 319, 1972.

Zellner, R., Exner, M., and Herrmann, H.: Absolute OH Quantum Yield in the Laser Photolysis of Nitrate, Nitrite and Dissolved H_2O_2 at 308 and 351 nm in the Temperature Range 278-353 K, J. Atmos. Chem., 10, 411 – 425, 1990.

Ziemann, P. J.: Aerosol products, mechanisms, and kinetics of heterogeneous reactions of ozone with oleic acid in pure and mixed particles, Faraday Discuss., 130, 1–22, 2005.

Zingler, J. and Platt, U.: Iodine oxide in the Dead Sea Valley: Evidence for inorganic sources of boundary layer IO, J. Geophys. Res., 110, D07 307, doi:10.1029/2004JD004 993, 2005.

Acknowledgements

First of all I would like to thank Dr. Roland von Glasow for supervising this thesis in the last three years. Many thanks to him for helpful discussions and for giving me the opportunities to present my work on several international conferences.

Furthermore, I would like to thank Prof. Ulrich Platt for taking the role of my official supervisor at the University of Heidelberg.

I am very grateful to the former group members Susanne Pechtl and Matthias Piot who both helped me especially at the beginning of the work on this thesis with a lots of questions regarding MISTRA or ferret!

I would like to thank my parents for always giving the the freedom to make my own decisions and having trust and faith in me. I thank Holger for always supporting me and standing at my side - even though I moved hundreds of kilometres away to Norwich.